NASA CR-72864

NAS3-13482
RR 71-02

STUDIES OF FOIL JOURNAL-BEARINGS FOR BRAYTON CYCLE TURBOMACHINERY

by

L. Licht

Ampex Corporation, Research Department

401 Broadway, Redwood City, California 94063

for

National Aeronautics and Space Administration

Lewis Research Center

21000 Brookpark Road, Cleveland, Ohio 44135

NASA CR-72864

Contract No. NAS3-13482

STUDIES OF FOIL JOURNAL-BEARINGS FOR BRAYTON CYCLE TURBOMACHINERY

FINAL REPORT

RR 71-02

February 16, 1971

Prepared by

Ampex Corporation, Research Department
401 Broadway, Redwood City, California 94063

for

National Aeronautics and Space Administration
Lewis Research Center
21000 Brookpark Road, Cleveland, Ohio 44135

Prepared by:

L. Licht, Principal Investigator

Approved by:

P. Szego, Manager, Mechanics Section

ABSTRACT

The content of this report pertains to further development of a foil-bearing support for an experimental, Brayton cycle turbo-alternator. In the course of previous investigations, reported in detail in references [1] through [4] *, it was demonstrated that high-speed rotors, supported in foil bearings, were free from whirl-instability and sensitivity to excitation at frequency equal half the rotor speed. The foil bearing was also shown to be capable of accommodating thermal and geometrical distortions, combining the foregoing attributes with excellent wipe-wear characteristics and tolerance of foreign particles.

The present investigation was directed toward the solution of two important problems in the practical application of foil bearings:

(a) To construct foil bearings of dimensions commensurate with rigid, tilting-pad bearings, and to produce a reliable rotor support with foil bearings reduced in length by a margin of 50%.

(b) To eliminate the need for an elaborate foil-lift system and to achieve multiple starts and stops without the aid of external pressurization.

This report contains a detailed description of experimental methods which lead to the realization of the foregoing objectives.

*Numbers in square brackets refer to the list of references on page 141 of this report.

ACKNOWLEDGMENTS

These studies were sponsored by the National Aeronautics and Space Administration, Lewis Research Center, Cleveland, Ohio, under NASA Contract No. NAS3-13482. Mr. William J. Anderson, Fluid System Components Division, NASA Lewis Research Center, was Project Manager and guided the research with respect to hardware requirements and technical objectives.

The experiments were conducted in the Mechanics Section of the Research Department of the Ampex Corporation. Mr. P. Szego, Section Manager, and Dr. A. Eshel made significant technical contributions and offered constructive criticism. The author gratefully acknowledges the cooperation of Mr. B. Lawson in the conduct of experiments and of Mr. F. Schneider in the construction of apparatus. Mrs. T. Kember was responsible for the numerical work.

TABLE OF CONTENTS

TABLE OF CONTENTS (cont)

LIST OF FIGURES

LIST OF FIGURES (cont)

LIST OF FIGURES (cont)

LIST OF FIGURES (cont)

LIST OF FIGURES (cont)

LIST OF FIGURES (cont)

LIST OF FIGURES (cont)

LIST OF FIGURES (cont)

LIST OF FIGURES (cont)

LIST OF FIGURES (cont)

LIST OF FIGURES (cont)

SYMBOLS

A	Refers to upper foil bearing and monitoring probes X_A and Y_A
$2A_r$	Orbit dimension at resonance, peak-to-peak
B	Refers to lower foil bearing and monitoring probes X_B and Y_B
$b =$	$(\sqrt{3}/3)\ (r_0-r_1)$
2b	Foil width
C	Refers to clamped condition
$C =$	$r_0 p_a/T$, Compressibility parameter
$\bar{C} =$	Nr_1^3/Dt (N is reaction force)
$D =$	$Et^3/12(1-\nu^2)$, Flexural rigidity
E	Modulus of Elasticity
$\hat{e}$	Displacement of journal center from reference axis
e_1	Component of displacement along bisector of wrap.
F	Reaction force
F_p	Piston force
f_B	Frequency of "free-free" vibration of rotor
f_n	Natural frequency of foil-rotor support
f_{SS}	Frequency of friction-induced vibration
h	Gap width (clearance)
h^*	Gap width in region of uniformity

I = $\frac{1}{2}\rho_a U^2/(T/r_0)$, Inertia parameter

k Bearing Stiffness

L Foil length

L Distance between balancing planes

L_o Initial foil length

ℓ_o Initial length of perfectly flexible foil

M_o Bending moment at journal

M_1 Bending moment at foil guide

m = W/g Rotor mass (g is acceleration of gravity)

N Rotor Speed

N Reaction force

O Refers to reference position in pressurized mode at zero speed

P Refers to pressurized mode of operation

p Pressure of fluid in foil bearing gap

p_a Ambient (atmospheric) fluid pressure

p_ℓ Foil-lift pressure

R Radius of curvature

r_0 Radius of journal

r_1 Radius of foil guide

r_p Radius of gyration of rotor, polar

r_t Radius of gyration of rotor, transverse

S	Refers to self-acting mode of operation
T	Tension per unit width
T_o	Preload tension per unit width
t	Foil thickness
t_1	Foil thickness, outer foil
t_2	Foil thickness, liner foil
$U \approx r_0\omega$	Journal surface velocity
$\bar{u}$	Imbalance
W	Rotor weight
x; z	Coordinates
$X_{A,B}$; $Y_{A,B}$	Displacements of journals in monitoring planes A and B
y; w	Deflections of foil
Y; W	Normalized deflections of foil

$\alpha = (b^2T/D)^{1/2}$, $[b = (\sqrt{3}/3)(r_0-r_1)]$

$\beta = b^2/r_1t$, $[b = (\sqrt{3}/3)(r_0-r_1)]$

$\gamma = r_1/t$

$\Delta\ell_p = (\ell_o/Et)(T-T_o) - h^*\theta + 2e\sin\frac{\theta}{2}$, "slack" length

$\delta = 2\bar{u}/W$, Eccentricity of imbalance

$\eta = r_1/r_0$

θ Angle of wrap

$\lambda = (r_1^2T/D)^{1/2}$

μ	Viscosity of fluid
ν	Poisson's ratio
ρ_a	Density of fluid , ambient
ω	Angular velocity of rotor

1.0 INTRODUCTION

The present report and its two forerunners, NASA CR-1157 [1] and NASA CR-1563 [3], contain a rather complete set of data and information pertinent to the design and the operating characteristics of high-speed rotors, supported by gas-lubricated foil bearings.

The historical aspects of foil-bearing development, as well as a review of "natural" foil-bearing applications in the manufacture, processing and transport of flexible media*, is beyond the scope of this narrative. For sources of information on the subject of foil bearings, their characteristics as well as applications, the reader is referred to the bibliographies and to the introductory chapters of references [1] through [13].

It is appropriate, however, to devote part of this introduction to reasons underlying the effort to develop foil-bearing supports for high-speed, high-temperature turbomachines and to point out a number of advantages inherent in their operating characteristics. Thus, without assigning an order of priority to the following considerations, the foil-bearing support is free from whirl-instability and from resonances due to excitation at frequency equal to half the rotational speed. The motion of the journal is not constrained by narrow confines of a clearance circle and both foil and rotor can displace while maintaining an adequate lubricating film. Furthermore,

* Metal foil, paper and plastic film are typical examples. Thus mills, printers, coating and developing processors, cameras, and magnetic-tape drives are representative of machines, in which foil bearings exist in one form or another.

the foil bearing accommodates distortion at elevated temperatures and in the presence of appreciable temperature gradients. Its performance is quite insensitive to geometrical imperfections and misalignments, and it is endowed with excellent wipe-wear characteristics and tolerance of foreign particles. Manufacture is relatively simple and poses no stringent requirements with regard to dimensional accuracy and roundness.

These proven characteristics of foil bearings permit a very favorable comparison with rigid, gas-lubricated bearings. Even the relatively low stiffness of the foil bearing can be considered a partial asset, since resonances of the rotor-bearing system occur at low speeds and, therefore, at low levels of centrifugal forces induced by remanent imbalance.* It is not suggested that foil bearings are uniformly and universally superior to each and every type of rotor support regardless of size and application, but lubrication problems posed by high-temperature, high-speed turbomachines make this unusual bearing a serious contender among the few, feasible alternatives.

The development and associated experiments described in this report were directed toward two objectives. The first objective was aimed at reducing the length of the foil bearings by a margin of 50% and to support a 21-lb rotor within space requirements commensurate with those of rigid bearings, without producing adverse effects on the operational characteristics of the system. The second objective was to achieve multiple starts and stops, with adequate preload tension applied to the foils, but without the aid of external pressurization ("dry" starting and stopping) and with satisfactory performance at all operating speeds. These efforts were limited to rotation in the vertical, that is radially unloaded attitude of the rotor.

*Unless the amount of added imbalance is specifically stated, response data in this report pertains to excitation by remanent imbalance in the order of 100 to 350 μin-oz.

The reduction of bearing length was dictated mainly by considerations of space requirements. The elimination of the very effective but elaborate foil-lift system, and of the complex method of pressurization via the interior of the rotor [3], represented a very desirable simplification. These tasks, though unrelated and independent of one another, were undertaken simultaneously and solved in parallel. This approach imposed a series of constraints on the choice of bearing parameters. For example, in reducing the effective bearing length and bearing span, no attempt was made to increase the preload tension to levels that would have precluded starting without the aid of external pressurization. On the other hand, the capability of "dry" starting and stopping in lightly preloaded foil bearings was never considered as an end in itself, without full consideration being given to the effect of reduction of preload on high-speed operation.

2.0 DESCRIPTION OF FOIL-BEARING SUPPORT. - INSTRUMENTATION AND ACCURACY

The experimental apparatus, with the exception of modifications discussed in this section, was identical with that described in NASA CR-1563 [3] and is depicted schematically in Fig. 1*. The foil and foil-guide arrangement remained as indicated in Fig. 1, but the number of foil rows was reduced from 4 to 2. Consequently, the tandem-foil support plates (3)** were replaced with modified, single-foil supports shown in Fig. 2. Also, since operation was restricted to the vertical attitude only, the counterbalances (12) were eventually eliminated in favor of foil-loading platforms illustrated in the left-hand side of Fig. 3. Shown also in the center of the photograph in Fig. 3 are two rotors, the journals of which were flame-plated with chromium oxide and aluminum oxide. To the right of the two rotors is a subassembly, consisting of split construction foil-supports, spacers, and inboard-facing foil guides and foil locks. Here, the outboard-facing guides and locks (see Fig. 1) have been removed and the foil-support precisely realigned with new spacers, maintaining a 9.0-inch span between the centers of 1.5-inch long foil guides.

A similar foil-support subassembly accommodating 2.0-inch wide foils is shown in Fig. 2. Another view of several components of the foil-rotor system is presented in Fig. 4. The location of receptacles for the capacitance probes in the foil-bearing support plates is clearly discernible

*Fig. 7 of NASA CR-1563.

**Numbers in parentheses refer to components of the apparatus in Fig. 1 and Fig. 2. A common legend is appended in Fig. 1.

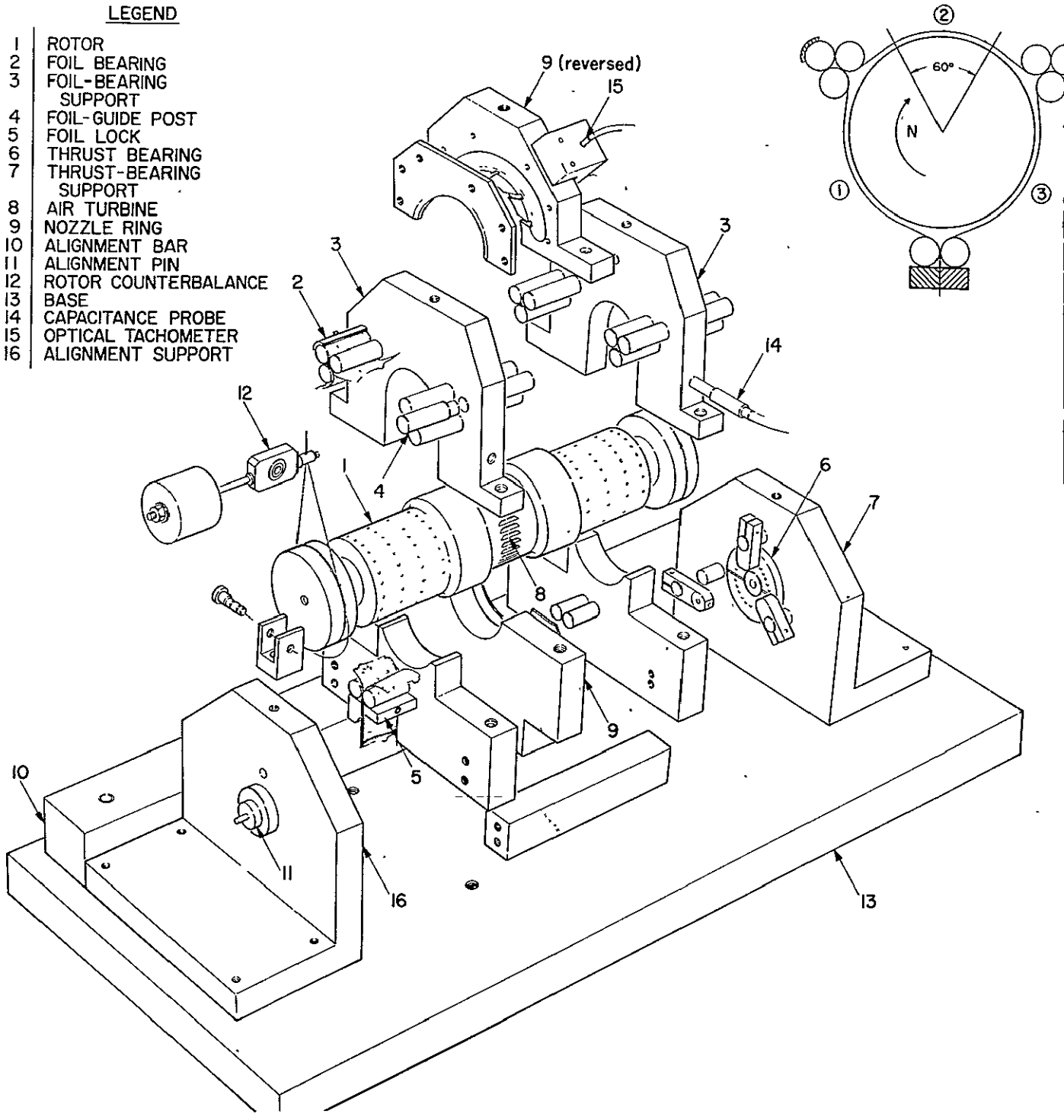

Fig. 1 Schematic Diagram of Experimental Apparatus
(Reproduced from reference [3])

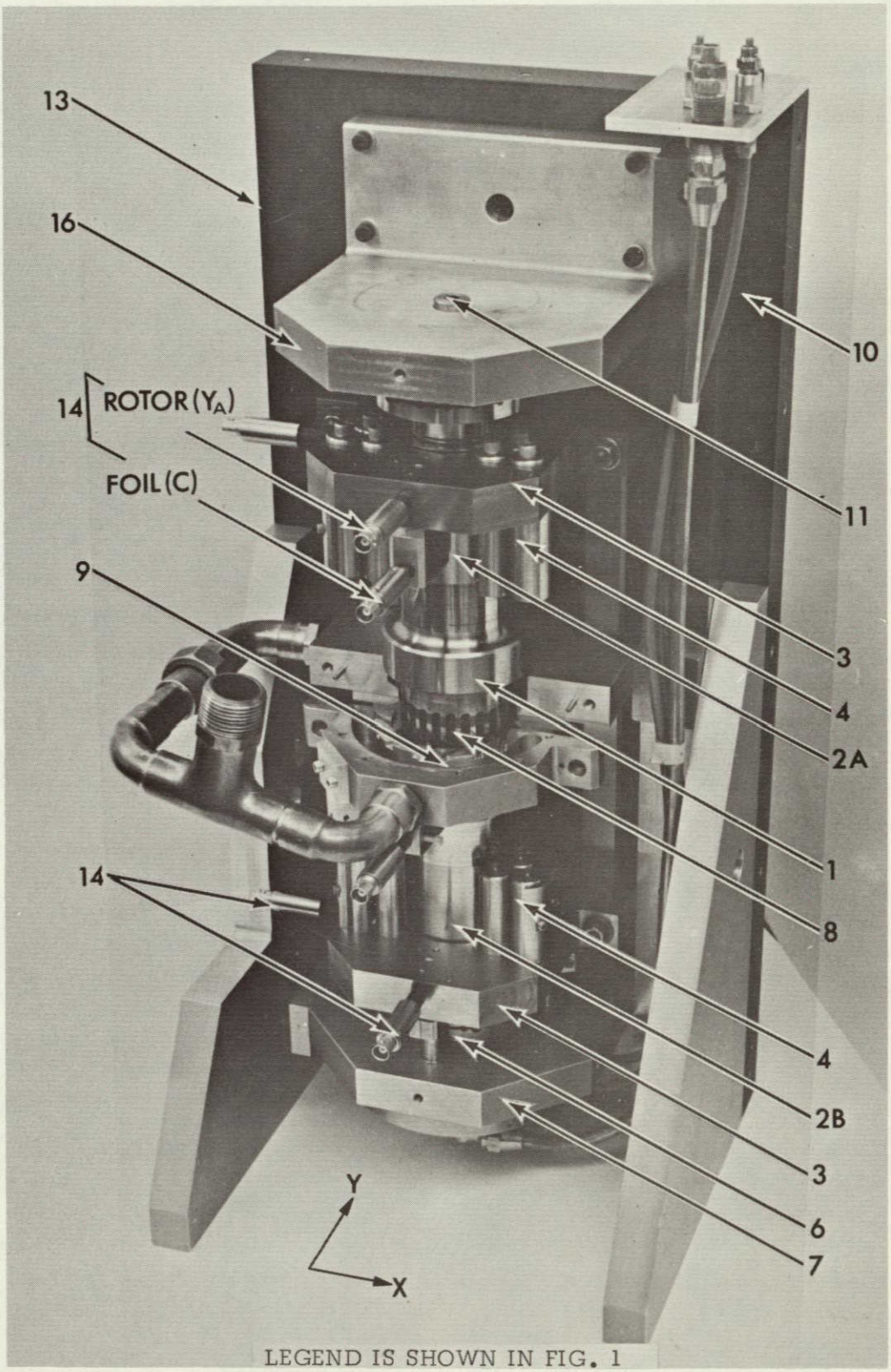

Fig. 2 View of Experimental Apparatus (Vertical Attitude)

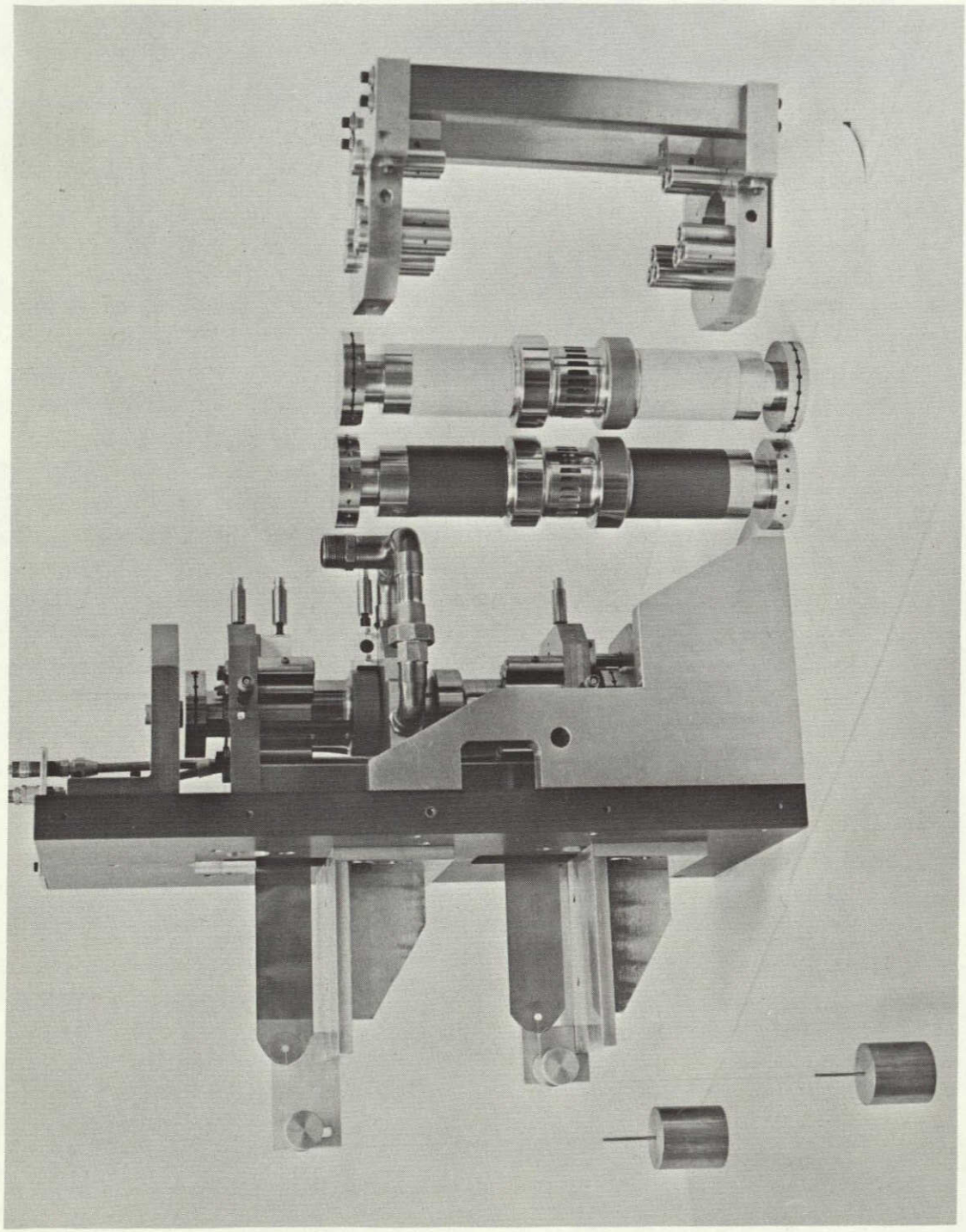

Fig. 3 View of Foil-Loading Attachments, Rotors and Foil Support Assembly

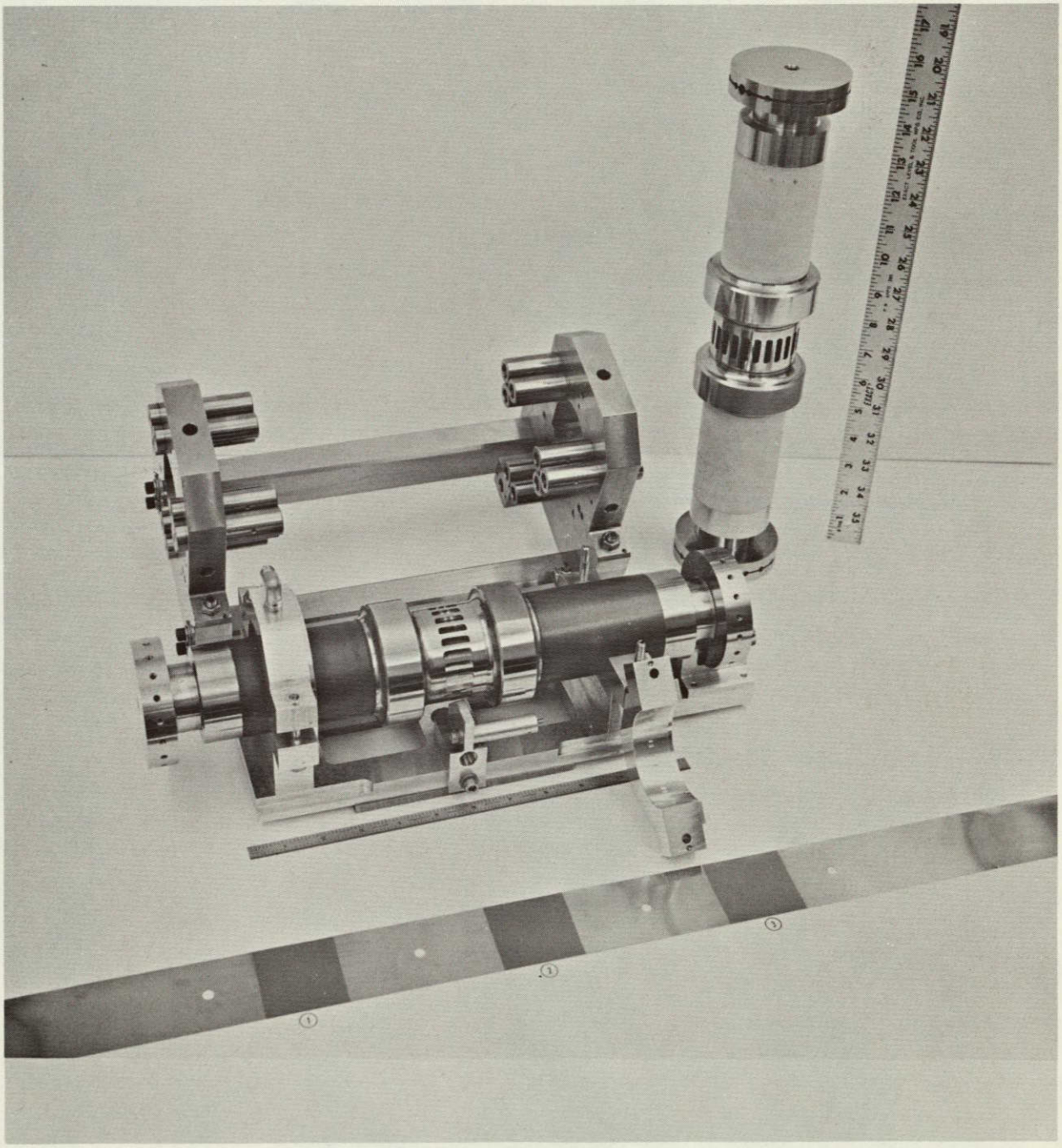

Fig. 4 View of Rotors, Foil Support, Balancing Fixture and Coated Foil

and it can be noted that sections of journals opposite the probes have not been flame-plated with oxides. The rotor with chromium oxide plating is located in a balancing fixture, in which the upper half of a pressurized air-bearing has been removed. In the foreground is a foil, with inorganically bonded MoS_2 film in the 3 regions of wrap. The view in Fig. 5 illustrates the rotor plated with aluminum oxide and the air-bearing fixture on the cradle of the balancing machine, surrounded by a sound-proof enclosure. The controls and vectorial displays of the balancing machine are seen in the left side of the photograph in Fig. 5.

The foils used in this series of experiments were molybdenum, of thickness varying between 0.001" and 0.002". Initially, some experiments were conducted with double-layer foils, using a 0.001" thick beryllium-copper foil as a liner. Attempts to utilize double-layer foil bearings were discontinued, however, because difficulties in uniform tensioning outweighed the advantages of this arrangement. Most foils, especially those used in operations involving starting and stopping unaided by external pressurization, were coated in the regions of wrap with an inorganically bonded, air-dried, MoS_2 lubricating film, approximately 100 to 200 microinches thick*.

Three rotors were used in the course of the experiments, and their outer geometry and inertial characteristics were very similar. The first was identical with the rotor used in experiments reported in references [3] and [4]. Each of the 4-inch long journals had 4 rows of 24, 0.020" dia. orifices. The inner rows of orifices of each journal were 1.5" apart and could be overlapped by 2-inch wide foils at a 9-inch bearing span. This rotor could also be operated at an 11.5-inch span, with 1.5-inch wide foils

*Dow-Corning, experimental coating designated as DC 1-3931. The bonded film is purported to be effective at temperatures the order of 1000°F.

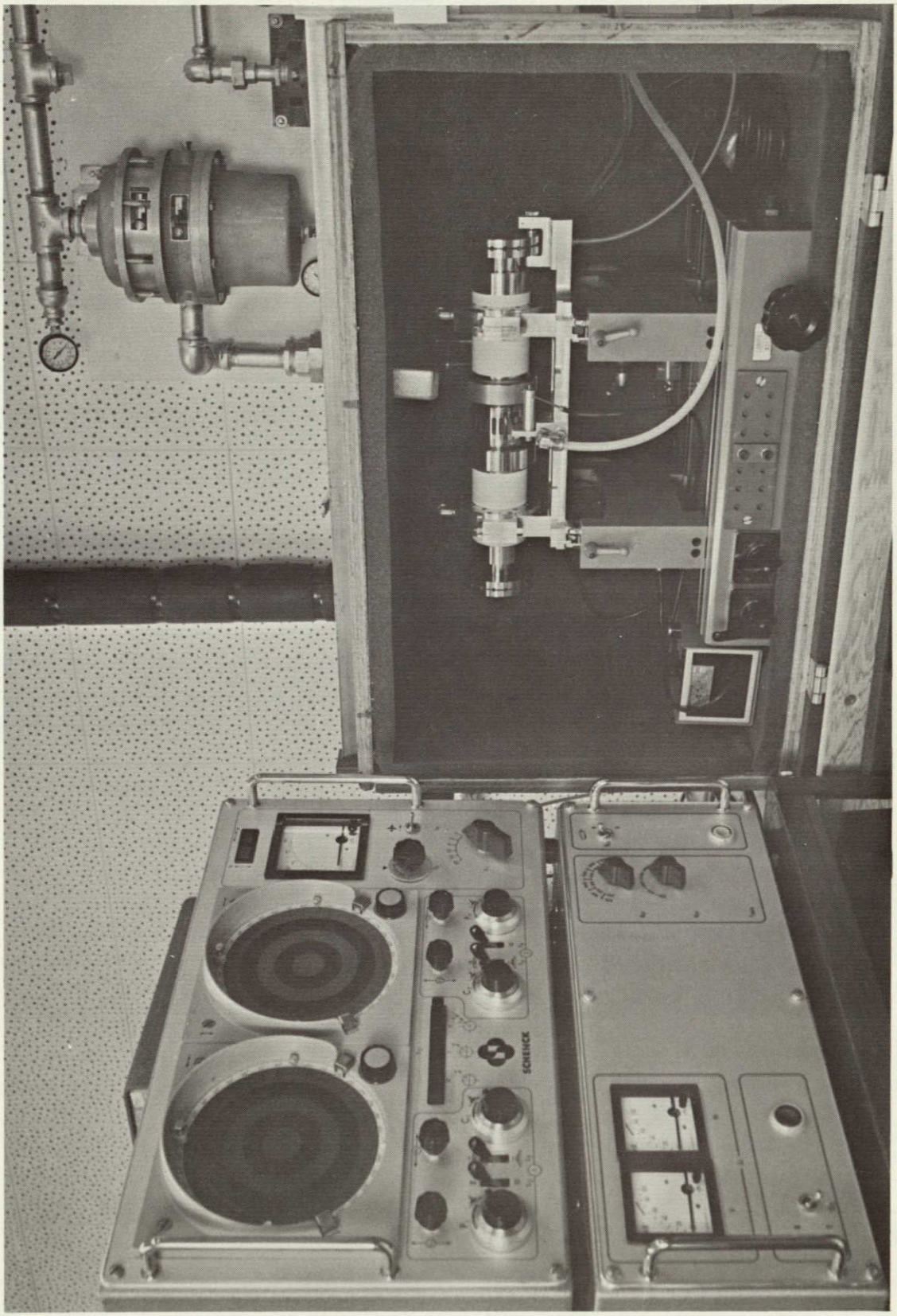

overlapping the outer rows of pressurization orifices of each journal. In both cases, the location of foil-lift orifices was 0.25" from the foil edges. The second rotor, intended for use in operations unaided by external pressurization, was a single unit, with the exception of two end-plugs pressed into the extremities of the 1.0-inch rotor bore. The journals were flame-plated with chromium oxide, except surfaces facing the capacitance probes. The third rotor, initially identical with the first and thus capable of being operated in the pressurized mode, had its journals ground to a smaller diameter and subsequently built up by flame-plated aluminum oxide. Particulars of the three rotors are listed below.

ROTOR No. ⟶		1	2	3
Overall Length	in	16.00	16.00	16.00
Journal Diameter	in	2.500	2.500	2.500
Thrust Collar Diameter	in	3.25	3.25	3.25
Thrust Bearing Clearance (Each Side)	in	0.003	0.003	0.003
Minimum Thrust Bearing Clearance (a)	in	0.0012	0.0012	0.0012
Rotor Weight	lb	20.90	21.25	20.50
Moment of Inertia, Transverse (b)	$in\text{-}lb\text{-}sec^2$	1.185	1.200	1.200
Radius of Gyration, Transverse	in	4.68	4.67	4.69
Moment of Inertia, Polar (b)	$in\text{-}lb\text{-}sec^2$	0.0595	0.0602	0.0564
Radius of Gyration, Polar	in	1.050	1.045	1.030
Remanent Imbalance (Each Plane) (c)	μin-oz	< 350	< 150	< 100
Distance Between Balancing Planes	in	15.25	15.25	15.25
Material	-	440-C	440-C	440-C
Journal Plating (d)	-	None, 440-C Rockwell C-56	Cr_2O_3	Al_2O_3
Construction	-	Shrunk on Sleeves; Orifices	One Piece No Orifices	Shrunk on Sleeves, Orifices

(a) With thrust bearing supporting the rotor weight
(b) Determined experimentally by pendulation
(c) Rotors balanced at 7200 RPM
(d) The Al_2O_3 flame-plated journals were subsequently coated with 100-200 microinches of inorganically bonded MoS_2 lubricant.

The foil-guide and foil-lock arrangement, the foil-lift (pressurization) system, the thrust bearing, and various other elements of the experimental apparatus have been described in considerable detail in reference [3]. In this section, the emphasis is on various modifications and additions. With regard to preload application, for example, the principle remained essentially unchanged, except that preloading in the horizontal position, Fig. 1, was changed to preloading in the vertical (operational) attitude. The tradeoff in this case was the elimination of counterbalancing (see item 12 in Fig. 1) in favor of doweled and removable loading platforms and carefully aligned idlers, as shown in Fig. 3. In addition, a more equitable sharing of the preload between the protruding extremities of the foil was provided by loading the free ends individually, rather than clamping the ends together and loading via a common holder*.

Initially, equalization of preload between 3 foil sectors was accomplished by utilizing the pressurization system to eliminate friction between the journal and the foil [3,4]. In the absence of pressurization orifices (Rotor No. 2), the adverse effect of friction on preload equalization was largely overcome by subjecting the foil-rotor system to small-amplitude vibrations. It is well known that friction forces can be reduced very appreciably by subjecting the contacting elements to vibrations [14,15]. In this case, the vibrations were transmitted to the structure by means of an eccentric, mounted on the spindle of a variable-speed motor attached to the base**. The vibrations proved more effective in the equalization of preload tension than pressurization. This was borne out by the fact that the same

*Holes were punched close to the foil extremities. The area around the holes was reinforced by thin, concentric washers, cemented to the foil. The load was applied equally to the free ends.

**Vibrations applied in this manner could also be utilized to reduce substantially the starting friction-torque.

weights applied to the foil ends produced consistently higher friction torques on starting, whenever equalization was effected through vibration. The reader should bear in mind, however, that values of preload tension T_o quoted in this report are nominal, and that the magnitudes correspond to the external load, divided by the width of the foil. These values, nevertheless, are estimated to be within 10% of the actual preload, except in cases of double-layer foil arrangements, for which the actual preload distribution was more uncertain.

Measurements performed in the course of experiments and described in the following sections involved the determination of motion of the rotor axis in two monitoring planes and of the relative displacement of the rotor and of the foil (i.e. the gap width) as a function of the rotational speed. An attempt was also made to measure the pressure in the lubricating air-film. Capacitance probes, used in conjunction with Wayne-Kerr DM 100 Displacement Meters, gave readings of displacement accurate to better than 5%. This estimate accounts for minor differences between all probe-meter-filter systems and for slight deviations from linearity of probe outputs in the range of measured displacements. Measurements of gap width, therefore, for which the differential output of 2 probes and meters was used, involved a maximum error not exceeding 10%. The frequency response of the instruments, inclusive of filters, was flat to approximately 2.5Kc and, therefore, quite adequate in the experimental speed range.

The speed was sensed by a photocell, via a bidirectional, optical fiber-tube, and displayed on a Hewlett-Packard 523B Electronic Counter. A digital-to-analog converter, integral with a Hewlett-Packard 560A Recorder, was used to convert the output of the counter to a speed-proportional d.c. signal driving the horizontal plates of an oscilloscope. This arrangement permitted simultaneous photographic recording of the X and Y components of motion, of gap width, and of pressure, as functions of the rotational speed.

In the recorded oscillograms, the maximum absolute error was in the order of 15 RPS, and was due mainly to slow instrument drift during the period of scan.

Most of the photographic data were obtained during coastdown of rotors from speed in excess of 750 RPS. At 750 RPS, deceleration was in the order of 8 RPS/sec. With a count time of 1 second and 1 second between counts, and with a typical human error of 1 second in actuating the camera shutter, possible deviations at 750 RPS were the order of 20 RPS, or less than 3%. Errors of this magnitude are reflected in the difference between the nominal speeds indicated along oscilloscope photographs of orbits, and the speeds derived from corresponding time-base oscillograms of capacitance probe outputs. Since such photographs are generally presented side by side in various figures of this report, the reader is alerted in advance to the existence of these minor discrepancies. The absolute error of the counter ($\pm$ 1 count) contributed little to inaccuracies, except at very low speeds. Additional errors of approximately 2% may have been involved in the calibration of the horizontal and vertical deflections of oscilloscope displays.

The determination of pressure variation in the foil-bearing gap as a function of speed presented a very difficult problem. These difficulties were a consequence of high velocity gradients across the gap width (order of 10^7 in/sec/in) and of unavoidable distortions caused by the attachment of pressure leads to the foil. The presence of a 0.005" dia. hole in a 0.001" thick foil, separated by a 0.0005" gap from a cylindrical surface moving at 5,000 in/sec, may have involved errors of considerable magnitude in the measurement of static pressure, especially in the presence of small protrusions and distortions along the perimeter of the pressure tap.

Three such pressure-tap holes were burned out by electric discharge along the centerline of a 60° foil sector, one in the center, and the

other two at 5° from the extremities of the region of wrap. The foil was then lightly lapped and the sector containing the holes wrapped around a 2.5" dia. plug-gauge. Three very flexible plastic tubes (Vinyl, 0.025" I.D and 0.063" O.D) were then attached with an adhesive to the convex side of the foil. The foil was carefully installed and the pressure tubes were supported at suitable locations to minimize foil distortion. A small capacity, diaphragm-type transducer was constructed to operate in conjunction with a capacitance probe and a Wayne-Kerr DM 100 meter. The pressure transducer was calibrated with a mercury manometer in the range 0-15 psi. and its readings were repeatable to within 0.3 psi. Because of low pneumatic capacitance and short pressure leads, the response time was more than adequate for monitoring pressures during rotor coastdown. The scans of pressure in the entrance and exit regions were not sufficiently reproducible and reliable to warrant publication. Two scans of pressure at the center of wrap, however, have been included and are discussed in a latter part of this report.

The fact notwithstanding that the performance of foil bearings is quite insensitive to an appreciable degree of misalignment, the best possible parallelism of foil guides and careful alignment of foil support assemblies with other components of the apparatus were insured. It is estimated that maximum deviation from parallelism between foil guides and rotor journals was less than 0.0003 in/in.

Because of the multiplicity of variables and impossibility to exercise selective control over many parameters affecting the performance of the foil-rotor system, a complete evaluation of errors and inaccuracies is not possible. The partial estimates presented in this section are intended to furnish the critical reader with means of assessing the general quality of experiments and data.

3.0 EXPERIMENTS

3.1 Review of Experiments and of Experimental Data

The first experiment of this series involved no changes in either foil width or foil spacing along the rotor axis. The configuration was identical with that maintained in the course of experiments reported in reference [3], Fig. 1. The tests were intended to assess the feasibility of using a double-layer foil support at a relatively light preload. This was followed by the removal of inner rows of foils and the operation of the rotor supported by outer rows of foils only (Section 3.2).

The potential advantages of the double-layer foil support were to decrease the undesirable bending rigidity, without sacrifice of extensional rigidity, and the minimization of contact in the edge zones, due to reduction of the anticlastic effect [13, 16, 17]. The intent was to maintain bearing stiffness by increasing foil thickness, while reducing the preload tension. The ultimate objective was to facilitate starting in the absence of external pressurization, without detriment to rotor performance in the speed-range 0-48,000 RPM. A possible advantage of additional damping, due to friction between adjacent foil layers, was also considered. At first, the double-layer arrangement appeared to be very attractive. In reality, it posed various problems related mainly to the application and equalization of preload tension, alignment, and foil handling. Thus, although the rotor performed quite satisfactorily with double-layer foil supports, this method was discontinued in subsequent experiments.

The removal of the inner rows of foils reduced the effective bearing length by 50%, but increased the span between the center-planes of bearings from 9" to 11.5", all of which could so far be accomplished without altering the foil-support assembly.* Several runs were made in this configuration, varying the foil thickness and the preload tension, thus gaining some insight into the response characteristic of the rotor supported by a single-row system (Section 3.3).

Subsequent tests required a new foil-support assembly, with 2.0" foil guides and a 9.0" bearing span. This configuration represented a reduction of total foil width by 33% and a possible saving of up to 50% in required journal length, while retaining the bearing span of the initial foil support. A major part of data presented in this report were obtained using the foregoing rotor support, including variations of foil thickness and preload tension, and excitation at various levels of symmetric and asymmetric imbalance (Sections 3.4 and 3.5).

Initially, pressurization was maintained to relatively high speed-limits prior to transition to the self-acting mode, with particular attention directed to rotor response in pressurized foil bearings. With self-acting operation extended later to speeds as low as 75 to 50 RPS, followed by coastdowns to a full stop unaided by pressurization, attention was also focused on self-acting performance in the low-speed range. Simultaneously, because of the unusual variation of gap width with speed in pressurized bearings, operation in the pressurized mode was routinely extended to speeds up to and in excess of 750 RPS. The effects of foil-lift pressure and of

*The foil-support system described in reference [3] required 4 inches of axial length at each journal, i.e. two 1.5" wide foils, separated by a 1" thick support plate. Although the radial stiffness is independent of the bearing span, the pitching stiffness varies with the square of the distance between the bearings.

preload tension on the gap width of a pressurized bearing were studied, and the effect of gap increase with temperature was demonstrated for the self-acting foil bearing. Measured also was the air-film pressure at the center of a foil sector (Section 3.6).

After the first successful attempts of starting without the aid of external pressurization with uncoated journals and foils and at moderate preloads, the overall performance was further improved by coating the bearing surface (or surfaces) with inorganically bonded MoS_2. Starting unaided by pressurization became then possible at higher preloads. Thus, with the feasibility of "dry" starting and stopping and satisfactory high-speed performance established on a firm foundation, subsequent experiments were directed to multiple start-stops and the study of rotor dynamics during the initial and final stages of rotation (Sections 3.7 and 3.8).

The present study culminated in a series of tests, wherein the foil width was reduced by an additional 25% (from 2.0" to 1.5"), without altering the 9.0" bearing span. These experiments involved also starting and stopping without the aid of pressurization and rotation with added symmetric and asymmetric imbalance (Section 3.9).

A careful, visual examination of journals and foils was performed after each bearing disassembly. Typical wear marks are illustrated in this report by profilometer traces, taken across circumferential wear tracks of a journal, and by photographs of magnified areas of coated foils in the entrance, exit and edge zones (Section 3.10).

The frictional power-loss can easily be determined from numerous coastdown curves presented in the last part of this chapter, and the bearing power-loss can be estimated from a comparison between deceleration in double-row and single-row foil bearings (Section 3.11).

The report contains also subsidiary information and data relevant to the effect of bending rigidity on clearance and bearing stiffness, to an

alternative starting method in the horizontal altitude, and to friction induced vibrations during starting and stopping, Appendices 1, 2 and 3. An improved bearing configuration is also suggested in Appendix 4.

The experimental data in this report consists largely of oscillograms pertaining to the dynamics of the rotor-foil system. Specifically, the data is presented in the following manner:

(a) Orbits in monitoring planes $(XY)_A$ and $(XY)_B$, containing two orthogonal sets of capacitance probes, Fig. 2. The orbits define the character of motion and the magnitude of rotor excursions.

(b) Motion in Y-Plane, recorded by parallel, coplanar probes Y_A and Y_B. These time-base records, when interpreted in conjunction with orbits and eccentricity loci, define the motion of the rotor axis.*

(c) Eccentricity loci in 2 monitoring planes at various rotational speeds, referred to the initial position of the stationary rotor. The loci define the mean displacement of the rotor axis from a reference position and provide a figure of merit with regard to departure of the foil bearings from perfect, 120-degree symmetry.

(d) Frequency scans of 4 amplitudes (X_A, Y_A and X_B, Y_B). The scans provide a continuous record of amplitudes up to 750 RPS and are particularly useful with regard to assessing the influence of system parameters on the bandwidth in which critical speeds occur.

*For a rigid rotor, these time-base records indicate the extent to which the motion is quasi-cylindrical or quasi-conical. They are helpful in assessing safe limits of rotor excursions and of imbalance. The choice of the Y-Probes, rather than the X-Probes, was arbitrary.

(e) Frequency scans of gap width. Although taken almost exclusively at the center of one foil sector, these records provide a great deal of information on the variation of gap width in pressurized and self-acting foil bearings. Supplementary information is furnished by a limited number of scans of gap width in the entrance and exit zones of the foil-wrap and also by time-base records of foil oscillations.

(f) Orbital motion in 2 monitoring planes at various stages of multiple start-stop cycling. These oscillographs furnish a history of motion during the initial and final stages of rotation and illustrate the effect of friction between foil and journal in the absence of pressurization.

(g) Scans of pressure at center of foil sector. Two scans of pressure included in this report furnish information complementary to simultaneously recorded scans of gap width.

All figures contain sufficient information pertinent to magnitudes of controllable parameters of the system. The inertial characteristics of all 3 rotors and their outer geometry were nearly identical. All journals were 2.5" in diameter and the extent of each region of wrap was 60°. The reader will note that the bearing span and the distance between the monitoring planes of the capacitance probes are clearly stated in schematic diagrams appended to various figures. The relative position of bearings and probes along the rotor axis should be taken into consideration in making quantitative comparisons between amplitudes of periodic excursions and mean displacements of the rotor axis.

The values of preload tension T_o quoted in this report are based on the load applied at the extremities of the foil, divided by the foil width. With the exception of double-layer foil bearings, an adequate equalization of tension in 3 foil sectors was probably insured by methods previously

described. The values of T_o, nevertheless, are approximate. Furthermore, the magnitudes of the operating tension T varied with temperature, which could not be kept constant and did not vary identically during each run. These, as well as other uncontrollable variables, may have obscured the effects of intended parametric variations.

Oscillograms of orbital motion and time-base traces of corresponding motion in the Y-plane are frequently placed side by side in various figures of this report. In the resonant range, the motion was recorded at speeds corresponding to maximum, or near maximum orbit dimensions. The reader should take into account possible discrepancies due to delay in human responses to a visual input (during coastdown) in the parallel actuation of 2 cameras. It should also be borne in mind that it has not always been possible to acquire all data pertinent to a given experiment simultaneously and during one run, and that operating conditions, and temperature in particular, may not have been quite identical during consecutive runs.

Most scans of amplitude and of gap width were obtained during coastdowns from 750 RPS, in the absence of both excitation by rotating air jets and convective cooling by turbine air discharge. In a number of cases, however, comparisons can be made between data obtained during slow acceleration and subsequent coastdown. All tests were conducted in the vertical, that is radially unloaded attitude.

With a few exceptions, experimental results have been presented chronologically. The organization of the report is based on the presentation of fairly complete sets of results pertinent to one bearing, rather than the grouping of one type of data extracted from test of various bearings. The narrative reflects the evolution of a simultaneous attack on the dual problem of the reduction of bearing length and the elimination of pressurization of the foil-support system during starting and stopping.

3.2 Double-Layer Foil Bearings and Reduction of Bearing Length through Elimination of Inner Rows of Foils

The point of departure from the set of experiments described in reference [3] was the introduction of a double-layer foil arrangement. The primary objective was to increase the resistance of the foil to extension and to avoid a large increase of flexural rigidity, which varies with the cube of foil thickness.* The increase of extensional rigidity Et through foil thickness was intended to compensate for the reduction of foil width, following the elimination of the inner rows of foils (See inboard-facing guides, item 2, Fig. 1). Other advantages anticipated from the double-foil arrangement were additional damping, due to friction between foil layers, and a reduction of the amplitude of anticlastic undulation in the edge zone [13,16,17].

Results relevant to the double-row system are presented in Fig. 6 and Fig. 7 and can be compared with the data of the single-row system in Fig. 8 and Fig. 9. The only change involved in this transition was the removal of the inner rows of foils, which lead to a reduction of bearing length, but also to an increase of bearing span.

The photographs (a), (b) and (c) in Fig. 6 and Fig. 8 illustrate rotor orbits in pressurized foil bearings and corresponding time-base oscillograms of motion in the Y-plane. Ultraharmonic resonances (fourth and second) occurred in the vicinity of the 2 lowest speeds. At the highest of of the three speeds, the loops had almost vanished and the transition to synchronous motion was nearly complete. The phenomenon of ultraharmonic resonances, which may be observed with various nonlinear systems

*The detrimental effect of flexural rigidity on bearing stiffness is reviewed on pp. 102-103 of reference [1]. Additional comments are made in Chapter 4 of this report. See also Appendix 1.

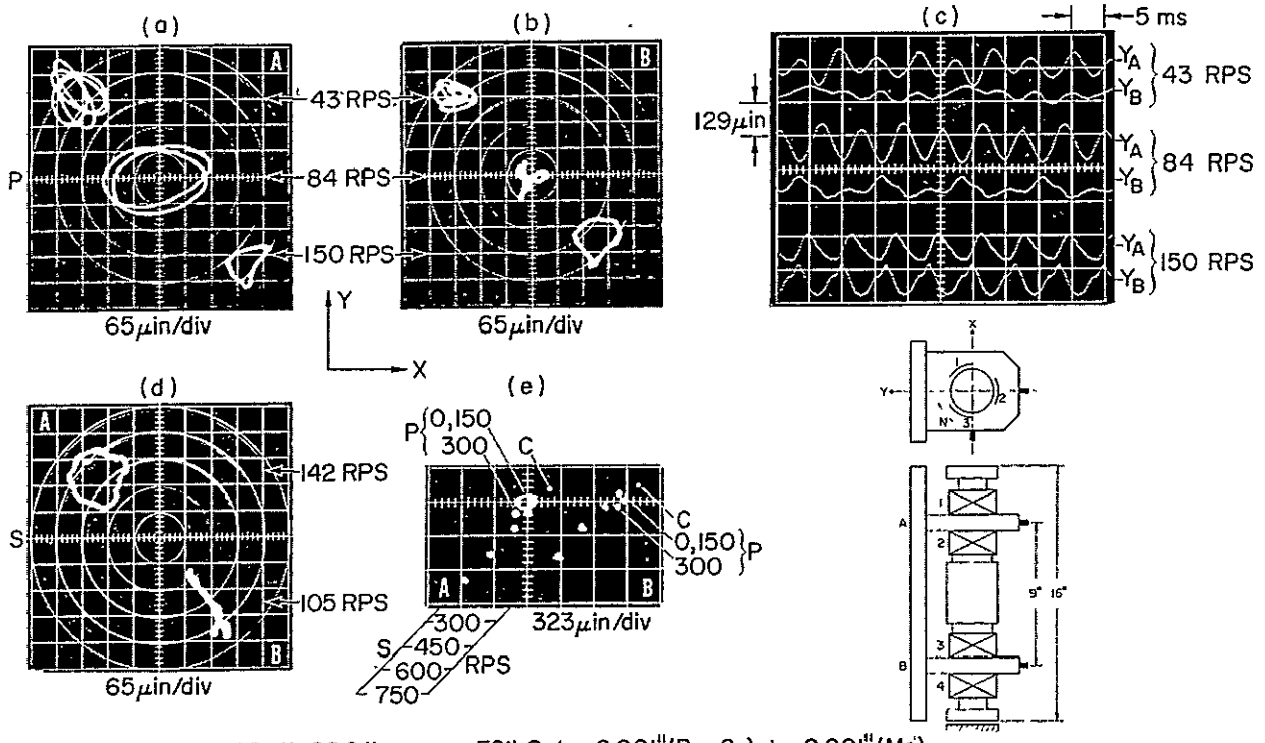

Fig. 6 Motion of Rotor in Double-Row, Double-Layer Foil Bearings (Bearing Span = 9"; Journal Length = 2 x 1.5")

(a), (b) Orbits in Resonant Range, Pressurized Bearings
(c) Motion in Y-Plane in Resonant Range, Pressurized Bearings
(d) Orbits in Resonant Range, Self-Acting Bearings
(e) Displacement of Rotor Axis with Speed

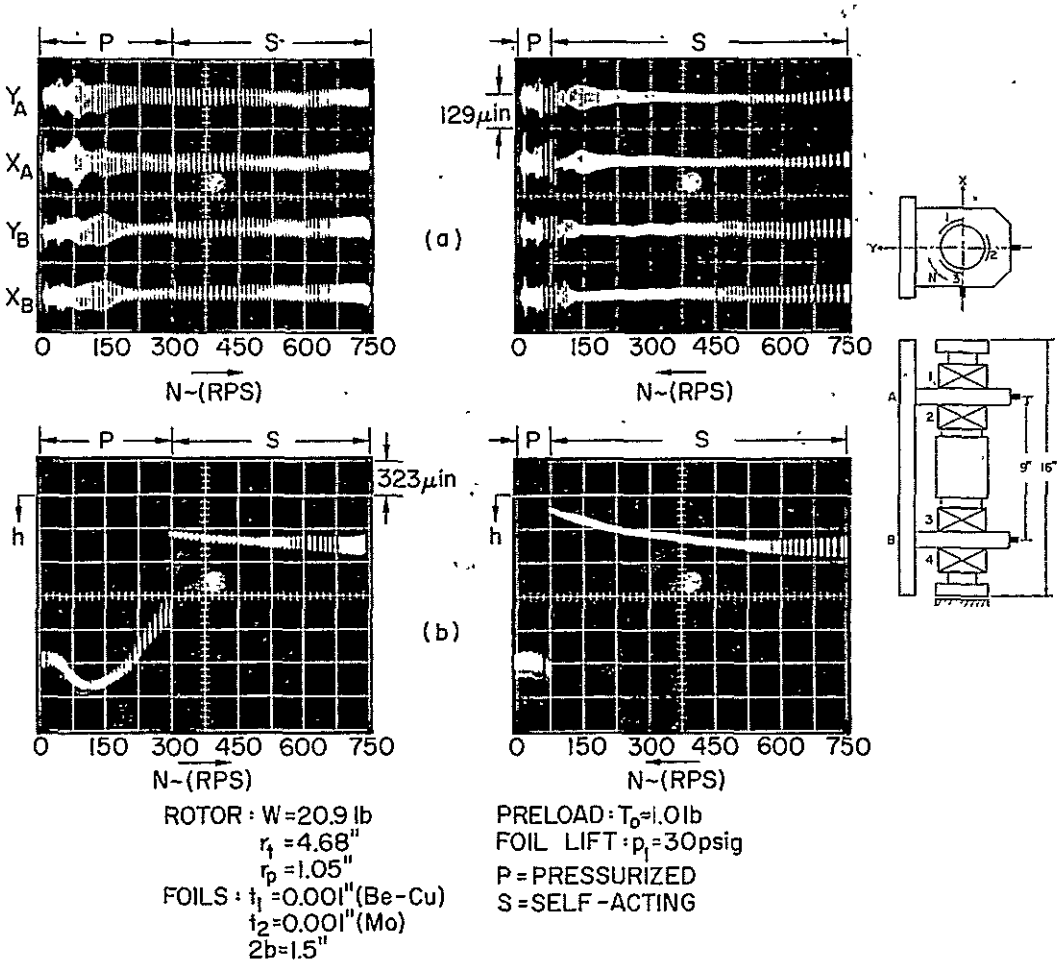

Fig. 7 Scans of Rotor Response and Gap Width in Double-Row, Double-Layer Foil Bearings (Bearing Span = 9", Journal Length = 2 x 1.5")

(a) Response to Remanent Imbalance
(b) Gap Width (Outer Foil, Sector A_2)

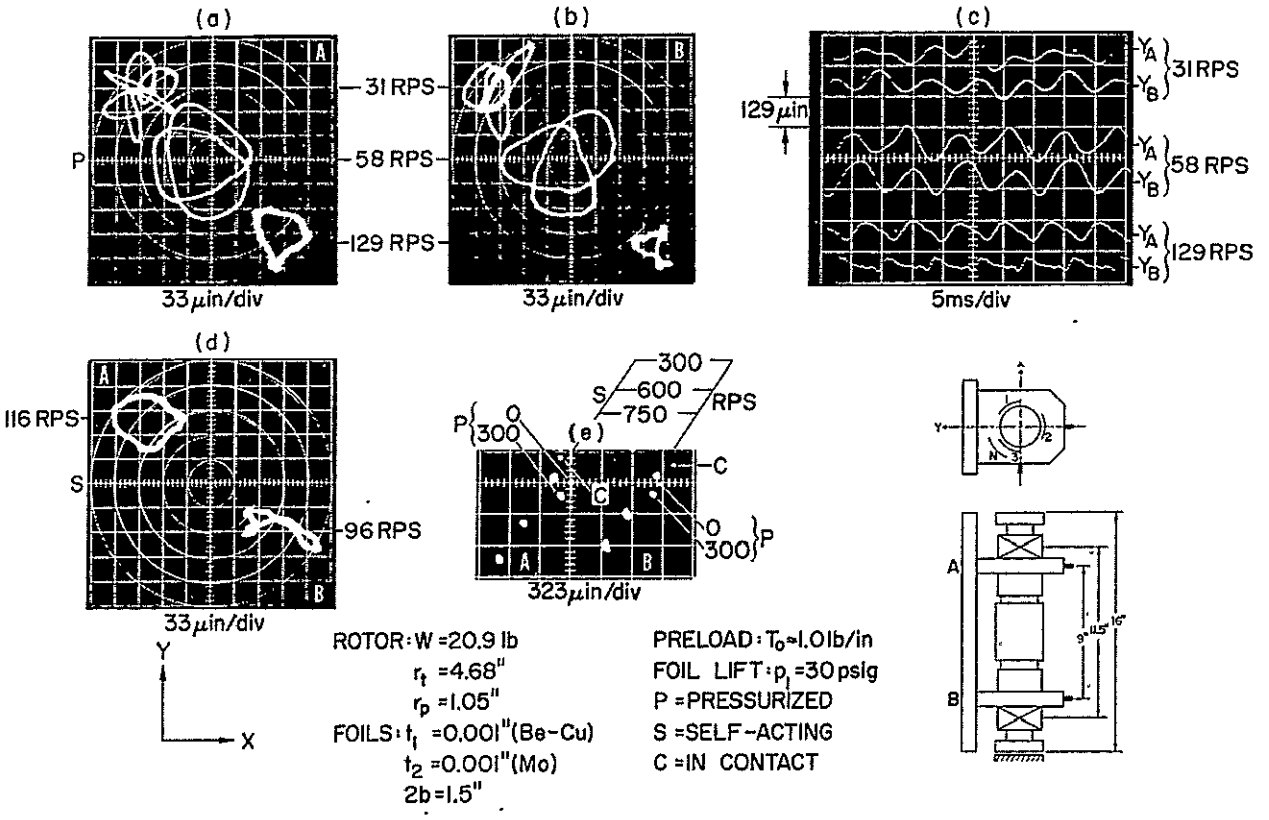

Fig. 8 Motion of Rotor in Single-Row, Double-Layer Foil Bearings (Bearing Span 11.5"; Journal Length = 1.5")

(a), (b) Orbits in Resonant Range, Pressurized Bearings
(c) Motion in Y-Plane in Resonant Range, Pressurized Bearings
(d) Orbits in Resonant Range, Self-Acting Bearings
(e) Displacement of Rotor Axis with Speed

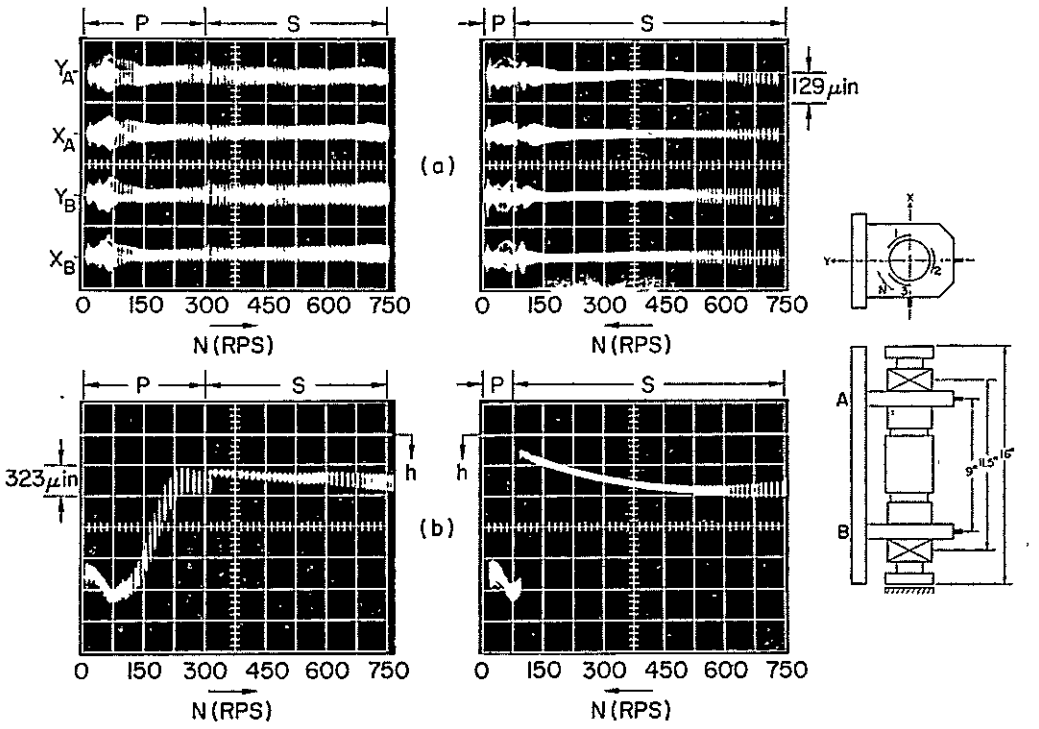

Fig. 9 Scans of Rotor Response and Gap Width in Single-Row, Double-Layer Foil Bearings (Bearing Span = 11.5", Journal Length = 1.5")

(a) Response to Remanent Imbalance
(b) Gap Width (Foil Sector A_2)

[18,19,20,21] is characteristic of pressurized foil bearings and was described in considerable detail in references [1] and [2].* In the present experiments, the reader may observe that the speed was approximately doubled with each successive resonance. The orbits in Fig. 6(d) and Fig. 8(d) were in the self-acting mode and corresponded to near-maximum rotor excursions in the resonant bandwidth. The reduction of bearing stiffness by a factor of 2, following the elimination of the inner rows of foils, was reflected consistently by a decrease in the magnitudes of resonant speeds in both modes of operation.

The displacement of the rotor axis with speed is shown in Fig. 6(e) and Fig. 8(e). The reference points in the monitoring planes A and B corresponded to the position of the rotor axis in the pressurized (P) foil bearings at zero speed (0). When the foil-lift pressure was cut off, the foils contacted the journals and the rotor axis was displaced to a new position (C). Starting at N = O in Fig. 6 and continuing in the pressurized mode, the next 2 positions were recorded at 150 RPS and at 300 RPS, the transition speed to the self-acting mode. The remaining points, up to 750 RPS, were obtained in the self-acting mode. The reader will note that the loci of points in the 3-rd quadrant were nearly straight lines, inclined at angles between 40° to 60° to the negative X-axis. The gradient of displacement increased with speed and the maximum displacement at 750 RPS was the order of 1.25×10^{-3} in. This magnitude exceeded substantially the maxima attained in all subsequent runs. The displacement with speed from the reference position reflected the degree of inherent dissymmetry of

*It was demonstrated in references [1] and [2] that the following relationship applies: $n \times N_n \approx N_s$, in which n is the number of the ultraharmonic, N_n is the rotational speed at which the ultraharmonic resonance occurs, and N_s is the speed of synchronous resonance.

geometry and tension. The corresponding differences in pressure distribution among the 3 foil sectors were amplified with speed, causing displacements of the rotor axis to new equilibrium positions.*

The frequency scans of amplitude response and of gap width for the double-row and single-row foil support systems are presented in Fig. 7 and Fig. 9. The transition speed during acceleration was 300 RPS, and approximately 75 RPS during coastdown. The oscillograms of amplitude response reflect the effect of changes in stiffness and bearing span, following the removal of the inner rows of foils. The unusual behavior of gap width in the pressurized mode of operation should be noted, pending further comments in Section 3.6.

Although performance in double-layer foil bearings was quite satisfactory throughout the entire operating speed-range, the mounting and tensioning of foils was difficult and cumbersome. Also, the equalization of the preload tension was inferior to that attainable with a single-layer bearing, and wear traces on the beryllium-copper foil, the liner foil, reflected an increase of misalignment. With the first reduction of bearing length accomplished, it was decided to explore operation with single foils, varying both thickness and preload. Several of these runs with 1.5" wide foils and a 11.5" bearing span are reviewed in the following section.

3.3 Operation with 1.5-inch Wide Foils at 11.5-inch Bearing Span

The exploratory runs described in this section were made with a bearing span approximately 2.5" longer than the span of a Brayton Cycle Unit undergoing tests at the NASA-Lewis Research Center. The anticipated effects of diminished bearing length, following the removal of 2 out

*In the present test rig, the rotor could be revolved in the clockwise sense only. Anticlockwise rotation [1] produced displacements in the 4-th quadrant, inclined at 40° to 60° to the positive X-axis.

of 4 rows of foils, were a decrease of radial stiffness and, to a lesser extent, a reduction of pitching stiffness. The parametric variations relevant to data presented in Fig. 10 through Fig. 15 involved changes of foil thickness and preload tension, from t = 0.0015" and $T_o \approx 1.0$ lb/in, to t = 0.002" and $T_o \approx 2.0$ lb/in.

Referring to the motion in the pressurized mode, the orbits in Fig. 10 and Fig. 13, and the scans of amplitude in Fig. 11 and Fig. 14, indicate that resonances occurred at nearly identical speeds and did not reflect the increase of foil thickness and of preload tension. The rotor axis described a complex, quasi-conical motion, and the ratio of speeds of synchronous and first ultraharmonic resonances was approximately 2. The shift in the resonant bandwidth in the self-acting mode was less significant than the change in the magnitudes of resonant-amplitudes. The maximum displacement of the rotor axis with speed was in the order of 950 μinches and 750 μinches, Fig. 10 and Fig. 13, with eccentricity vectors in the 3-rd quadrant of planes A and B inclined angles approximately 45° to 60° to the negative X-axis.

The variation of gap width with speed in the self-acting mode appears not to have been influenced greatly by changes of foil thickness and of preload. The foregoing can be surmised from corresponding scans of gap width during coastdown in Fig. 11 (lower right) and in Fig. 15 (upper, b). The reader will also note the apparent insensitivity of gap width to foil thickness and preload tension in the pressurized foil bearing. For example, the clearance at the center of a pressurized foil sector at zero speed is nearly identical in Fig. 11 and Fig. 12 (t = 0.0015"; $T_o \approx 1.0$ lb/in) and in Fig. 15 (t = 0.002 and $T_o \approx 2.0$ lb/in). This apparent inconsistency may be attributed to the effect of flexural rigidity, as shown in Appendix 1 and discussed in Chapter 4 (See also reference [1]).

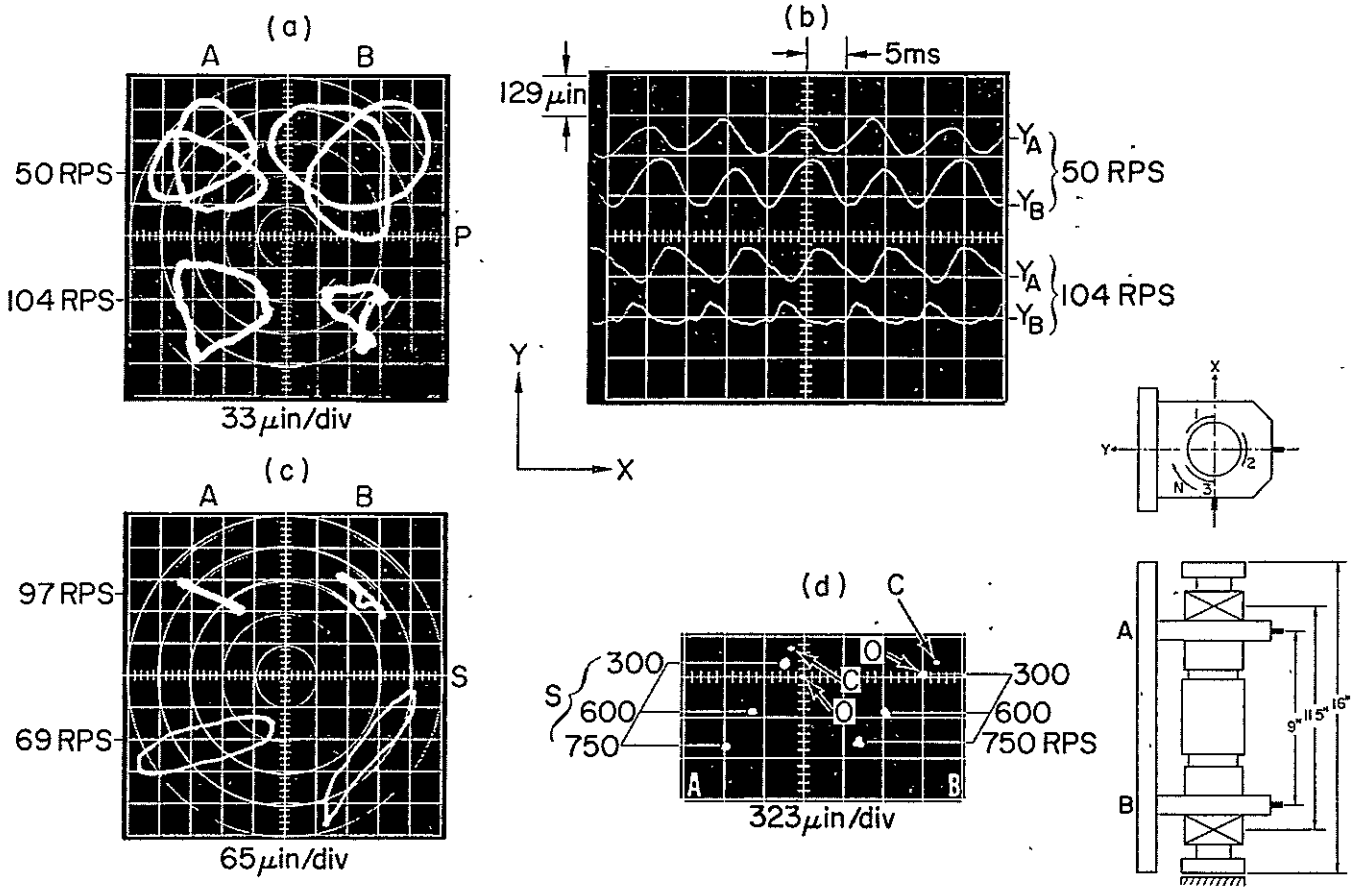

ROTOR : W = 20.9 lb
r_t = 4.68"
r_p = 1.05"
FOILS : t = 0.0015" (Mo)
2b = 1.5"

PRELOAD : $T_0 \approx 1.0$ lb/in
FOIL LIFT : p_l = 30 psig
P = PRESSURIZED
S = SELF-ACTING

Fig. 10 Motion of Rotor in Single-Row Foil Bearings (Bearing Span = 11.5"; Journal Length = 1.5")

(a) Orbits in Resonant Range, Pressurized Bearings
(b) Motion in Y-Plane in Resonant Range, Pressurized Bearings
(c) Orbits in Resonant Range, Self-Acting Bearings
(d) Displacement of Rotor Axis with Speed

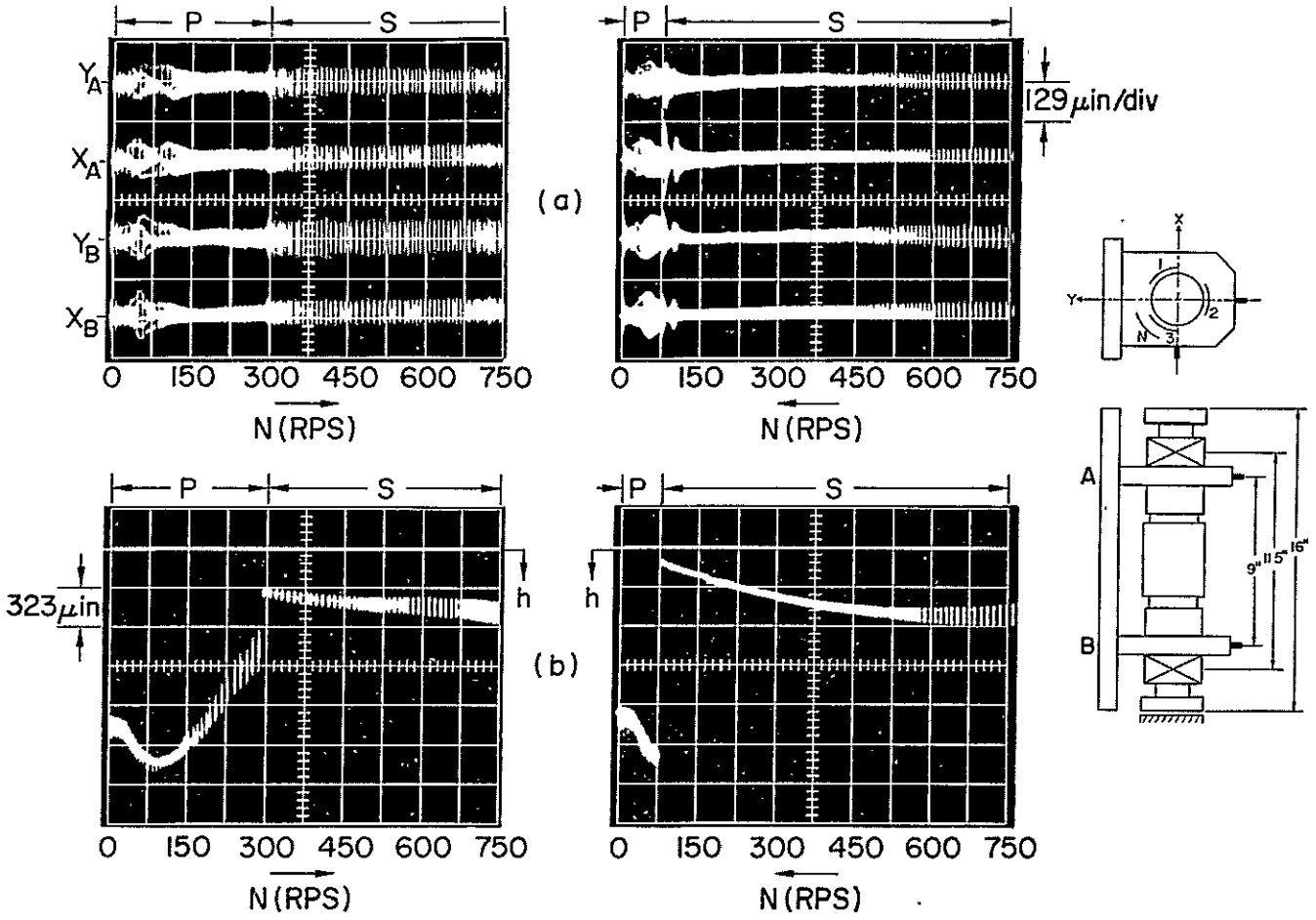

Fig. 11 Scans of Rotor Response and Gap Width in Single-Row Foil Bearing (Bearing Span = 11.5"; Journal Length = 1.5")

(a) Response to Remanent Imbalance
(b) Gap Width (Foil Sector A_2)

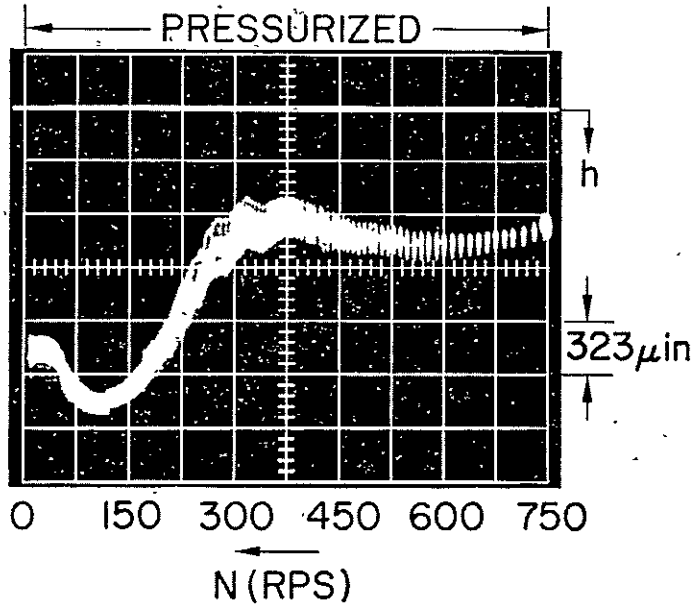

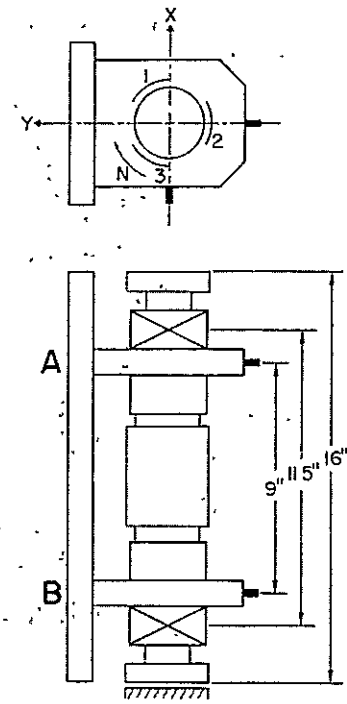

ROTOR: W=20.9 lb
r_t =4.68"
r_p =1.05"
FOIL LIFT: p_l =30psig

FOILS: t =0.0015"(Mo)
2b=1.5"
PRELOAD: $T_o \approx 1.0$ lb/in

Fig. 12 Scan of Gap Width in Pressurized Foil Bearing (Foil Sector A_2)

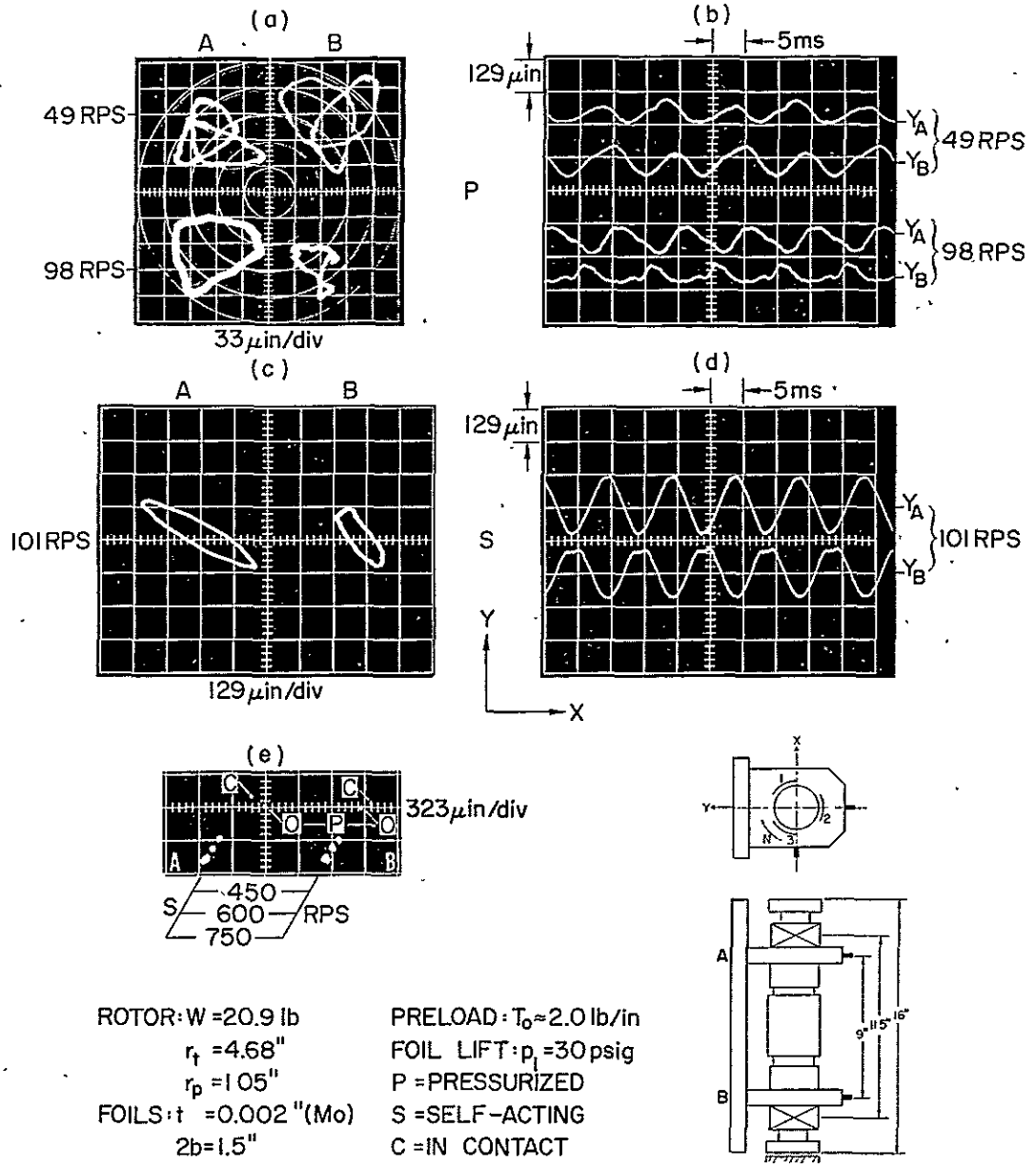

Fig. 13 Motion of Rotor in Single-Row Foil Bearings (Bearing Span = 11.5"; Journal Length = 1.5") - Increase of Foil Thickness and Preload

(a) Orbits in Resonant Range, Pressurized Bearings
(b) Motion in Y-Plane in Resonant Range, Pressurized Bearings
(c) Orbits in Resonant Range, Self-Acting Bearings
(d) Motion in Y-Plane in Resonant Range, Self-Acting Bearings
(e) Displacement of Rotor Axis with Speed

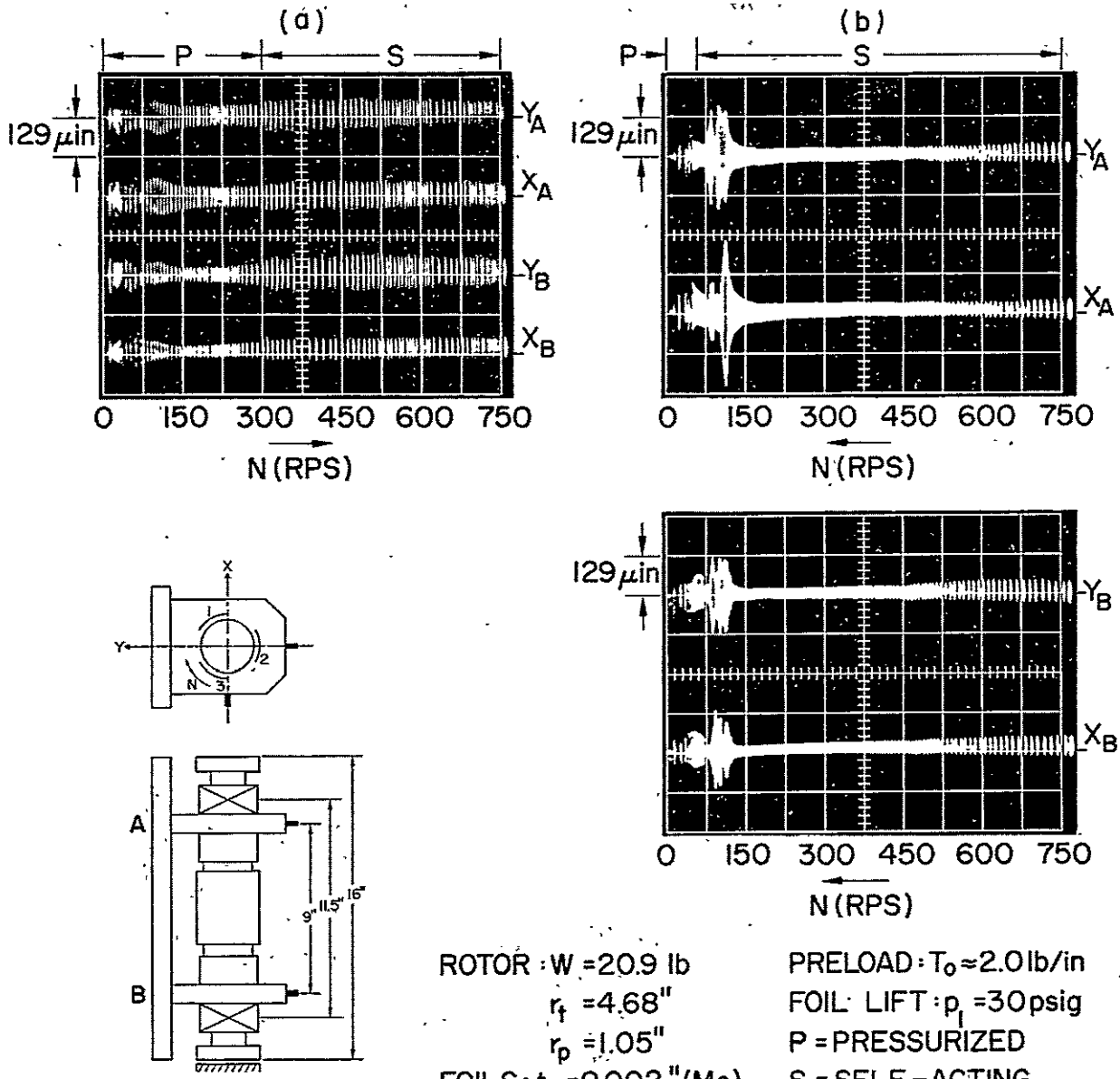

Fig. 14 Scans of Response in Single-Row Foil Bearings (Bearing Span = 11.5"; Journal Length = 1.5") - Increase of Foil Thickness and Preload

(a) Response to Remanent Imbalance, Increasing Speed
(b) Response to Remanent Imbalance, Decreasing Speed

It was considered that some discrepancies in gap measurements may have been due to the noncollinearity of the journal probe (Y_A) and the parallel foil probe, spaced 1.25" apart. The individual outputs of these probes are presented together with the differential outputs in Fig. 15. The reader will note that both the absolute and differential measurements gave the same values of clearance, within limits of experimental error. Comments on the unusual trend in the variation of gap width with speed in pressurized foil bearings are postponed till Section 3.6.

At this stage of the investigation, it appeared that little was to be gained with regard to bearing stiffness by increasing the foil thickness, at least not within the limits of preloads compatible with starting without the aid of external pressurization.

3.4 Operation with 2.0-inch Wide Foils at 9.0-inch Bearing Span, - Part I: Response to Excitation by Symmetric and Asymmetric Imbalance. Self-Acting Coastdown and Stop

The experiments described in the preceding section required no other changes from the 4-row configuration than the elimination of the inner rows of foils. All subsequent experiments, with the exception of those described in Section 3.9, were carried out with a new foil-support assembly, which accommodated 2.0" wide foils. The assembly had a 9.0" bearing span and contained the monitoring probes in planes 12.0" apart. Referring to Fig. 1, it will be noted that there were 8 rows of orifices in the rotor; 4 at each journal and 2 per each foil of the original, double-row bearing support. In order to use the existing rotors and fixed foil-lift orifices in conjunction with single-row foil bearings, the feasible alternatives were: (a) to place 1.5" wide foils at an 11.5" bearing span and overlap the rows 1, 2 and 7, 8, or (b) locate 2.0" wide foils at a 9.0" span and pressurize through orifice rows 2,3 and 6,7. The latter arrangement corresponded to the configuration illustrated in Fig. 2.

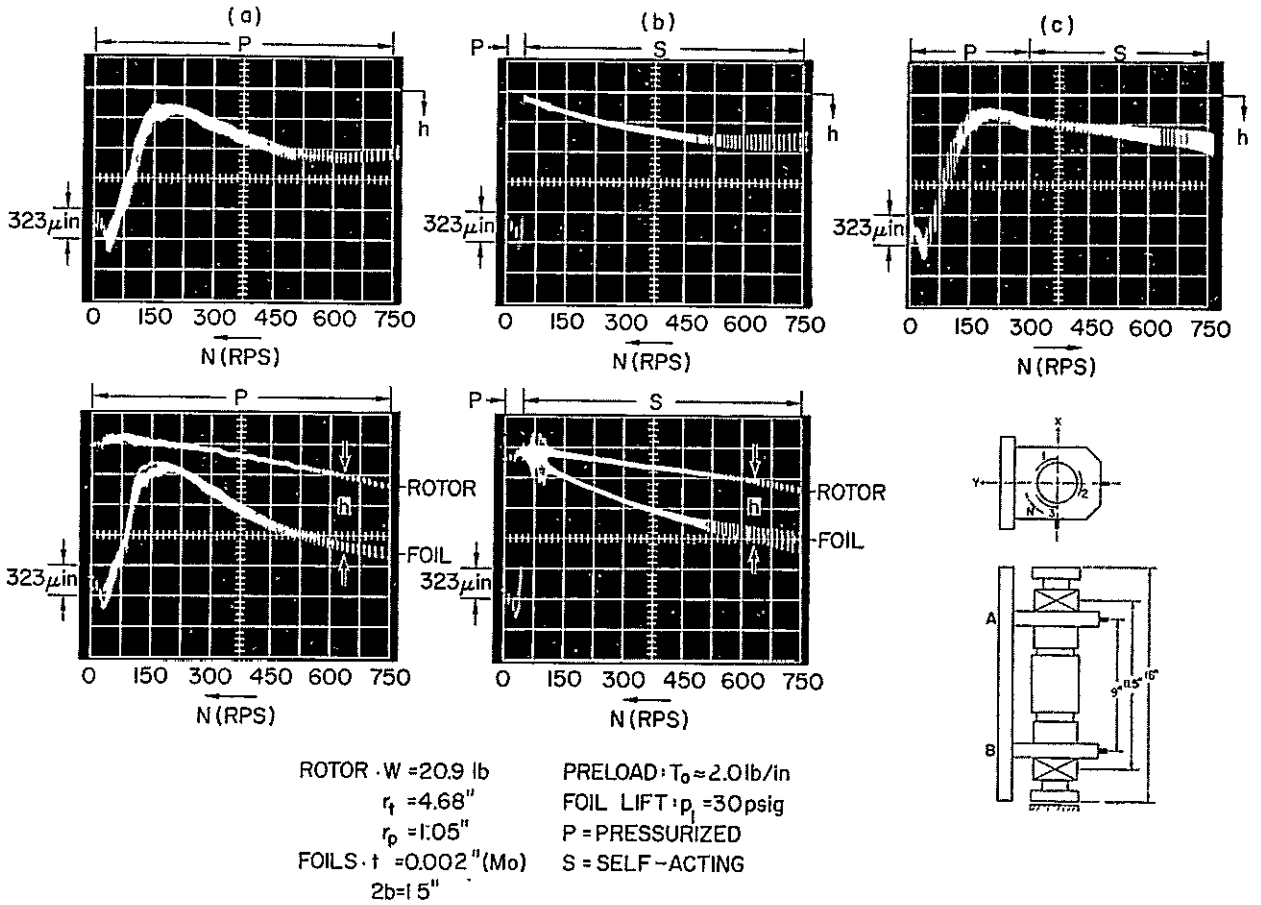

Fig. 15 Scans of Gap Width in Single-Row Foil Bearing (Foil Sector A_2; Bearing Span = 11.5"; Journal Length = 1.5") - Increase of Foil Thickness and Preload

(a) Gap Width, Pressurized Bearing and Decreasing Speed
(b) Gap Width, Self-Acting Bearing and Decreasing Speed to 75 RPS
(c) Gap Width, Pressurized Bearing and Increasing Speed

The data relevant to this section are presented in Fig. 16 through Fig. 26. The oscillograms in Fig. 16 and Fig. 17 pertain to the response of the rotor to remanent imbalance ($\bar{u} < 350\mu$in-oz). The resonant bandwidths in both the pressurized and in the self-acting modes overlapped in a relatively low speed range. In the pressurized mode, the motion was characterized by now familiar ultraharmonics, and the largest orbits in the self-acting mode, approximately 900 μinches peak-to-peak, occurred at 56 RPS, Fig. 16. A complex quasiconical motion prevailed in the region of resonances, while in the high-speed range, at 750 RPS, the motion was nearly cylindrical, Fig. 16(g) and Fig. 16(h).

Referring to Fig. 17, a remarkable aspect of the response was an apparent growth of amplitudes with speed to the right of the resonant bandwidth. Although the rotor was very rigid and the resonant frequency in the first bending mode well outside the operating speed range, the steady growth or orbits with speed, Fig. 17(e), as well as the "flaring out" of scans of amplitude and of gap width, Fig. 17(a) through Fig. 17(d), could, nevertheless, be attributed to bending of the rotor under the influence of centrifugal forces. Additional results substantiating this conclusion are presented in Section 3.5.

The scan of gap width in the pressurized mode in Fig. 17 is yet another example of the unusual variation of clearance with speed at the center of wrap. The scan of gap width in the self-acting mode was obtained during coastdown to a full stop without pressurization. Smooth rotation and gradual deceleration were maintained down to between 30 and 20 RPS, and stopping without the aid of external pressurization became henceforth standard practice. The reader may follow the position of the rotor axis in Fig. 17(e), starting with zero speed (0). The displacement from the reference position (P) in the pressurized bearings to the second reference position (C), when pressurization was discontinued and the preloaded foils contacted the journals, was in the order of 250 μinches. The

mean displacement in the A-plane at 750 RPS (from C to the center of the largest orbit) was approximately 800 μinches. The corresponding displacement in the B-plane was nearly 520 μinches. Both displacements were in the 3-rd quadrant, subtending angles 40° to 45° with the negative X-axis.

In all previous experiments with foil bearings of reduced length, excitation was provided mainly by a small amount of remanent imbalance. The tests described in the remaining part of this section were conducted with synchronous excitation furnished by 26,100 μin-oz of symmetric imbalance and 15,350 μ-in-oz of asymmetric imbalance, added in 2 planes 15.25" apart. The foil thickness and preload in these runs were identical with those maintained during runs with residual imbalance, Fig. 16 and Fig. 17. The results of runs with symmetric imbalance are contained in Fig. 18 through Fig. 21.

Comparing the largest orbits in the pressurized and in the self-acting modes in Fig. 18 and Fig. 19, it will be noted that maxima occurred at relatively low speeds, differing by less than 10%, and that the self-acting orbits were the largest by far (2380 μinches peak-to-peak). It would appear, therefore, that pressurization contributed appreciably to damping. The disparity between the orbits A and B in Fig. 19, and the fact that a sensibly symmetric imbalance excited motion in the pitching mode, reflected both the residual dissymetries and the coalescence of resonances in a narrow speed range.

With increasing speed, the rotor entered into a second zone of resonances, characterized by subharmonic motion. Typical orbits, recorded at speeds corresponding to local maxima of journal excursions, are illustrated in Fig. 20. In the first row of photographs, at 123 RPS, the large orbit at A can be retraced along the path of a distorted figure-8, starting at a point where Y is maximum and moving to the right. This path evolved with increasing speed from a triple-loop orbit, similar to that described by the rotor axis at B. The latter can be traced out in a clockwise

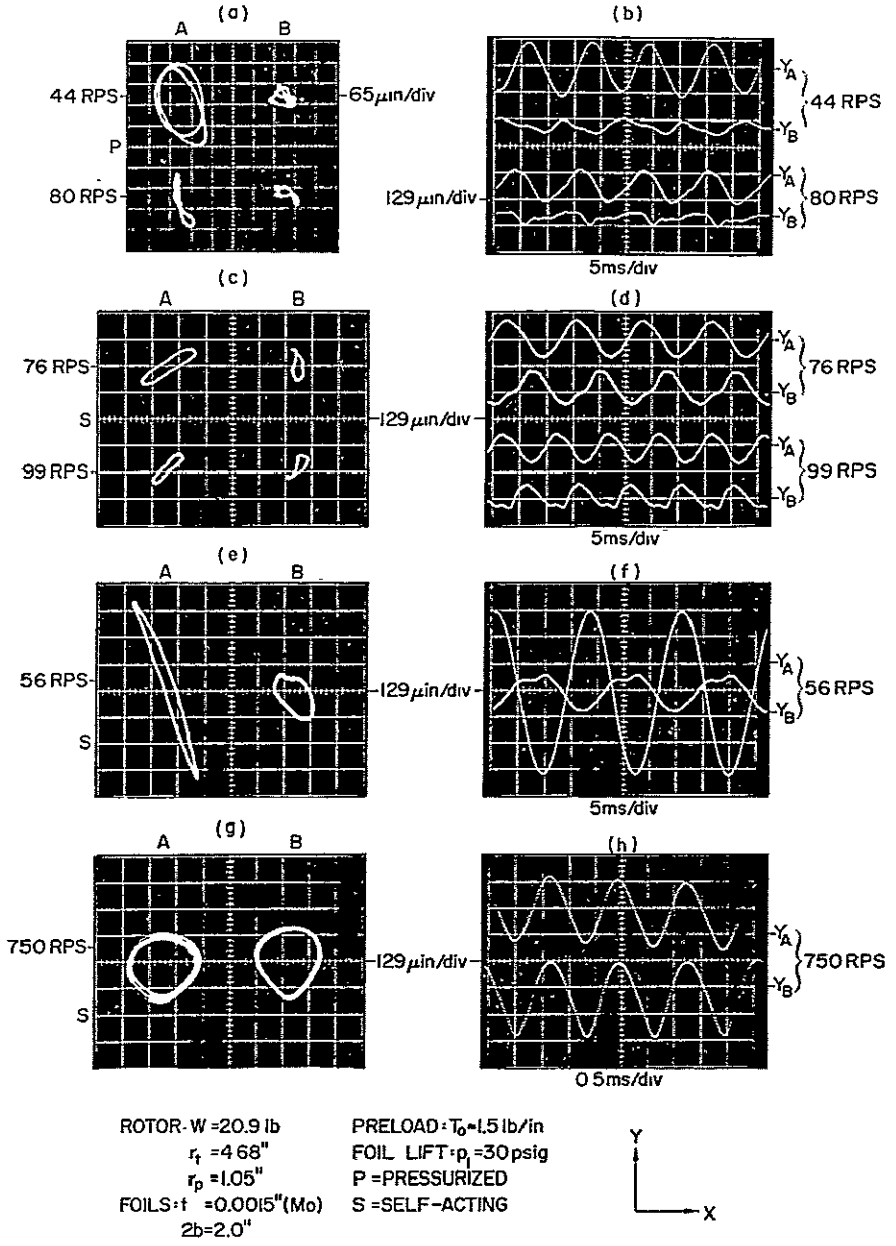

Fig. 16 Motion of Rotor in Foil Bearings at 9.0" Span and 2.0" Journal Length

(a) Orbits in Resonant Range, Pressurized Bearings
(b) Motion in Y-Plane in Resonant Range, Pressurized Bearings
(c), (e) Orbits in Resonant Range, Self-Acting Bearings
(d), (f) Motion in Y-Plane in Resonant Range, Self-Acting Bearings
(g) Orbits in Self-Acting Bearings at 750 RPS
(h) Motion in Y-Plane in Self-Acting Bearings at 750 RPS

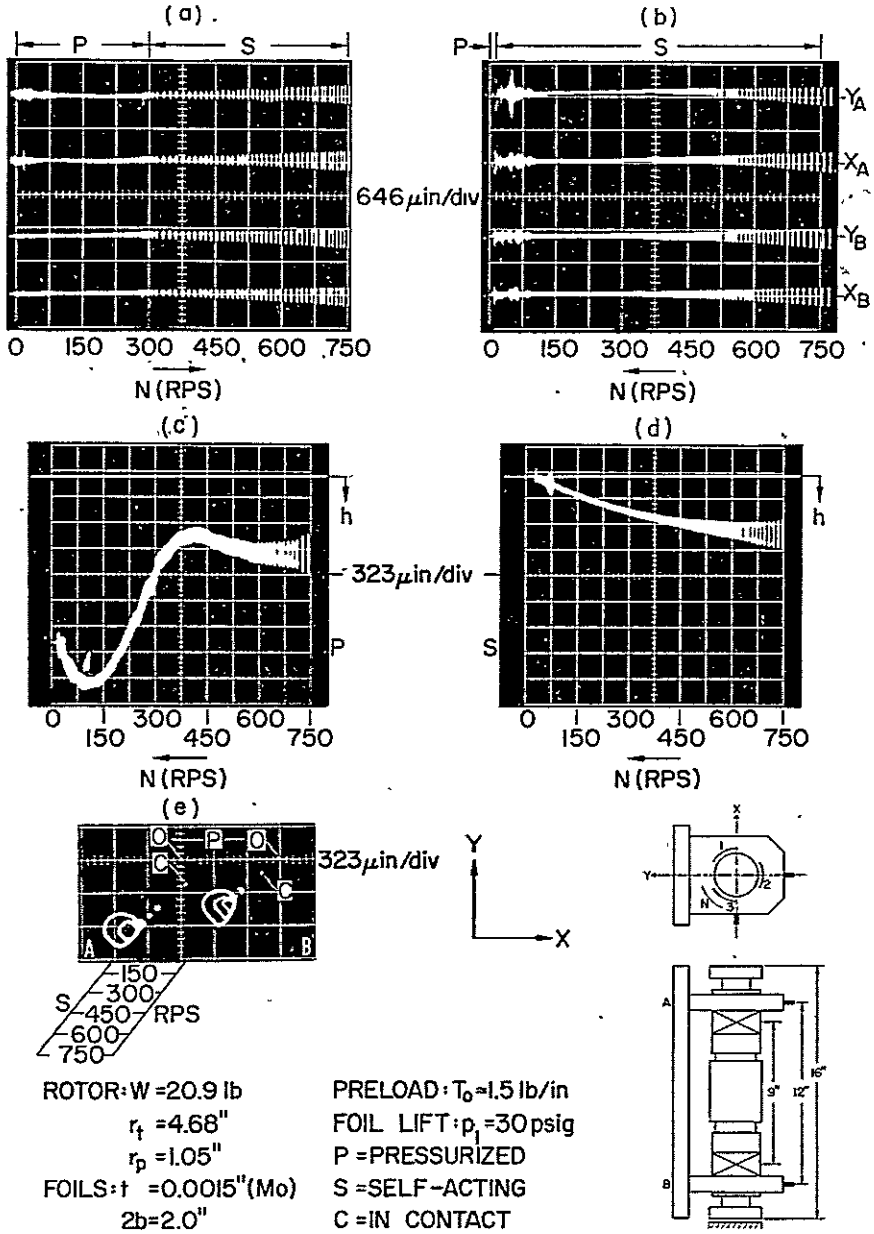

Fig. 17 Scans of Response and Gap Width (Foil Sector A_2). - Displacement of Rotor Axis (Bearing Span = 9"; Journal Length = 2.0")

(a), (b) Response to Remanent Imbalance (Acceleration and Coastdown)

(c) Gap Width, Coastdown in Pressurized Bearings

(d) Gap Width, Coastdown in Self-Acting Bearings

(e) Displacement of Rotor Axis with Speed

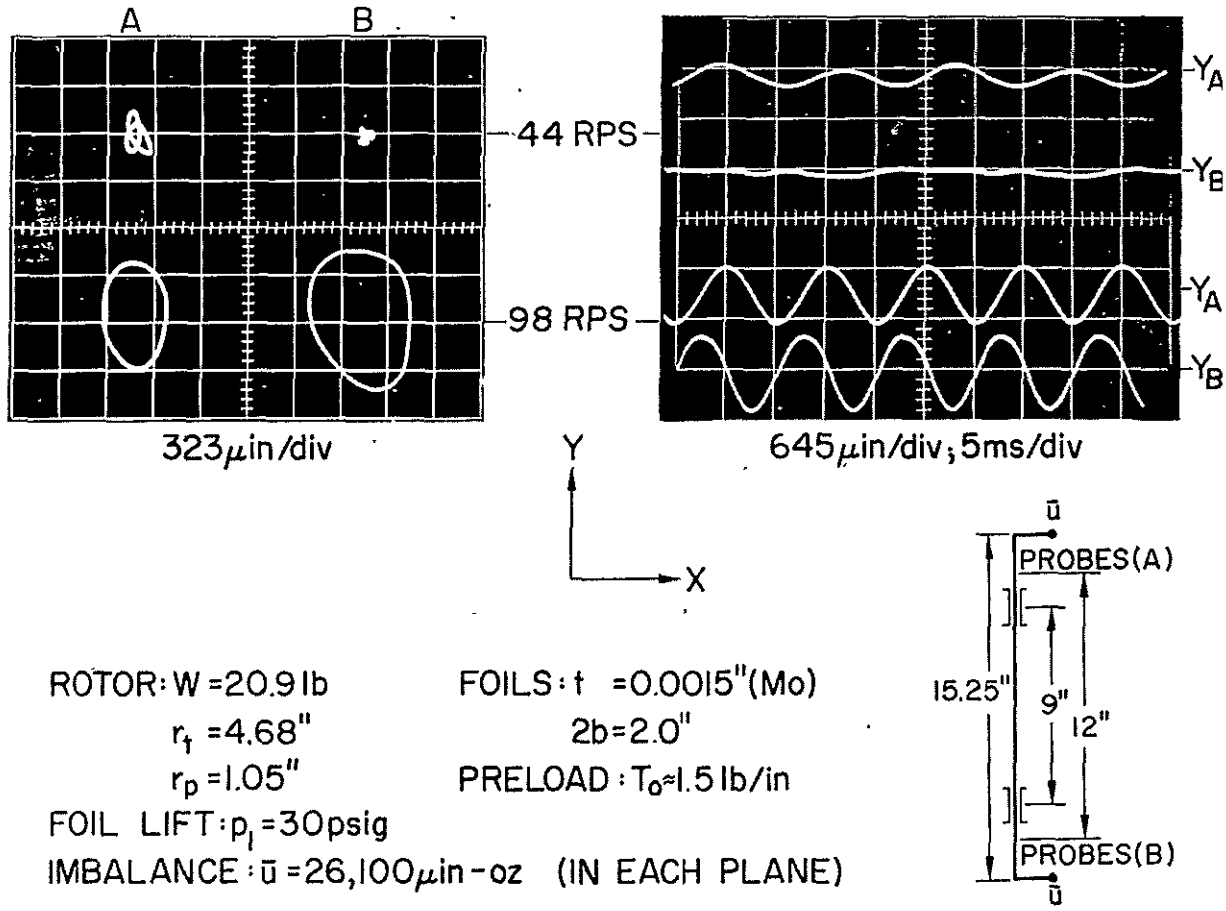

Fig. 18 Motion of Rotor with Symmetric Imbalance in Pressurized Foil Bearings in Resonant Range (Bearing Span = 9.0"; Journal Length = 2.0")

sense, which is apparent from the corresponding time-base display of Y_B at 123 RPS. From the time-base oscillograms in the second column of Fig. 20 and the appended values of rotational speeds, it is clear that each orbit was described in 2 revolutions of the rotor about its axis.* The rather striking appearance of multiple orbits at 155 RPS was due to a low-frequency amplitude modulation. The orientation of the loops remained essentially unchanged and the successive states of orbit growth were obtained during an exposure time of 0.1 seconds. A number of oscilloscope photographs of this type, and of associated time-base displays recorded at very low sweep rates, are presented in the latter part of this chapter.

The orbits and time-base traces of motion in the Y-plane in Fig. 19 and Fig. 20 are complemented by the frequency scans of amplitude response in Fig. 21(c). The amplitude peaks in the bandwidth of approximately 60 to 90 RPS correspond to the synchronous motion illustrated in Fig. 19, and those in the bandwidth of approximately 115 to 185 RPS represent maximum excursions of subharmonic resonances shown in Fig. 20. The reader may also note that the scans of amplitude reflect the occurrence of "jump" phenomena, which are frequently encountered in systems characterized by spring rates that increase or decrease with displacement [19, 20, 21]. The amplitude Y_B, for example, displayed a very abrupt increase at 180 RPS during coastdown. At high-speed, the motion with symmetric imbalance was nearly cylindrical, as indicated by the oscillograms in the upper row of photographs in Fig. 21.

The addition of a large amount of symmetric imbalance in one single step was risky because of the lack of operational experience with foil bearings of reduced length. The asymmetric imbalance involved addi-

*The subharmonic resonance of order one half should not be confused with a type of instability of rotors supported in fluid film bearing, loosely referred to in literature as "half-frequency whirl", or "fractional-frequency whirl" [21].

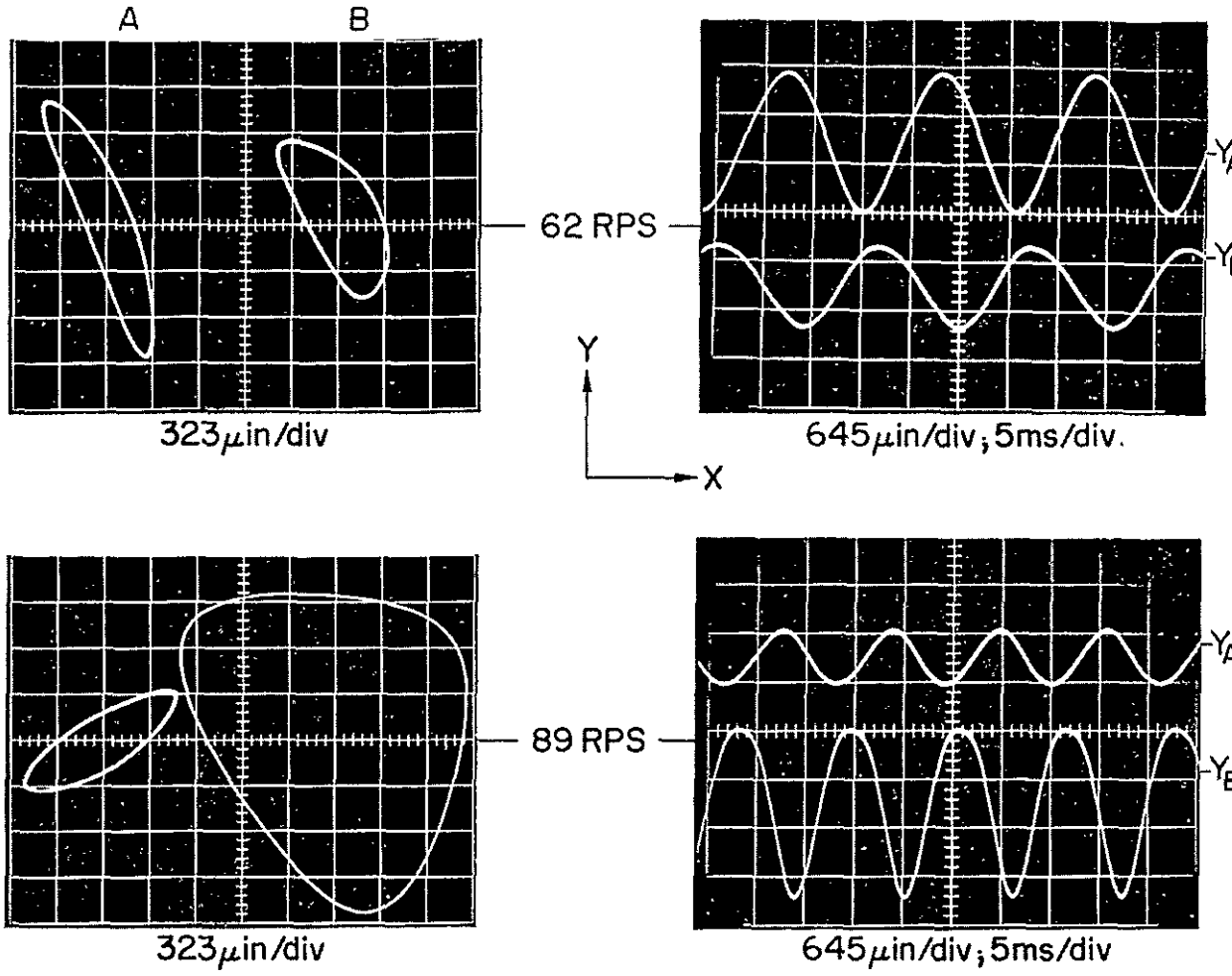

ROTOR: W=20.9 lb
r_f =4.68"
r_p =1.05"
IMBALANCE: $\bar{u}$ =26,100μin-oz (IN EACH PLANE)

FOILS: t =0.0015"(Mo)
2b=2.0"
PRELOAD: T_o≈1.5 lb/in

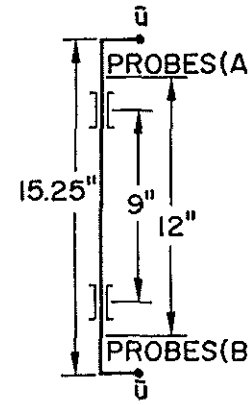

Fig. 19 Motion of Rotor with Symmetric Imbalance in Self-Acting Foil Bearings in Resonant Range (Bearing Span = 9.0"; Journal Length = 2.0")

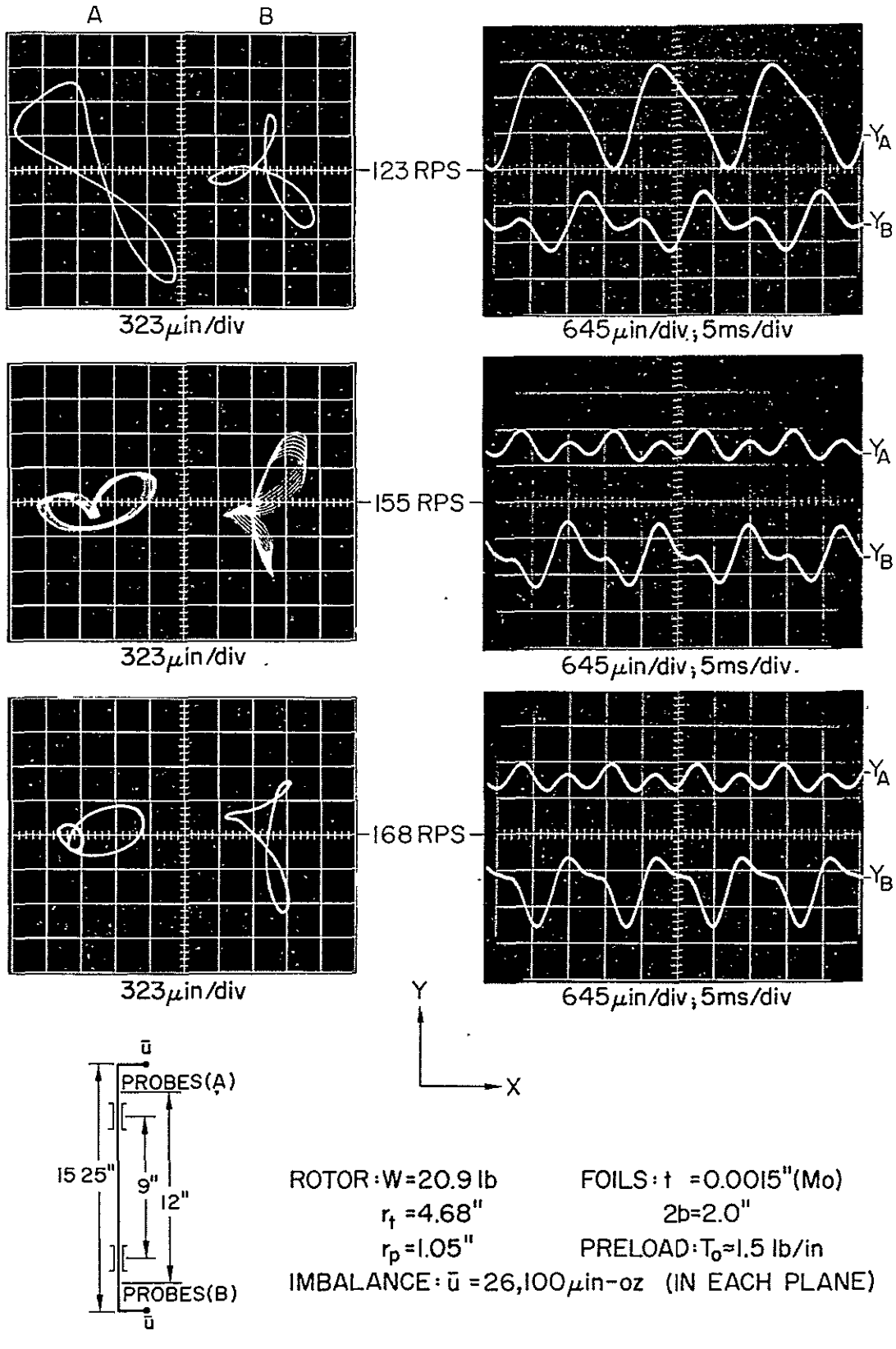

ROTOR: W = 20.9 lb FOILS: t = 0.0015" (Mo)

r_t = 4.68" 2b = 2.0"

r_p = 1.05" PRELOAD: T_o = 1.5 lb/in

IMBALANCE: ū = 26,100 μin-oz (IN EACH PLANE)

Fig. 20 Subharmonic Motion and Resonance of Rotor with Symmetric Imbalance in Self-Acting Foil Bearing (Bearing Span = 9.0"; Journal Length = 2.0")

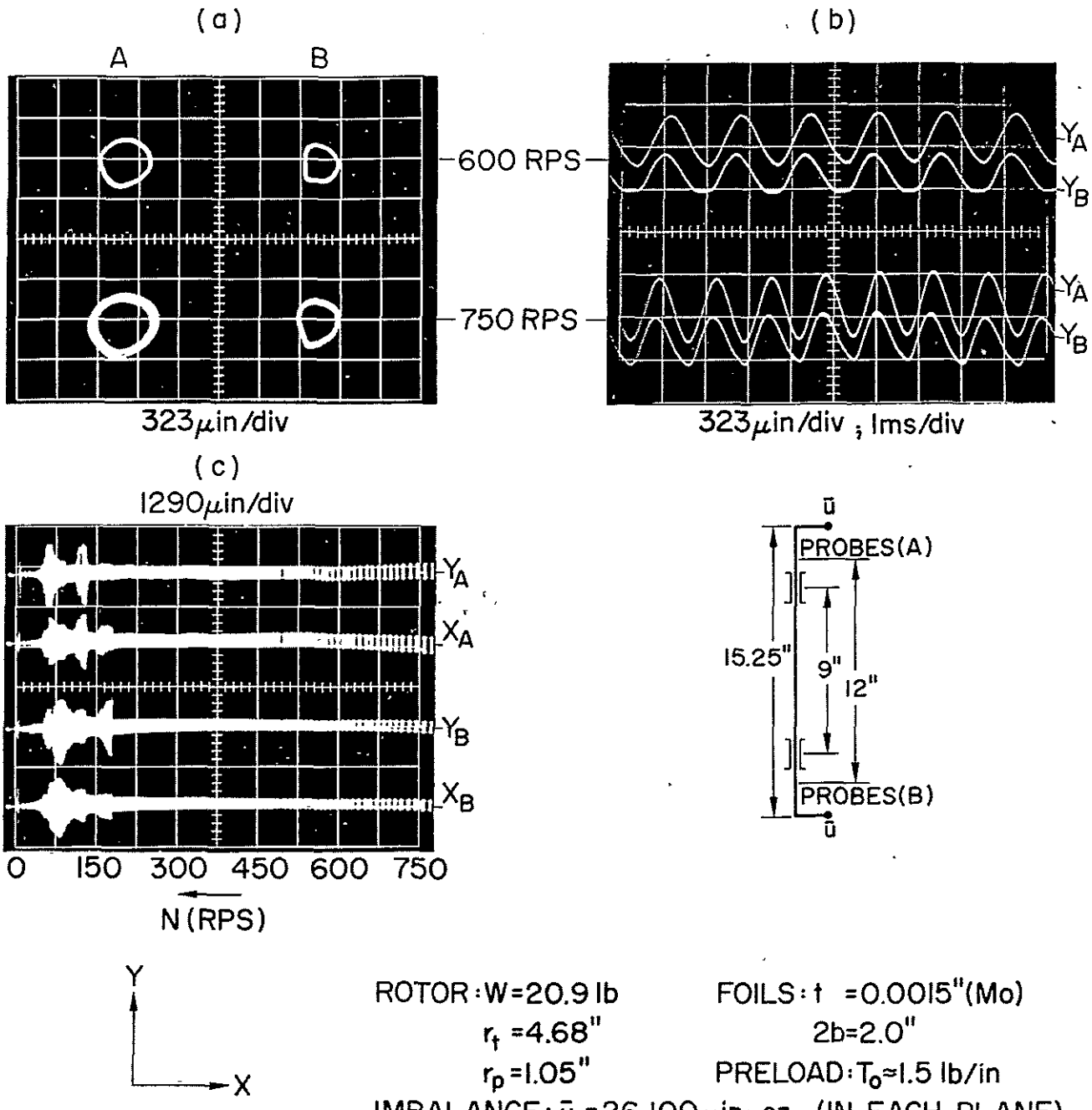

Fig. 21 Motion of Rotor with Symmetric Imbalance in Self-Acting Foil Bearings and Scans of Response (Bearing Span = 9.0"; Journal Length = 2.0")

(a), (b) Orbits and Motion in Y-Plane at 600 and 750 RPS
(c) Scans of Response

tional hazards, especially the increased danger of wiping, or impacting the thrust bearing during resonance in the pitching mode.* With a tolerable magnitude of symmetric imbalance established, the magnitude of allowable asymmetric imbalance was estimated by assuming the system to be linear, symmetric and uncoupled. The motion could thus be characterized by 2 resonances, one in the cylindrical and the other in the conical mode. Constraining the permissible excitation by requiring the resonant amplitudes at the bearings to be equal for both modes of motion, and assuming the damping coefficients to be equal in both cases, the relation between the asymmetric ($\bar{u}_a$) and symmetric ($\bar{u}_s$) imbalances is:

$$\bar{u}_a \approx \bar{u}_s \ (2\, r_t/L)$$

with r_t the transverse radius of gyration of the rotor, and L the distance between planes of imbalance.** The amount of asymmetric imbalance added was based on the foregoing relation and the maximum amplitudes recorded with both types of imbalance were commensurate.

The results of runs with asymmetric imbalance are presented in Fig. 22 through Fig. 25. The resonant orbits in the pressurized mode, Fig. 22, were again smaller than in the self-acting mode of operation, Fig. 23. In both modes, resonances occurred in nearly coincident bandwidths. Since the mean thickness of the self-acting film was much smaller than that of the pressurized film, vibration produced quantitatively varying

*Closure of the operating gap (0.0012") at the edge of the lower thrust plate (1.5" rad.) corresponded to a 0.0036" pitching amplitude at the journal bearings (0.0072" peak-to-peak).

**Gyroscopic effects were neglected in this estimate since all resonances occurred at relatively low speeds.

effects. In the self-acting film, apart from the average throughflow, the air is trapped locally and there is little additional flow in the lateral directions. This increases the stiffness, but adds little to damping. In the thicker, pressurized film, the air is partly trapped and partly squeezed out from the region of wrap. The latter effect is dissipative and enhances damping. The additional damping was considered to be responsible for limiting the resonant amplitudes in the pressurized mode of operation. The largest peak-to-peak excursions in the bandwidth of synchronous resonances, Fig. 23, were in the order of 3880 μinches at 64 RPS, with the rotor axis pitching along narrow, crescent-like loci. The second and third rows of photographs in Fig. 23 correspond to other local maxima in the resonant range. With the sense of rotation known (clockwise, looking from A to B), two types of oscillograms, as in Fig. 23 for example, are sufficient to reconstruct the surface traced out by the rotor axis in space. The reader may note the progress in phase difference between A and B with variation of speed in Fig. 23.

The asymmetric imbalance excited also subharmonic resonances, very approximately at twice the speed of synchronous resonances. The orbits, which with variation in speed transformed from clover-leafed shapes to distorted, or folded figure-8 forms, are shown in the left column of Fig. 24. The corresponding time-base traces are illustrated in the right column of the same figure. Each orbit was described in 2 revolutions of the rotor about its axis, and the time-base oscillograms displayed generally a series of major and minor maxima and minima in the Y-plane.* Similar remarks apply to motion with symmetric imbalance, Fig. 20. It is of

*The choice of the Y-plane, as one of the possible reference planes normal to the monitoring planes, was arbitrary. The major and minor stationary points may be indistinguishable, or degenerate to inflection points, depending on the direction of the reference plane.

interest to note the relationship between the excursions Y_A and Y_B. In the case of symmetric imbalance, Fig. 20, the correspondence at 155 RPS is approximately as follows:

Y_A	MAX	MIN	max	min
Y_B	max	MIN	MAX	min

while in the case of asymmetric imbalance, Fig. 24, the sequence at 152 RPS is:

Y_A	MAX	MIN	max	min
Y_B	min	MAX	MIN	max

in which majors are capitalized, and minors appear in lower case letters.

The orbits at 152 RPS in Fig. 24, and those at 150 RPS in Fig. 25, were excited by asymmetric imbalance and were similar to the subharmonic motion with symmetric imbalance at 155 RPS , Fig. 20. The amplitude of motion was modulated by a low frequency beat (approximately 2.15 CPS, in Fig. 25), with the orientation of the "pulsating" orbits remaining sensibly unchanged. The oscillograms in Fig. 25 give the illusion of 2 superimposed traces. In reality, the slow sweep rate produced an oscillogram, in which the lighter shading of the central section was due to twice the density of nearly vertical lines present in the outer zones of the trace. The time-varying limits of both major and minor excursions are clearly discernible in the Y_B - trace.

Motion with asymmetric imbalance in the high-speed range is illustrated in Fig. 26(a) and Fig. 26(b). The amplitude scans in Fig. 26(c)

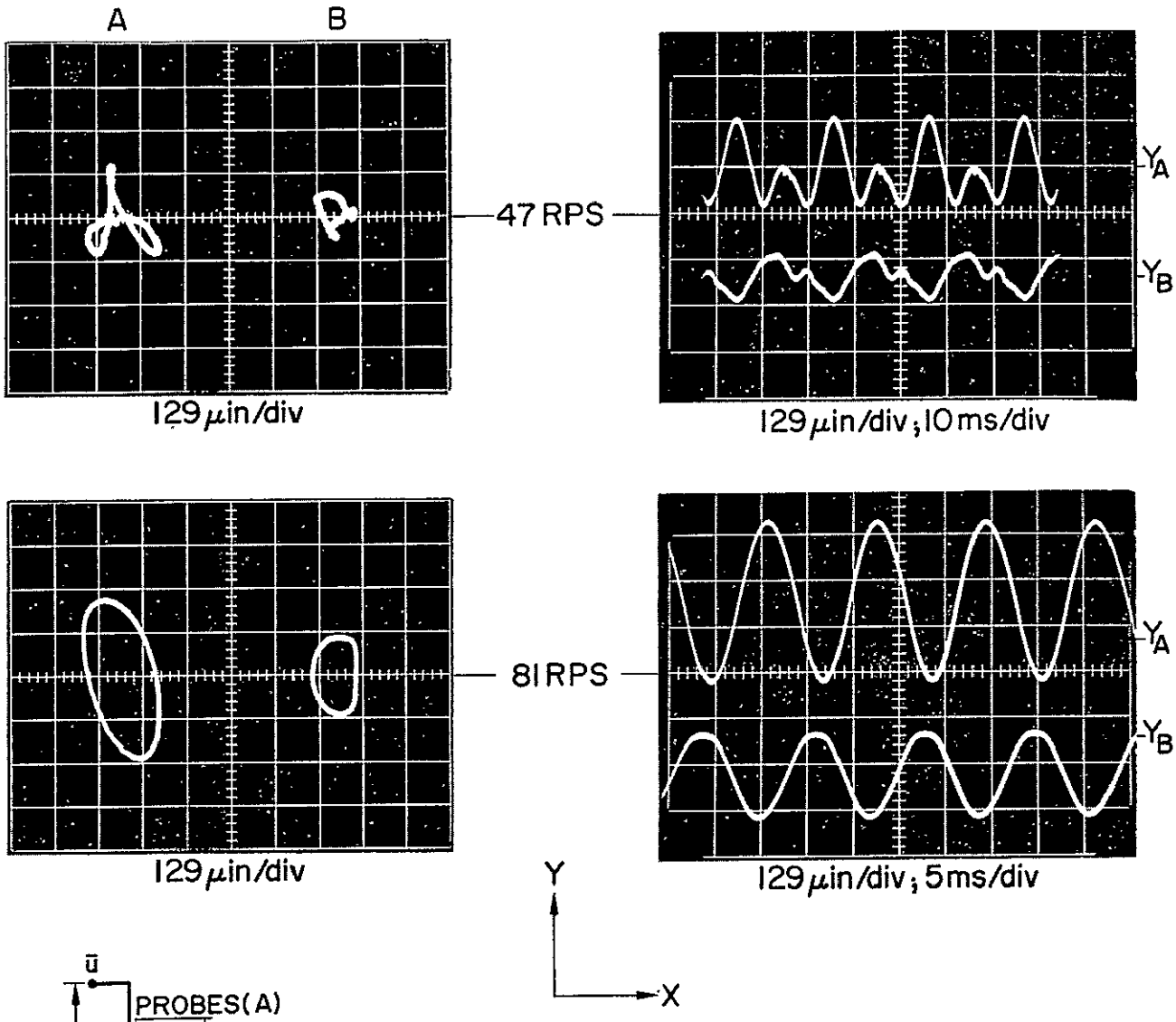

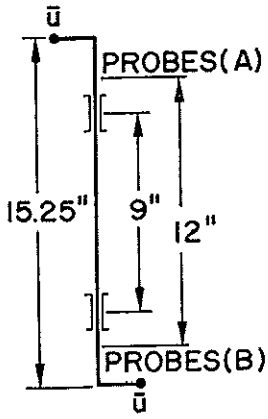

ROTOR: W = 20.9 lb
r_t = 4.68"
r_p = 1.05"
FOIL LIFT: p_l = 30 psig
IMBALANCE: ū = 15,350 μin-oz (IN EACH PLANE)

FOILS: t = 0.0015" (Mo)
2b = 2.0"
PRELOAD: T_o ≈ 1.5 lb/in

Fig. 22 Motion of Rotor with Asymmetric Imbalance in Pressurized Foil Bearings in Resonant Range (Bearing Span = 9.0"; Journal Length = 2.0")

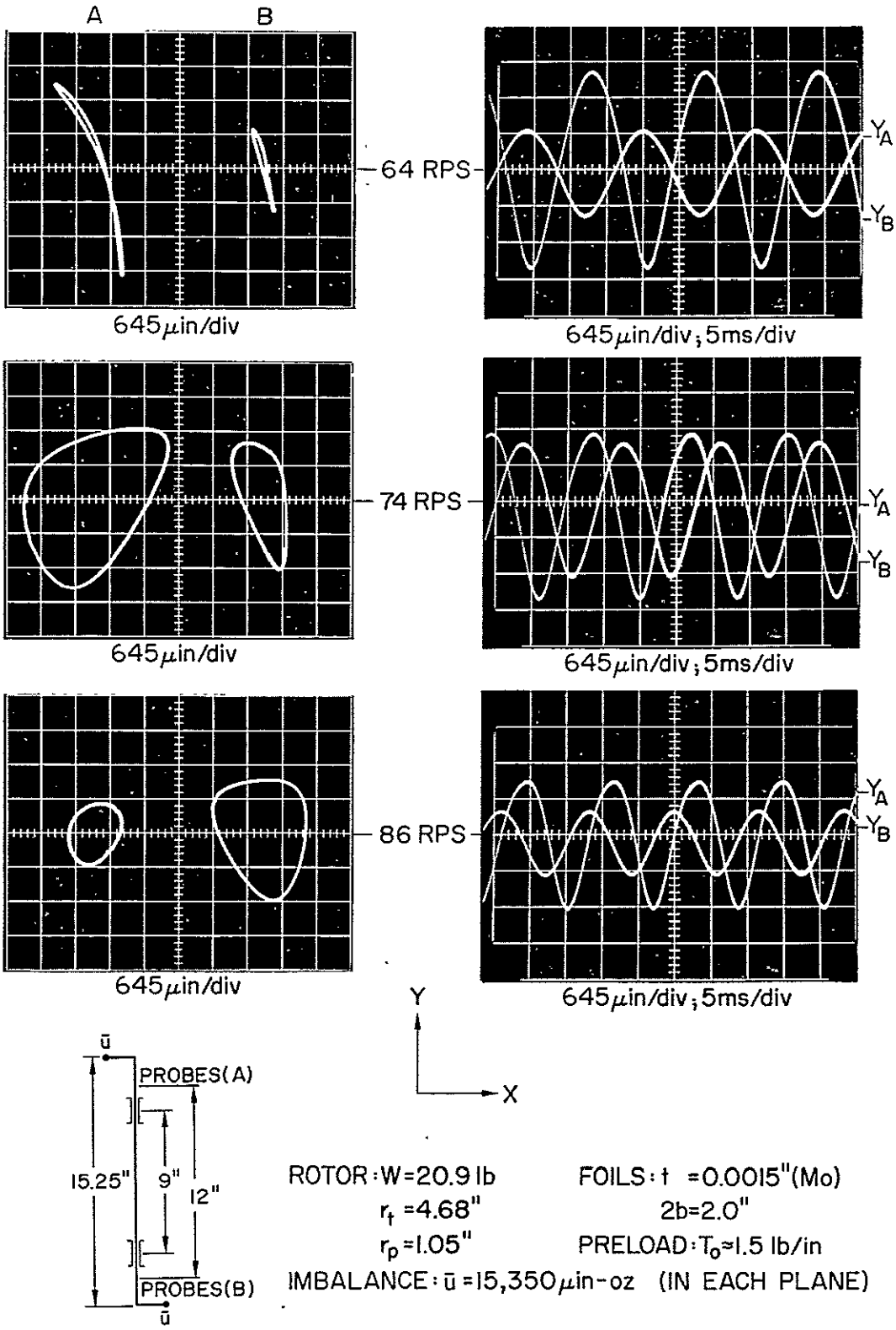

ROTOR: W=20.9 lb FOILS: t =0.0015"(Mo)
r_t =4.68" 2b=2.0"
r_p =1.05" PRELOAD: T_o≈1.5 lb/in
IMBALANCE: ū =15,350μin-oz (IN EACH PLANE)

Fig. 23 Motion of Rotor with Asymmetric Imbalance in Self-Acting Foil Bearings in Resonant Range (Bearing Span = 9"; Journal Length = 2.0")

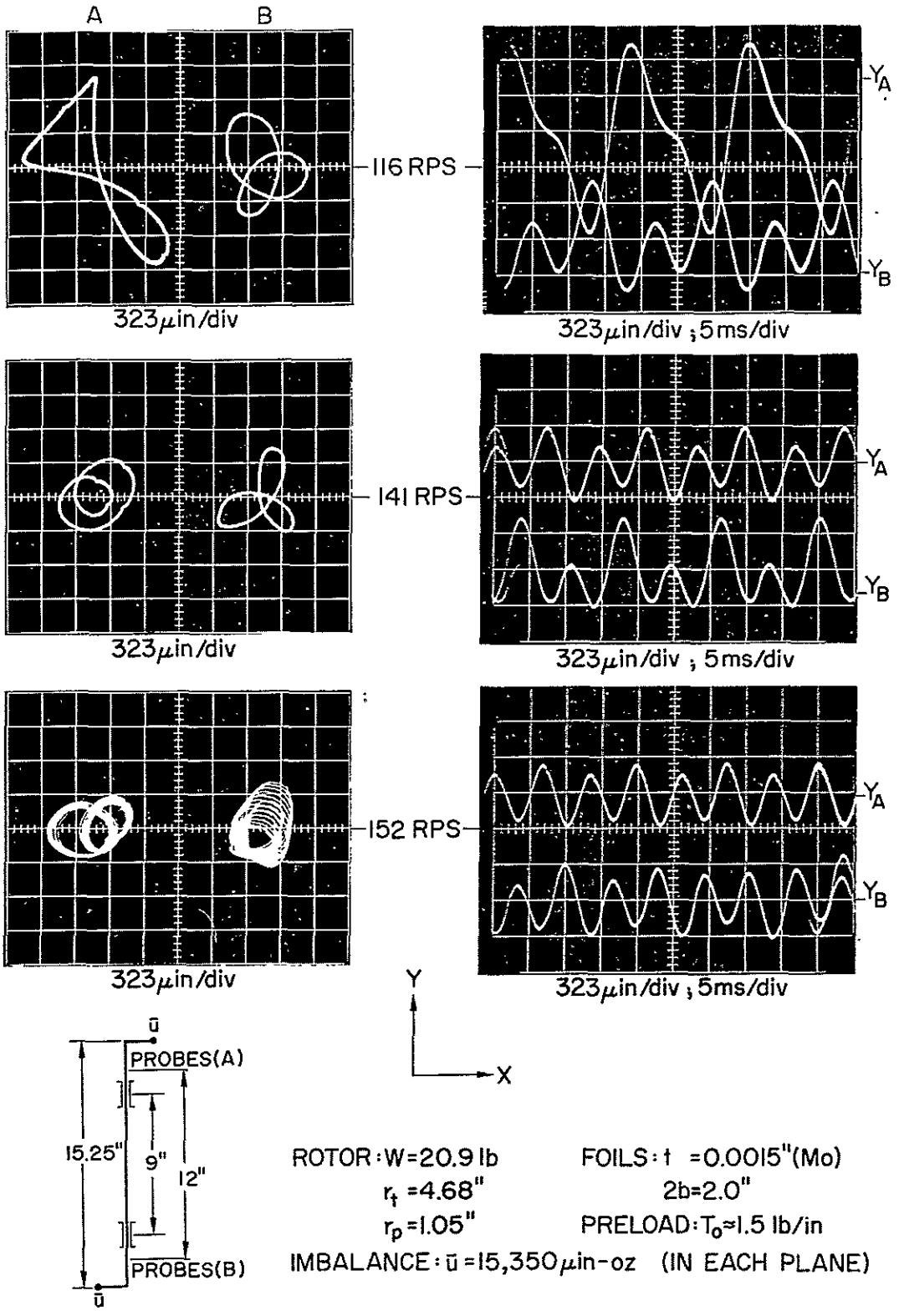

Fig. 24 Subharmonic Motion and Resonance of Rotor with Asymmetric Imbalance in Self-Acting Foil Bearings (Bearing Span = 9.0"; Journal Length = 2.0")

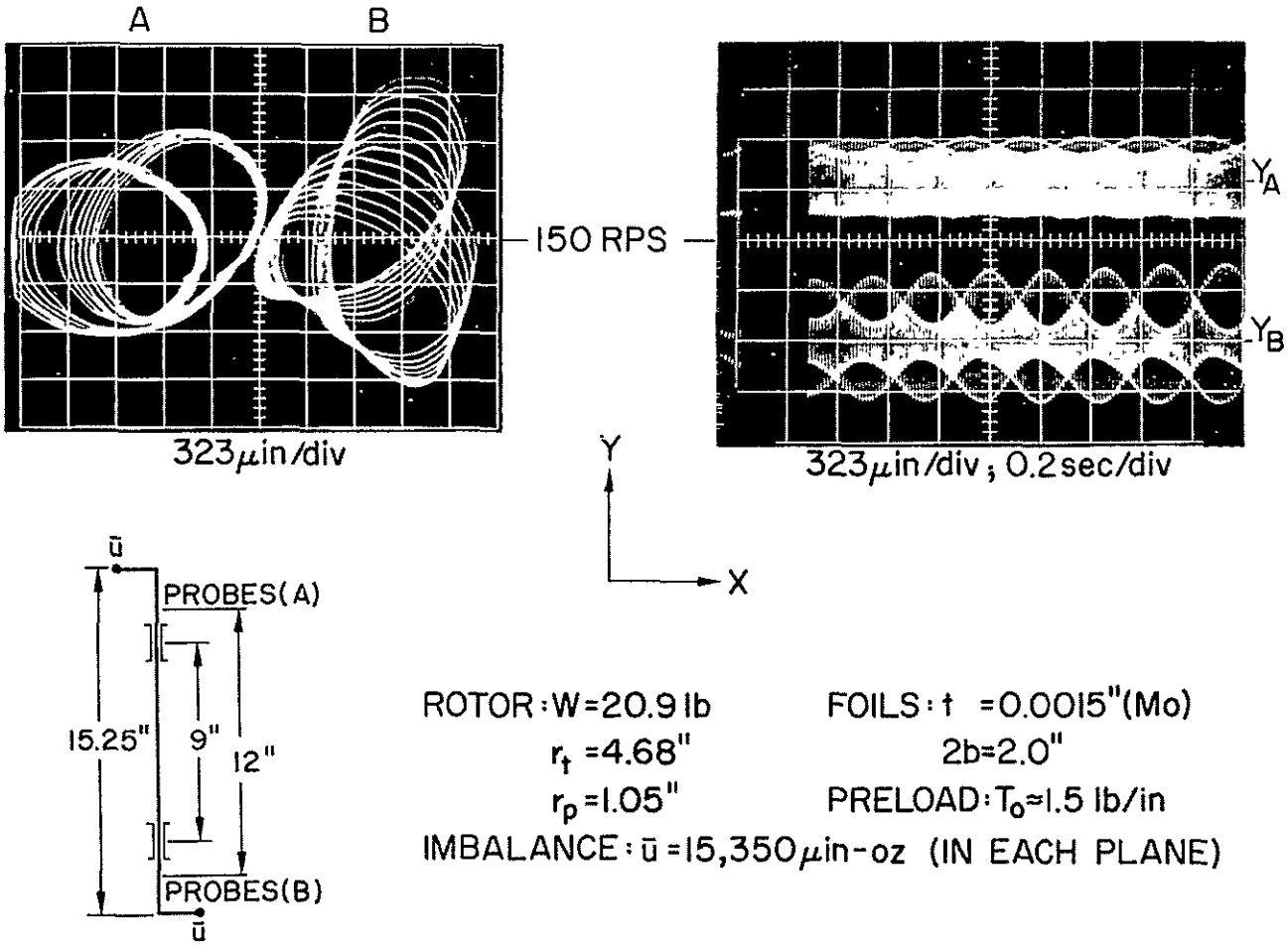

Fig. 25 Subharmonic Motion and Resonance of Rotor with Asymmetric Imbalance in Self-Acting Foil Bearings. Low-Frequency Beats (Bearing Span = 9.0"; Journal Length = 2.0")

and Fig. 26(d) contain the maxima of synchronous resonances in the bandwidth 60-80 RPS, and the subharmonic maxima in the bandwidth 110-155 RPS. The stepped appearance of the amplitude scans in Fig. 26 is due to sampling of speed over discrete time intervals. In addition, one may observe larger discontinuities in amplitude, for example X_A at 68 RPS, Y_A at 120 RPS, or Y_B at 72 RPS. These correspond to "jumps", or amplitude instabilities of nonlinear systems.

3.5 Operation with 2.0-inch Wide Foils at 9.0-inch Bearing Span, -Part II: Effect of Foil Thickness and Preload Tension. Bending of Rotor at High Speeds. Further Experiments with Symmetric and Asymmetric Imbalance

In an idealized configuration and with perfectly flexible foils, both the preload T_o and the extensional rigidity Et tend to increase the foil-bearing stiffness. Since reduction of preload would facilitate starting, an increase in foil thickness was considered as a logical method of compensation for the reduction of foil width. Unfortunately, however, an increase of foil thickness was accompanied by an increase of flexural rigidity ($D \sim t^3$), which appeared to have a detrimental effect on the performance of the system. While a comprehensive discussion of the adverse influence of flexural rigidity is postponed till Chapter 4, the results presented in Fig. 27 point to the necessity of increasing the preload in parallel with foil thickness. Shown in Fig. 27 are high-speed orbits of a rotor supported by relatively thick foils (0.002") at 3 levels of preload tension. The first photograph shows an unstable orbit at N = 690 RPS, at which speed the turbine air was cut off and the rotor allowed to coast down. Although the maximum dimension of the orbit envelope at 690 RPS did not exceed 650 μinches and exhibited no catastrophic rate of growth, rotation under marginal conditions was not considered a satisfactory solution. Referring now for comparison to Fig. 17 and Fig. 21, the reader

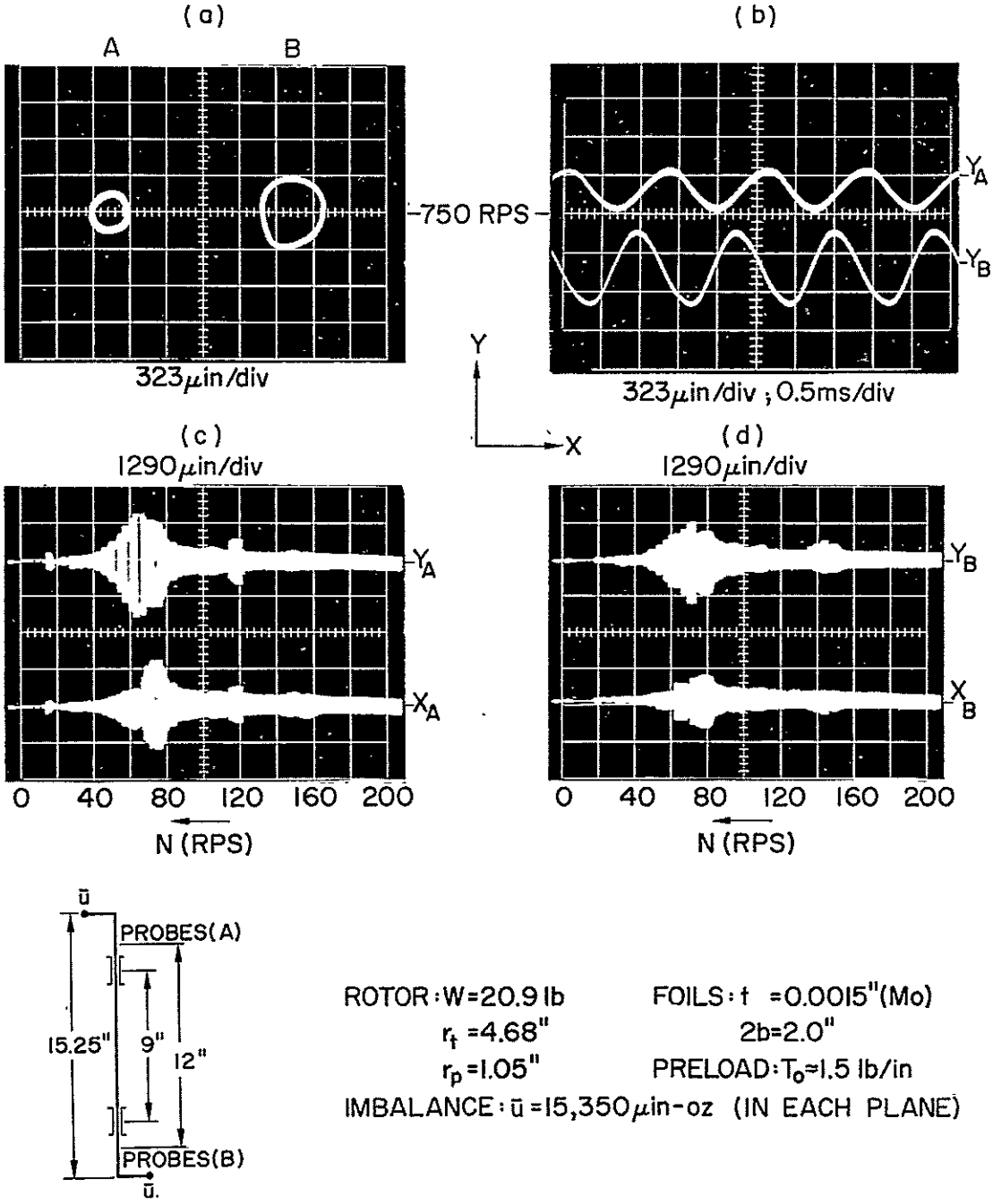

Fig. 26 Motion of Rotor with Asymmetric Imbalance in Self-Acting Foil Bearings and Scans of Response (Bearing Span = 9.0") Journal Length = 2.0")

(a), (b) Orbits and Motion in Y-Plane at 750 RPS
(c), (d) Scans of Response

may note that no difficulty has been experienced with 0.0015" thick foils when operating at the preload of 1.5 lb/in. Returning now to the second and third photographs in Fig. 27, it will be noted that consecutive increases of preload, from 1.5 lb/in to approximately 1.875 lb/in, and then to 2.25 lb/in, had a salutary effect on high-speed operation. The slow whirling was progressively suppressed with increasing preload tension.

The high-speed orbits illustrated in various figures of the preceding sections were always larger than the orbits in the low-speed range, with the exception possibly of excursions in regions of resonances. This growth with speed was apparent in the amplitude scans, and also in the scans of gap width. It was suspected that the cause of the apparent amplitude growth was the bending of the rotor under the influence of centrifugal forces caused by internal dissymmetries. To show this, a third probe Y_C was placed between and in line with the probes Y_A and Y_B. The time-base outputs of these probes at various rotational speeds are shown in Fig. 28, together with a schematic diagram indicating the location of probes relative to the bearings. Starting with the oscillogram corresponding to 750 RPS, it can be seen that excursions at Y_A and Y_B were approximately equal and in the same direction, and that a larger excursion in the opposite direction was recorded at Y_C. A similar relation persisted down to 300 RPS, except that at lower speeds harmonic components were superposed on the synchronous motion. Bending, however, became progressively less significant. The high-speed traces indicate that the rotor axis was bent in a plane and described a nearly symmetrical surface of revolution, with nodal points spaced approximately 9.0" apart.

The effect of bending was also reflected in the measurements of gap width determined by subtracting the output voltages of two parallel probes, one facing the foil at the center of wrap, the other monitoring the journal excursion just outside the foil edge. When a nodal point was close to the bearing midplane, the foil excursion was very small in

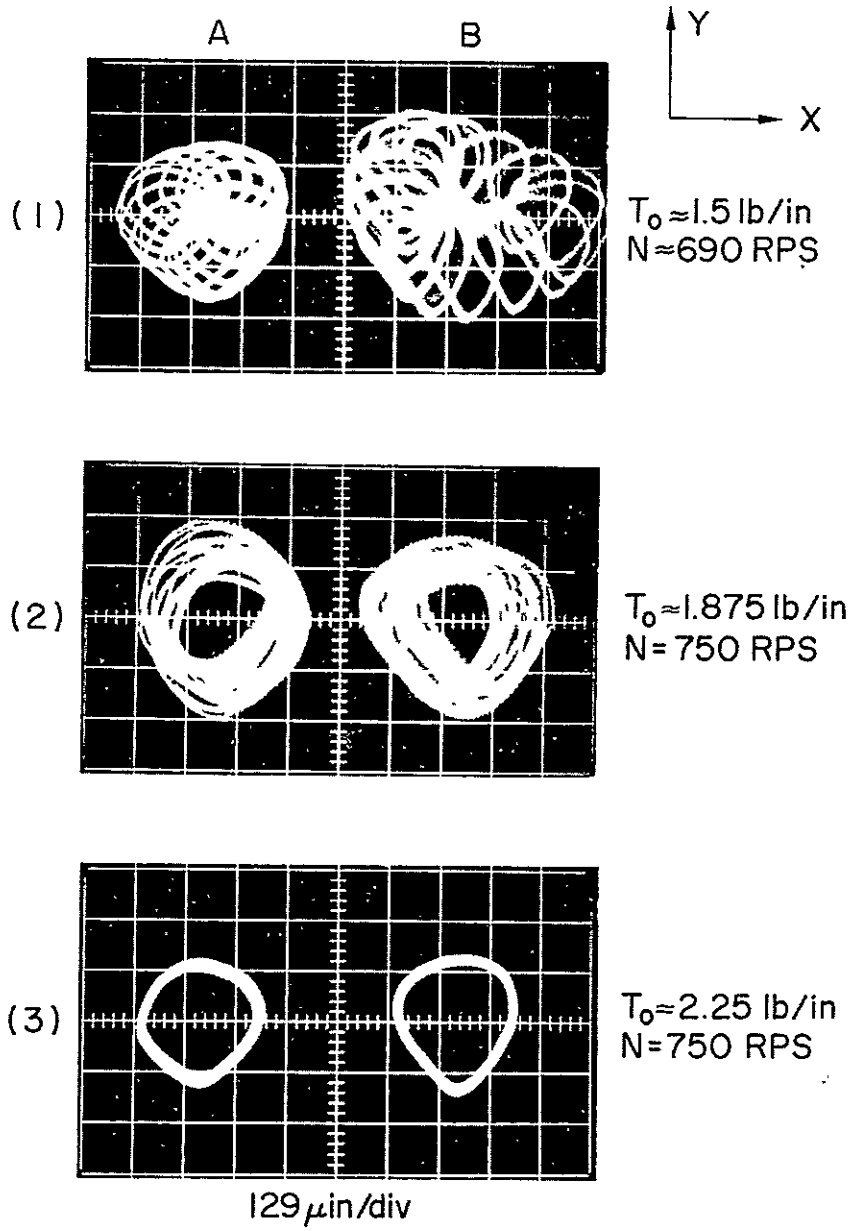

Fig. 27 Comparison of High-Speed Orbits in Self-Acting Mode in a Relatively Inflexible Foil-Bearing at Various Preload Tensions (Bearing Span = 9.0"; Journal Length = 2.0")

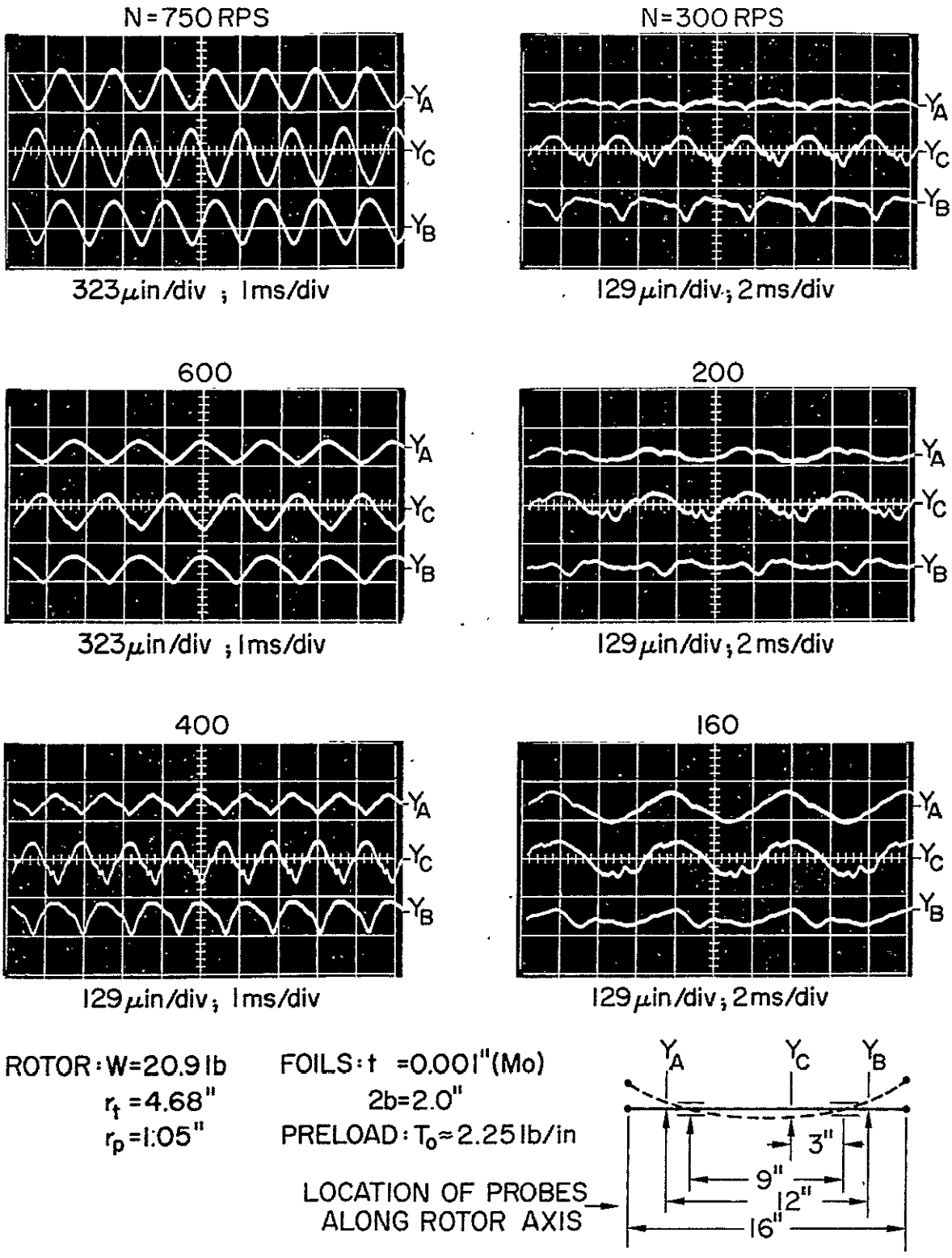

Fig. 28 Bending of Rotor due to Centrifugal Forces (Bearing Span = 9.0"; Journal Length = 2.0")

comparison with the motion of the journal. Conversely, with the journal probe in the vicinity of a nodal point, the motion of the foil was large in comparison. Whichever the case, either motion modulated the differential output and manifested itself as an apparent increase of "noise" with speed . Hence the "flared out" appearance of traces, characteristic of most scans of gap width in the high-speed range. The foregoing inferences are substantiated by the oscillograms presented in Fig. 29. The upper photograph at N = 750 RPS corresponds to a configuration, in which a nodal point was nearly coincident with the journal probe Y_A. In the two lower photographs of Fig. 29, at 600 RPS and 750 RPS, the nodal point was very close to the bearing center, as evidenced by the flatness of the traces A_2. It may be inferred, therefore, that the nodal span was approximately 9.0", regardless of bearing span. This also shows that at high speeds the motion was not affected by the position of the bearings, since the latter were very compliant in comparison with the rotor. The motion of the rotor could thus be considered as very close to a "free-free" vibration.

The natural frequency of such "free-free" vibrations was determined for rotors No. 1 and No. 2. The first rotor was of multicomponent construction, while the second was virtually monolithic. Both rotors were mounted in identical foil bearings and impacted in the midplane normal to the axis. The monolithic rotor was more rigid, as indicated by the frequencies of "free-free" vibrations superposed on the rapidly decaying traces of the main excursion of the body, Fig. 30.

Since the tests involving the determination of adequate preloads for 0.002" thick foils showed that 2.25 lb/in was quite sufficient, operational data were obtained for this combination of parameters. Results are presented in Fig. 31, and it appears that no significant shift of resonant speeds was precipitated through simultaneous increases of thickness and of preload. The resonant bandwidth in the self-acting mode was approximately 80 to 100 RPS, and the motion at resonance was quasi-conical.

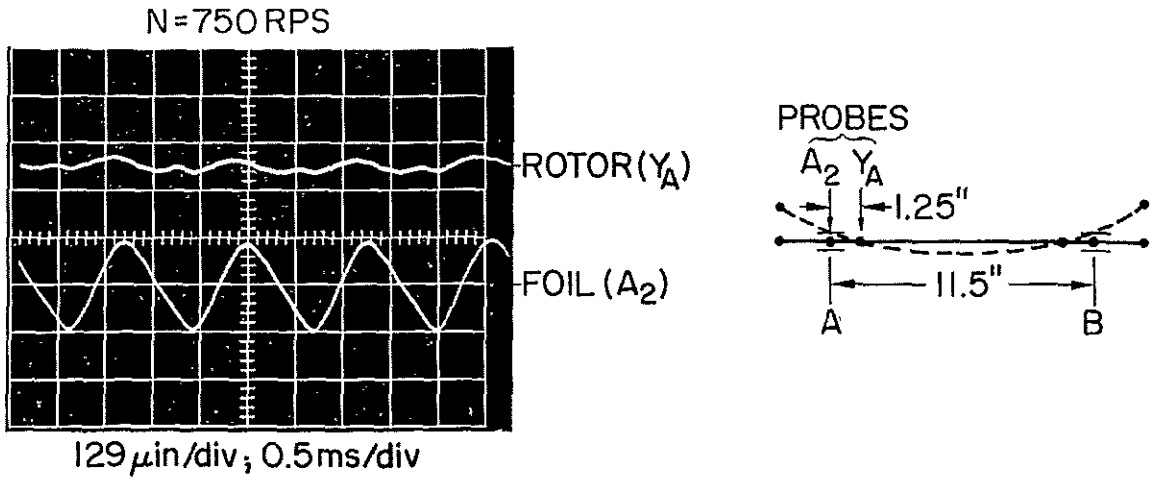

ROTOR: W=20.9 lb
r_t =4.68"
r_p =1.05"
BEARING SPAN =11.5"

FOILS: t =0.002"(Mo)
2b=1.5"
PRELOAD: T_o≈2.0 lb/in

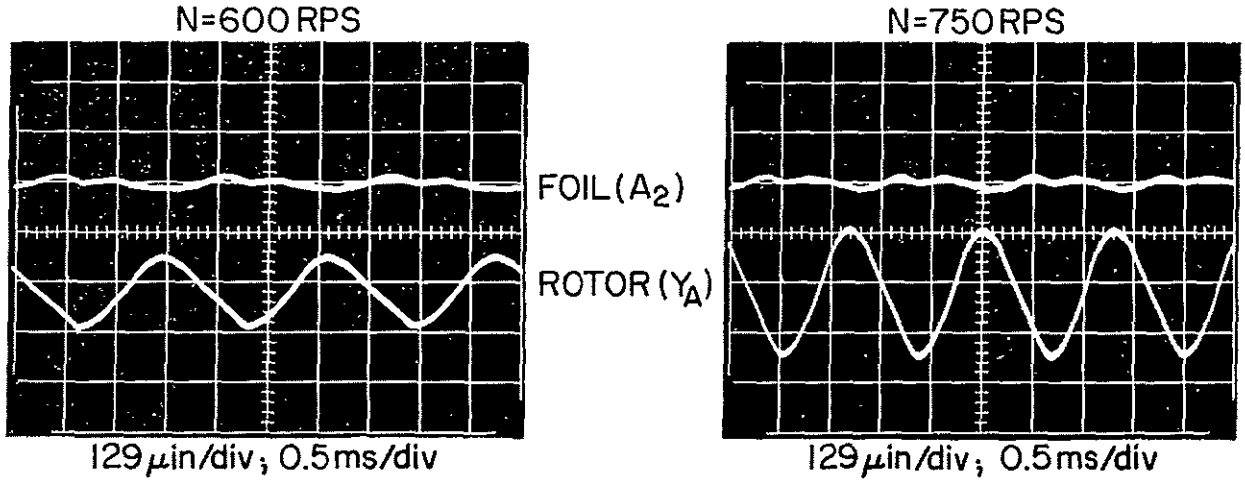

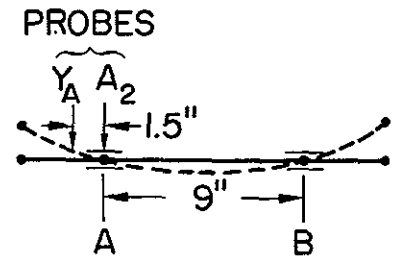

ROTOR: W=20.9 lb
r_t =4.68"
r_p =1.05"
BEARING SPAN =9"

FOILS: t =0.001"(Mo)
2b=2.0"
PRELOAD: T_o≈2.25 lb/in

Fig. 29 Effect of Rotor Bending on Measurement of Gap Width - Relative Motion of Rotor and Foil at Adjacent Monitoring Probes (Bearing Span = 11.5" and 9.0"; Journal Length = 1.5" and 2.0")

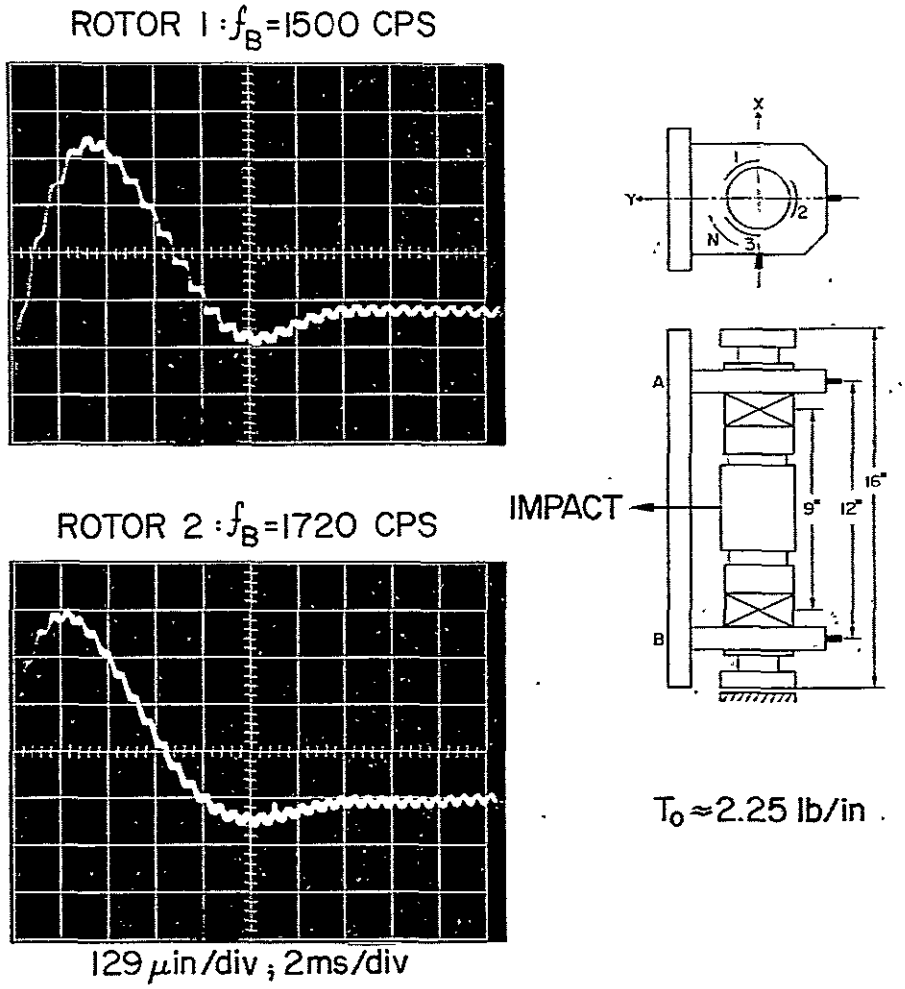

Fig. 30 Determination of Frequencies of Gravest Mode of Bending Vibrations for Composite (1) and One-Piece (2) Rotors.

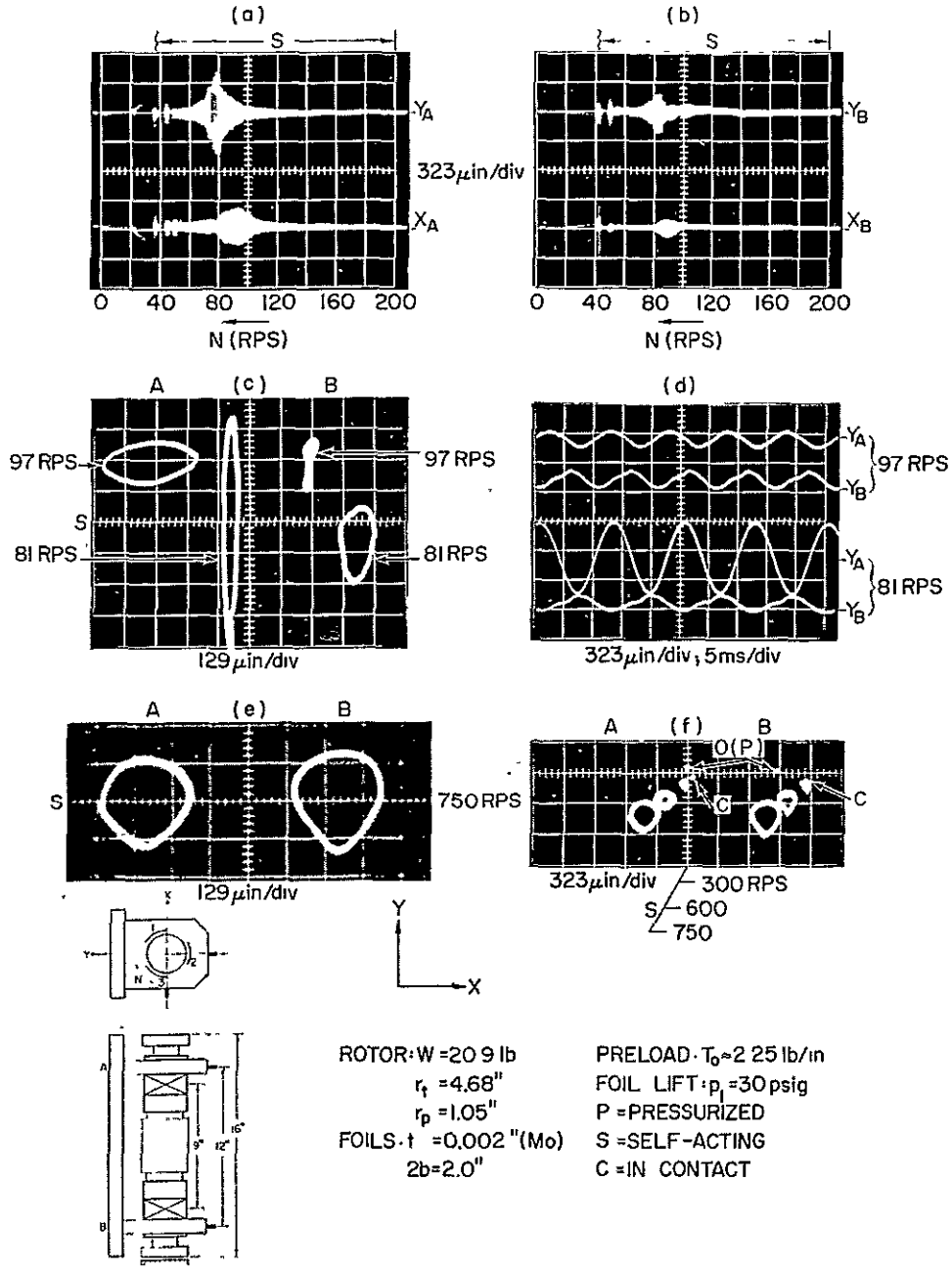

Fig. 31 Motion of Rotor and Scans of Response in Self-Acting Foil Bearing. - Increase of Foil Thickness and Preload (Bearing Span = 9.0"; Journal Length = 2.0")

(a), (b) Scans of Response to Remanent Imbalance
(c), (d) Orbits and Motion in Y-Plane in Resonant Range
(e) Orbits at 750 RPS
(f) Displacement of Rotor Axis with Speed

The displacement of the rotor axis with speed was of the same order of magnitude as in previous experiments. Self-acting coastdown to a full stop was characterized by rather rapid deceleration below 50 RPS, indicating early contact between the journal and the thicker, and more heavily preloaded foil.

Since the variation of gap width in the pressurized foil bearing continued to be of interest, the clearance was measured not only at the center, but also 0.125" from the foil edge. In both positions, the probes were located in a plane bisecting the region of wrap A_2. The scans, in both the pressurized and in the self-acting modes, are presented in Fig. 32. It can be seen, that although the corresponding clearances at the center and at the edge differed perceptibly, the unusual behavior in the pressurized mode was very similar at both monitoring stations. The reader may note once again the characteristic variation of gap width in the mid-plane of a pressurized foil-sector, particularly the steep transition joining the minima and maxima, the "jump" in the vicinity of a minimum, and the fact that at high speeds the clearances of the pressurized and of the self-acting bearings were quite commensurate. Further details relevant to variations of gap width are given in Section 3.6.

Unable to derive significant advantages from the use of thicker foils, and surmising that loss of flexibility hampered equalization of preload and increased the residual slack, subsequent experiments were conducted almost exclusively with 0.001" thick foils. Also, with stopping without the aid of external pressurization now an established practice showing no apparent detrimental effect on performance, experiments were concentrated progressively more on the self-acting mode of operation.

The performance characteristics of a rotor supported by 0.001" thick foils, preloaded to 1.5 lb/in, are depicted in Fig. 33 through Fig. 39. The first 2 figures of this sequence, Fig. 33 and Fig. 34,

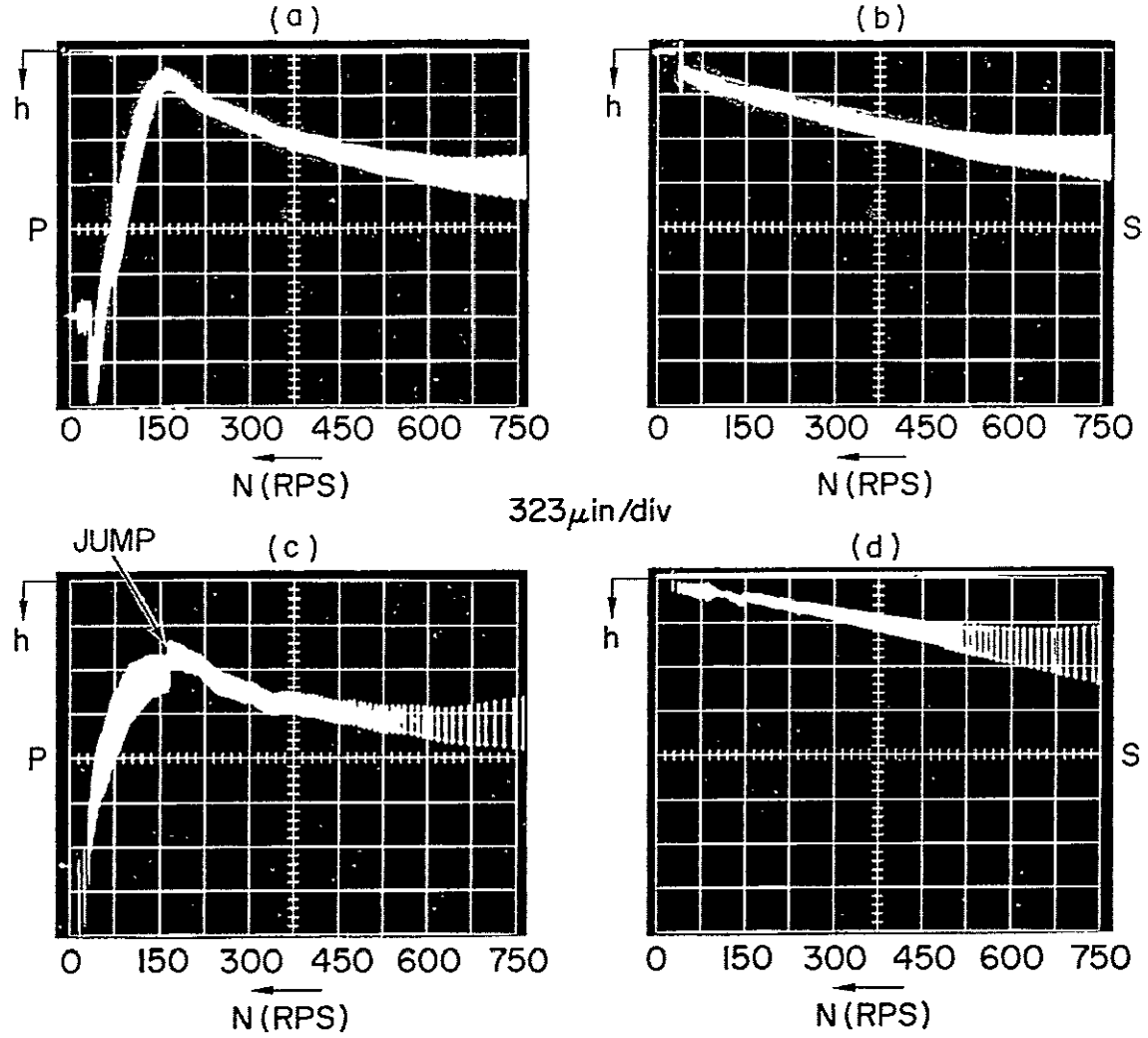

ROTOR: W = 20.9 lb
r_t = 4.68"
r_p = 1.05"
FOILS: t = 0.002" (Mo)
2b = 2.0"

PRELOAD: T_o ≈ 2.25 lb/in
FOIL LIFT: p_l = 30 psig
P = PRESSURIZED
S = SELF-ACTING

Fig. 32 Scan of Gap Width at Center and in Edge Zone in Pressurized and Self-Acting Foil Bearings. (Foil Sector A_2; Bearing Span = 9.0"; Journal Length = 2.0")

(a), (b) At center of Wrap
(c), (d) At 0.125" from Edge, at Bisector of Wrap

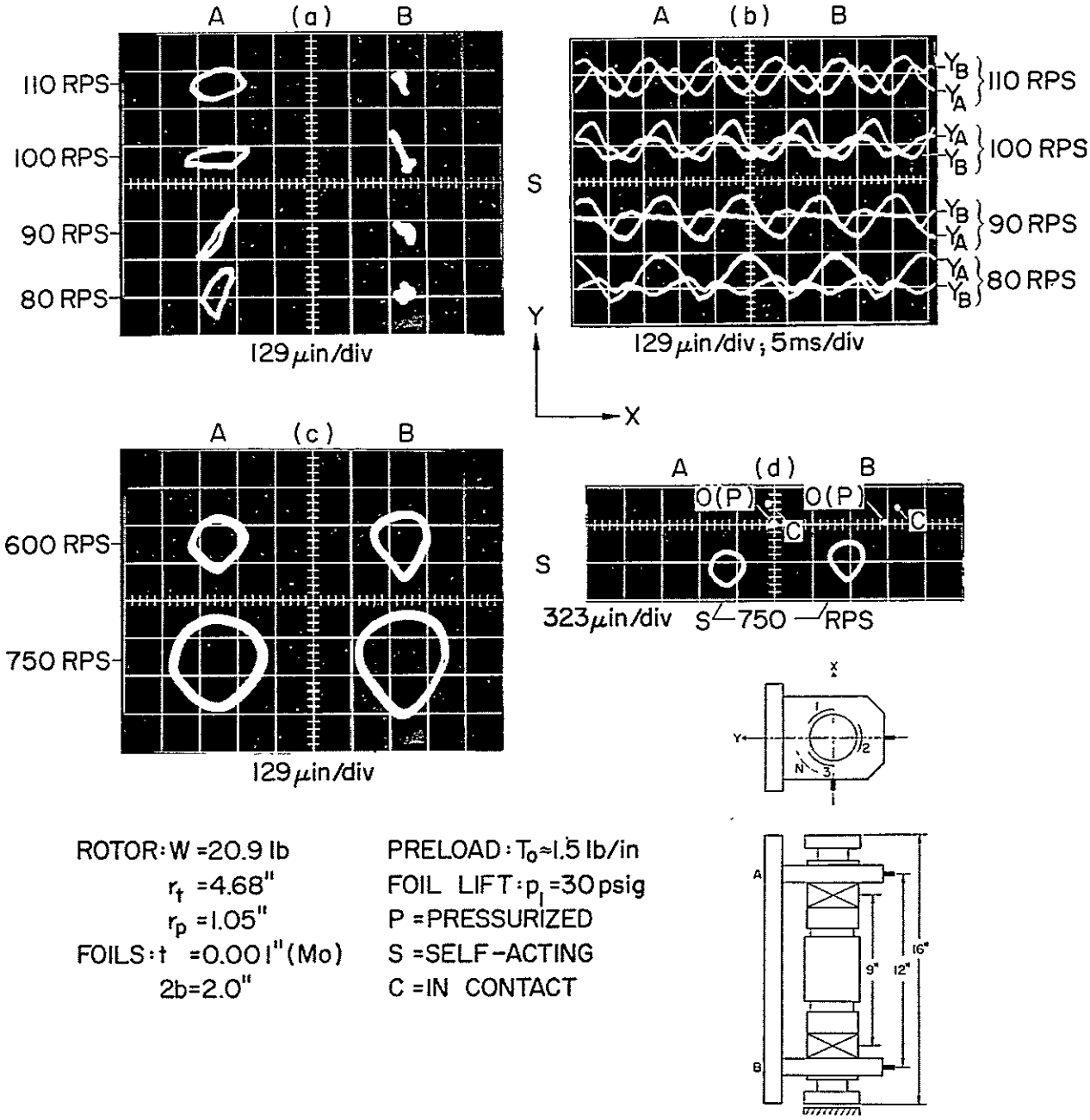

Fig. 33 Motion of Rotor in Self-Acting Foil Bearings. - Decrease of Foil Thickness at Moderate Preload (Bearing Span = 9.0"; Journal Length = 2.0")

(a) Orbits in Resonant Range
(b) Motion in Y-Plane in Resonant Range
(c) Orbits at 600 and 750 RPS
(d) Displacement of Rotor Axis with Speed

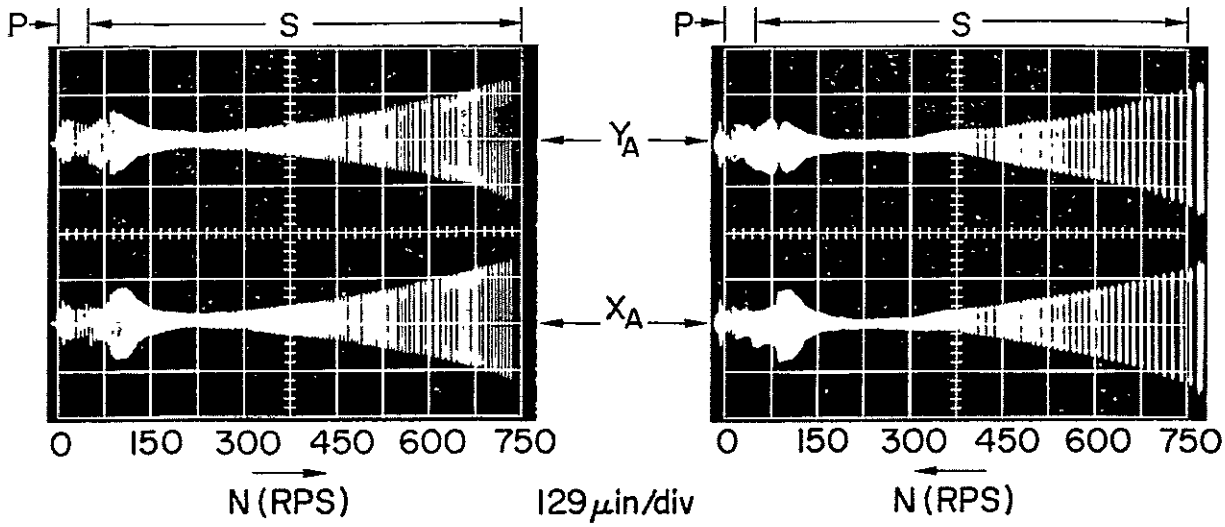

ROTOR: W = 20.9 lb
r_t = 4.68"
r_p = 1.05"
FOILS: t = 0.001"(Mo)
2b = 2.0"

PRELOAD: $T_o \approx 1.5$ lb/in
FOIL LIFT: p_l = 30 psig
P = PRESSURIZED
S = SELF-ACTING

Fig. 34 Scans of Response in Self-Acting Foil Bearings. Decrease of Foil Thickness at Moderate Preload (Bearing Span = 9.0"; Journal Length = 2.0")

contain data pertinent to motion with remanent imbalance. The following figures, Fig. 35 through Fig. 39, are relevant to rotation with symmetric and asymmetric imbalance. A direct comparison can also be made between the results contained in Fig. 33 and Fig. 34 and the data presented in Fig. 40, with regard to changes effected by an increase of preload from 1.5 to 2.25 lb/in.

Referring to Fig. 33 and Fig. 34, it can be seen that resonances in the self-acting mode occurred in the bandwidth 75-100 RPS. The resonant orbits were relatively small, smaller in fact than those recorded at 750 RPS. Apparently bending at high RPS overshadowed the effect of remanent imbalance at resonance. In the resonant bandwidth, one could also discern ultraharmonic components of motion in the self acting mode, particularly at 80 RPS, Fig. 33 (b). The mean displacement was, as usual, in the 3-rd quadrant, subtending an angle of approximately 45° with the negative X-axis.

It is convenient at this point to compare the foregoing data with the results in Fig. 40. In this case, the increase of preload from 1.5 to 2.25 lb/in was accompanied by a shift of the resonant bandwidth from 75-100 RPS to approximately 90-150 RPS. The motion in the resonant zone was quasi-conical, with the "apex" located approximately in the plane of the B-probes. At high speed, the motion of the bent rotor appeared to trace a very symmetrical surface of revolution.

Turning now to the operation at 3 levels of symmetric imbalance with a preload of 1.5 lb/in, the responses can be compared by reference to the first rows of photographs in Fig. 35, Fig. 36 and Fig. 37. An increase of imbalance appears to have produced no definite stiffening effect and no significant shift in the resonant bandwidth. The amplitudes increased nearly linearly with excitation, reaching a maximum peak-to-peak orbit of 1550 μinches at 105 RPS, with 26,100 μin-oz of symmetric imbalance.

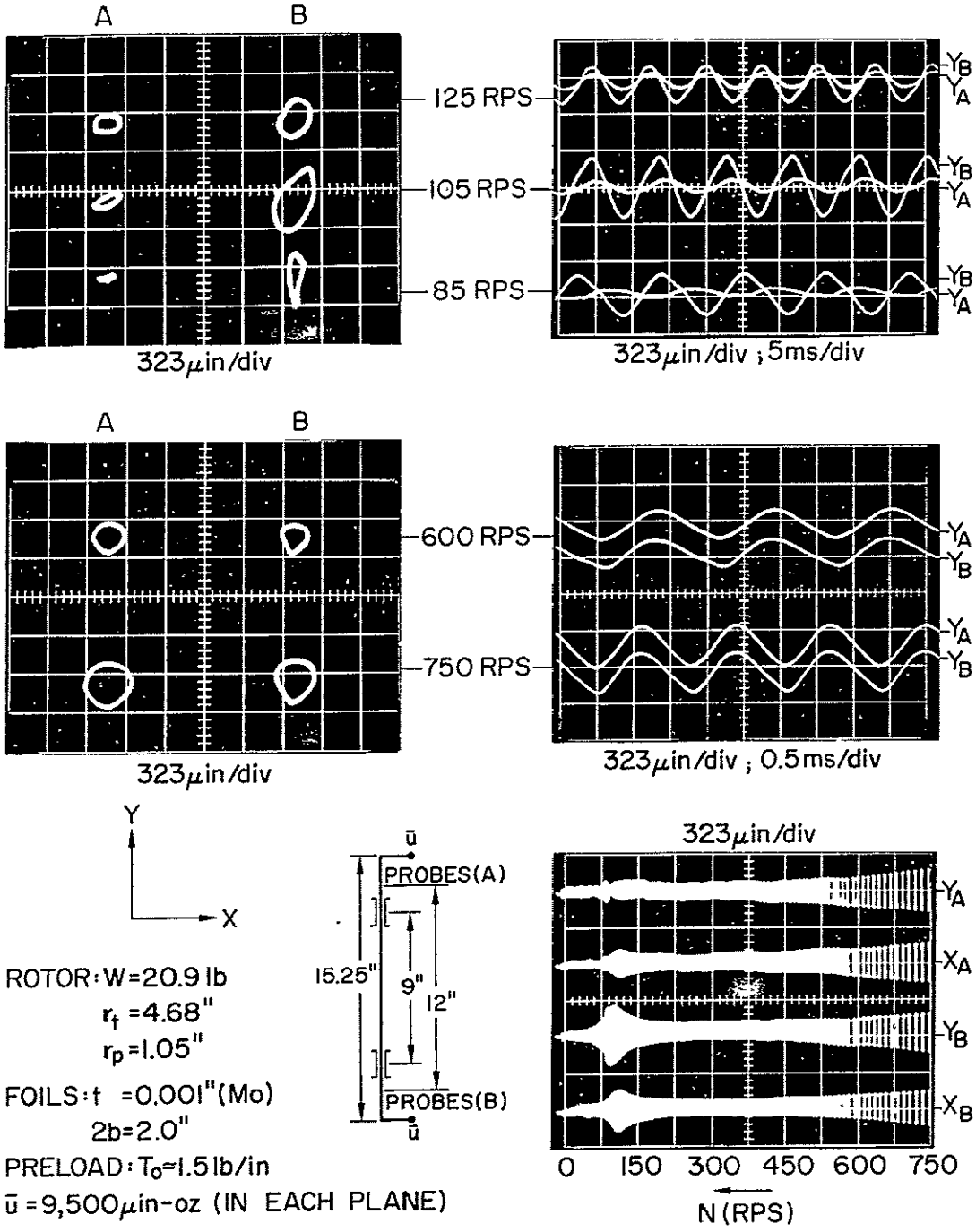

Fig. 35 Excitation with Symmetric Imbalance 1. - Motion of Rotor and Scans of Response in Self-Acting Foil Bearings in Resonant and High-Speed Range (Bearing Span = 9.0"; Journal Length = 2.0")

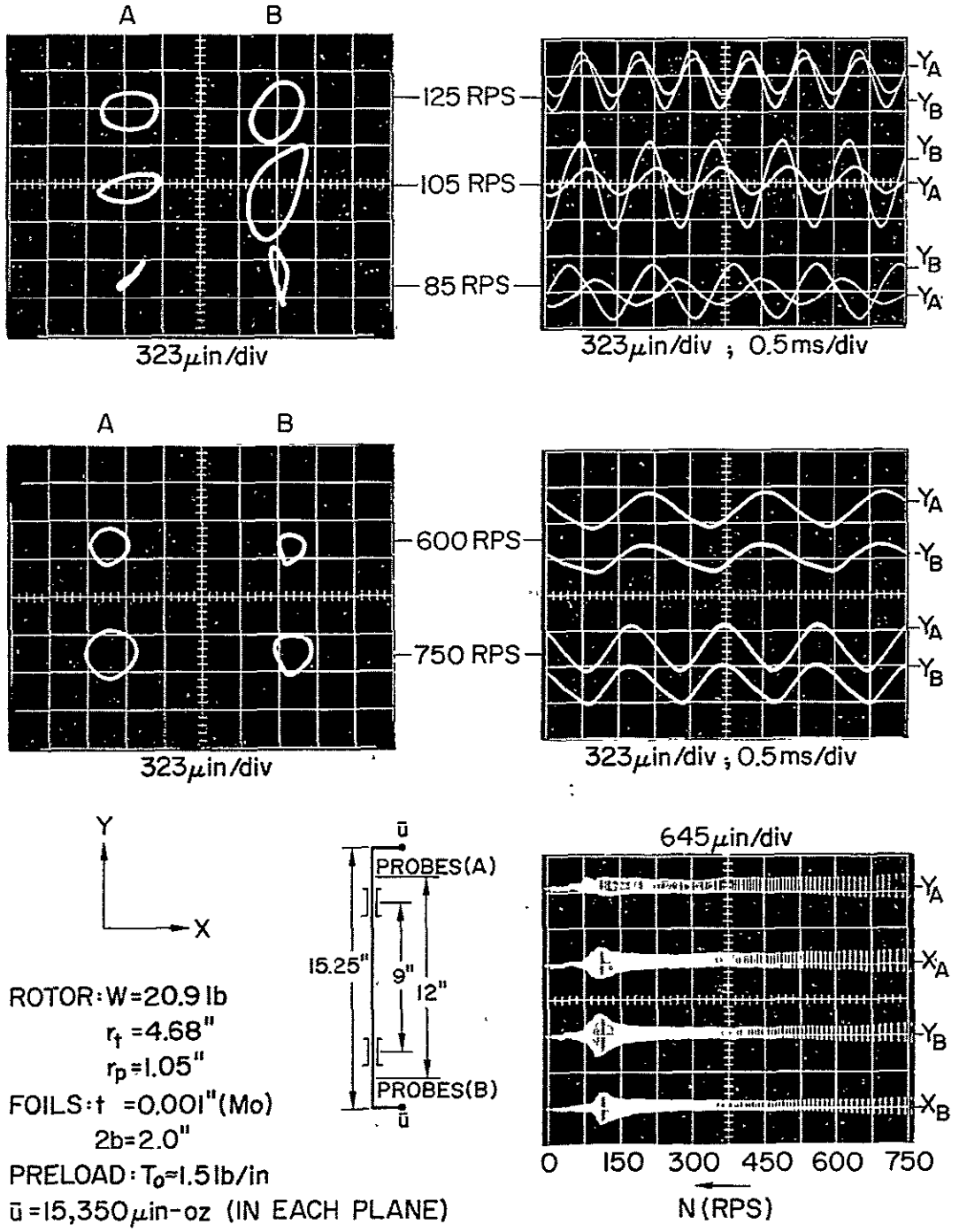

Fig. 36 Excitation with Symmetric Imbalance 2.- Motion of Rotor and Scans of Response in Self-Acting Foil Bearings in Resonant and High-Speed Range (Bearing Span = 9.0"; Journal Length = 2.0")

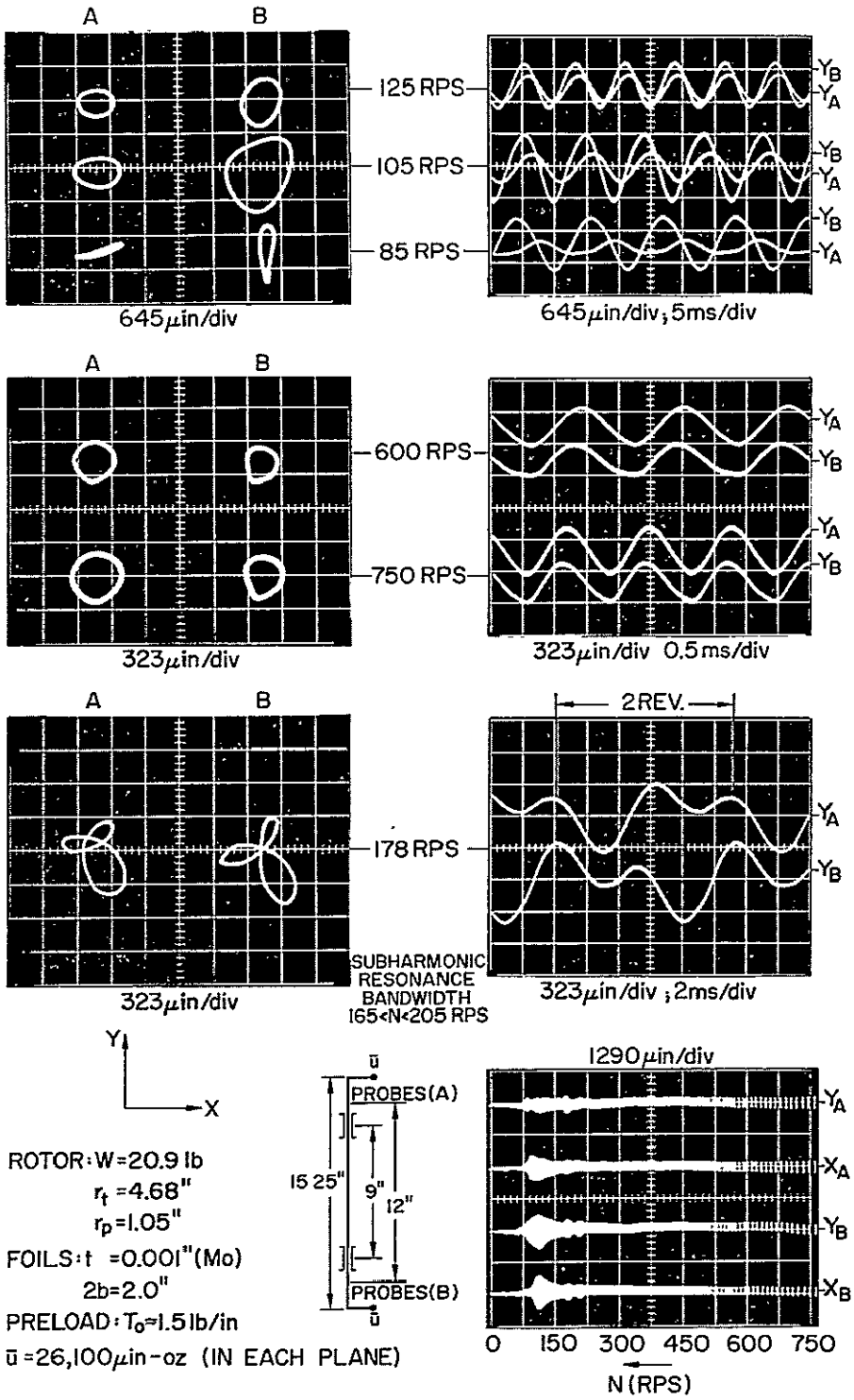

Fig. 37 Excitation with Symmetric Imbalance 3;-Motion of Rotor and Scans of Response in Self-Acting Foil Bearings in Resonant and High-Speed Range. Subharmonic Resonance (Bearing Span = 9.0"; Journal Length = 2.0")

The reader may note the progressive change in the attitude of the rotor axis from the time-base traces of the Y-probes, corresponding to an increase in speed from 85 RPS to 125 RPS. While only synchronous resonances were excited at lower levels of excitation, the largest symmetric imbalance induced subharmonic resonances in the bandwidth $165 < N < 205$ RPS, as illustrated in the 3-rd row of photographs in Fig. 37. Inspection of the time-base traces and of the clover-shaped orbits indicates that the axis precessed in the sense of rotation (clockwise), and the motion can be visualized by noting the coincidence of minor and major excursions in the Y-plane at A and at B. The complex motion in the resonant zones can be contrasted with the regularity of high-speed motion. At high RPS, the rotor revolved in a bent configuration, without pitching, and with no significant influence of imbalance on orbit size.

The responses to excitation by asymmetric imbalance are shown in Fig. 38 and Fig. 39. The highest level of 15,350 μin-oz in each balancing plane resulted in a maximum peak-to-peak excursion of 2200 μinches, at 102 RPS. No significant translation of the resonant bandwidth with increasing imbalance was observed, and such differences in resonant speeds as may be observed in Fig. 38 and Fig. 39 may have been due to temperature changes between corresponding, consecutive runs. At resonance, as well as at high speeds, the asymmetry of imbalance gave prominence to the pitching component of motion. This is reflected in the time-base traces of motion in the Y-plane in Fig. 38 at 110, 125, 600 and 750 RPS. While no subharmonic motion was excited at the lower level of imbalance, an increase of imbalance produced minor subharmonic resonances of order 1/2 in the bandwidth 180-200 RPS. The amplitudes of motion were modulated by a slow beat, approximately 1/20 of the rotational frequency. The subharmonic motion, depicted in the 3-rd row of oscillograms

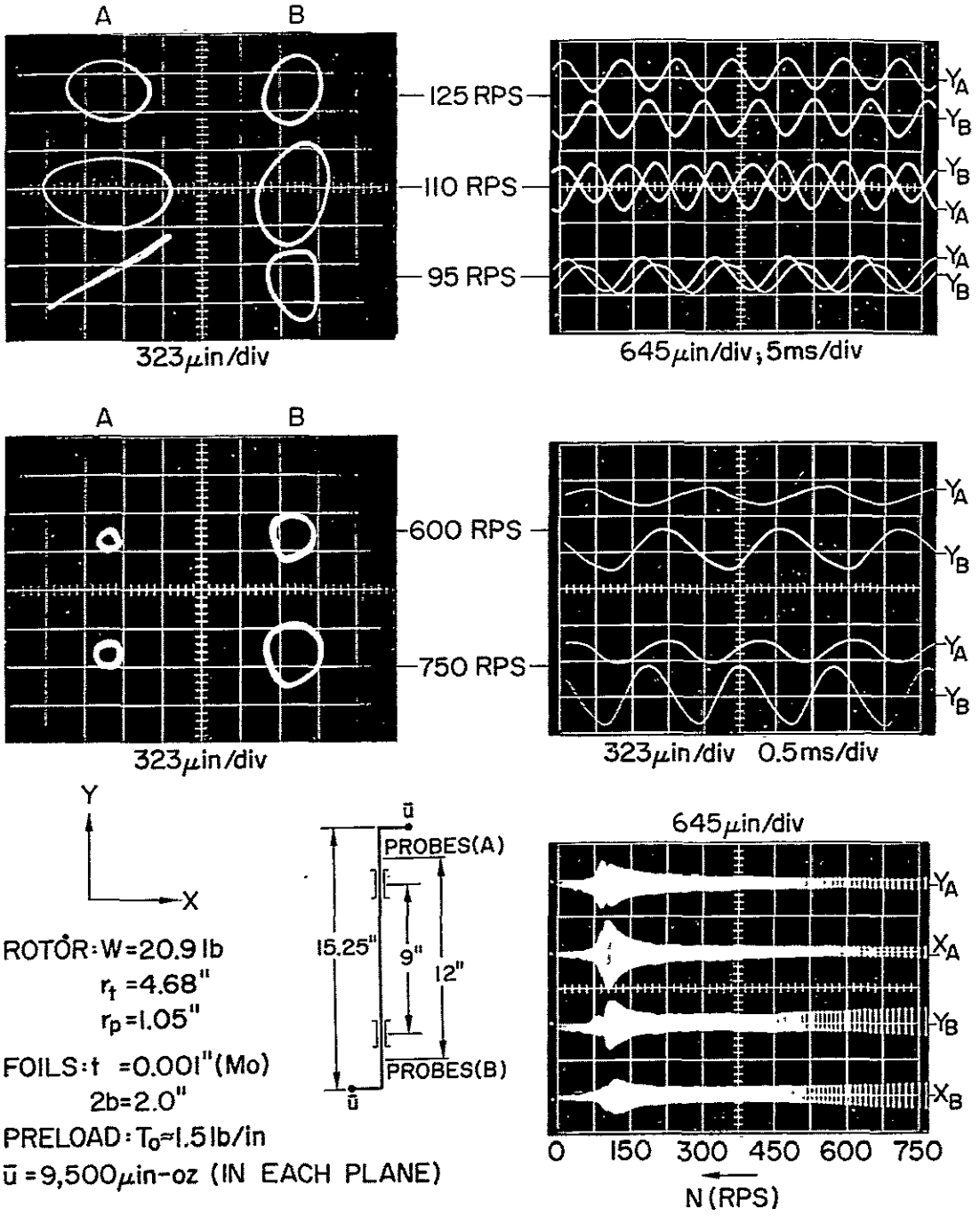

Fig. 38 Excitation with Asymmetric Imbalance 1. - Motion of Rotor and Scans of Response in Self-Acting Foil Bearings in Resonant and High-Speed Range (Bearing Span = 9.0", Journal Length = 2.0")

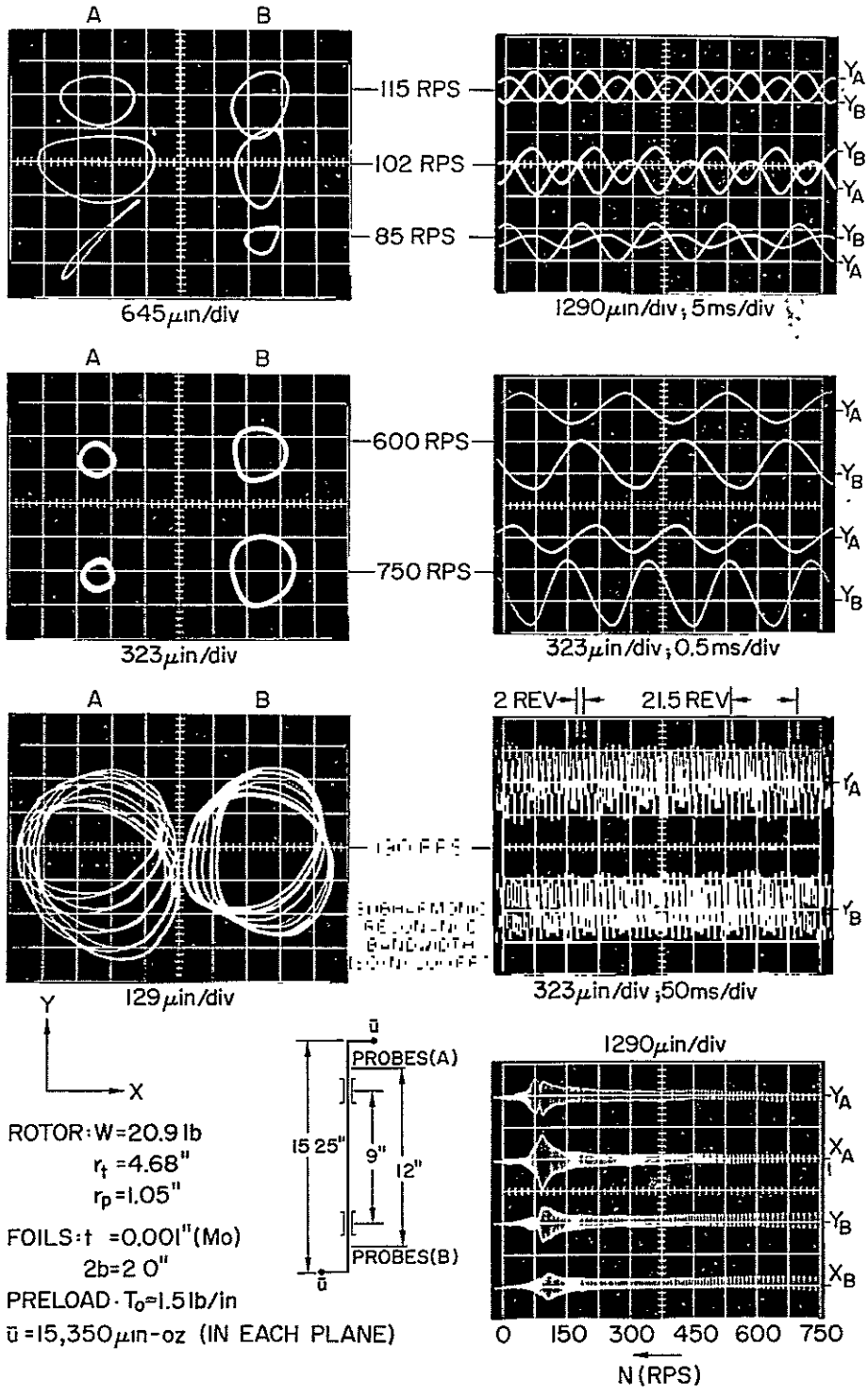

Fig. 39 Excitation with Asymmetric Imbalance 2. - Motion of Rotor and Scans of Response in Self-Acting Foil Bearings, in Resonant and High-Speed Range. Subharmonic Resonance. (Bearing Span = 9.0"; Journal Length = 2.0").

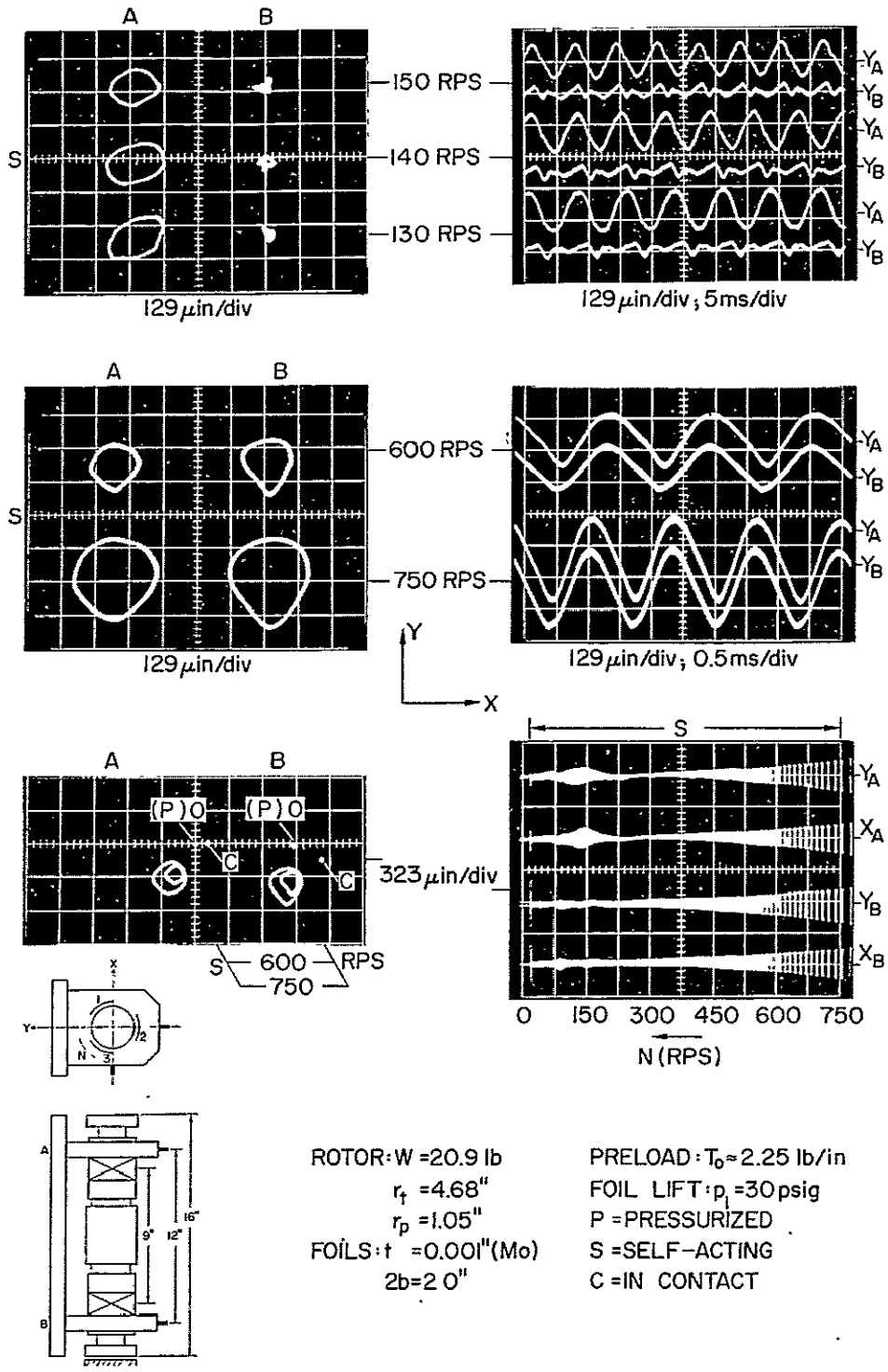

Fig. 40 Motion of Rotor and Scans of Response to Remanent Imbalance in Self-Acting Foil Bearings in Resonant and High-Speed Range. Displacement of Rotor Axis with Speed - Flexible Foil and High Preload (Bearing Span = 9.0"; Journal Length = 2.0")

in Fig. 39, was qualitatively identical with previously encountered, nonlinear phenomena illustrated in Fig. 29, Fig. 24 and Fig. 25.

The experiments reported in this and in the previous sections showed that very satisfactory performance could be achieved with relatively thin and lightly preloaded foils, and that relatively large amounts of imbalance could be accommodated with 2.0" wide foils at a 9.0" bearing span. It appeared that an increase of foil thickness had few advantages to offer and that no significant shift of resonances from a bandwidth centered at approximately 100 RPS (6,000 RPM) was to be anticipated. The ability to operate at relatively low levels of preload and of coasting down repeatedly to a full stop were encouraging with regard to possibility of starting without the aid of pressurization. The foil-lift system, however, which served so well in the past and presented so far the only proven means of starting, required a better understanding with respect to variation of the clearance topography with speed and of parameters influencing the unusual trend previously observed. A series of experiments relevant to this topic are described in the following section.

3.6 Gap Width Characteristics of Pressurized and Self-Acting Foil Bearings. Determination of Pressure at Center of Wrap. Thermal Relaxation

Intuitively, one might expect the self-acting effect to augment the pressurization, with the net result of increasing the mean gap width. In reality, however, the interaction of the two effects does not increase the mean clearance and produces a rather complex gap topography. Measurements of clearance at the center of wrap, reported in numerous figures of the preceding sections, pointed to the complexity of the gap distribution and the high sensitivity to variation of speed. Since the maintenance of an adequate gap width during the initial and final stages of rotation was the prime purpose of the foil-lift system, the variation of

clearance distribution in the pressurized bearing was examined in greater detail.

The scanning of the gap width by means of a rotating probe integral with the journal [13] was not feasible in this apparatus. The measurements, therefore, were limited to 3 fixed stations along the foil centerline and required 3 pairs of radially mounted, parallel probes. The first measurements involved the parametric variation of the foil-lift supply pressure and were limited to clearances at the center of wrap. The results, presented in Fig. 41, Fig. 42 and Fig. 43, contain scans of clearance and of amplitudes of motion of the foil and of the rotor in the plane of the bisector of a foil segment. Shown also are the time-base displays of foil and rotor amplitudes at specific rotational speeds.

Starting at the highest supply pressure p_ℓ = 50 psig in Fig. 41, and continuing through p_ℓ = 20 psig to the self-acting case p_ℓ = 0, the following can be observed:

(a) The gap at the center of wrap, at zero speed, varied approximately linearly with the supply pressure.

(b) All scans were characterized by an initial increase of gap width with speed to a maximum, followed by a very steep transition to a minimum, at which the gap width was but a fraction of the initial value.

(c) With decreasing supply pressure, both stationary points occurred at lower speeds, resulting in very steep transition gradients.

(d) With further reduction of the supply pressure, one or more "jumps" were observed during transition, an indication of possible instability of local gap configuration. (Fig. 41, at 23 and 20 psig. Also Fig. 42 at 15 and 10 psig).

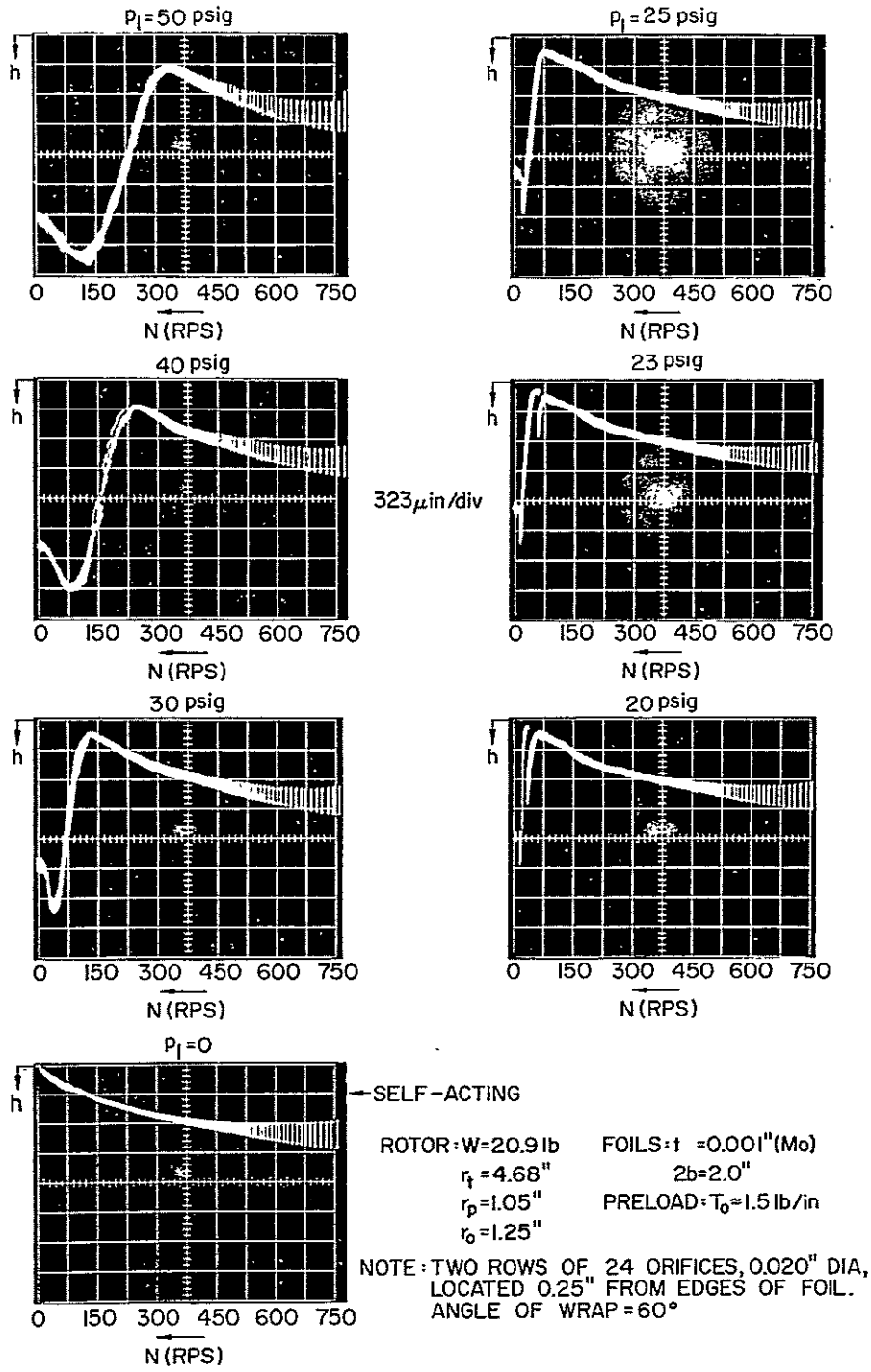

Fig. 41 Scans of Gap Width at Center of Wrap. Effect of Foil-Lift Pressure Variation at Constant Preload $T_o \approx 1.5$ lb/in (Bearing Span = 9.0"; Journal Length = 2.0")

(e) To the right of the minimum, and with increasing speed, the gap width at the center of wrap varied in a manner similar to that of the self-acting foil-bearing.

The upper row of photographs in Fig. 42 consists of three oscillograms, recorded at p_ℓ = 30 psig. The scan of gapwidth, and the corresponding scans of foil and rotor excursions, indicate that the transition zone between 20 RPS and 120 RPS contained a foil resonance, centered at approximately 97 RPS (i.e. close to the speed where the gap was minimum). Furthermore, the time-base trace of foil motion showed that the fundamental vibration of the foil was synchronous with the speed of rotation. The amplitude was approximately 400 μinches peak-to-peak, despite the fact that the excursions of the rotor were quite negligible in comparison.

An even more complex transition could be observed with a foil-lift pressure p_ℓ = 20 psig, for which the following sequence of events is depicted in the scans of Fig. 43. With decreasing speed, and upon passing through a minimum at 55 RPS, the gap began to increase. The increase was followed by a foil resonance at approximately 40 RPS (III) and a sudden decrease to a vanishingly small gap (II). With further reduction in speed, the gap increased rapidly again and the foil experienced a second resonance (I). The gap growth continued to a maximum at approximately 20 RPS, decreasing slightly thereafter to 1250 μinches at zero speed. The second row of photographs in Fig. 43 illustrates the motion of the foil in two regions of resonance, (I) and (III), and at an intermediate speed (II). At (II), the clearance was vanishingly small, and foil and rotor moved in unison. The motion of the foil in the vicinity of the two resonances was large in comparison with the excursions of the rotor. Various harmonics were superposed on the synchronous motion, including the clearly discernible response to excitation by 24 impinging air jets. The sequence

of events , as related here, was in the order of occurrence during coast-down. Although the responses were not fully identical in the course of acceleration and deceleration, the general trend and the type of phenomena observed were similar.

An increase of the preload tension produced effects very similar to the reduction of the foil-lift pressure. Both caused a shift of the gap transition-zone at the center of wrap in the direction of lower speed, Fig. 41 and Fig. 44. Data relevant to the variation of foil-lift pressure at a higher level of preload tension $T_o \approx 2.25$ lb/in are presented in Fig. 44 and Fig. 45. The oscillograms display sharp transitions and discontinuities, as well as foil resonances in the bandwidth of transitions. The results may be compared with the data corresponding to lower preload tension $T_o \approx 1.5$ lb/in, Fig. 41 through 43.

The results of measurements described in the foregoing paragraphs pertain to the center of wrap. It was also demonstrated in Section 3.5 that the variation of gap width with speed was similar at the center and in the vicinity of the edge, when measured in the plane bisecting the angle of wrap, Fig. 32. The scans of gap width presented in the first row of photographs in Fig. 46 were obtained at three locations along the foil centerline; at the center of wrap (C), and at 5° from the inlet and exit terminals of the 60° angle of wrap (I and E). These photographs permit a semi-quantitative reconstruction of gap profiles along the centerline of the foil at all speeds and afford thereby an insight into the spatial variation of gap topography.

The second row of oscillograms in Fig. 46 illustrates the corresponding variation of gap width in the case of the self-acting foil bearing. The third row of photographs in Fig. 46 contains simultaneous scans of the

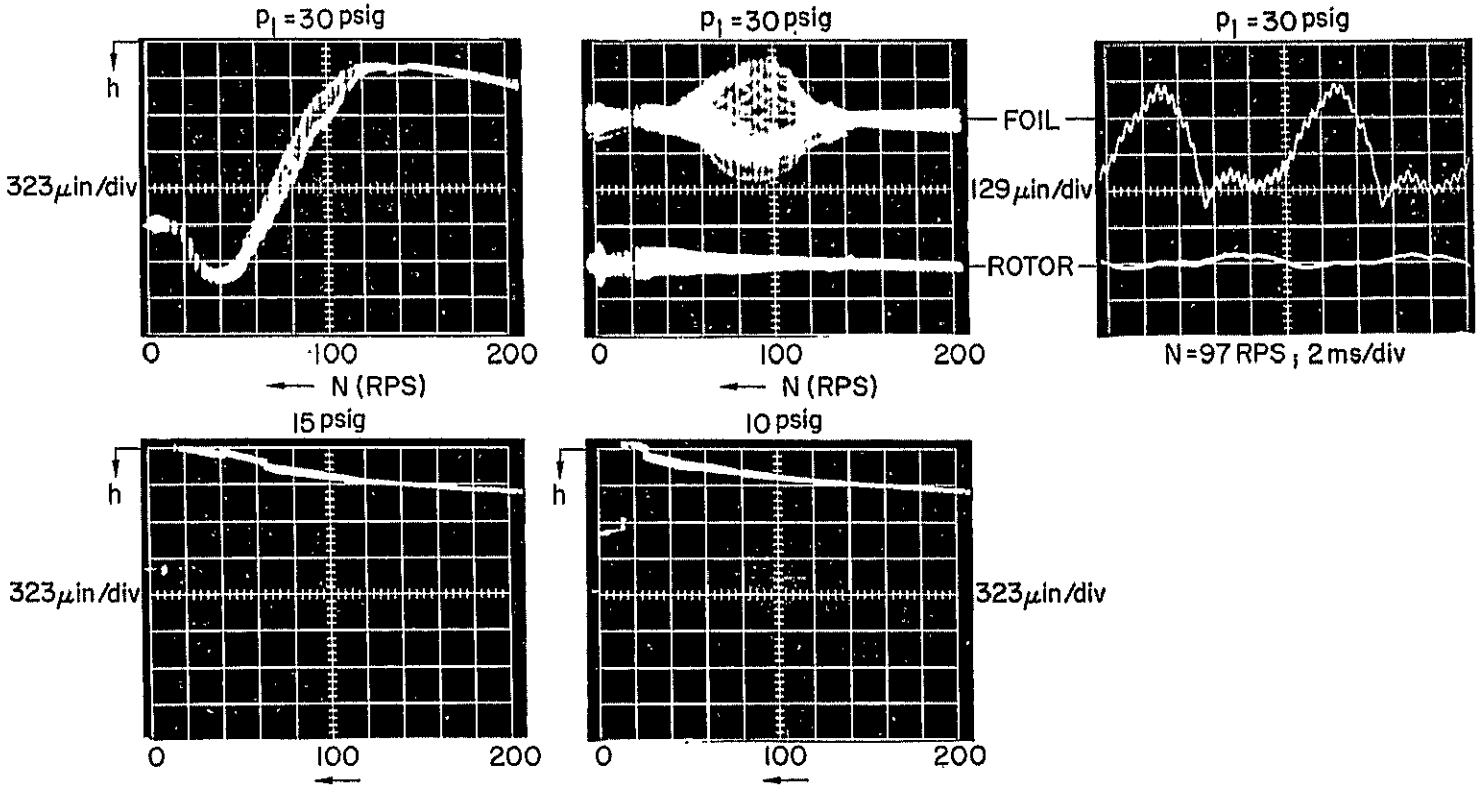

ROTOR: W = 20.9 lb
r_t = 4.68"
r_p = 1.05"
r_o = 1.25"

FOILS: t = 0.001" (Mo)
2b = 2.0"
PRELOAD: T_o ≈ 1.5 lb/in

NOTE: TWO ROWS OF 24 ORIFICES, 0.020" DIA, LOCATED 0.25" FROM EDGES OF FOIL. ANGLE OF WRAP = 60°

Fig. 42 Scans of Gap Width at Center of Wrap. Effect of Foil-Lift Pressure Variation at Constant Preload $T_o \approx 1.5$ lb/in. - Motion of Foil in Transistion Zone at Foil Lift Pressure p_l = 30 psig (Bearing Span = 9.0"; Journal Length = 2.0")

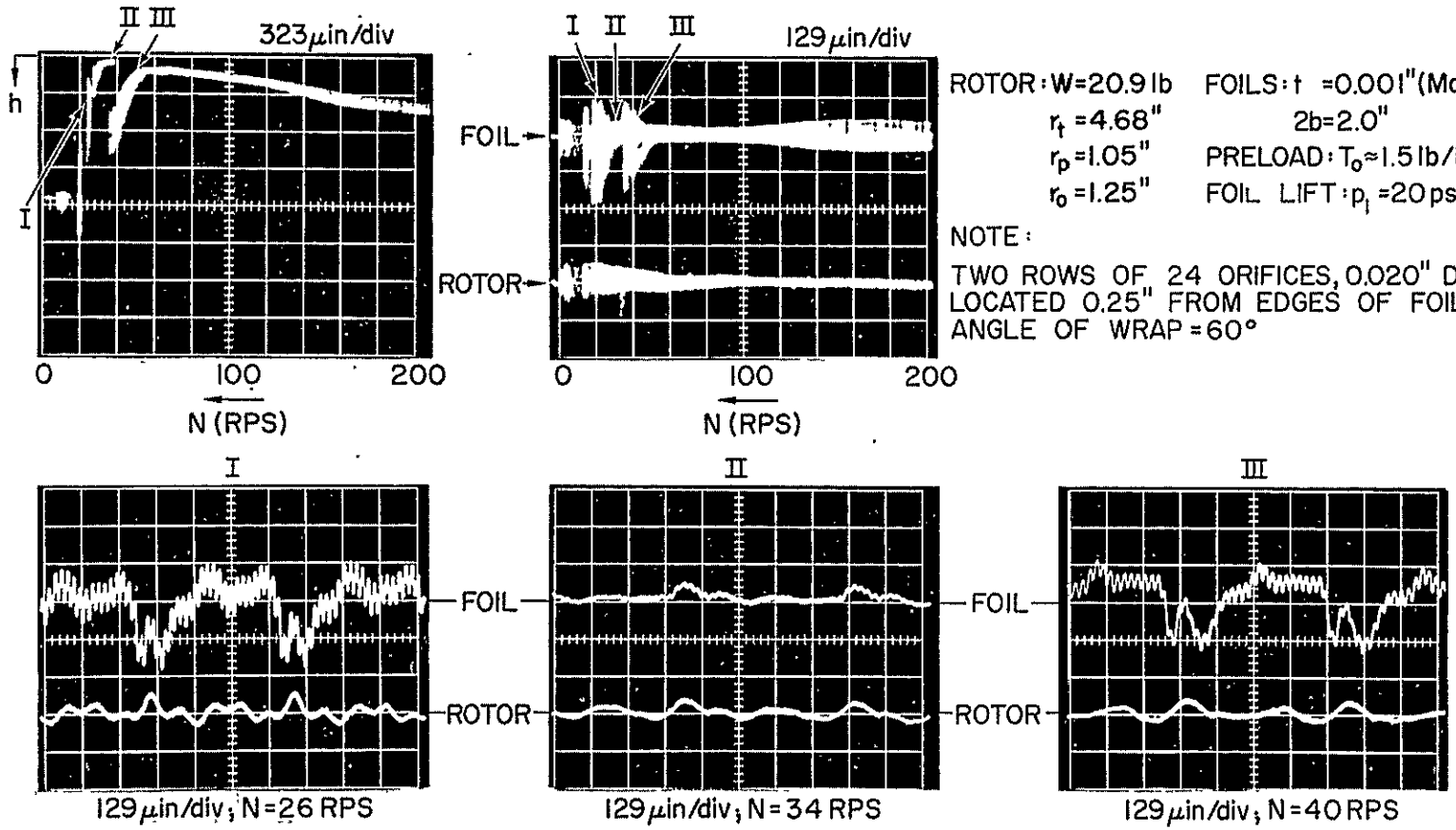

Fig. 43 Scan of Gap Width at Center of Wrap and Motion of Foil in Transition Zone at $T_o \approx 1.5$ lb/in and $p_\ell = 20$ psig (Bearing Span = 9.0"; Journal Length = 2.0")

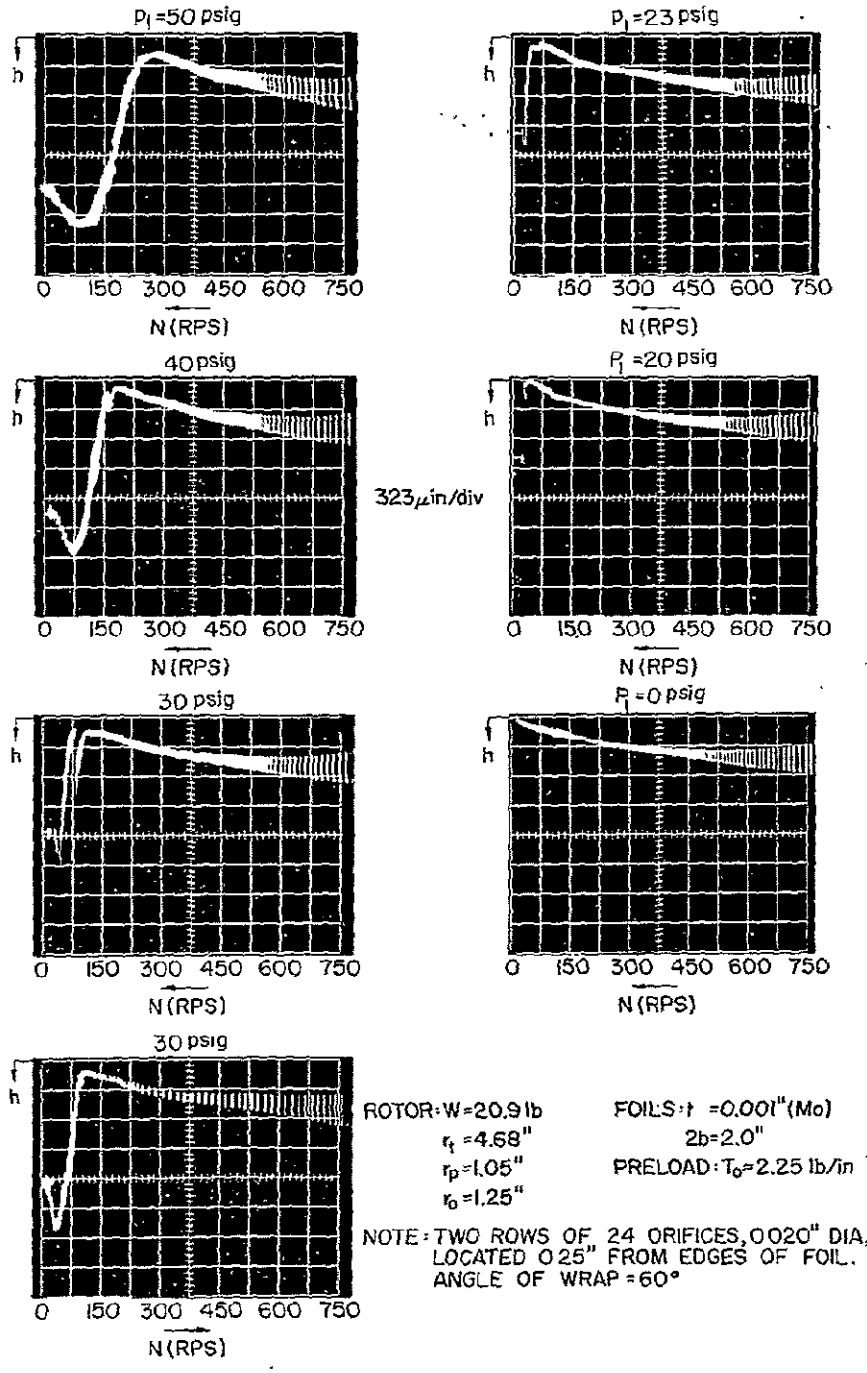

Fig. 44 Scans of Gap Width at Center of Wrap. Effect of Foil-Lift Pressure Variation at Constant Preload $T_o \approx 2.25$ lb/in (Bearing Span = 9.0"; Journal Length = 2.0")

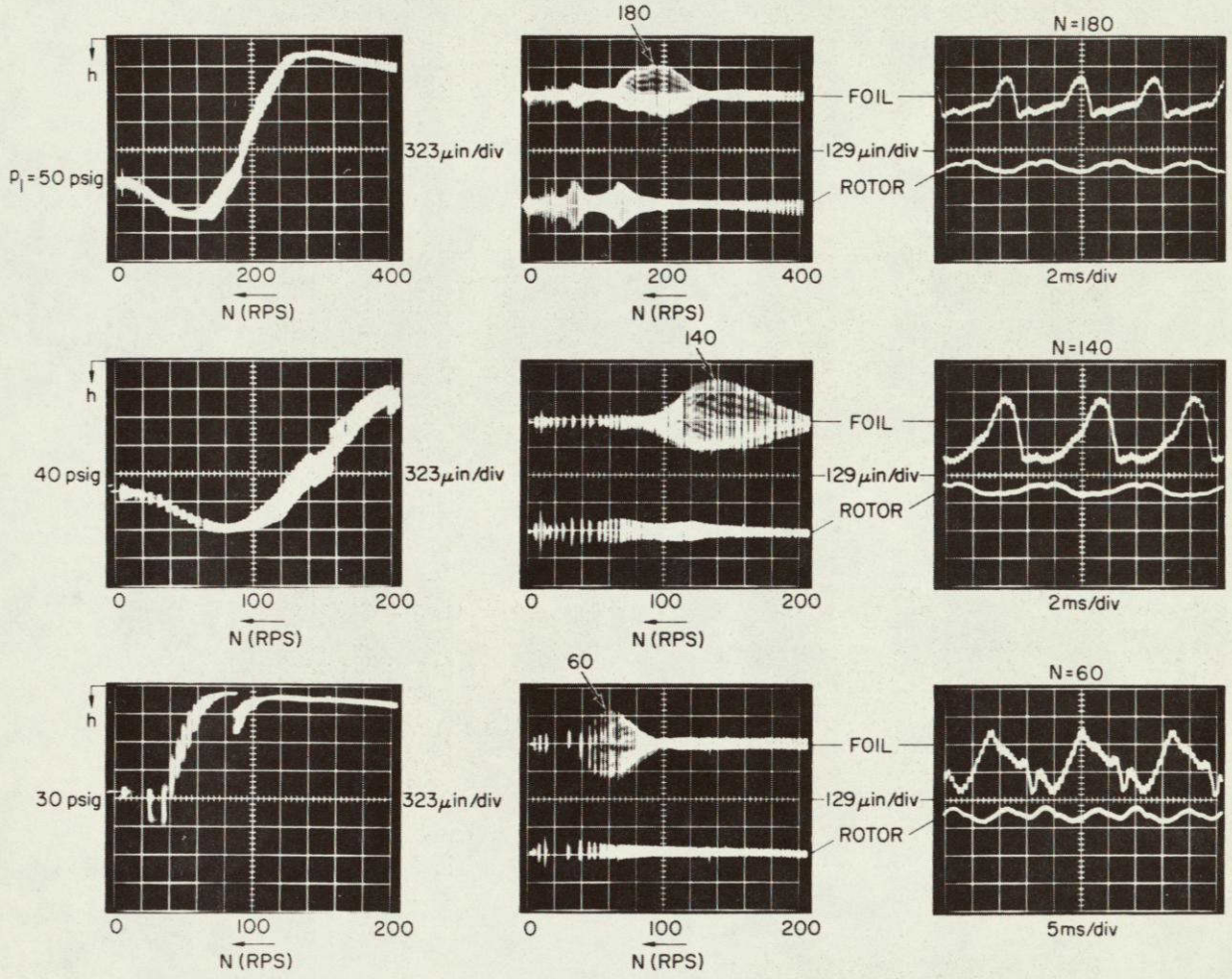

ROTOR: W = 20.9 lb
r_t = 4.68"
r_p = 1.05"
r_o = 1.25"

FOILS: t = 0.001" (Mo)
2b = 2.0"
PRELOAD: T_o = 2.25 lb/in

NOTE: TWO ROWS OF 24 ORIFICES, 0.020" DIA, LOCATED 0.25" FROM EDGES OF FOIL. ANGLE OF WRAP = 60°

Fig. 45 Scans of Gap Width at Center of Wrap. Effect of Foil-Lift Pressure Variation at $T_o \approx 2.25$ lb/in. Motion of Foil in Transition Zone (Bearing Span = 9.0"; Journal Length = 2.0")

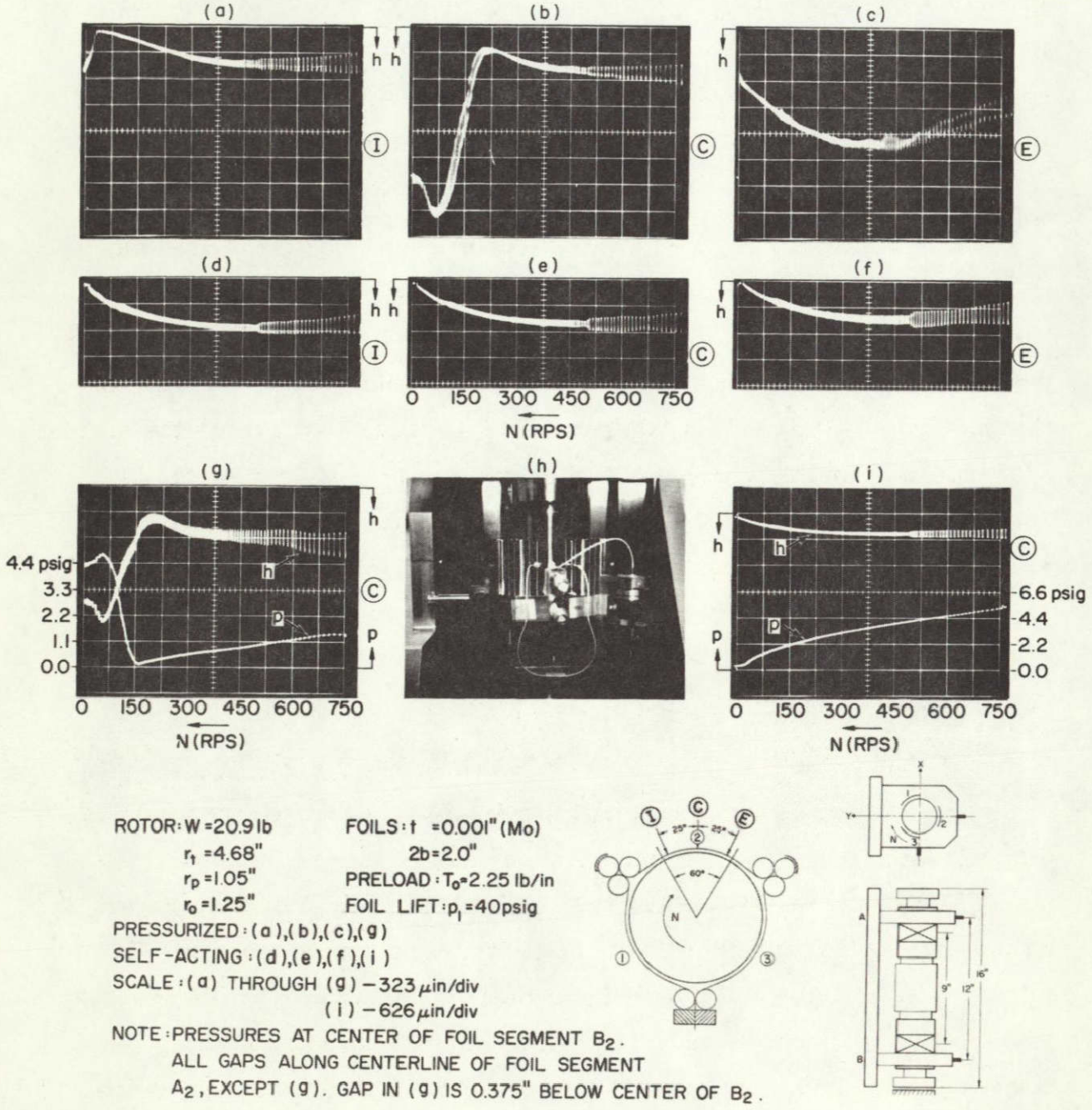

ROTOR: W = 20.9 lb
r_1 = 4.68"
r_p = 1.05"
r_o = 1.25"

FOILS: t = 0.001" (Mo)
2b = 2.0"
PRELOAD: T_o = 2.25 lb/in
FOIL LIFT: p_i = 40 psig

PRESSURIZED: (a), (b), (c), (g)
SELF-ACTING: (d), (e), (f), (i)
SCALE: (a) THROUGH (g) − 323 μin/div
(i) − 626 μin/div

NOTE: PRESSURES AT CENTER OF FOIL SEGMENT B_2.
ALL GAPS ALONG CENTERLINE OF FOIL SEGMENT A_2, EXCEPT (g). GAP IN (g) IS 0.375" BELOW CENTER OF B_2.

Fig. 46 Scans of Gap Width and Pressure in Self-Acting and Pressurized Foil Bearing. (Bearing Span = 9.0"; Journal Length = 2.0")

gap width and of pressure at the center of wrap, for both the pressurized (g) and for the self-acting (i) bearings. Shown also is a closeup photograph of the foil sector B_2. Two parallel capacitance probes used in gap measurement are discernible in the foreground, and the pressure transducer connected to the center tap of the foil can be seen on the right hand side of the insert photograph.

The scans of gap width in the pressurized mode indicated the following. At zero speed, the profile along the centerline bulged at the midspan and sagged at the extremities of the wrap. With increasing speed, the self-acting effect was washed downstream, making itself felt first in the inlet zone. The profiles (a), (b) and (c) in Fig. 46 constitute the source of the semi-quantitative gap profiles at various speeds shown in Fig. 47. The profile at zero speed leaves little doubt with regard to symmetry and the profile at 75 RPS, though similar, reflects the initial effect of the "self-acting distortion". Proceeding in the same manner to successive profiles at higher speeds, and guided at each speed by 3 definite data points, the transition of topography can be traced from a purely pressurized foil bearing to the high-speed range, where the self-acting effect is dominant.

The oscillograms (g) and (i) in Fig. 46 are unique, inasmuch as they represent the only simultaneous scans of pressure and gap width included in this report. The pressure changes at the center of wrap appear to have paralleled the variation of gap width. At a supply pressure p_ℓ = 40 psig (g), the pressure at the center of wrap at zero speed was 4.4 psig, dropping to nearly atmospheric at 150 RPS, and rising to barely 1.4 psig at 750 RPS. In contrast, the pressure induced at 750 RPS at the center of wrap of the self-acting bearing, Fig. 46(i), was 5.3 psig, or nearly 4 times as much as at the center of the pressurized bearing sector.

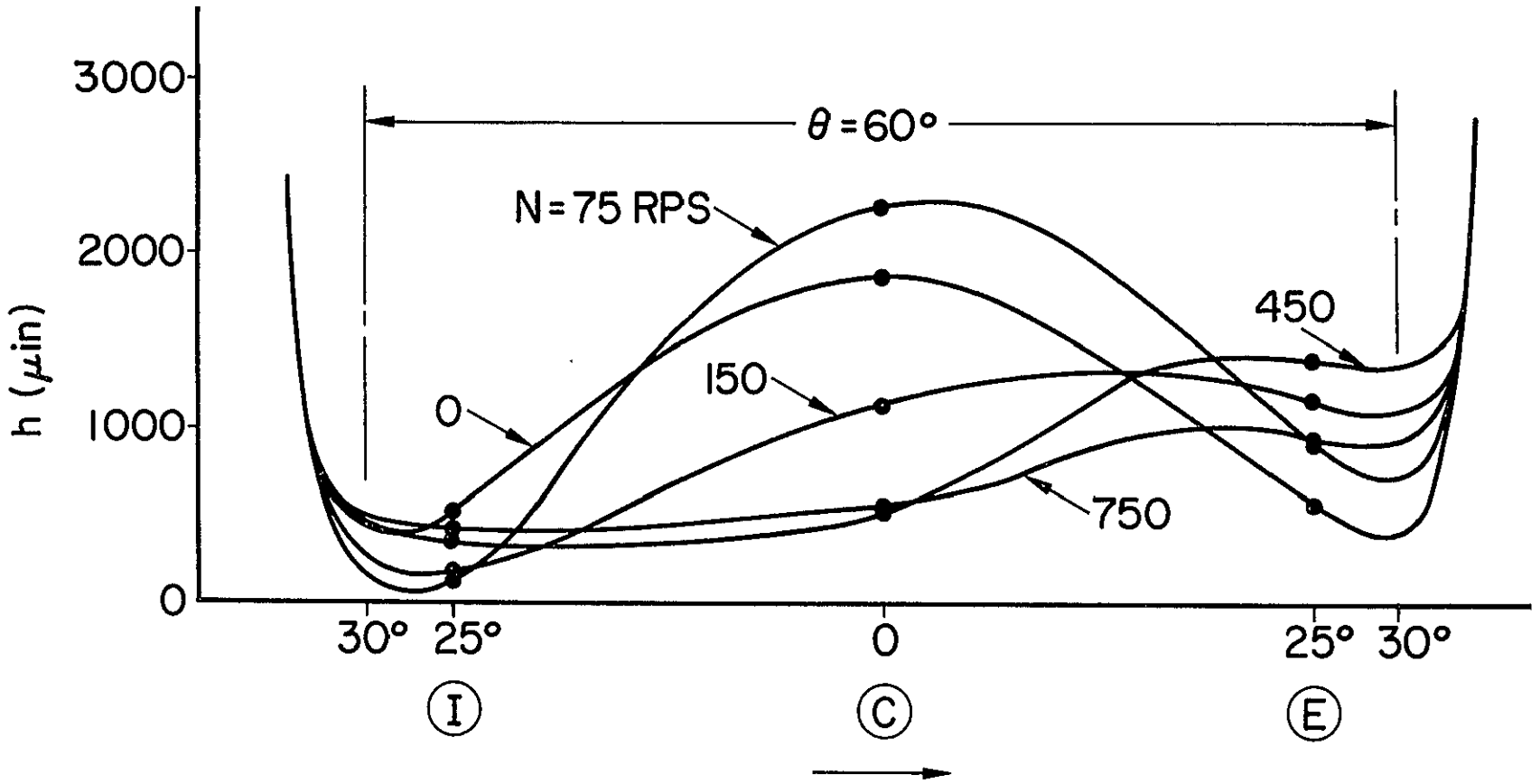

Fig. 47 Semi-Quantitative Representation of Gap Profiles Along Centerline of Pressurized Foil Bearing (Data points from first row of oscillograms in Fig. 46)

If we relate the measured pressure to the average tension in the self-acting case:

$$p-p_a = T/r_0 \approx 5.3 \text{ psi}$$

then the inertia parameter and the reciprocal of the compressibility parameter assume, approximately, the following values:

$$I = \tfrac{1}{2} \rho_a U/(T/r_0) \approx 0.35$$

$$1/C = T/(r_0 p_a) \approx 0.36$$

and the gap width can be determined from the expression [9]

$$h^* = H^*(I,C)\, r_0 (6\mu U/T)^{2/3}$$

in which, using the foregoing values of I and 1/C,

$$H^* = 0.643 + 0.286I + 1.905I^2 - \frac{0.183}{C} \approx 0.92$$

Rewriting the expression of h^* in the form:

$$h^* = 0.92 r_0 [12\pi\mu N/(p-p_a)]^{2/3}$$

and substituting $r_0 = 1.25"$, $\mu = 2.7 \times 10^{-9}$ lb-sec/in; N = 750 RPS, the calculated gap width, based on the experimentally determined gauge pressure $p-p_a = 5.3$ psi, becomes:

$$h^* \approx 680 \text{ } \mu\text{inches}$$

while the gap width scaled directly from either oscillogram (i) or (e) in Fig. 46 gives:

$$h^* \approx 510 \ \mu\text{inches}$$

If, in addition to errors inherent in instrumentation, one bears in mind the effect of local foil-distortion on both pressure and gap measurements, a discrepancy of only 30% reflects favorably on the correlation. Furthermore, the expression of H^* is based on an approximate theory, which at $H^* \approx 0.92$ involves an uncertainty the order of $\pm 15\%$ [9].

The last figure in this section, Fig. 48, illustrates the influence of thermal transients. Shown are scans of gap width in the self-acting mode, obtained at three locations along the sector A_2. Each scan was recorded during a cycle consisting of acceleration to over 750 RPS, followed by an abrupt cutoff of turbine air and a coastdown to standstill.* Some gap growth due to heating undoubtedly occurred during acceleration to top speed, despite heat convection enhanced by discharge of turbine air. (Were it not so, the scans with increasing speed in Fig. 48 would be concave upward, rather than nearly rectilinear, or even convex.) It is also reasonable to assume that the expansion of journals contributed little to the variation of clearance, because the journal mass and that of the entire rotor constituted a much larger heat reservoir than the foils. With convective cooling diminished appreciably during the coastdown part of the cycle, a drastic increase of gap width occurred above the corresponding values of clearance recorded during acceleration, especially

*The observant reader will note that Fig. 48 is one of the exceptions to the chronological order of presentation. The oscillograms indicate that both starting and stopping were unaided by pressurization.

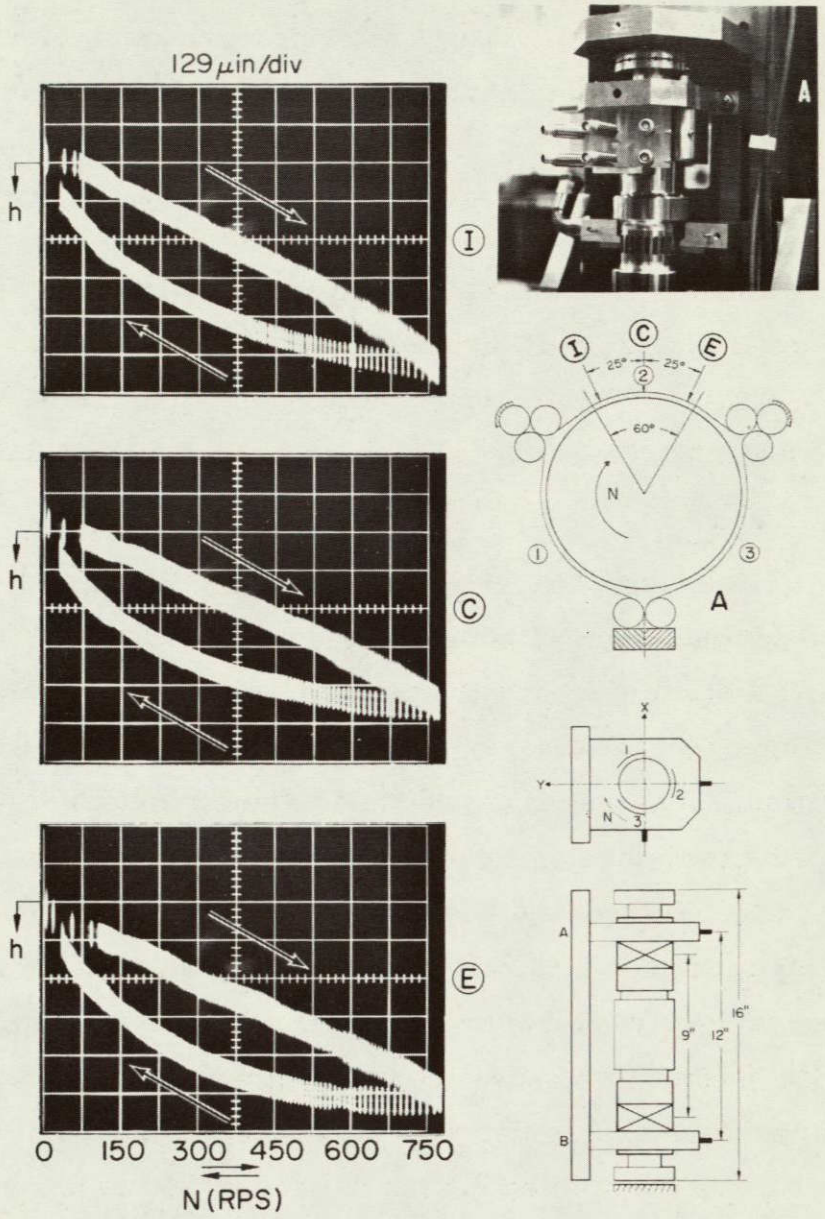

ROTOR : W = 21.25 lb ; r_t = 4.67" ; r_p = 1.045"
FOIL : t = 0.001" (Mo) ; 2b = 2.0"
PRELOAD : $T_o \approx 2.25$ lb/in
SURFACE TREATMENT : Cr_2O_3 FLAME-PLATED JOURNAL AND MoS_2-COATED FOIL

Fig. 48 Scans of Gap Width at 3 Positions along Sector of Self-Acting Foil Bearing during Slow Acceleration and Coastdown (Bearing Span = 9.0"; Journal Length = 2.0")

in the lower speed range. It became evident, therefore, that thermal growth associated with transients of this type was of significance commensurate with the preload tension T_o, the extensional rigidity Et, the flexural rigidity $D = Et^3/12(1-\nu^2)$ (Appendix 1), and the fluid inertia [1,9].

3.7 Operation Without Aid of External Pressurization with 2.0-inch Wide Foils at 9-inch Bearing Span, - Part I: Initial Start-Stops. Effect of Dry Lubricant. Additional Experiments with Symmetric and Asymmetric Imbalance. First Series of Multiple Starts and Stops

It was not difficult to overcome the initial friction torque at low levels of preload, even with a relatively inefficient air turbine. The mere capability of starting rotation, however, was not an end in itself. Rapid acceleration to a speed high enough to maintain adequate gas-lubrication was required. The preload tension had to be sufficiently low to permit rapid starting, yet high enough to furnish adequate constraint during rotation. The danger existed that relatively low preloads would lead to difficulties at high speeds, even if it were possible to traverse the resonant zone within acceptable amplitude limits.* Furthermore, it was not possible to predict in advance how the rotor would respond to appreciable frictional excitation anticipated during the initial stages of rotation.

The first attempts of starting without the aid of external pressurization, therefore, were accompanied by considerable apprehension. Preparations involved the enlargement of air passages leading to the nozzle ring, and the machining of additional nozzles, in line with the buckets to enhance the starting torque (See Fig. 1, item 9). A pattern of 10 alternatively

*See also Section 3.5, Fig. 27.

reflecting and light-scattering sectors was added to the end-face of each rotor. The pattern gave ten pulses per revolution, rather than one, so that scans of amplitudes during rapid acceleration could be recorded photographically with an adequate count density. The friction torque was measured at various preload tensions and it was finally decided to attempt the first "dry start" with a preload of $T_o \approx 1.5$ lb/in. The fully hardened, 440-C journals and the molybdenum foils were thoroughly cleaned with a solvent (tetrahydrofuran), and the average breakaway friction torque was $M_f \approx 3.95$ in-lb.*

The scans of amplitudes recorded during the first "dry start" with a preload of 1.5 lb/in, and the corresponding coastdown scans, are shown in Fig. 49. The time required to attain 150 RPS was 4 seconds, as compared with 235 seconds required for coastdown from the same speed. The peak-to-peak amplitudes of motion in the resonant bandwidth did not exceed 250 μinches. The difference between the envelopes of scans during acceleration and deceleration is quite apparent. Although differences in response with increasing and decreasing speed, due to both temperature changes and nonlinear effects, have been observed in the course of previous experiment, the additional factor in this case was the very rapid passage through the resonant bandwidth.

Encouraged by initial success, "dry starting" was next attempted with nominal preload tension increased by 25%, from $T_o \approx 1.5$ lb/in to $T_o \approx 1.875$ lb/in. The average breakaway friction torque in this case was $M_f \approx 5.35$ in-lb. The results of this test, illustrated in Fig. 50, were similar to those presented in Fig. 49. The retensioning of foils increased only slightly the overall stiffness, but had an appreciable effect on friction, as evidenced by an almost fourfold decrease in coastdown time from 150 RPS.

*Average of 10 torque readings. After each clockwise slip, the rotor was turned counterclockwise, then clockwise again before each torque measurement.

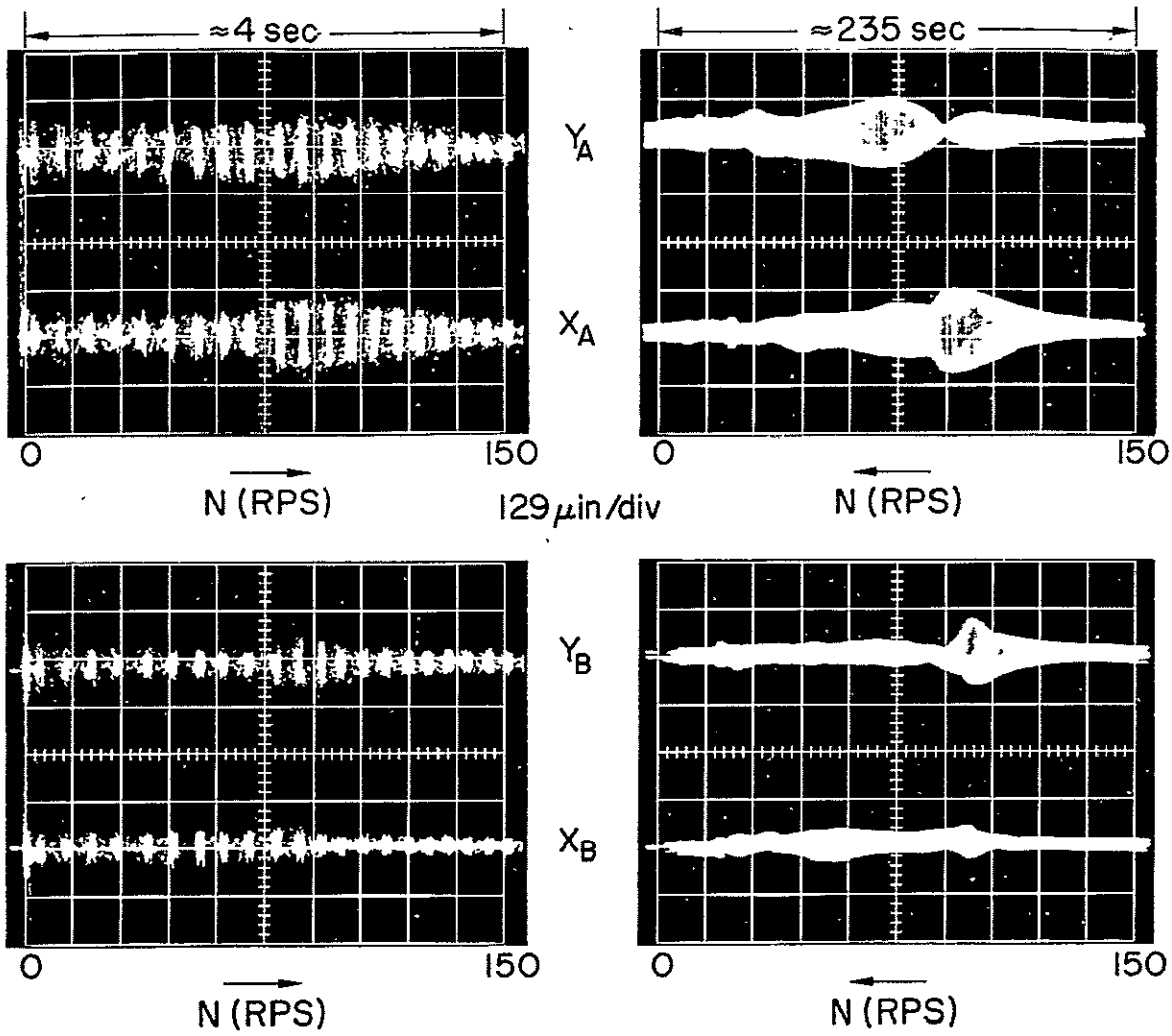

ROTOR : W=20.9 lb ; r_p=1.05" ; 440-C (ROCK. C-56)
FOILS : t =0.001" (Mo) ; 2b=2.0"
PRELOAD: $T_o \approx 1.5$ lb/in
STARTING FRICTION-TORQUE : $M_f \approx 3.95$ in-lb

Fig. 49 Scans of Response During Starting and Stopping Unaided by External Pressurization. - First Trial with Plain Molybdenum Foil and 440-C Journals at $T_o \approx 1.5$ lb/in (Bearing Span = 9.0"; Journal Length = 2.0")

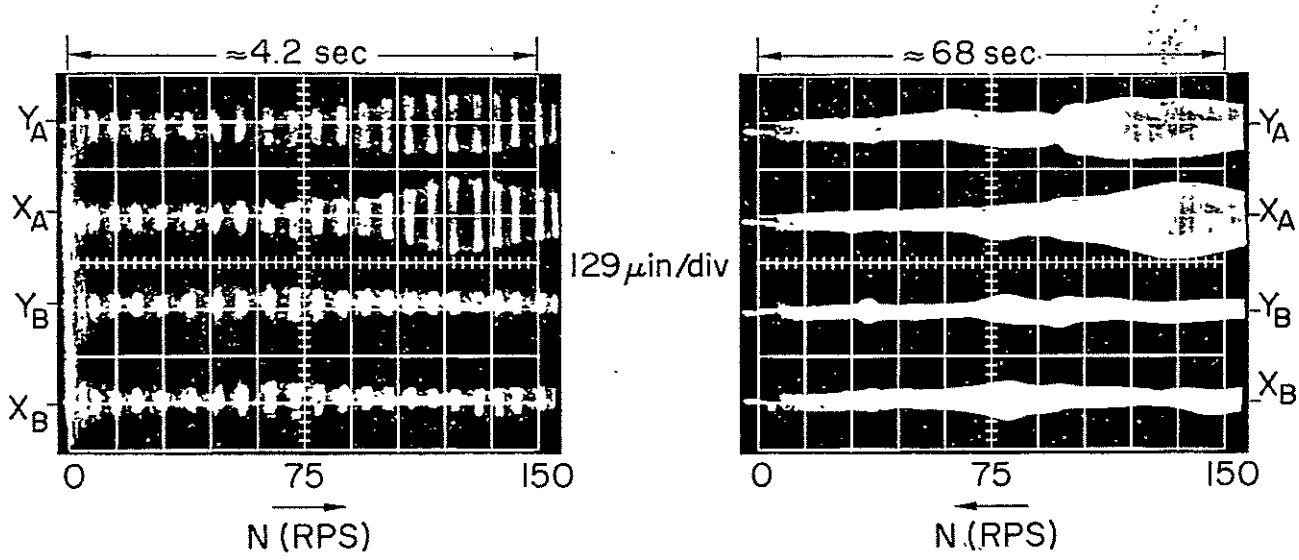

ROTOR : W = 20.9 lb ; r_p = 1.05" ; 440-C (ROCK. C-56)
FOILS : t = 0.001" (Mo) ; 2b = 2.0"
PRELOAD : $T_o \approx 1.875$ lb/in
STARTING FRICTION-TORQUE : M_f = 5.35 in-lb

Fig. 50 Scans of Response During Starting and Stopping Unaided by External Pressurization. - Second Trial with Plain Molybdenum Foils and 440-C Journals at $T_o \approx 1.875$ lb/in. (Bearing Span = 9.0"; Journal Length = 2.0")

Although repeated starts and stops with plain foils and journals caused no degradation of performance, further improvement was expected if the foils, or the journals, or both surfaces could be coated with a dry lubricant. Since the foils were molybdenum, in situ deposition of MoS_2 was first considered [22,23]. The idea was abandoned, however, because of inherent difficulties in treating molybdenum, and foils in particular. An inorganically bonded, air-dried MoS_2 - film was applied instead.* The first foil specimens were prepared by the manufacturer, but since the process required thorough degreasing, cleaning and spraying only, the art of application was perfected in our laboratory. The films were applied with a cup-fed spray gun to an average and sensibly uniform thickness of 100-200 μinches, then gently buffed and polished to smooth the initially granular surface-texture.

The first set of foils coated with MoS_2 was used in conjunction with rotor No. 2. The rotor had no orifices and was, with the exception of end plugs, made of a single piece of 440-C steel. It had less tendency to bend at high RPS, probably because of greater internal symmetry and slightly greater stiffness. The journals were flame plated with Cr_2O_3 prior to grinding. The porous chromium oxide was very compatible with the MoS_2 film and the average breakaway friction torque was only 3.23 in-lb, despite an additional increase of preload to $T_o \approx$ 2.25 lb/in. Starting and stopping was uneventful and the resonant amplitudes were very small, probably because of the smallness of the residual imbalance ($u < 150$ μin-oz). The results corresponding to the foregoing test condition are presented in Fig. 51. The largest orbit in the resonance zone during coastdown, at approximately 80 RPS, was actually much smaller than the excursions associated with the initial stages of rotation. The motion at resonance was quasi-conical and the displacement of the rotor axis at 750 RPS was 800 μinches, in the

*Dow Corning designation DC 1-3931. The manufacturer claims the bond of the film is effective to temperatures the order of 1000°F.

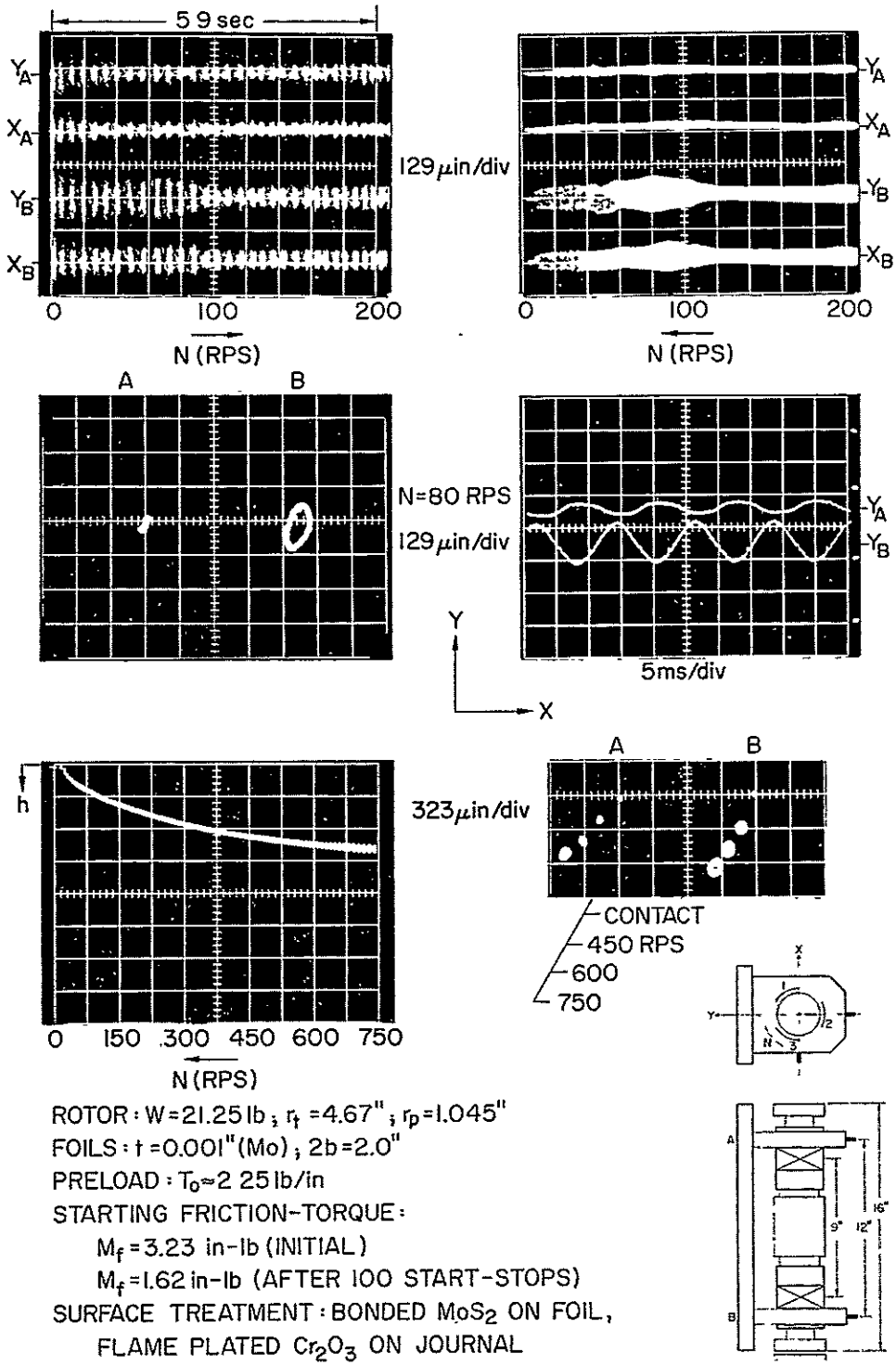

Fig. 51 Motion of Rotor near Resonance and Scans of Response. Starting and Stopping Unaided by Pressurization. - Scan of Gap Width and Displacement of Rotor Axis with Speed (Bearing Span = 9.0"; Journal Length = 2.0")

3-rd quadrant and inclined at 45°-60° with the negative X-axis. The scan of clearance in Fig. 51 is probably one of the most clearly defined traces recorded in the course of this investigation. The clearance at the foil sector A_2 was 790 μinches at 600 RPS and 830 μinches at 750 RPS. Following a limited number of "dry" starts and stops performed in the course of gathering the data presented in Fig. 51, the rotor was subjected to 100 consecutive start-stops. The procedure was to crack the turbine throttle wide open, to accelerate to approximately 50 to 75 RPS, and to cut off the turbine air and coast down to standstill. As soon as the rotor came to a full stop, the sequence was repeated again. No change in performance was observed, but the breakaway friction torque was reduced from 3.23 in-lb to approximately 1.62 in-lb, probably because of the initial wear-in process of the MoS_2 film and the porous Cr_2O_3 coating.

In order to gain further confidence in starting unaided by pressurization, the rotor was started and operated throughout the entire speed range, with excitation furnished by the largest amounts of symmetric and asymmetric imbalance yet applied in the course of these experiments. The motion excited by a symmetric imbalance of $\bar{u}$ = 28,300 μin-oz is illustrated in Fig. 52. A quasi-cylindrical resonance at 75 RPS was followed by a subharmonic resonance, with maximum amplitude at 114 RPS. The largest peak-to-peak amplitudes were of the order of 1480 μinches. The reader will note again the rather interesting mode of motion in the zone of subharmonic resonance. Each clover-leaf orbit was described in 2 clockwise revolutions, and major and minor maxima and minima occurred almost simultaneously in the Y-plane. The high-speed orbits were less than 200 μinches, peak-to-peak, and the motion was nearly cylindrical. Scans of response during acceleration and during coastdown are shown in Fig. 53. To be noted is the fact that the excursions following starting appeared to be commensurate with resonant amplitudes, both synchronous and subharmonic.

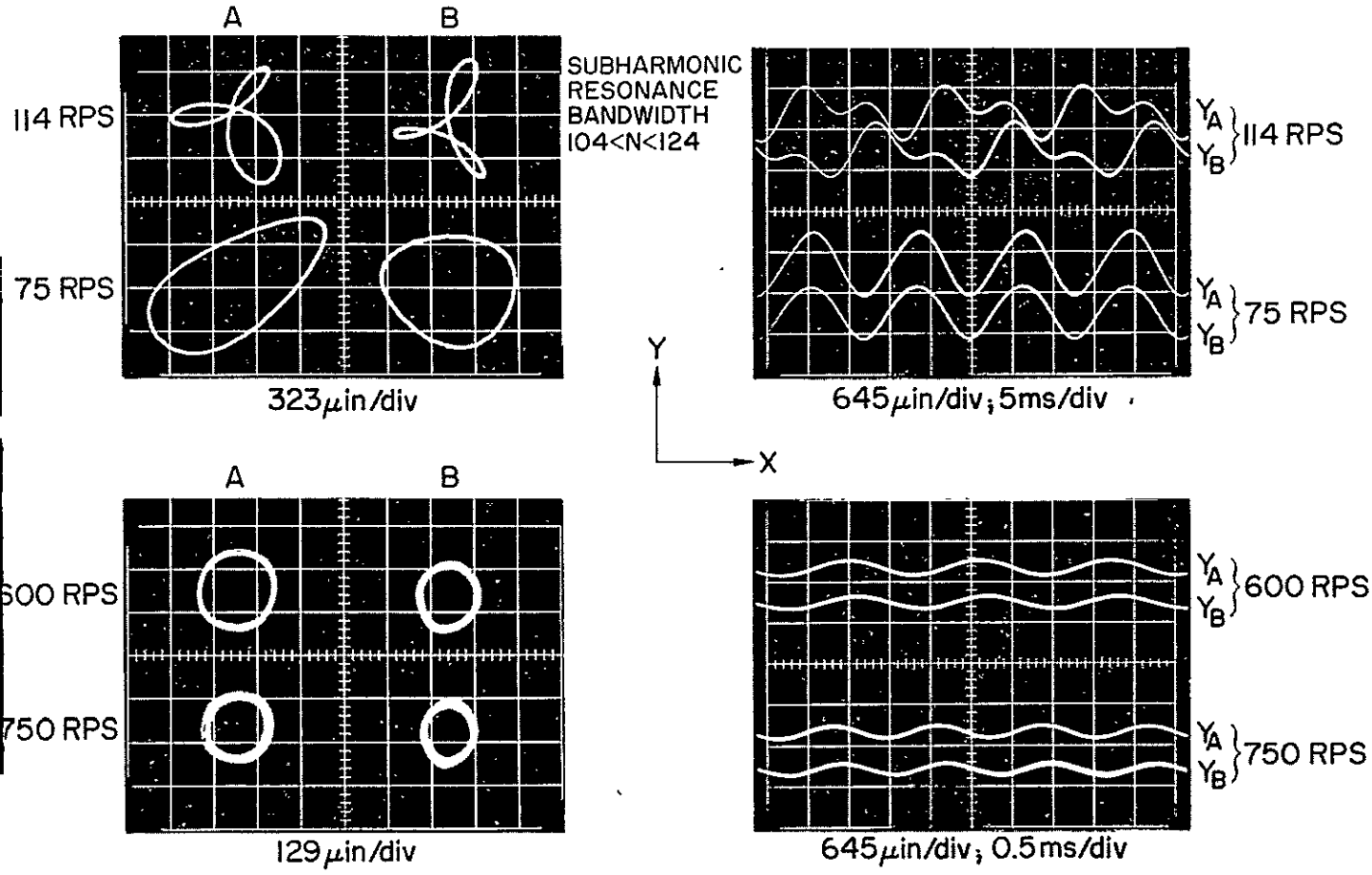

ROTOR : W = 21.25 lb ; r_f = 4.67" ; r_p = 1.045"
FOILS : t = 0.001"(Mo) ; 2b = 2.0"
PRELOAD : $T_o \approx 2.25$ lb/in
STARTING FRICTION-TORQUE :
M_f = 3.23 in-lb (INITIAL)
M_f = 1.62 in-lb (AFTER 100 START-STOPS)
SURFACE TREATMENT : BONDED MoS_2 ON FOIL,
FLAME PLATED Cr_2O_3 ON JOURNAL
IMBALANCE : $\bar{u}$ = 28,300 μin-oz (IN EACH PLANE)

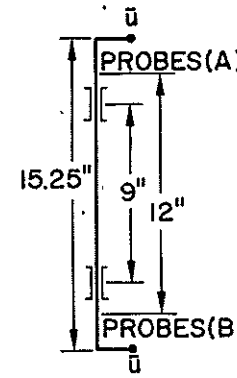

Fig. 52 Motion with Symmetric Imbalance. - Orbits and Motion in Y-Plane in Resonant and High-Speed Range. Subharmonic Resonance. Starting and Stopping Unaided by Pressurization (Bearing Span = 9.0"; Journal Length = 2.0")

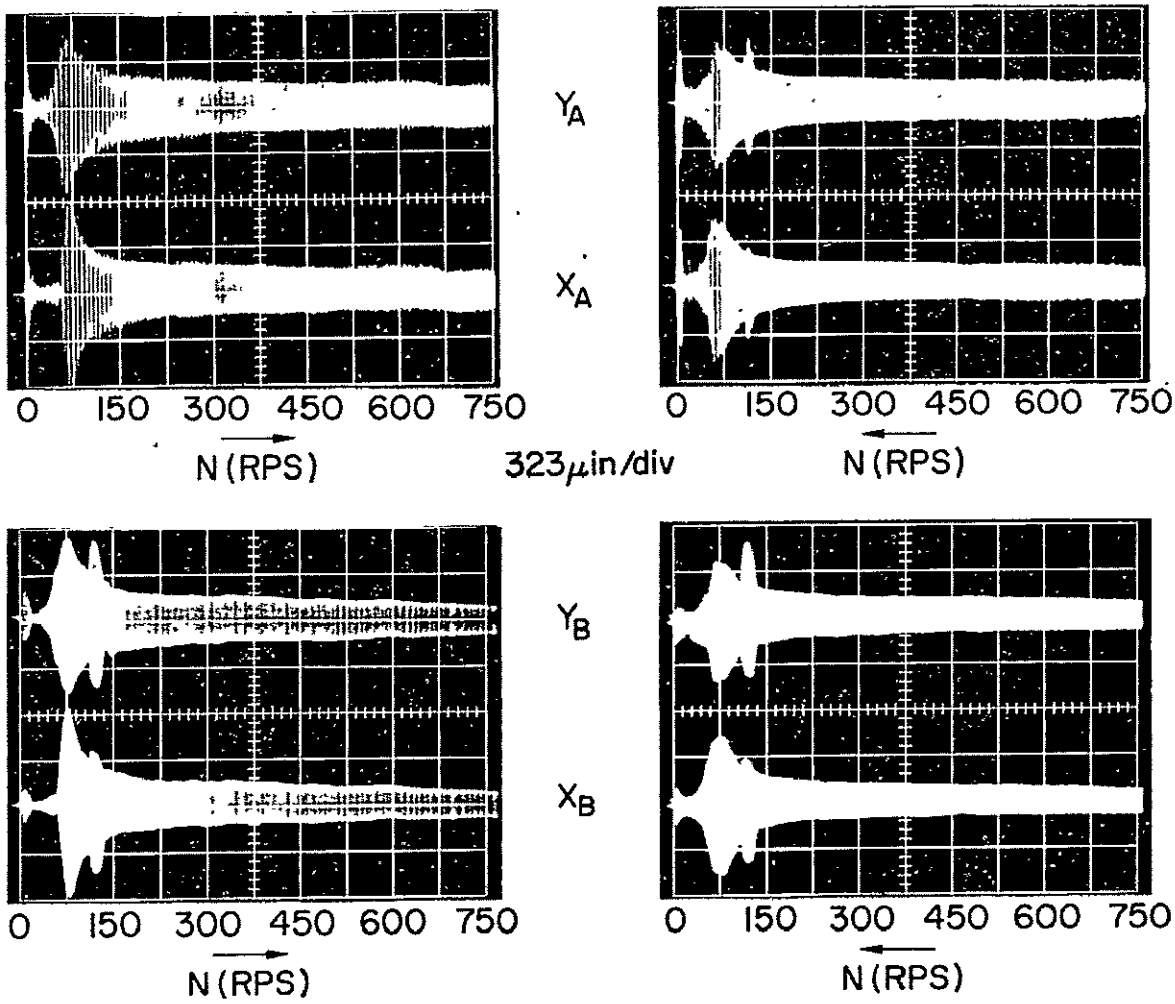

ROTOR : W = 21.25 lb ; r_t = 4.67" ; r_p = 1.045"
FOILS : t = 0.001" (Mo) ; 2b = 2.0"
PRELOAD : $T_0 \approx 2.25$ lb/in
STARTING FRICTION-TORQUE :
M_f = 3.23 in-lb (INITIAL)
M_f = 1.62 in-lb (AFTER 100 START-STOPS)
SURFACE TREATMENT : BONDED MoS_2 ON FOIL,
FLAME PLATED Cr_2O_3 ON JOURNAL
IMBALANCE : $\bar{u}$ = 28,300 μin-oz (IN EACH PLANE)

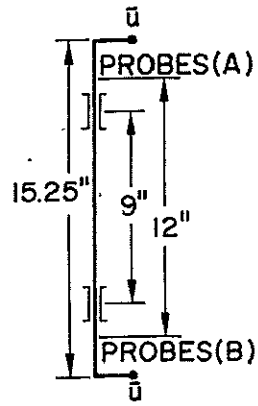

Fig. 53 Scans of Rotor Response with Symmetric Imbalance. Starting and Stopping Unaided by Pressurization (Bearing Span = 9.0"; Journal Length = 2.0")

The motion excited by an asymmetric imbalance of $\bar{u} = 15{,}600$ μin-oz is illustrated in Fig. 54. No subharmonic resonance was observed in the course of this run,* and the largest synchronous orbits, approximately 1800 μinches peak-to-peak, were observed at 72 RPS. The motion was conical throughout the speed range and the scans of amplitudes during acceleration and deceleration are shown in Fig. 55. The series of tests, results of which are contained in Fig. 52 through Fig. 55 included a total of over 150 starts and stops unaided by external pressurization, in the course of which no degradation of operational characteristics could be observed.

3.8 Operation Without Aid of External Pressurization with 2.0-inch Wide Foils at 9-inch Bearing Span, -Part II: Multiple Start-Stops and Motion During Initial and Final Stages of Rotation

When starting and stopping without the aid of external pressurization, the time required to complete the first and last 10 to 20 revolutions was too short to assess visually the magnitude of excursions from the oscilloscope displays. In subsequent multiple start-stop tests, therefore, rotor orbits were recorded during the initial and final stages of rotation. The oscilloscope camera-shutter was held open until the rotor reached the speed of 30 to 50 RPS, and the converse procedure applied during coastdown. Oscillograms of this type were obtained at regular intervals, usually after each 20-th or 25-th coastdown. It was anticipated that the frictional excitation during the initial and final stages of rotation, though essentially torsional, would induce also lateral and pitching components because of inherent dissymmetries between bearings, bearing sectors, and turbine nozzles. The objective was to record the rotor response to this type of excitation and thus to determine not only the magnitude of the

*Compare with results presented in Fig. 24 and Fig. 39.

⊕ 3

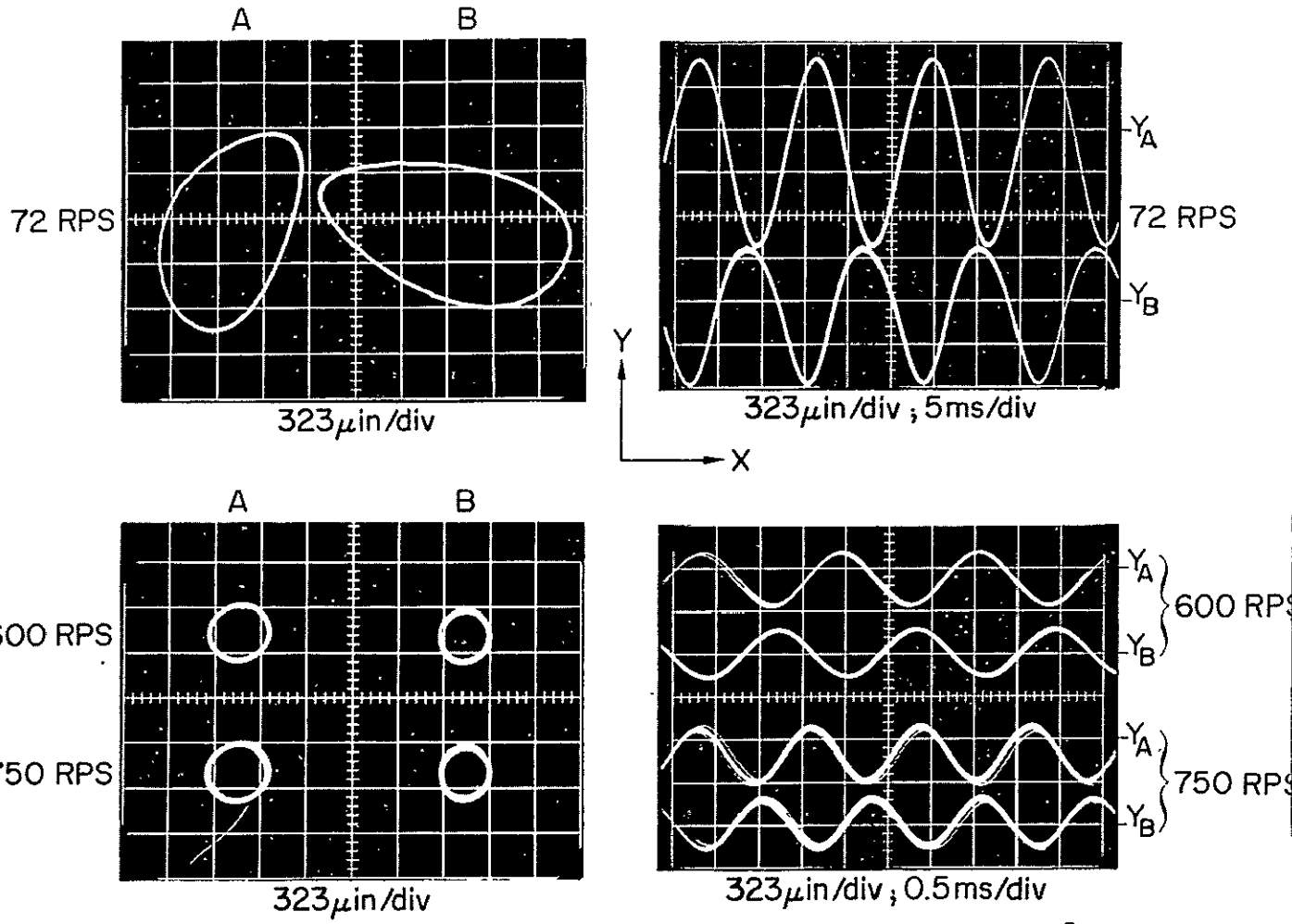

ROTOR : W = 21.25 lb ; r_f = 4.67" ; r_p = 1.045"
FOILS : t = 0.001" (Mo) ; 2b = 2.0"
PRELOAD : $T_o \approx 2.25$ lb/in
STARTING FRICTION-TORQUE :
M_f = 3.23 in-lb (INITIAL)
M_f = 1.62 in-lb (AFTER 100 START-STOPS)
SURFACE TREATMENT : BONDED MoS_2 ON FOIL,
FLAME PLATED Cr_2O_3 ON JOURNAL
IMBALANCE : $\bar{u}$ = 15,600 μin-oz (IN EACH PLANE)

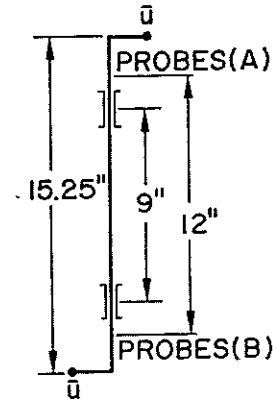

Fig. 54 Motion with Asymmetric Imbalance. - Orbits and Motion in Y-Plane in Resonant and High Speed Range. Starting and Stopping Unaided by Pressurization (Bearing Span = 9.0"; Journal Length = 2.0")

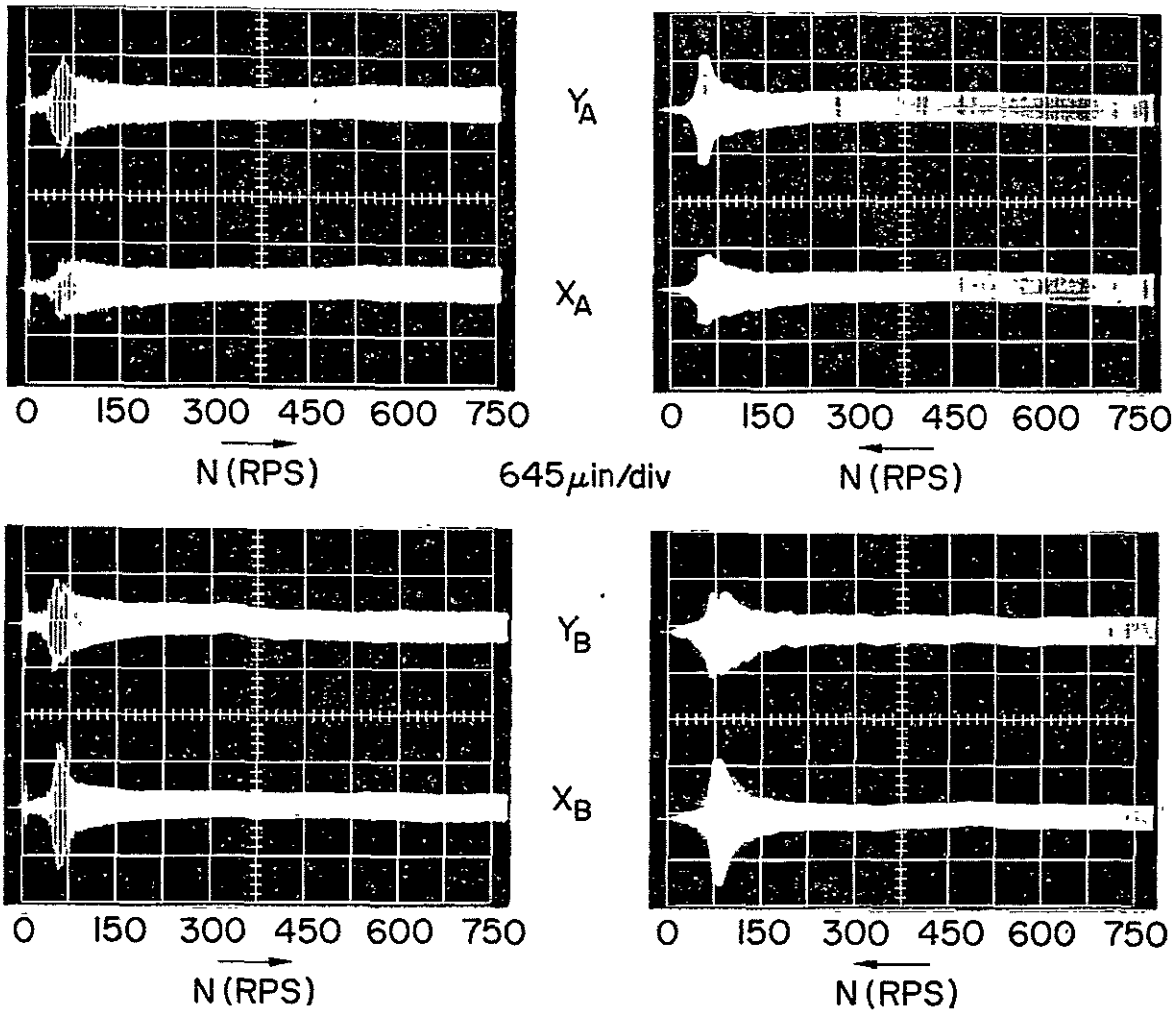

ROTOR : W = 21.25 lb ; r_f = 4.67" ; r_p = 1.045"
FOILS : t = 0.001" (Mo) ; 2b = 2.0"
PRELOAD : $T_o \approx 2.25$ lb/in
STARTING FRICTION-TORQUE :
M_f = 3.23 in-lb (INITIAL)
M_f = 1.62 in-lb (AFTER 100 START-STOPS)
SURFACE TREATMENT : BONDED MoS_2 ON FOIL,
FLAME PLATED Cr_2O_3 ON JOURNAL
IMBALANCE : $\bar{u}$ = 15,600 μin-oz (IN EACH PLANE)

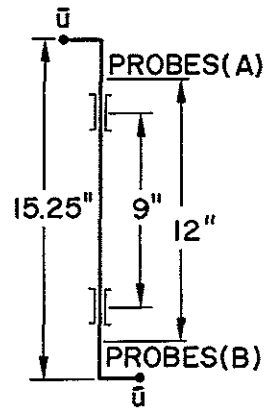

Fig. 55 Scans of Rotor Response with Asymmetric Imbalance. Starting and Stopping Unaided by Pressurization (Bearing Span = 9.0"; Journal Length = 2.0")

initial and final excursions, but also whether the trend developed with the number of start-stop cycles was random or regular.

The first series of such oscillograms is presented in Fig. 56 and Fig. 57. The results apply to rotor No. 1, the journals of which were 440-C steel, hardened to approximately C-56 Rockwell. The molybdenum foils were MoS_2-coated, as described in Section 3.7, and preloaded to $T_o \approx 2.25$ lb/in. The average breakaway friction torque was initially $M_f = 4.25$ in-lb. The left column of oscillocope photographs in Fig. 56 contains histories of initial rotation, while the oscillograms in the right column portray the final stages of rotation. The observed trend in starting, following the 21-st cycle, was a steady decrease of maximum excursions, from approximately 930 μinches peak-to-peak at the 21-st start, to 260 μinches after the 101-st. The orbital motion during the final stages of rotation produced smaller excursions and displayed consistently regular, inwardly spiralling paths. Maxima, prior to stopping, did not exceed 325 μinches peak-to-peak. It is of interest to note that on starting the orbits were larger at A, while during coastdown the excursions were larger at B.

Upon completion of the 101-st cycle, both bearings were thoroughly flushed with freon. This eliminated a considerable amount of MoS_2 and binder debris from the bearing interspace, resulting no doubt in the relaxation of the initial preload tension due to removal of the worn portion of the MoS_2 film. The 102-nd cycle, Fig. 57, produced, consequently, an increase of orbit size during starting and stopping, the largest orbits of 1615 μinches peak-to-peak occurring now exclusively at A. The foils were subsequently unlocked and preloaded again to the initial value of $T_o \approx 2.25$ lb/in. The average starting torque increased to $M_f = 5.25$ in-lb. The retensioning resulted in a considerable reduction of excursions, as evidenced by the start-stop history of the 103-rd cycle.

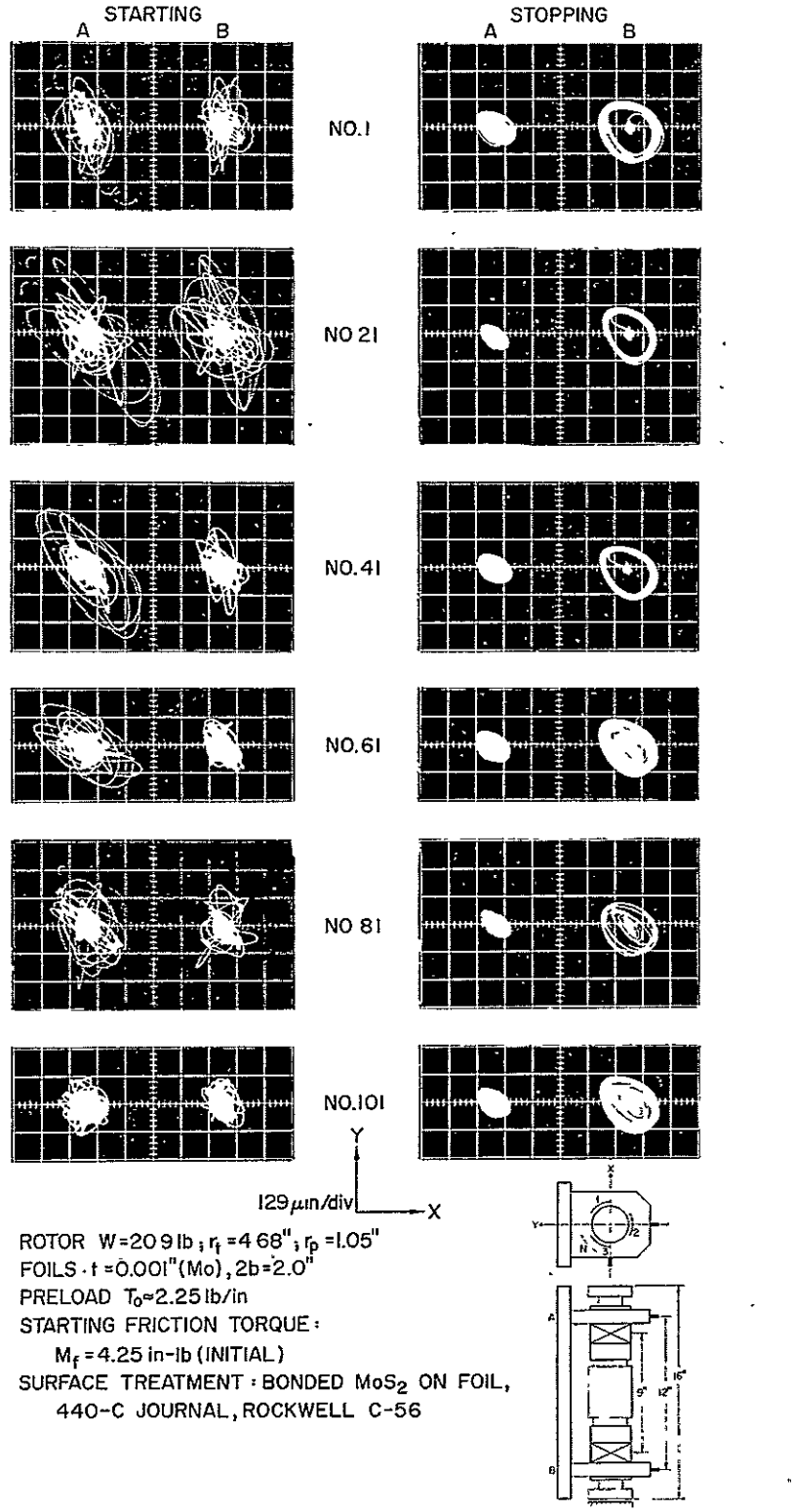

Fig. 56 Rotor Orbits During Starting and Stopping. - 101 Consecutive Start-Stops Unaided by Pressurization with 440-C Journal and MoS_2 - Coated Foil (Bearing Span = 9.0"; Journal Length = 2.0")

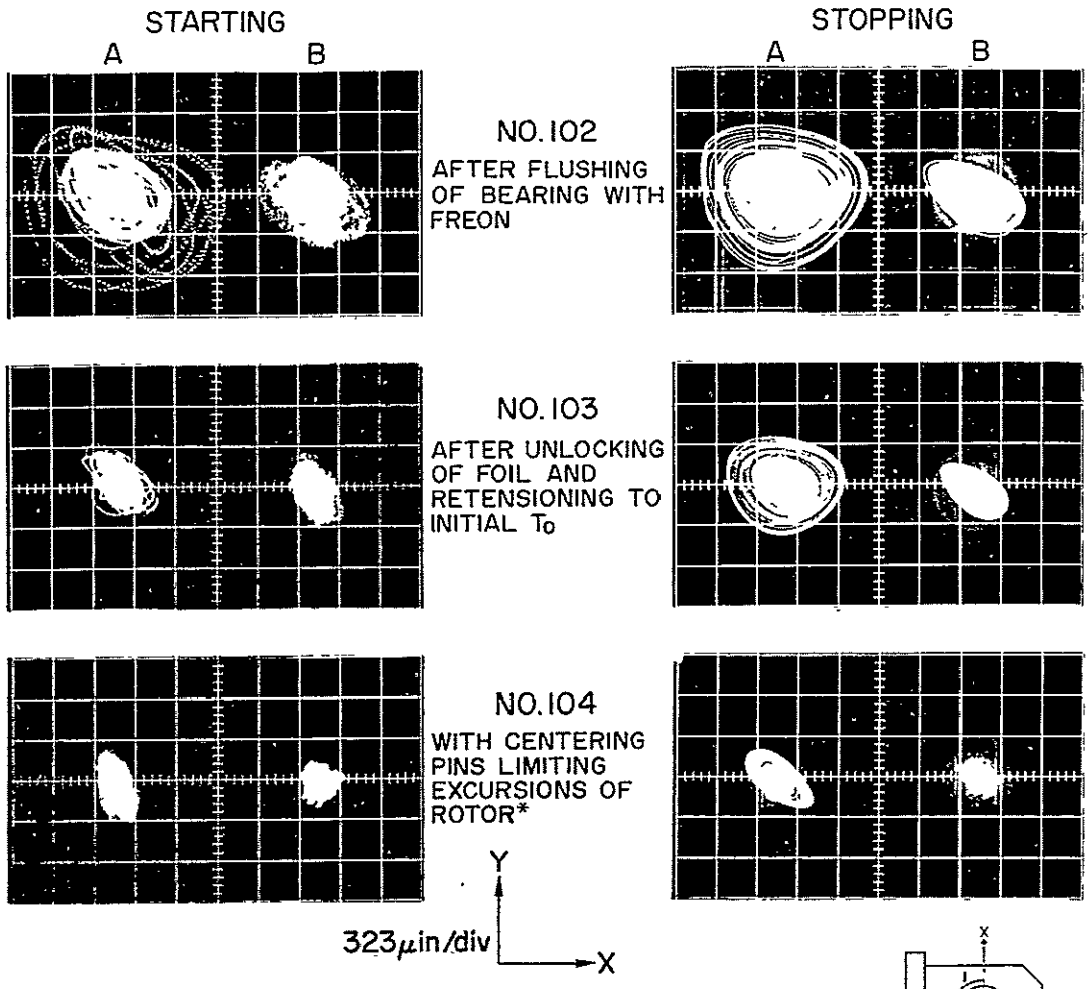

ROTOR: W=20.9 lb; r_f =4.68"; r_p=1.05"
FOILS: t =0.001" (Mo); 2b=2.0"
PRELOAD: T_o≈2.25 lb/in
STARTING FRICTION-TORQUE: M_f =4.25 in-lb (INITIAL)
M_f =5.25 in-lb (AFTER 102 START-STOPS, FLUSHING AND RETENSIONING)
SURFACE TREATMENT: BONDED MoS_2 ON FOIL AND 440-C JOURNAL, ROCKWELL C-56.
*MAXIMUM CLEARANCE CIRCLE DIAMETER 0.0015"

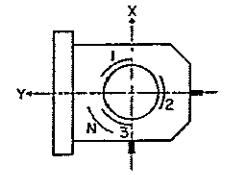

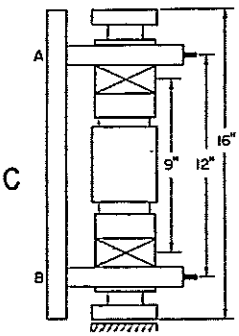

Fig. 57 Rotor Orbits During Starting and Stopping after 101 Consecutive Start-Stops, Flushing of Bearings and Retensioning to Initial Preload (440-C Journals and MoS_2 - Coated Foils. Bearing Span = 9.0"; Journal Length = 2.0")

At this point, an attempt was made to investigate, however superficially, the effect of mechanical stops on limiting the rotor excursions at low speeds. The centering pins and alignment holes at the ends of the rotor, Fig. 1, were useful for this purpose. The actual diametral clearance of these 0.3125" dia. pins was less than the nominal 0.0015". The pins were very effective as mechanical stops, as illustrated by the oscillograms of the 104-th cycle in Fig. 57*.

The next and last series of multiple starts and stops unaided by pressurization was conducted with rotor No. 3, the journals of which were flame-plated with aluminum oxide. It was decided to apply a MoS_2-coating to both the foil and the $A\ell_2O_3$-plated journals. The mating surfaces were sprayed as evenly as was feasible to a thickness of 100 to 200 μinches of dry lubricant.

No special effort was made to control the thickness and texture to a high degree of uniformity and accuracy beyond what could be achieved by a skilled hand and a spray gun. The results of this test are presented in Fig. 58 and Fig. 59 in a manner analogous to Fig. 56 and Fig. 57. The initial breakaway friction torque, at a preload $T_o \approx 2.25$/in, was $M_f = 5.1$ in-lb. The number of consecutive start-stop cycles in this test was increased to a total of 156. The orbits during starting were larger than in the case of the untreated steel-journal, Fig. 56 and Fig. 57. The maximum peak-to-peak excursions increased at first, but did not vary greatly between the 26-th and the 151-st cycle, Fig. 59. The largest peak-to-peak excursion recorded at the 76-th start was approximately 2000 μinches, as compared with 520 μinches prior to stopping, Fig. 58. The coastdown orbits, in

*A small concentric pin has an obvious advantage over a stop acting at the journal periphery. The frictional moment and the ensuing excitation are reduced, but this arrangement may not always be possible.

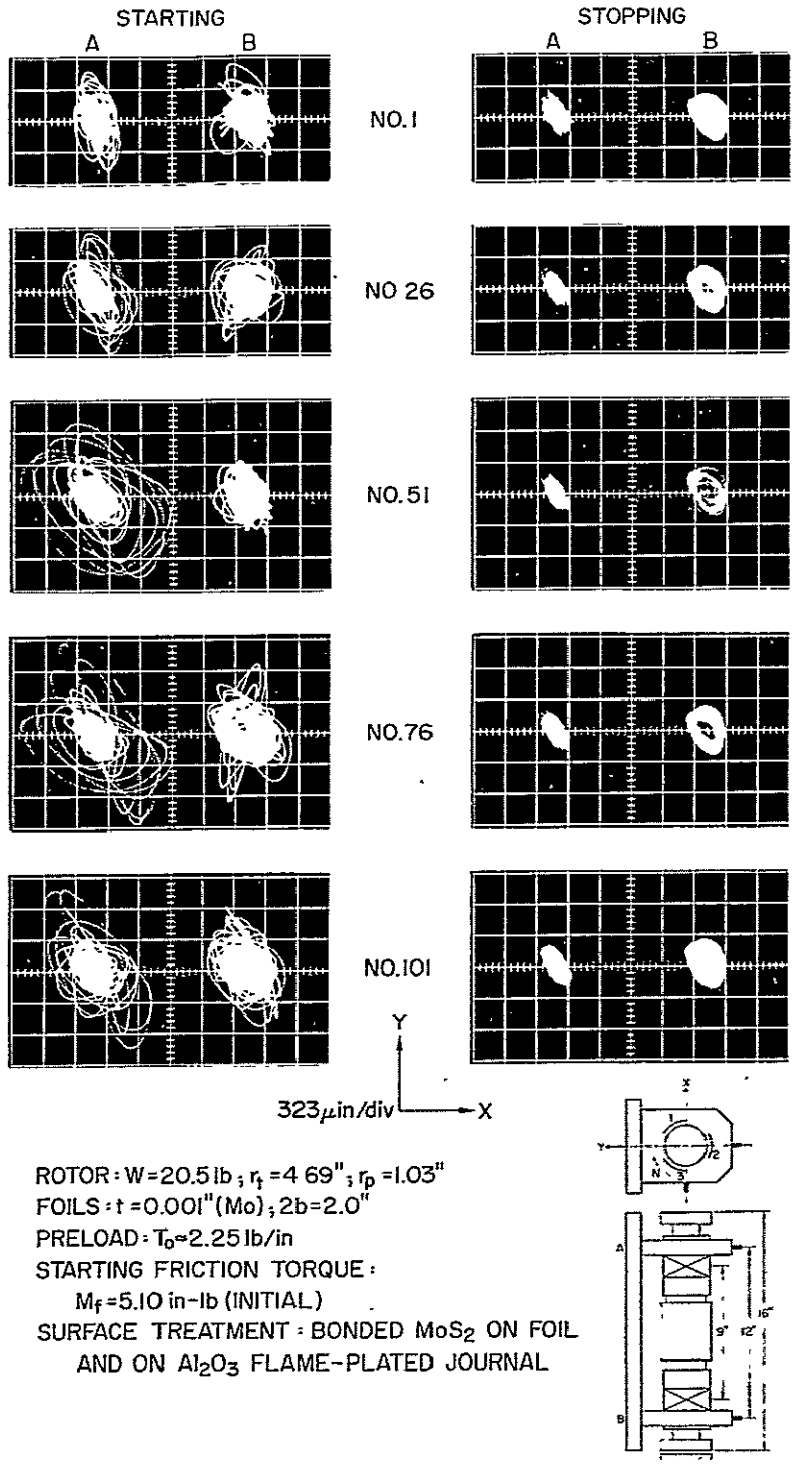

Fig. 58 Rotor Orbits During Starting and Stopping. - 101 Consecutive Start-Stops Unaided by Pressurization with Foils and Al_2O_3 Flame-Plated Journals Coated with MoS_2 (Bearing Span = 9.0"; Journal Length = 2.0")

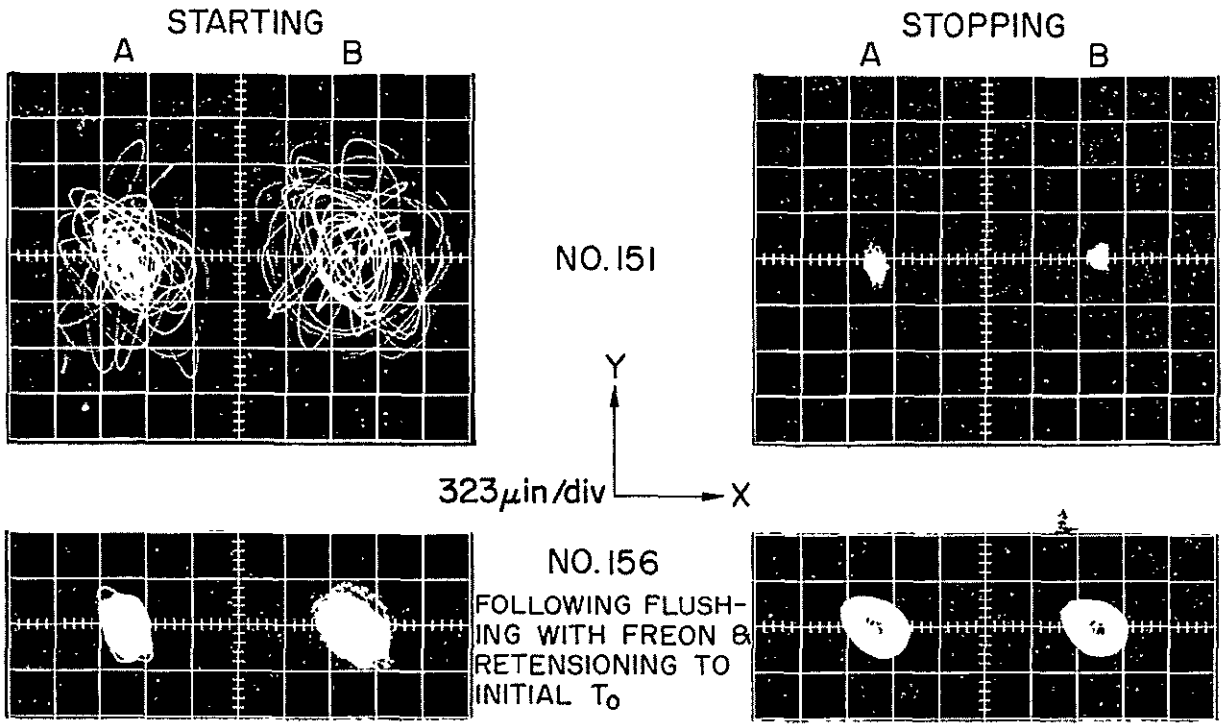

ROTOR : W = 20.5 lb ; r_t = 4.69" ; r_p = 1.03"
FOILS : t = 0.001"(Mo) ; 2b = 2.0"
PRELOAD : $T_o \approx 2.25$ lb/in
STARTING FRICTION TORQUE :
M_f = 5.10 in-lb (INITIAL)
M_f = 4.20 in-lb (FOLLOWING FREON FLUSH AND RETENSIONING AFTER 151 START-STOPS)
SURFACE TREATMENT : BONDED MoS_2 ON FOIL AND ON Al_2O_3 FLAME-PLATED JOURNAL

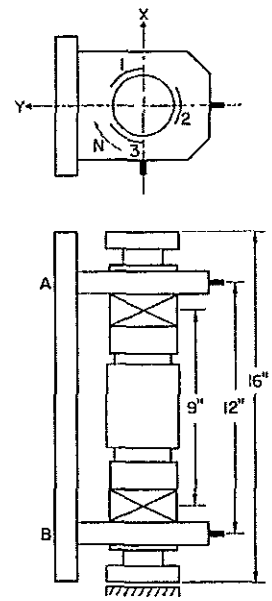

Fig. 59 Rotor Orbits During Starting and Stopping Following 150 Consecutive Start-Stops and after Flushing of Bearings and Retensioning to Initial Preload (Foils and Al_2O_3 Flame-Plated Journal Coated with MoS_2. (Bearing Span = 9.0"; Journal Length = 2.0")

addition to being relatively small in size, exhibited also a regular, inwardly spiralling pattern.

The effect of frictional excitation on the magnitude of excursions appeared to be much more pronounced during the rapid transient of initiating the motion, rather than in the course of the more gradual coastdown and in the absence of excitation originating in the turbine. Upon completion of the 151-st cycle, the foils were unlocked and the system copiously flushed with freon. Following the retensioning of the foils to the initial preload of $T_o \approx 2.25$ lb/in, the average breakaway friction torque decreased to $M_f = 4.20$ lb/in. The drastic reduction of orbit size during starting, to a peak-to-peak maximum of approximately 650 μinches at the 156-th start, is illustrated in the last row of oscillograms in Fig. 59.

The multiple start-stop tests described in Sections 3.7 and 3.8 exceeded all expectations. It appeared feasible that the number of cycles could be increased by an order of magnitude, without rendering the foil-bearing support inoperative. Furthermore, starting and stopping was possible with both coated and uncoated bearing surfaces, and with preloads adequate to ensure satisfactory operation at low and at high speeds.

3.9 Operation Without Aid of External Pressurization with 1.5-inch Wide Foils at 9-inch Bearing Span, -Part III: Further Reductions of Foil Width. Effect of Friction on Starting. Excitation by Symmetric and Asymmetric Imbalance

The experimental results summarized in this section represent a step above and beyond the objectives set forth in the beginning of this investigation. Described in the following paragraphs are comprehensive performance tests of a foil rotor-support, in which the bearing length was reduced by an additional 25%, from 2b = 2.0" to 2b = 1.5", without increasing the 9" bearing span. The experiments, in addition to proving

the supportworthiness of a relatively short foil bearing, produced important information with regard to frictional effects during the initial and final stages of rotation. The latter constitute the starting point of the present narrative and additional details are presented in Appendix 3.

The first preload applied to 1.5" wide foils was approximately 2.25 lb/in. The foils were MoS_2-coated and supported the rotor with Cr_2O_3-plated journals. Although no difficulty was experienced in starting, the excursions were excessive. The preload tension was subsequently reduced in several steps, until at $T_o = 1.5$ lb/in the maximum orbits on starting were less than 750 μinches peak-to-peak. Subsequent tests, described in Appendix 3, showed a definite correlation between the frequency of the quasi-harmonic motion, induced by friction at slow rotation, and the resonant frequency of the rotor supported by the foils. These frequencies were nearly coincident at $T_o \approx 2.25$ lb/in and diverged with the reduction of initial tension. The obvious inference was that the large orbits encountered during the first attempts of "dry" starting at higher preloads were caused by the proximity of the frequency of frictional excitation to the resonant bandwidth of the foil-rotor system. This discovery was useful from a practical point of view, to say the least.

Having established a preload level suitable for starting, the rotor was put through the usual series of tests. The response to remanent imbalance ($\bar{u} < 150$ μin-oz), the displacement of the rotor axis with speed, and the gap measurement at the foil sector A_2, both during acceleration and coastdown, are presented in Fig. 60. Resonances occurred close to 95 RPS and exhibited very small orbits. High-speed operation presented no problems, and the maximum displacement of the rotor axis was of the order of 550 μinches at 750 RPS, in the 3-rd quadrant and at 45° - 60° with the negative X-axis. The gap width attained 520 μinches at 750 RPS and was larger during coastdown, but the increase was much less pronounced than in Fig. 48.

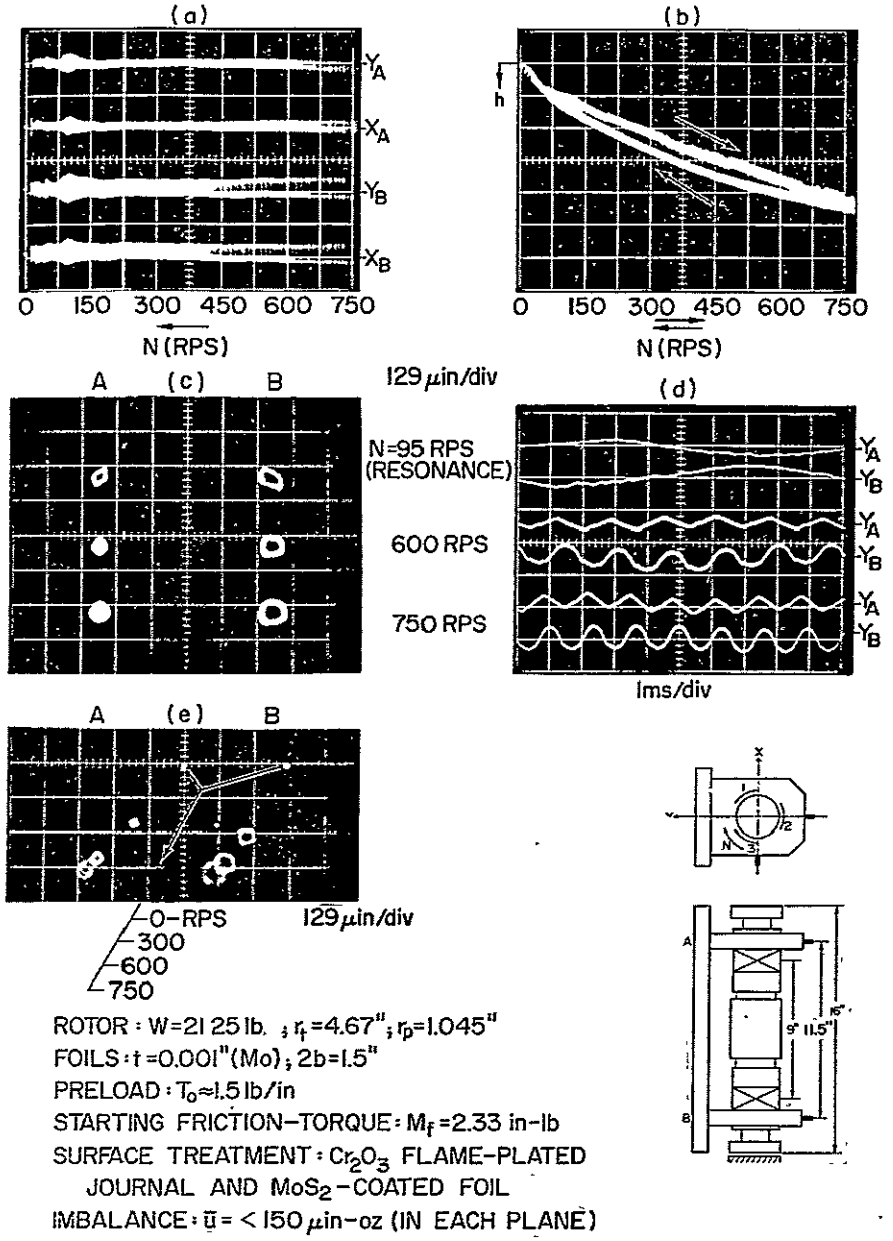

Fig. 60 Motion of Rotor in Self-Acting Foil Bearings and Scans of Response to Remanent Imbalance in Resonant and High-Speed Range. Displacement of Rotor Axis with Speed. (Bearing Span = 9.0"; Journal Length = 1.5")

(a) Scans of Response to Remanent Imbalance
(b) Scans of Gap Width
(c), (d) Orbits and Motion in Y-Plane in Resonant and High Speed Range
(e) Displacement of Rotor Axis with Speed

The response to symmetric imbalance of $\bar{u}$ = 15,600 μin-oz exhibited a maximum orbit of 930 μinches peak-to-peak at 105 RPS. The orbits are illustrated in Fig. 61(c), (d) and (e), of which (e) contains a superposition of several orbits in the resonant bandwidth $90 < N < 120$ RPS. The motion was nearly cylindrical at 105 RPS, Fig. 61(d), and a subharmonic resonance occurred in the interval $175 < N < 185$ RPS. Very symmetric, subharmonic orbits, and a superposition of several such orbits, are illustrated in Fig. 61(f) and (h). The corresponding motion in the Y-plane, Fig. 61(g), shows again the correspondence of minima and maxima in the monitoring planes A and B. In addition, Fig. 61 contains also amplitude scans, (a) and (b), and oscillograms of the cylindrical motion at 600 and 750 RPS, (i) and (j). Comparing the magnitudes of imbalance and the maximum amplitudes relevant to data presented in Fig. 52 and Fig. 61, it is self evident that an appreciably larger, symmetric imbalance than $\bar{u}$ = 15,600 μin-oz could be safely accommodated by the bearings, despite the reduction in length from 2.0" to 1.5".

The response to excitation by an asymmetric imbalance of $\bar{u}$ = 9,750 μin - oz is illustrated in Fig. 62. The oscillograms (a) and (b) contain scans of amplitude response during coastdown. The largest orbit, at A, was 920 μinches peak-to-peak, and the motion was nearly conical. The orbits in the resonant bandwidth and the time-base traces of motion in the Y-plane are shown in the second row of photographs in Fig. 62. The motion at high speed is illustrated in the same figure in the oscillograms (f) and (g). The reader may compare the results of Fig. 62 with those of Fig. 54 and conclude that, in this case also, the safe limit of asymmetric imbalance could have been considerably higher.

The tests described in this section represent the culminating point of this investigation and show beyond any doubt that both starting and stopping without the aid of pressurization, and operation at high

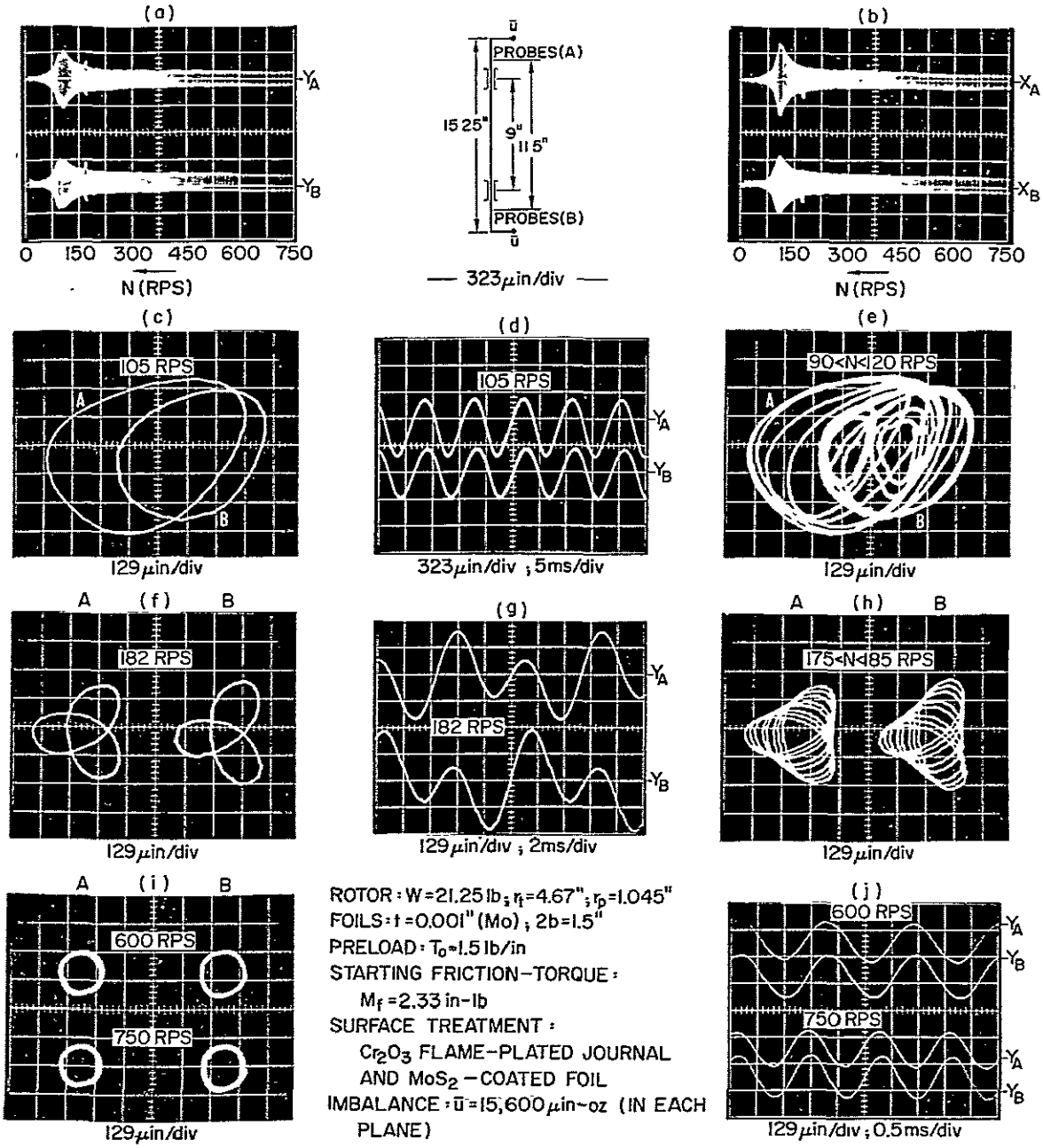

Fig. 61 Motion with Symmetric Imbalance in Self-Acting Foil Bearings (Bearing Span = 9.0"; Journal Length = 1.5")

(a), (b) Scans of Response

(c), (d), (e) Orbits and Motion in Y-Plane near Synchronous Resonance

(f), (g), (h) Orbits and Motion in Y-Plane near Subharmonic Resonance

(i), (j) Orbits and Motion in Y-Plane in High-Speed Range

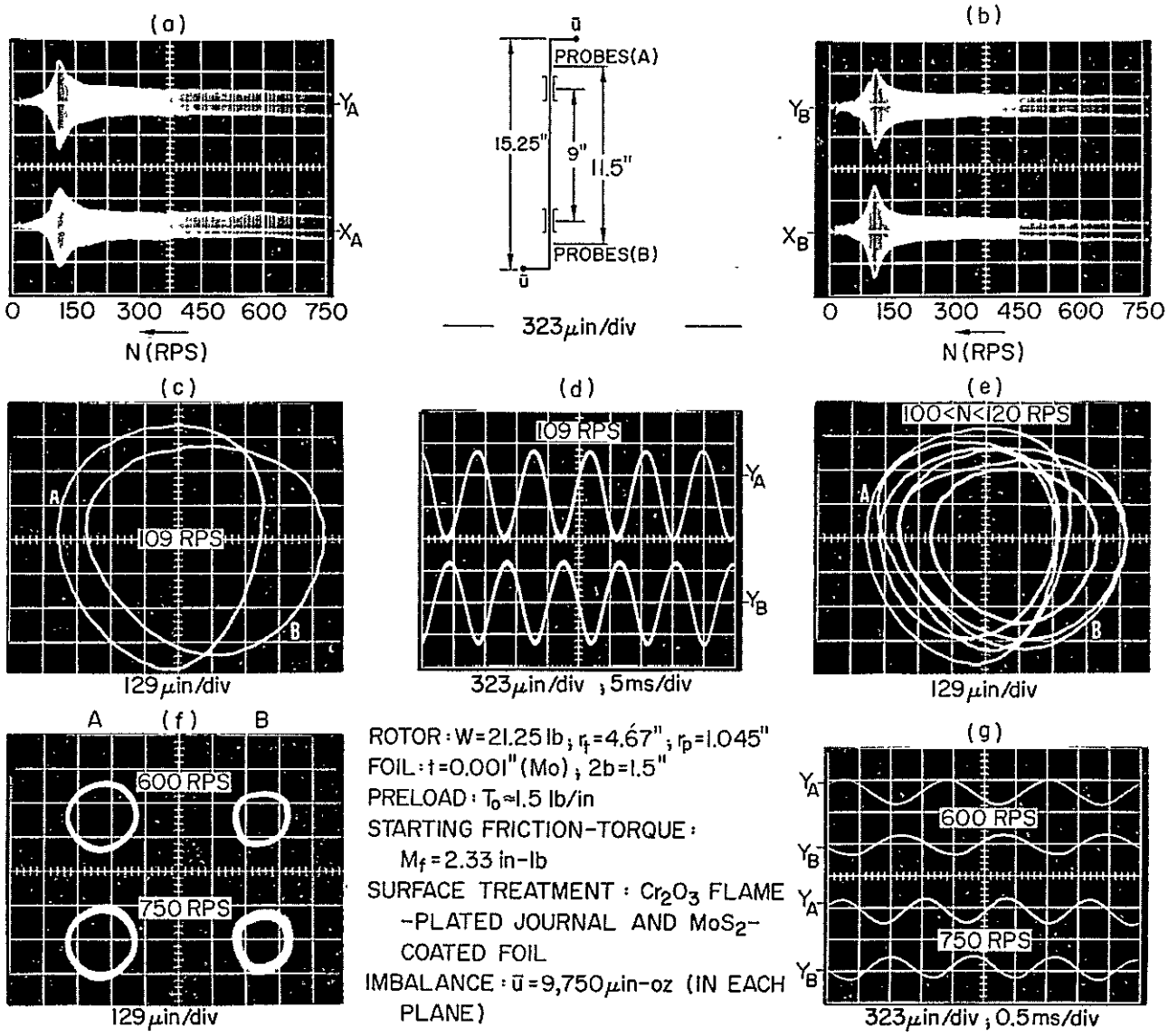

Fig. 62 Motion with Asymmetric Imbalance in Self-Acting Foil Bearings (Bearing Span = 9.0"; Journal Length = 1.5")

(a), (b) Scans of Response
(c), (d), (e) Orbits and Motion in Y-Plane near-Synchronous Resonance
(f), (g) Orbits and Motion in Y-Plane in High-Speed Range

speeds, are feasible with foil bearings of length comparable with other types of fluid-film bearings.

3.10 Wipe-Wear Characteristics of Foil Bearings.

- Cumulative Wear of Journal. Wear of MoS_2 Coated Foils

The report would not be complete without a summary of wear characteristics of foil bearings. The inherent advantages due to the flexibility of the foil, the ability of the foil bearing to accommodate geometrical and thermal distortion and to tolerate dirt and foreign particles, and the excellent wipe-wear characteristics have been documented and discussed in considerable detail in references [1] through [4]. Additional evidence is included in Fig. 63. Shown therein are profilometer traces across a variety of wear tracks. The numbers under the traces and their magnified photographs correspond to the tracks, numbered consecutively on the appended photograph of one journal. These tracks represent the cumulative wear of the A-journal of rotor No. 1. The wear was incurred at various locations corresponding to variations of both foil width and of bearing span. They include a very large number of stops unaided by pressurization, the initial "dry" starts, and all use and abuse accumulated in the course of actual and preparatory runs relevant to data reported in Fig. 6 through Fig. 50.

Most tracks correspond to the edge zones, in which wear occurred first along the major troughs of the anticlastic undulation, brought into contact with the journal in the region of rapidly decreasing pressure along the foil edges [13,17]. Some wear occurred also in the pressurized mode of operation, particularly in the sagging entrance zone, Fig. 47.*

*See also reference [1], pp. 154-165.

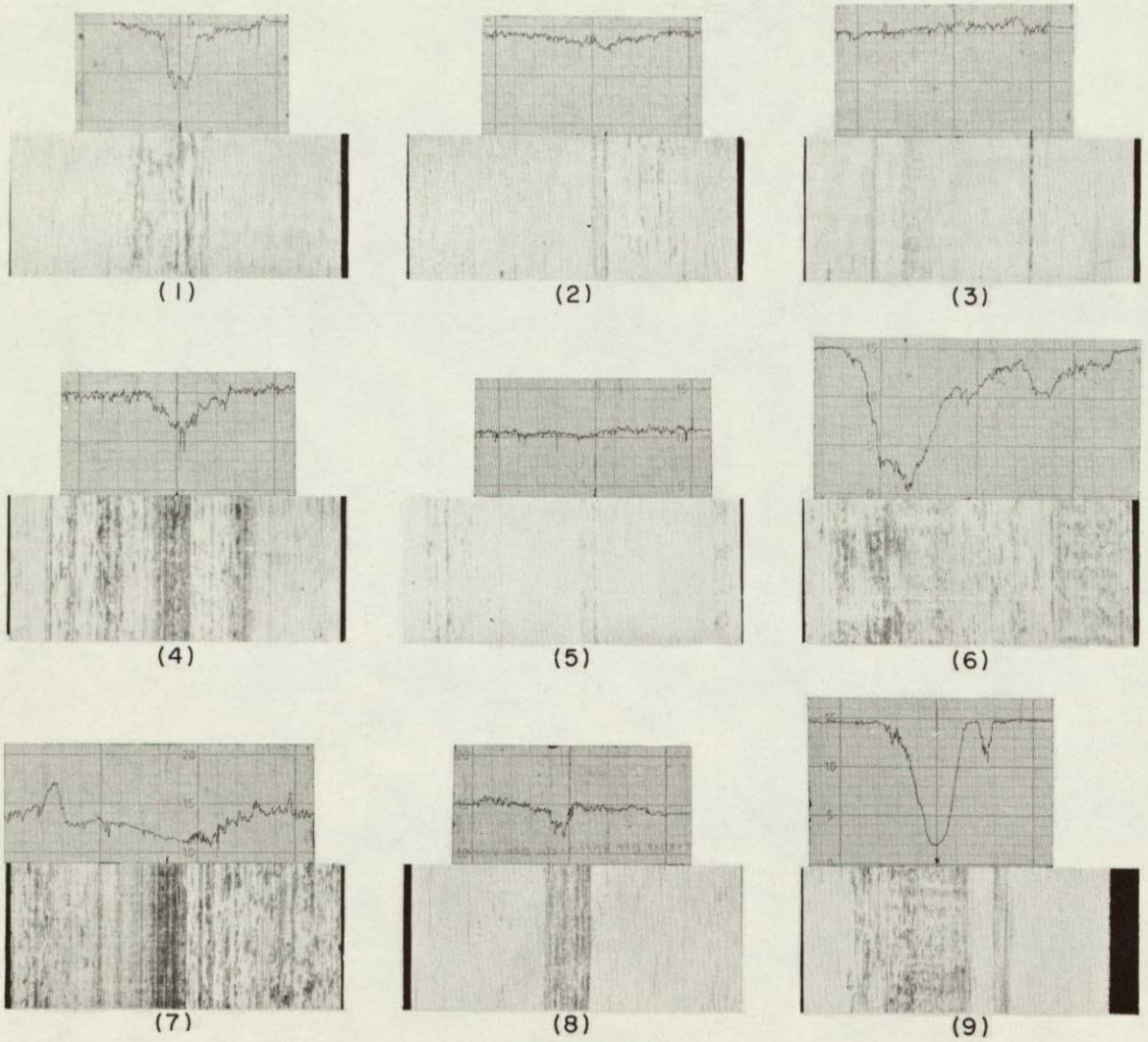

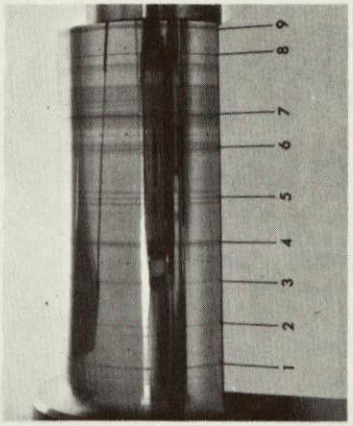

H = HORIZONTAL

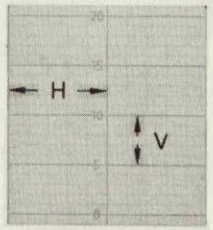

V = VERTICAL

No.	H	V
1	0.05"	25 μin
2	0.05"	25 μin
3	0.05"	25 μin
4	0.05"	25 μin
5	0.05"	25 μin
6	0.05"	50 μin
7	0.05"	50 μin
8	0.05"	25 μin
9	0.05"	50 μin

Fig. 63 Cumulative Wipe-Wear Traces on Rotor Journal

Some inconspicuous, but deeper tracks were evidently the work of sharp, hard particles entering the foil-bearing clearance.(It is an astounding feat in itself that no failures occurred in the course of this investigation, despite the fact that not even minimal precautions were taken to prevent dust, dirt and debris from entering the foil-bearing gap.)

Referring to Fig. 63, the deepest grooves, (6) and (9), were only 140 and 130 μinches deep. The wear marks denoted by (5) were along the center of a 2" wide foil and were distinguishable in the profilometer trace only by the burnishing of the initial surface roughness. The deepest grooves, (6) and (9), corresponded to the outer, 1.5" wide foil and a bearing span of 9". The wear did not appear to have an adverse effect on the operation of the rotor, although the degree of wear depicted in Fig. 63 represented a situation much worse than could be expected under normal operating conditions.

A complementary set of photographs is presented in Fig. 64. Shown are magnified portions of MoS_2-coated foils, in the inlet and exit regions and close to the foil edge. While the legend is self-explanatory, the reader may contrast the virgin and worn portions of the coating, noting that the narrow strip along the edge remained untouched, because it curled away from the journal [13,16]. Although much detail is missing in the reproduction of Fig. 64, the MoS_2-film was never worn through and had a typically glossy, graphite-like appearance. The photograph (b) shows the uncoated molybdenum foil on the left, the virgin coating in the center, and the polished protruberances of the granular film surface in the entrance zone on the right. It is felt that relatively thin, pre-burnished films were most suitable for this application. The combination of 100 μinches of dry lubricant, bonded to the foil surface, and a journal flame-plated with Cr_2O_3, appeared to be very compatible. The gradual wear of the film and the complementary impregnation of the porous Cr_2O_3 surface may have

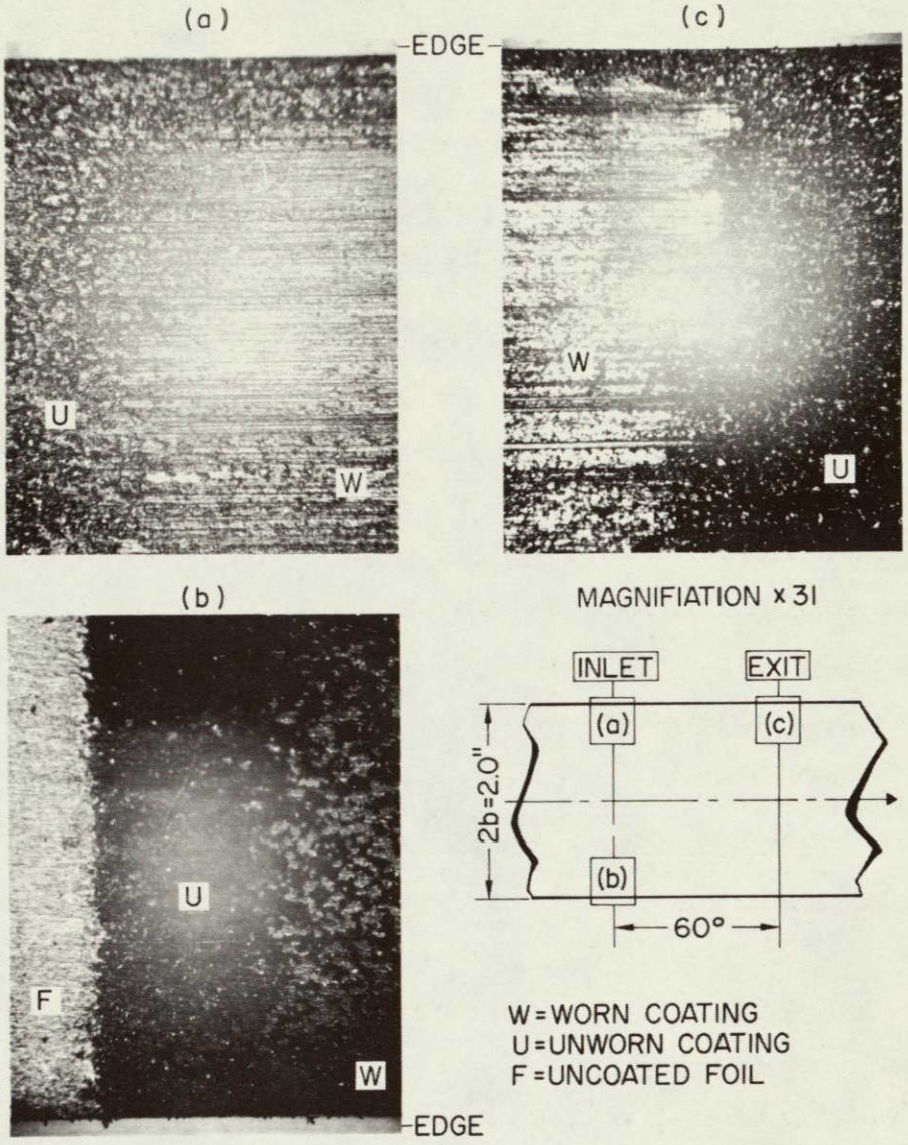

JOURNALS

(a) Cr_2O_3 FLAME-PLATED

(b) 440-C, ROCKWELL C-56

(c) Al_2O_3 FLAME-PLATED AND MoS_2-COATED

FOILS

MOLYBDENUM, t=0.001", INORGANICALLY BONDED MoS_2 (0.0001" TO 0.0002"), $T_o \approx 2.25$ lb/in

(a),(b)—OVER 100 START-STOPS

(c)—OVER 150 START-STOPS

Fig. 64 Wipe-Wear Traces on MoS_2-Coated Foils Following Multiple Start-Stops Unaided by Pressurization

been responsible for the satisfactory results. A view of three rotors, in the state following the conclusion of all experiments described in this report, is presented in Fig. 65.

3.11 Friction Power-Loss and Estimates of Power Loss in Foil Bearings. Effect of Foil Thickness.

The variation of speed with time during coastdown was recorded under various conditions and 11 deceleration curves have been plotted in Fig. 66 through Fig. 70. Each of these figures contains a table of data pertinent to the graph, including the values of the deceleration $\ddot{\theta}$ at 480, 600 and 720 RPS.* The coastdown curves are useful in the determination of total power losses, but it is difficult to apportion the loss due to the foil bearings. The total power dissipation due to fluid friction can be easily determined from the formula:

$$\mathcal{P}_T = 2\pi W r_p^2 N\ddot{\theta}/g .$$

At N = 600 RPS, the total loss was of the order of 820 watts, of which the foil-bearing contributed very approximately 20%. If laminar, Couette flow is assumed, than the contribution of 2 single-row bearings is given by:

$$\mathcal{P}_b = 16\mu b\pi^3 r_0^3 N^2/h^* .$$

With h^* = 590 μinches, a typical value at 600 RPS, the entire foil-bearing loss becomes approximately 133 watts for a bearing length 2b = 1.5.

*The values are based on data points in the range 300 < N < 750 RPS, to which a cubic was least-square fitted.

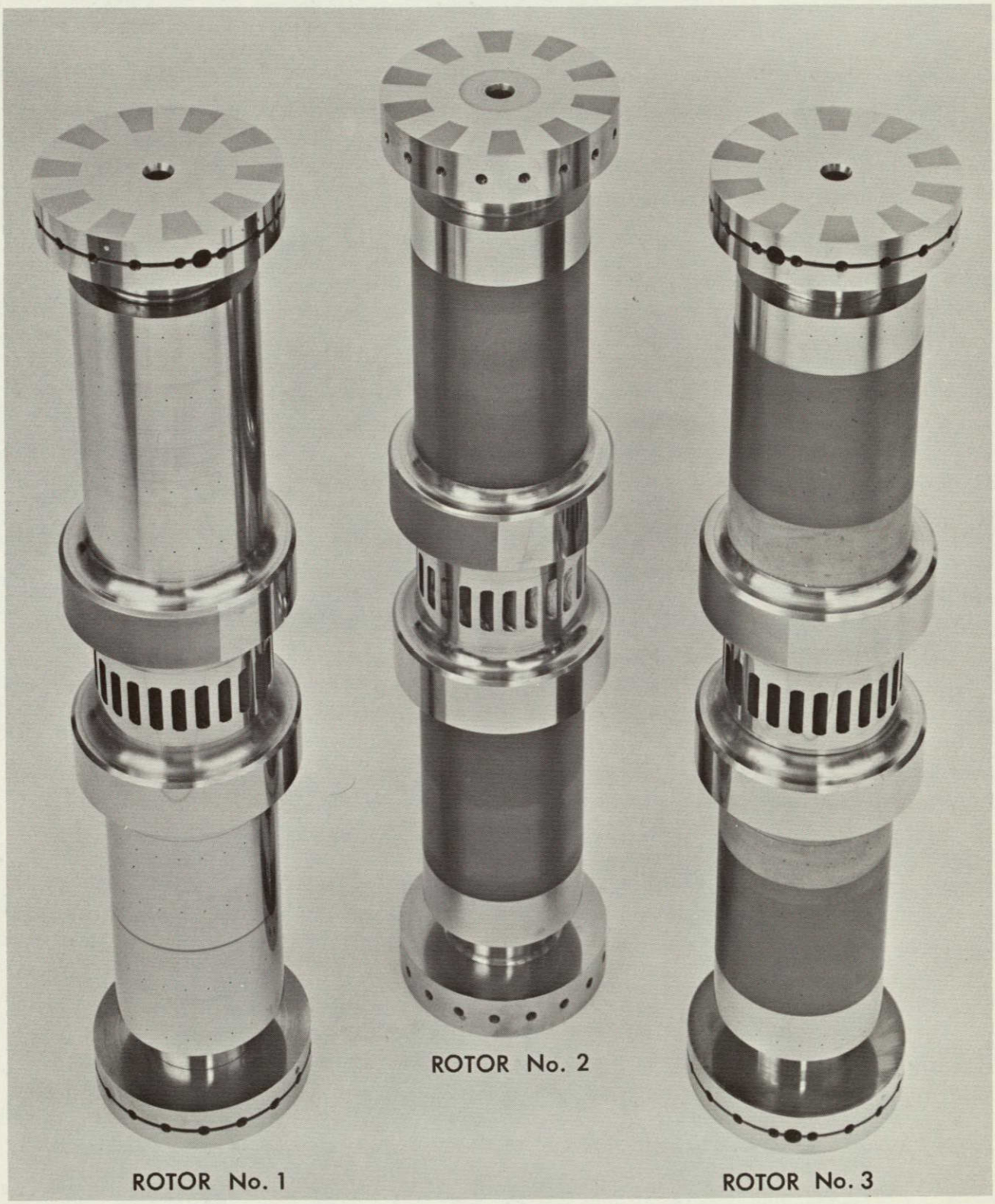

Fig. 65 View of Three Rotors in State Following Conclusion of Experiments

The coastdown curves in Fig. 66 were obtained with double-row and single-row bearings. If one neglects the additional windage, then the removal of one row of foils allows the determination of the power loss incurred in the remaining, single-row bearings. For the case at hand, the power loss established on the basis of data appended in Fig. 66 was 167 watts at 600 RPS. Similar estimates can be made by utilizing the information relevant to 2.0" long and 1.5" long bearings, operated under identical, or similar conditions. Such calculations, however, involve differences of numbers ($\ddot{\theta}$) which do not differ greatly in magnitude, and this may lead to very appreciable error. It is evident that at high speeds the major losses were due to windage, and it was shown in the preceding sections that the clearance, and the bearing loss therefore, were influenced by temperature transients. The separation of the energy dissipation occurring in the foil-bearing gap from the total loss involves a large degree of uncertainty, but such estimates are nevertheless useful and complementary to more elaborate calculations.

A comparison between coastdown curves in the pressurized and self-acting modes in Fig. 67 and Fig. 68 shows that pressurization involved larger friction losses. Inasmuch as differences are bound to exist between the characteristics of pressurized and self-acting bearings (See Section 3.6), an increase in energy dissipation may have been partly due to rotating air jets issuing from the uncovered orifices, resulting in additional windage.

The coastdown curves in Fig. 69 are relatively steep and reflect the influence of large preload tension. These curves are of particular interest, because the only difference in the parameters involved (at least nominally) is the foil thickness. The thicker and, therefore, the less flexible foil appears to have supplied sufficient slack at low speed to increase the bearing clearance, reducing thereby the shear rate. Note, however, that the thinner foil produced an appreciably smaller deceleration

in the final stages of rotation. This behavior indicates that the thicker foil contacted the journal at a higher speed, probably because of greater proximity of the first anticlastic trough to the journal surface [13,17]. Three additional coastdown curves are presented in Fig. 70. The difference between curves (9) and (11), which are nearly congruent, except at low speed, is the preload tension. The slower deceleration of (9) during the final stages of rotation is consistent with the lower preload. Similar conclusions may be drawn with regard to curve (10) and (11), in view of differences of foil thickness and width.

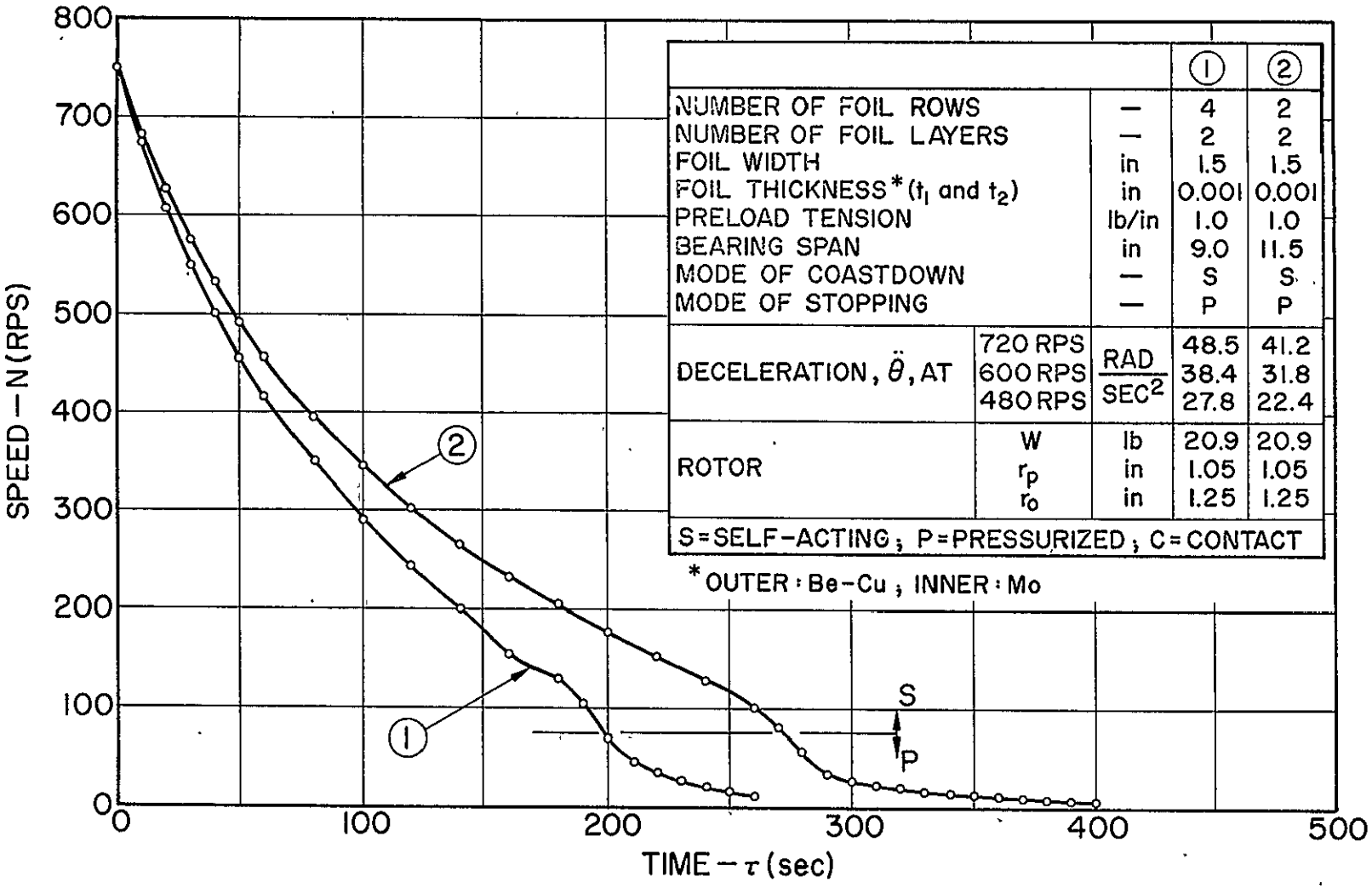

			①	②
NUMBER OF FOIL ROWS		—	4	2
NUMBER OF FOIL LAYERS		—	2	2
FOIL WIDTH		in	1.5	1.5
FOIL THICKNESS* (t_1 and t_2)		in	0.001	0.001
PRELOAD TENSION		lb/in	1.0	1.0
BEARING SPAN		in	9.0	11.5
MODE OF COASTDOWN		—	S	S
MODE OF STOPPING		—	P	P
DECELERATION, $\ddot{\theta}$, AT	720 RPS	$\frac{RAD}{SEC^2}$	48.5	41.2
	600 RPS		38.4	31.8
	480 RPS		27.8	22.4
ROTOR	W	lb	20.9	20.9
	r_p	in	1.05	1.05
	r_o	in	1.25	1.25

Fig. 66 Comparison of Coastdowns in Double-Row and Single-Row Foil Bearings

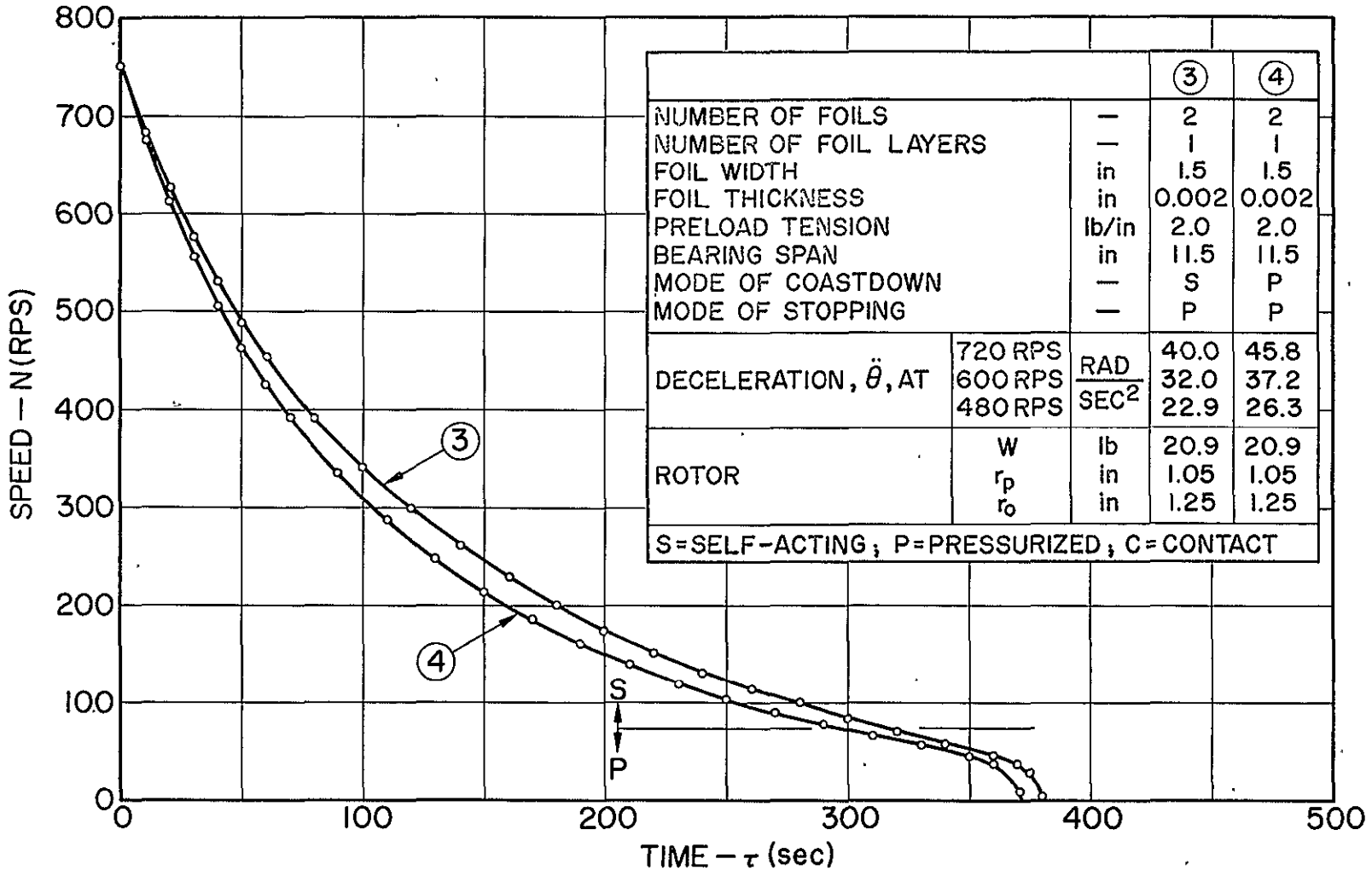

			③	④
NUMBER OF FOILS		—	2	2
NUMBER OF FOIL LAYERS		—	1	1
FOIL WIDTH		in	1.5	1.5
FOIL THICKNESS		in	0.002	0.002
PRELOAD TENSION		lb/in	2.0	2.0
BEARING SPAN		in	11.5	11.5
MODE OF COASTDOWN		—	S	P
MODE OF STOPPING		—	P	P
DECELERATION, $\ddot{\theta}$, AT	720 RPS	RAD/SEC^2	40.0	45.8
	600 RPS		32.0	37.2
	480 RPS		22.9	26.3
ROTOR	W	lb	20.9	20.9
	r_p	in	1.05	1.05
	r_o	in	1.25	1.25
S=SELF-ACTING; P=PRESSURIZED; C=CONTACT				

Fig. 67 Comparison of Coastdowns in Pressurized and Self-Acting Foil Bearings (First Comparison)

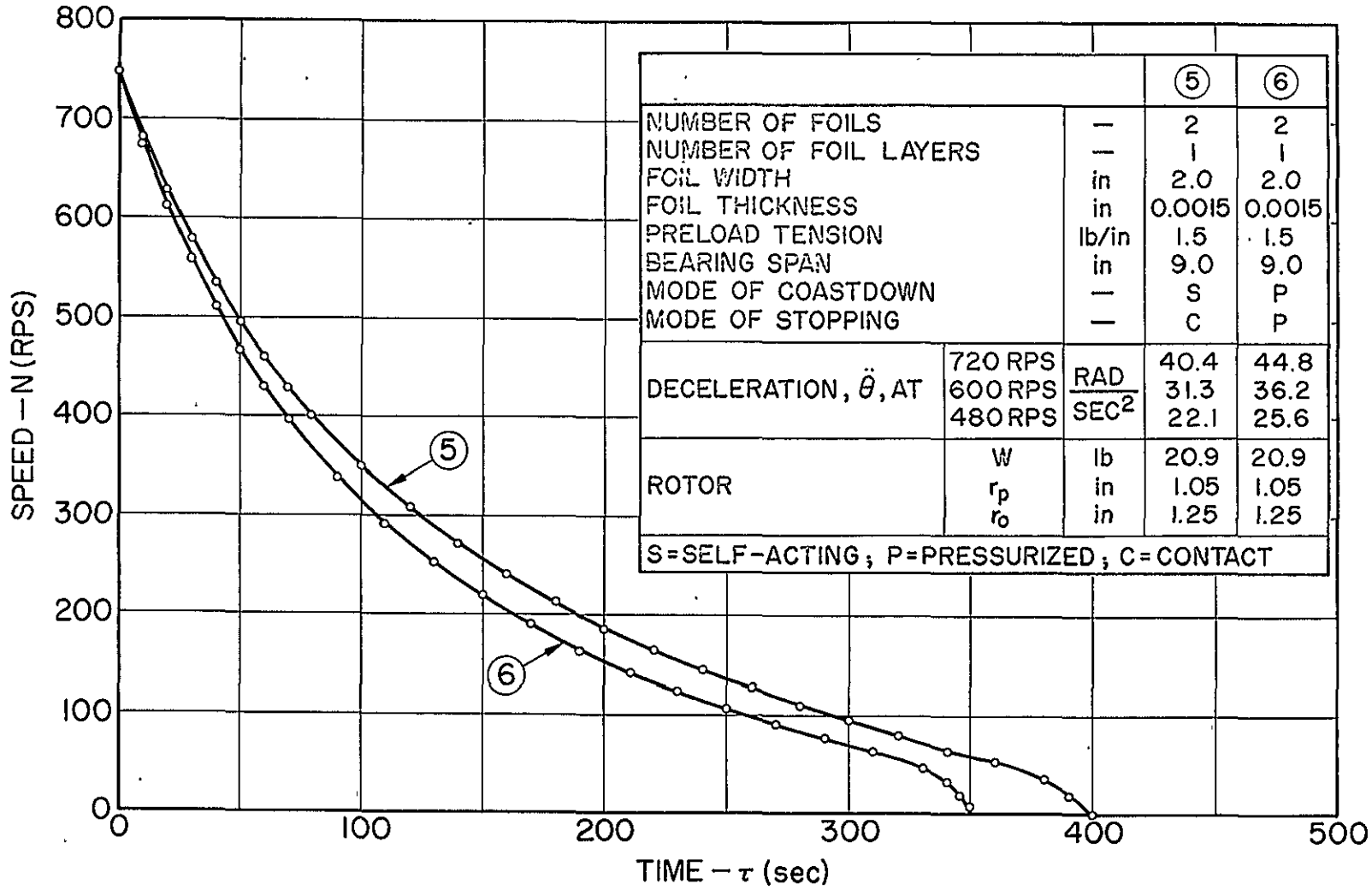

Fig. 68 Comparison of Coastdowns in Pressurized and Self-Acting Foil Bearings (Second Comparison)

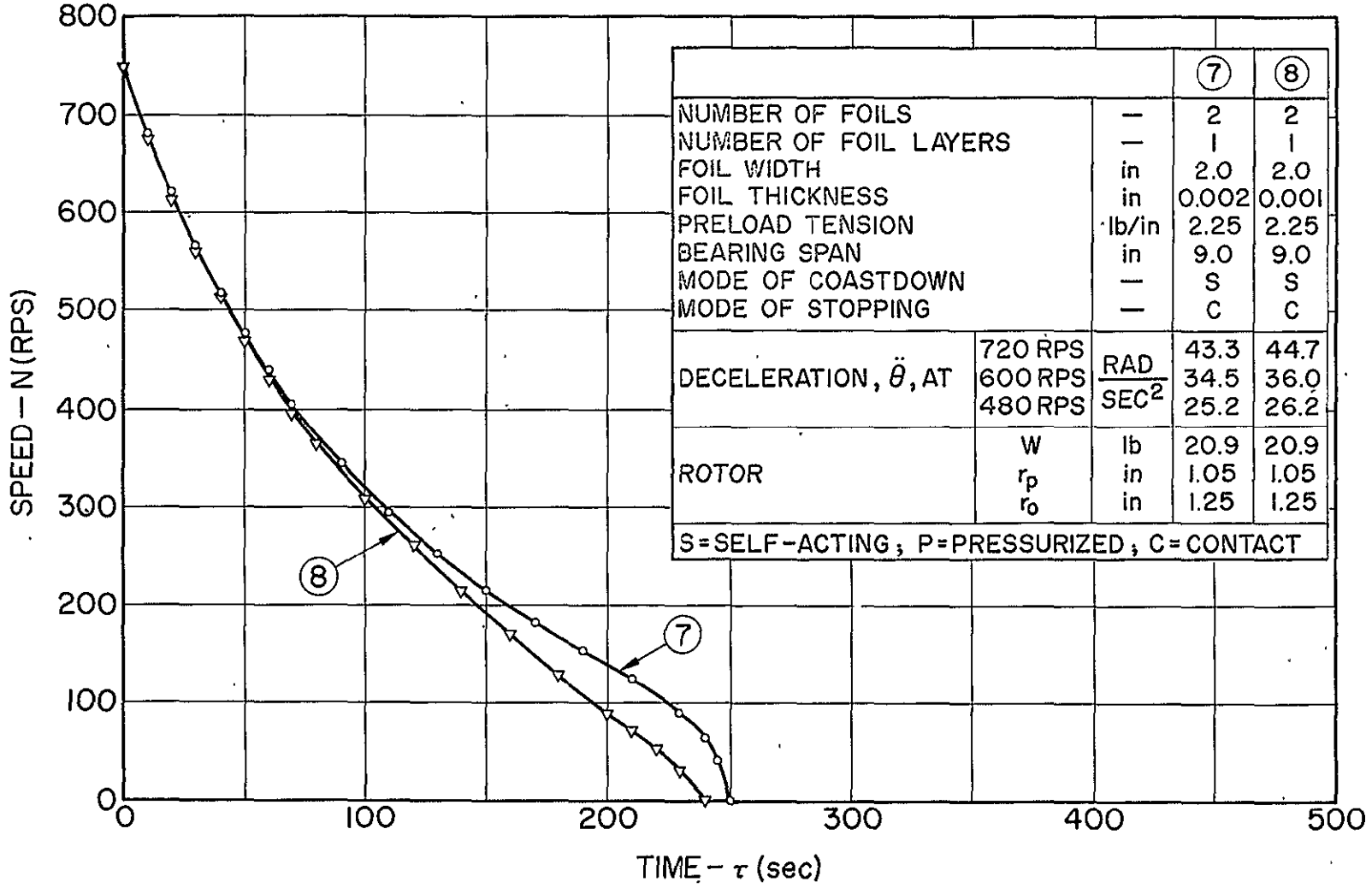

Fig. 69 Comparison of Coastdowns in Self-Acting Foil Bearings. - Variation of Foil Thickness

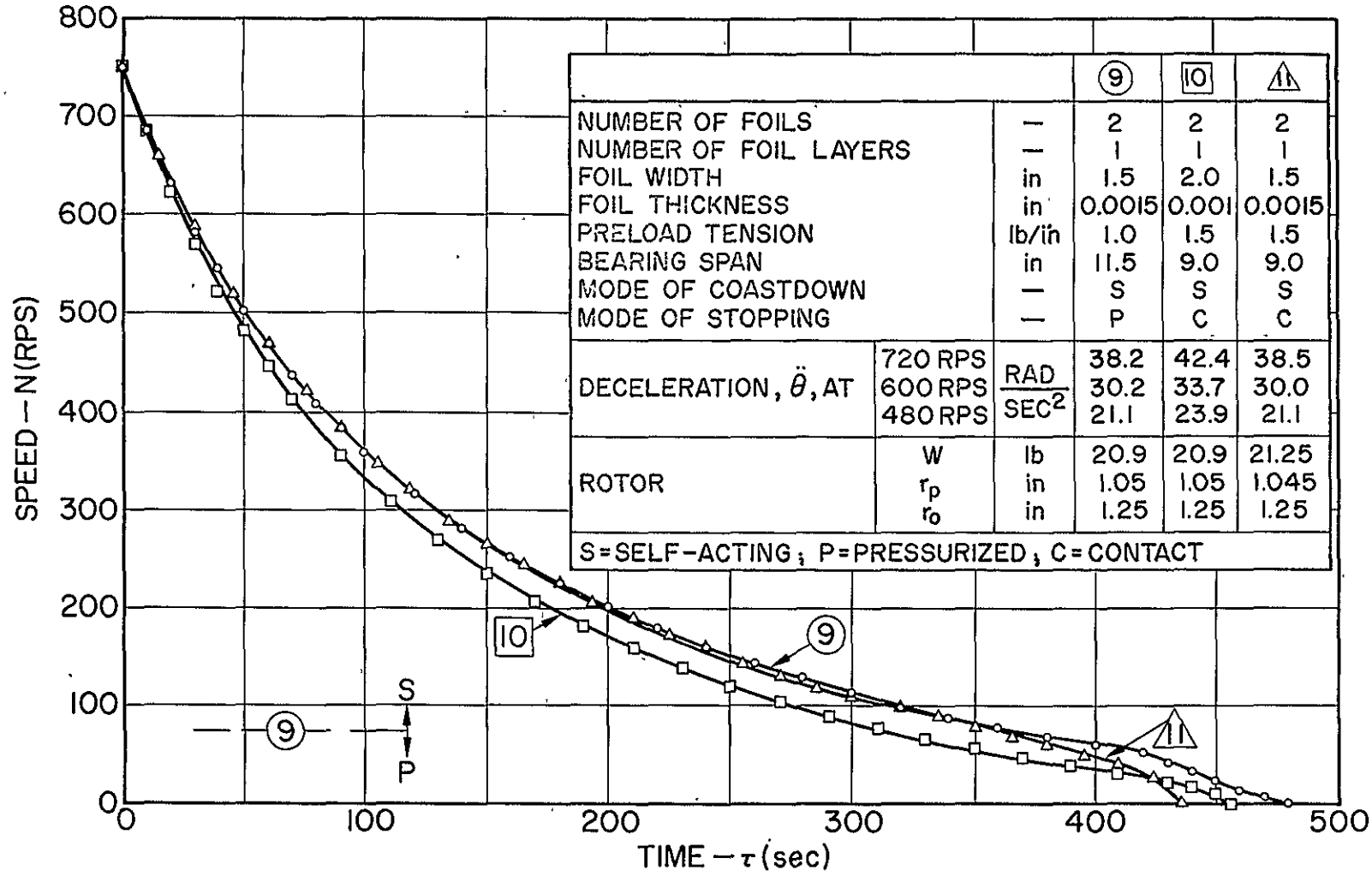

			9	10	11
NUMBER OF FOILS		—	2	2	2
NUMBER OF FOIL LAYERS		—	1	1	1
FOIL WIDTH		in	1.5	2.0	1.5
FOIL THICKNESS		in	0.0015	0.001	0.0015
PRELOAD TENSION		lb/in	1.0	1.5	1.5
BEARING SPAN		in	11.5	9.0	9.0
MODE OF COASTDOWN		—	S	S	S
MODE OF STOPPING		—	P	C	C
DECELERATION, $\ddot{\theta}$, AT	720 RPS	RAD/SEC^2	38.2	42.4	38.5
	600 RPS		30.2	33.7	30.0
	480 RPS		21.1	23.9	21.1
ROTOR	W	lb	20.9	20.9	21.25
	r_p	in	1.05	1.05	1.045
	r_o	in	1.25	1.25	1.25

S = SELF-ACTING ; P = PRESSURIZED ; C = CONTACT

Fig. 70 Comparison of Coastdowns in Self-Acting Foil Bearings. - Variation of Foil Thickness, Width and Preload

4.0 DISCUSSION OF RESULTS

The objectives of this investigation were fully realized. It was demonstrated that the effective bearing length could be reduced by as much as 50% from the value reported in reference [3], while retaining a bearing span of 9". Perhaps the most encouraging aspect of the present experiments was proof that rotors could be started and stopped without the aid of external pressurization. The advantages of "dry" starting and stopping can be fully appreciated, only if one considers the degree of simplification ensuing from the elimination of the elaborate foil-lift system [1,3]. While rotation could undoubtedly be initiated at sufficiently low preloads, the reduction of the initial tension below a certain minimum would have precluded acceleration through the resonant bandwidth and operation in the high-speed range. The fact, therefore, that multiple start-stops could be performed at levels of preload tension more than adequate to ensure successful high-speed operation constitutes a significant achievement.

The experiments described in this report were directed toward the development of supportworthy foil bearings for a specific application. The tests were numerous, but it has not been possible to engage in a basic study, in which full control could be exercised over most parameters, while observing the effects of deliberate variations of selected parameters only. No attempt will be made, therefore, in this discussion to account in detail for apparent inconsistencies with regard to the effect of preload tension T_o and foil thickness t on the magnitude of clearance and, indirectly, on the speeds at which resonances occurred. Here, in addition to inherent dissymmetries and differences between nominal and actual values of preload, the main

source of apparent inconsistencies can be attributed to the variability of temperature between various runs. Furthermore, while the direct influence of bending rigidity of the foil on the magnitude of gap width in the region of uniformity is not very significant [7], the indirect effect through the production of "curvature slack", as illustrated qualitatively in Fig. 71 and estimated in Appendix 1, was to increase the gap width significantly in the lower speed-range. The seemingly paradoxical influence of foil thickness on bearing stiffness, therefore, was to increase it through the extensional rigidity Et, and to diminish it simultaneously because of the increase in bending rigidity $Et^3/12(1-\nu^2)$ and the ensuing "slack".*

A sufficient number of tests were conducted however to establish representative orders of magnitude of various operational characteristics. Considering thus the coalescence of 4 modes of vibration in a relatively narrow bandwidth, maximum amplitudes at synchronous resonances of all runs occurred in the range $55 < N < 145$ RPS, the average speed being approximately 95 RPS (5700 RPM).** Representative values of gap width, established by the averaging of all recorded values, were 620 μinches at 750 RPS and 590 μinches at 600 RPS. Since most scans were recorded under transient conditions and during coastdown, the foregoing gap magnitudes reflect a smaller difference than observed during accleration. (See also Fig. 48 and Fig. 60). Similarly established values of the average displacement of the rotor axis with speed from an initial reference position gave 560 μinches at 600 RPS and 760 μinches at 750 RPS. The "eccentricity"

*See also reference [1], pp. 102-103.

**If one extrapolates from a linear, symmetric and isoelastic case, the system may be characterized by two resonant speeds which are nearly coincident ($N_a/N_S \approx 0.96$). Although the present system is nonlinear, maximum amplitudes (X_A, X_B, Y_A, Y_B) of synchronous resonances were grouped almost invariably within a relatively narrow bandwidth of approximately 90 RPS.

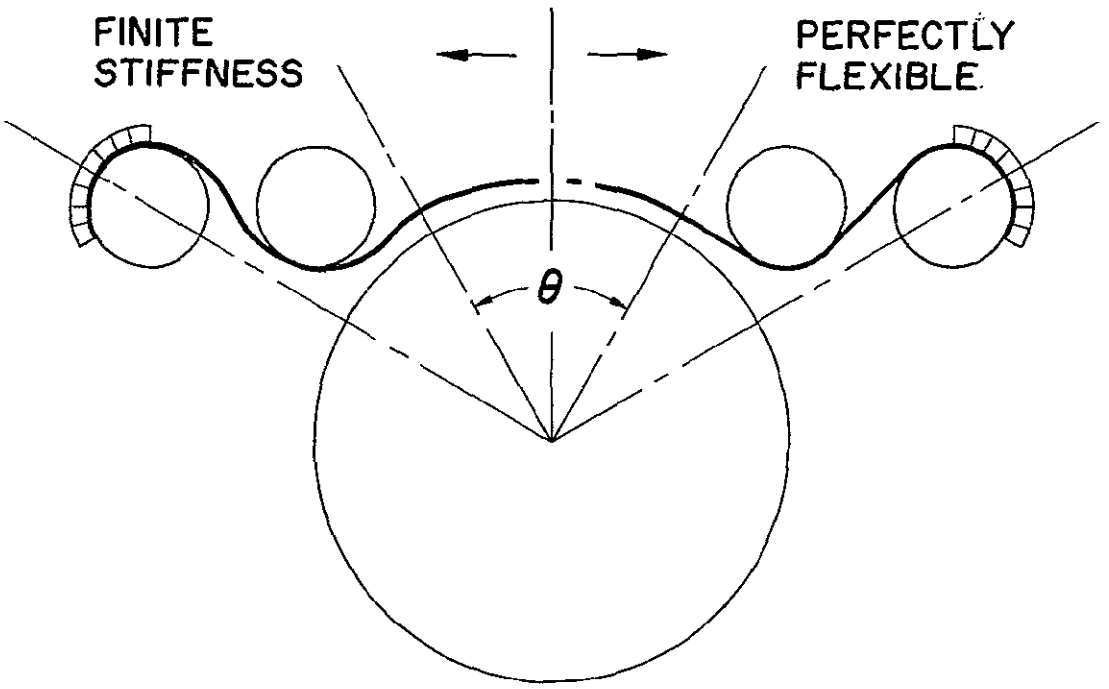

Fig. 71 Schematic Illustration of the Effect of Flexural Rigidity of Foils

loci were nearly straight lines in the 3-rd quadrant, inclined at a mean angle of approximately 45° to the negative X-axis.

It is of interest to compare this data with the loci presented in Fig. 4.28 and Fig. 4.37 of reference [1]. If differences in the orientation of the axes are taken into consideration and all displacements are referred to the present system of coordinates, the loci in reference [1] fall in the 4-th quadrant and are inclined approximately at an angle of 45° to the positive X-axis. The difference in the orientation of the loci was due to the fact that the rotors used in present and previous experiments [1] revolved in opposite directions. It is to be noted that the bearings were geometrically similar and symmetrical about the bisector of foil segment No. 2, located opposite the foil lock, Fig. 1. Since loads were applied evenly to the free ends of the foil, the tensions in sectors 1 and 3 were sensibly equal to each other, but probably higher than in Sector 2. An inherent tendency existed, therefore, for the rotor to displace in the direction of the negative Y-axis, i.e. away from the foil lock. An additional dissymmetry was introduced through rotation and amplified with speed,* giving rise to a second component of displacement in the negative or positive direction of the X-axis, according to whether rotation was clockwise or counterclockwise. Prior knowledge of anticipated displacement can be useful if it is desired to offset the foil supports to a predetermined eccentricity with respect to a reference axis. The displacement of the rotor, however, was insignificant at low speeds, so that excursions at resonance would be considered with reference to the initial position. Furthermore, displacements of the rotor in order of 750 μinches are not excessive and can be generally accommodated with ease within the clearance circle of labyrinth seals.

*The pressure field of each bearing sector is not symmetrical, especially if comparisons are made between the inlet and exit zones [6,12,13]. Inertia effects amplify the dissymmetry at high speed.

It is well known that the stability of rigid-surface gas bearings is extremely sensitive to operation in the concentric, that is radially unloaded attitude, and that the threshold speed of whirl is lowered by increasing the mass (or transverse inertia) of the rotor [24,25]. Various elaborate methods of stabilization were suggested to increase the operational speed-range of gas bearings [26], including radial loading by external pressurization, mounting of rigid bearings on flexible supports, and supporting rotors on pivoted shoes.

In contrast, the operation of rotors supported by foil bearings, so in the course of present experiments as in the course of experiments reported in references [1] through [4], showed that stability was maintained at speeds in excess of 50,000 and 70,000 RPM, with no radial load applied to the rotor, and with the mass per unit projected bearing area increased progressively in the ratio $1 \div 2.4 \div 2.8 \div 5.6$.* A theoretical analysis, reference [27], lends additional support to the claim that foil-bearings of the present and of similar configurations are inherently stable. Also, while flexible mounting of rigid bearings may or may not enhance stability, it does not possess the advantages of the inherent flexibility of foil bearings with regard to accommodation of thermal distortions, forgiveness of geometrical imperfections, and tolerance of foreign particles. Furthermore, since flexibly mounted bearings and pivoted shoes are far more massive than foils, the use of such elements in rotor support-systems may induce various high-speed resonances, shoe-flutter, and other problems that may be avoided with foil bearings.

One of the most important aspects of this investigation was the determination of maximum excursions induced by imbalance at resonance,

*The largest mass per unit projected bearing area was 2.8 lb/in^2.

and by friction during the initial and final stages of rotation. The asymmetric imbalance is, of course, more dangerous than the symmetric. The estimate, made in Section 3.4 on the basis of extrapolation from a simplified linear system, showed that equality of resonant amplitudes at the bearings, in both conical and cylindrical modes, required a ratio of asymmetric to symmetric imbalance $\bar{u}_a/\bar{u}_s = 2r_t/L \approx 0.615$. With the limit of the safer symmetric imbalance established, the ratio of 0.615 was used as an approximate guideline in all tests involving synchronous excitation.

The results of these tests are summarized in the following tabulation, which gives the amount of imbalance added in each plane and the equivalent eccentricity δ, on the assumption of one half of the rotor mass being concentrated in each balancing plane. Given also is the peak-to-peak amplitude $2A_r$ of the largest resonant orbit and the corresponding speed N_r.

Fig. No.	$\bar{u}$		δ	T_o	t	2b	N_r	$2A_r$	Remarks
	μin-oz	Type	μin	lb/in	in	in	RPS	μin	—
19	26,100		156	1.5	0.0015	2.0	89	2380	a,c
23	15,350		92				64	3880	a,c,*
37	26,100		156	1.5	0.001	2.0	105	1550	a,c
39	15,350		92				102	2200	a,c
52	28,300		166	2.25	0.001	2.0	75	1480	b,c
54	15,600		92				72	1800	b,c
61	15,600		92	1.5	0.001	1.5	105	930	b,c
62	9,750		58				109	920	b,d

a) Rotor No. 1: - W = 20.9 lb; r_t = 4.68"; r_p = 1.05"

b) Rotor No. 2: - W = 21.25 lb; r_t = 4.67"; r_p = 1.045"

c) Probe Span = 12"

d) Probe Span = 11.5"

With the exception of the asymmetric imbalance corresponding to Fig. 23 (i.e. the second entry in the foregoing table), all peak-to-peak maxima were less than 0.0025.* Rotor excursions of this magnitude may be assumed to represent the worst possible condition, but should be accommodated comfortably within a representative seal clearance. The most adverse condition is represented by a purely conical motion with the apex of the cone at the center of the symmetric rotor. With the outer edges of seals at 7" from the apex, a peak-to-peak excursion of 0.0025" at the monitoring station 6" from the rotor center corresponds to (7/6)(0.0025) = 0.0029" at the outer edge of the seal. Such amplitudes could certainly be accommodated within the confines of a nominal clearance circle the order of 0.008", and even within the confines of clearance reduced to 0.004" by differences in thermal expansion of shaft and seal.

A point of additional interest is that pitching of the rotor could be accommodated within the operational clearance of approximately 0.0012" between the runner and the 3.0" diameter thrust plate. A safety estimate, made with assumptions analogous to the case of seals, shows that a peak-to-peak pitching excursion of 0.0025" at the location of the probes reduced the spacing at the edge of the pressurized thrust bearing to 0.0006", or to 50% of the parallel clearance.

The observations made in the preceding paragraphs with respect to response to excitation by rotating imbalance emphasize the supportworthiness of foil bearings. It is not expected that the imbalance under operating conditions should be either purely asymmetric, or 50 to 100 times

*The magnitude of response to asymmetric imbalance in Fig. 23 is inconsistent with the results of all subsequent tests, Fig. 39 for example. Note that maximum orbits produced by symmetric and asymmetric imbalance occurred at nearly equal speeds, except in Fig.19 and Fig.23. It is suspected that insecure clamping may have been at fault.

greater than the magnitude of remanent imbalance that can be achieved with little effort on a good balancing machine.

The latter part of this investigation was devoted to starting without the aid of external pressurization. These tests were highly successful and indicated that multiple start-stops, possibly several hundreds, could be achieved without rendering the foil bearings inoperative. Recalling that multiple start-stops could be achieved at adequate preloads even without the aid of dry lubricants, it appears that with proper chemistry and refinement of bonding, and with proper film thickness control, the useful life of the foil bearing could be extended to a thousand start-stop cycles, or more.

The most important problem in "dry" starting is the control of friction-induced vibration. The phenomena observed during the initial and final stages of rotations are typical of a class of problems, which have been studied over a number of years, and of which references [28] through [32] constitute a representative sample. The envelopes of initial excursions did not exceed 0.0021", Fig. 58, but they were commensurate in size with resonant orbits excited at maximum levels of rotating imbalance. The correlation between frequencies of the quasi-harmonic oscillations induced by friction and the resonant frequencies of a foil-supported rotor in Appendix 3 points to the difficulties that may be encountered if the two frequencies coincide. It is fortunate that friction-induced vibrations were associated with very low speeds and that their amplitudes were not excessive. Their existence, however, and need of control during initial and final stages of rotation cannot be ignored.

The last part of this chapter is devoted to a number of observations with regard to nonlinear phenomena noted in the course of this investigation. The motion of a rotor supported in foil bearings involves restoring and damping forces which are unknown functions of displacement

and its derivatives with respect to time. The complex elasto-hydrodynamic interactions, in the presence of thermal and frictional effects, lead to great difficulties in a realistic formulation of governing equation of motion and of boundary conditions. Linearized solutions, useful in studies of stability in the small, cannot predict the motion in response to large excitation, while parametric computer studies (orbit programs) do not afford a general insight into the characteristics of the system. In the absence of analytic solutions, observations can be made only with regard to similarities with simpler, non-linear systems characterized by similar phenomena, or with respect to other experimental results relevant to the response of flexibly mounted rotors.

The motion in pressurized foil bearings, for example, was characterized by ultraharmonic resonances, Figures 6, 8, 10, 13, while subharmonic resonances occurred mainly in the self-acting mode, Figures 20, 24, 25, 37, 39, 52, 61. The rotational speeds at which ultraharmonic resonances occurred were shown to be related by nearly integral numbers to each other and to the speed of synchronous resonance [1,2]. An analogous relation was shown to exist in the case of systems represented by Duffing-type equations by Burgess [18], and experimentally by Atkinson [19], who studied the ultraharmonic response by simulation on an analog computer. He produced a series of odd ultraharmonic resonances and "backbone" curves, characteristic of a symmetric (cubic) restoring force. Carnegie and Reif [20] showed theoretically and by simulation that both odd and even overharmonics existed in the case of asymmetries, and that the multivalued response curves reflected complex "jump" phenomena. Both even and odd ultraharmonics have been observed with pressurized foil bearings in the course of previous studies [1,2,3,4] and during the present investigation, Fig. 8 for example. The response was frequently associated by amplitude instability ("jumps").

Only subharmonic resonances of order 1/2 were observed in the course of the present investigation, as in Fig. 61 for example. The subharmonic motion was always excited at appreciable levels of imbalance and was otherwise absent. In a number of cases, the amplitude of subharmonic motion was modulated by a frequency approximately 1/20 the rotational speed, Fig. 25 and Fig. 39. Various pertinent remarks were made by Tondl [21], who investigated nonlinear phenomena associated with turbomachinery. He points out that subharmonic resonances were frequently confused with self-excited vibrations and that loose mounting of cylindrical oil-bearings had the effect of suppressing whirl, while introducing ultraharmonic, subharmonic, and other types of nonlinear resonances. If oil surrounded the loose bearing in the experiments described in reference [21], the dissipative contribution of the squeeze-film may have effected stabilization, because, as pointed out by Lund [33], and Marsh [34], flexible mounts are effective as whirl suppressants only if the compliance of the mounts has damping in parallel. Linearized analyses, however, of which references [27] and [33] are typical, while useful in assessing stability in the small and the response to weak excitation, preclude by their nature an insight into non-linear phenomena observed in the course of foil-bearing studies.

From the operational point of view, the maximum amplitudes of ultraharmonic and subharmonic resonances were generally smaller, and at most commensurate with magnitudes of excursions at synchronous resonances. On the other hand, operation was not limited by instability and no self-excited vibrations were detected at operational speeds approaching at times the 54,000 RPM mark.

5.0 CONCLUSIONS AND RECOMMENDATIONS

Previous experiments [1,3] and the present investigation have shown that gas-lubricated foil bearings are endowed with a unique combination of useful properties. The latter suggest that considerable advantages may be derived in the application of foil bearings to high-speed, high-temperature turbomachinery. Possible applications suggest themselves also in cryogenics (expanders) optics (rotating mirrors and scanners), in biochemical devices (centrifuges), and many others. The list of useful properties is extensive and only the salient ones are listed herewith:

a) Stability. Self-excited vibrations induced through the fluid film and commonly referred to in the literature as "half-frequency" or "fractional-frequency" whirl, do not occur in foil bearings. In contrast with foil bearings, the onset of whirl puts severe limitations on the maximum operating speed of rotors supported by rigid gas bearings, particularly when the revolving mass is large and the radial load is small.* Also, excitation at frequency equal half the speed of rotation has no adverse effects on the operation of the foil bearing.

b) Distortions. Thermal distortions, geometrical imperfections and misalignment can be accommodated readily because of the flexibility and extensibility of the foil. A properly designed foil bearing will operate successfully at elevated temperatures and in the presence of appreciable temperature gradients.

*Numerous papers, possibly several hundreds, have been devoted to the subject of whirl-instability of gas and liquid-lubricated bearings [35]. Research expenditures have been commensurate.

c) Wear and Particles. The passage of foreign particles and of debris through the clearance is aided by the flexibility of the foil and its ability to deform locally.* A multiplicity of asperities is involved when bearing surfaces approach in the region of wrap, so that contact is distributed, rather than concentrated. Since both journal and foil can deflect, motion is not constrained by the narrowest confines of the clearance circle. Excursions can be relatively large, without destroying the effectiveness of the lubricating film. The foil is forgiving and the wear is benign. "Dry" starting poses fewer problems than with rigid-surface gas bearings.

d) Manufacture. No special requirements exist with respect to journal size and roundness. No stringent tolerance need be maintained with regard to bearing dimensions, since the foil will conform with the size of the journal.

Previous objections to foil bearings have been largely removed as a result of the present investigation.- Specifically:

a) Successful operation was achieved with bearings of greatly reduced length, and of overall dimensions commensurate with other types of fluid-film bearings.

b) It has been shown that the efficient but nevertheless elaborate foil-lift system is not an indispensable prerequisite to starting. Multiple start-stops were accomplished successfully without the aid of external pressurization.

*No precautions were taken with regard to cleanliness. Dust, dirt and debris entered the foil-bearing gap in abundance, but no foil-bearing failures were ever experienced.

The foil-bearing is relatively compliant (10^4 to 2×10^4 lb/in). The stiffness is, nevertheless, commensurate with that of pivoted-shoe bearings used in the support of small turbo-alternators [36]. Furthermore, since low stiffness produces resonances in the low-speed range, the synchronous excitation by imbalance, and the corresponding rotor excursions in the resonant bandwidth,are diminished accordingly. Moreover, the inherent flexibility of the foil furnishes an inherently stable support and eliminates the need for elaborate stabilization systems.

It is recommended that a foil-bearing support be designed and manufactured for the specific purpose of adapting the support to an existing NASA Brayton Cycle Unit and testing it in the actual machine. One possible configuration is illustrated schematically in Fig. 79, Appendix 4. It is also suggested that foil bearings be incorporated, whenever feasible, into various types of high-speed turbomachines, in which rotor stability, thermal distortion, misalignment and sensitivity to particles preclude the reliable use of various types of rigid gas-bearings. Above all, it is advisable to consider the use of foil-bearings in new machines, in order to achieve their rational integration in the design ab initio. Finally, the attention of all concerned is drawn to possible advantages of foil-bearing applications in cryogenics, optical instruments, centrifuges, and to yet unexplored possibilities of utilizing liquid-lubricated foil bearings in rotary pumps.

REFERENCES

1. Licht, L. and Eshel, A., "Study, Fabrication and Testing of a Foil-Bearing Rotor Support System", NASA CR-1157, November 1968, prepared by the Ampex Corporation under Contract NASW-1456, NASA, Washington, D.C.

2. Licht, L., "An Experimental Study of High-Speed Rotors Supported by Air-Lubricated Foil Bearings - Part 1: Rotation in Pressurized and Self-Acting Foil Bearings and Part 2: Response to Impact and to Periodic Excitation", Journal of Lubrication Technology, Trans. ASME, Vol. 91, Series F, No. 3, 1969, pp. 477 - 505.

3. Licht, L., "Design, Fabrication and Testing of a Foil Gas-Bearing Test Rig", NASA CR-1563, May 1970, prepared by the Ampex Corporation under Contract NAS3-11826, NASA Lewis Research Center, Cleveland, Ohio.

4. Licht, L., "The Dynamic Characteristics of a Turborotor Simulator Supported on Gas-Lubricated Foil Bearings. - Part 1: Response to Rotating Imbalance and Unidirectional Excitation, and Part 2: Operation with Heating and Thermal Gradients", Journal of Lubrication Technology, Trans. ASME, Vol. 92, Series F, No. 4, 1970, pp. 630-660.

5. Barlow, E. J.; "Derivation of Governing Equations for Self-Acting Foil Bearings", Journal of Lubrication Technology, Trans. ASME, Vol. 89, Series F, No. 3, 1967, pp. 334-340.

6. Eshel, A. and Elrod, H.G., Jr., "The Theory of the Infinitedly Wide, Perfectly Flexible, Self-Acting, Foil Bearing", Journal of Basic Engineering, Trans. ASME, Vol, 87, Series D, No. 4, 1965, pp. 831-836.

7. Eshel, A. and Elrod, H.G., Jr., "Stiffness Effects on the Infinitely Wide Foil Bearing", Journal of Lubrication Technology, Trans. ASME, Vol. 89, Series F, No. 1, 1967, pp. 92-97.

8. Eshel, A., "Compressibility Effects on the Infinitely Wide, Perfectly Flexible Foil Bearing", Journal of Lubrication Technology, Trans. ASME, Vol. 90, Series F, No. 1, 1968, pp. 221-225.

9. Eshel, A., "On Fluid Inertia Effects in Infinitely Wide Foil Bearings", Ampex Report RR 68-15, July 1968.

10. Wildmann, M., "Foil Bearings", Journal of Lubrication Technology, Trans. ASME, Vol. 91, Series F, No. 1, 1969, pp. 37-44.

11. Ma, J.T.S., "An Investigation of Self-Acting Foil Bearings", Journal of Basic Engineering, Trans. ASME, Vol. 87, Series D, No. 4, 1965, pp. 837-846.

12. Barlow, E.J., "Self-Acting Foil Bearings of Infinite Width", Journal of Lubrication Technology, Trans. ASME, Vol. 89, Series F, No. 3, 1967, pp. 341-345.

13. Licht, L., "An Experimental Study of Elastohydrodynamic Lubrication of Foil Bearings - Part 1: Displacement in the Central Zone and Part 2: Displacement in the Edge Zone", Journal of Lubrication Technology, Trans. ASME, Vol. 90, Series F, No. 1, 1968, pp. 199-220.

14. Mitskevich, A.M., "Motion of Body Over a Tangentially Vibrating Surface, Taking Account of Friction", Soviet Physics, Acoustics, Vol. 13, No. 3, 1968, pp. 348-351.

15. Lenkiewicz, W., "The Sliding Friction Process-Effect of External Vibrations", Wear, Vol. 13, No. 2, 1969, pp. 99-108.

16. Ashwell, D.G., "The Anticlastic Curvature of Rectangular Beams and Plates", Journal of Royal Aeronautical Society, Vol. 54, No. 479, 1950, pp. 708-715.

17. Eshel, A. and Elrod, H.G., Jr., "Finite Width Effects on the Self-Acting Foil Bearing", Columbia University, Lubrication Research Laboratory, Report No. 6, August 1966.

18. Burgess, J.C., "Harmonic, Superharmonic and Subharmonic Response for Single Degree of Freedom Systems of the Duffing Type", Stanford University, Division of Engineering Mechanics, Technical Report. No. 27, September 1954 (Based on Ph.D. dissertation of the author, September 1954).

19. Atkinson, C.P., "Superharmonic Oscillations as Solutions to Duffing's Equation as Solved by an Electronic Differential Analyzer", Journal of Applied Mechanics, Trans. ASME, Vol. 24, No. 4, 1957, pp. 520-525.

20. Carnegie, W. and Reif, Z.F., "Ultraharmonic Resonance of a System With an Asymmetrical Restoring Force Characteristic", Journal of Mechanical Engineering Science, Vol. II, No. 6, 1969, pp. 592-597.

21. Tondl, A., "Notes on the Problem of Self-Excited Vibrations and Non-Linear Resonances of Rotors Supported in Several Journal Bearings", Wear, Vol. 8, No. 5, 1965, pp. 349-357.

22. Vest, C.E., "Adaptation of an MoS_2 'In Situ' Process for Lubricating Spacecraft Mechanical Components", NASA TN-D-2288, May 1964, Washington, D.C.

23. Di Sapio, A. and Maloney, J., "The Lubricating Performance of an 'In Situ' Process MoS_2 Film in Air and In Liquids", Trans. ASLE, Vol. 11, No. 1, 1968, pp. 56-63.

24. Gross, W.A., Gas Film Lubrication, John Wiley and Sons, New York, 1962.

25. Constantinescu, V.N., Gas Lubrication, Produced by the National Science Foundation, published by A.S.M.E.,New York, 1969.

26. Mechanical Technologv Inc. and Rensselaer Polytechnic Institute, Design of Gas Bearings, Vol. I, 1966.

27. Eshel, A., "Dynamic Analysis of Three-Foil Rotor Support-System in Zero Gravity Enrironment", Journal of Lubrication Technology Trans. ASME, Vol. 92, Series F, No. 4, 1970, pp. 617-629.

28. Tolstoi, D.M., "Significance of the Normal Degree of Freedom and Natural Normal Vibrations in Contact Friction", Wear, Vol. 10, No. 3, 1967, pp. 199-213.

29. Singh, B.R., "Study of Critical Velocity of Stick-Slip Sliding", Journal of Engineering for Industry, Trans. ASME, Vol. 82, Series B, No. 4, 1960, pp. 393-398.

30. Brockley, C.A., Cameron, R. and Potter, A.F., "Friction-Induced Vibration", Journal of Lubrication Technology, Trans. ASME, Vol. 89, Series F, No. 2, 1967, pp. 101-108.

31. Brockley, C.A. and Ko, P.L., "Quasi-Harmonic Friction Induced Vibrations", Journal of Lubrication Technology, Trans. ASME, Vol. 92, Series F, No. 4, 1970, pp. 550-556.

32. Banerjee, A.K., "Influence of Kinetic Friction on the Critical Velocity of Stick-Slip Motion", Wear, Vol. 12, 1968, pp. 107-116.

33. Lund, J.W., "The Stability of an Elastic Rotor in Journal Bearings With Flexible, Damped Supports", Journal of Applied Mechanics, Trans. ASME, Vol. 32, Series E, No. 4, 1965, pp. 911-920.

34. Marsh, H. "The Stability of Self-Acting Gas Journal Bearings With Noncircular Members and Additional Elements of Flexibility", Journal of Lubrication Technology, Trans. ASME, Vol. 91, Series F, No. 1, 1969, pp. 113-119.

35. Sternlicht, B. and Rieger, N.F., "Rotor Stability", Proc. Instn. Mech. Engrs., Vol. 182, Part 3A, 1967/1968, pp. 82-99.

36. Airesearch Manufacturing Co., "Brayton Cycle Rotating Unit and Associated Hardware", Report No. APS-5227-R8, Contract No. NAS3-9427, March 15, 1967.

APPENDIX I

EFFECT OF BENDING RIGIDITY ON GAP WIDTH AND FOIL BEARING STIFFNESS

It is assumed for the purpose of this estimate that the foil bearing consists of 3 identical sectors, equally spaced at 120°. The foil guides are considered smooth and the ends of each foil segment are clamped, as shown in Fig. 72. Temperature effects, compressibility and fluid inertia are purposely neglected, in order to focus attention on the influence of bending rigidity on clearance and bearing stiffness.

When the foil guides are very far from the region of wrap, the flexural rigidity has a weak influence on the magnitude of the gap width in the region of uniformity [7]. For a perfectly flexible and extensible foil, the bearing consists of sectors which are circular or linear, except in short transition zones at the terminals of wrap. If on the other hand the foil is capable of offering resistance to bending, all sectors of the bearing become curved. It will be demonstrated that the flexural rigidity tends to increase the clearance in the region of uniformity and to decrease the bearing stiffness.

With the foregoing assumptions, the gap width in the region of uniformity may be calculated from the expression [6]:

$$h^* \doteq 0.643 r_6 (6\mu r_6 \omega / T)^{2/3}, \qquad (1)$$

and the stiffness in the concentric position may be evaluated from the equation [1]:

$$k = \frac{6\sin^2\frac{\theta}{2}}{\frac{l_o}{Et} + \frac{\partial \Delta l_p}{\partial T} + \frac{2}{3}\frac{\theta h^*}{T}}, \qquad (2)$$

in which Δl_p is an increase in length due to factors other than simple extension. For the case at hand, Δl_p can be considered the difference in length between two foil sectors; one perfectly flexible and resisting extension only, the other characterized by both extensional and bending rigidities [Et and $Et^3/12(1-\nu^2)$].

Referring to Fig. 72, the initial length of a perfectly flexible foil-sector at tension T_o and in the absence of rotation is:

$$l_o = r_o\theta + 2r_1\theta + 2r_1 + 2b. \qquad (3)$$

The equivalent expression for the initial length of foil of finite bending rigidity is:

$$L_o = r_o\theta + 2r_1\theta + 2\int_o^b \left(1+\tfrac{1}{2}y_o'^2\right)dx + 2\int_o^{r_1}\left(1+\tfrac{1}{2}w_o'^2\right)dz, \qquad (4)$$

and the length corresponding to a state characterized by tension T, gap width h^*, and journal displacement $\vec{e}$ can be expressed as:

$$L = r_o\theta + 2r_1\theta + 2\int_o^b \left(1+\tfrac{1}{2}y'^2\right)dx + 2\int_o^{r_1}\left(1+\tfrac{1}{2}w'^2\right)dz - 2e_1\sin\frac{\theta}{2} + h^*\theta. \qquad (5)$$

In the foregoing, it was assumed that the curvatures of non-circular foil sectors and the changes in angles of wrap were sensibly small, so that the approximations made in equations (4) and (5) are consistent with those made in the derivation of equation (2) in reference [1].

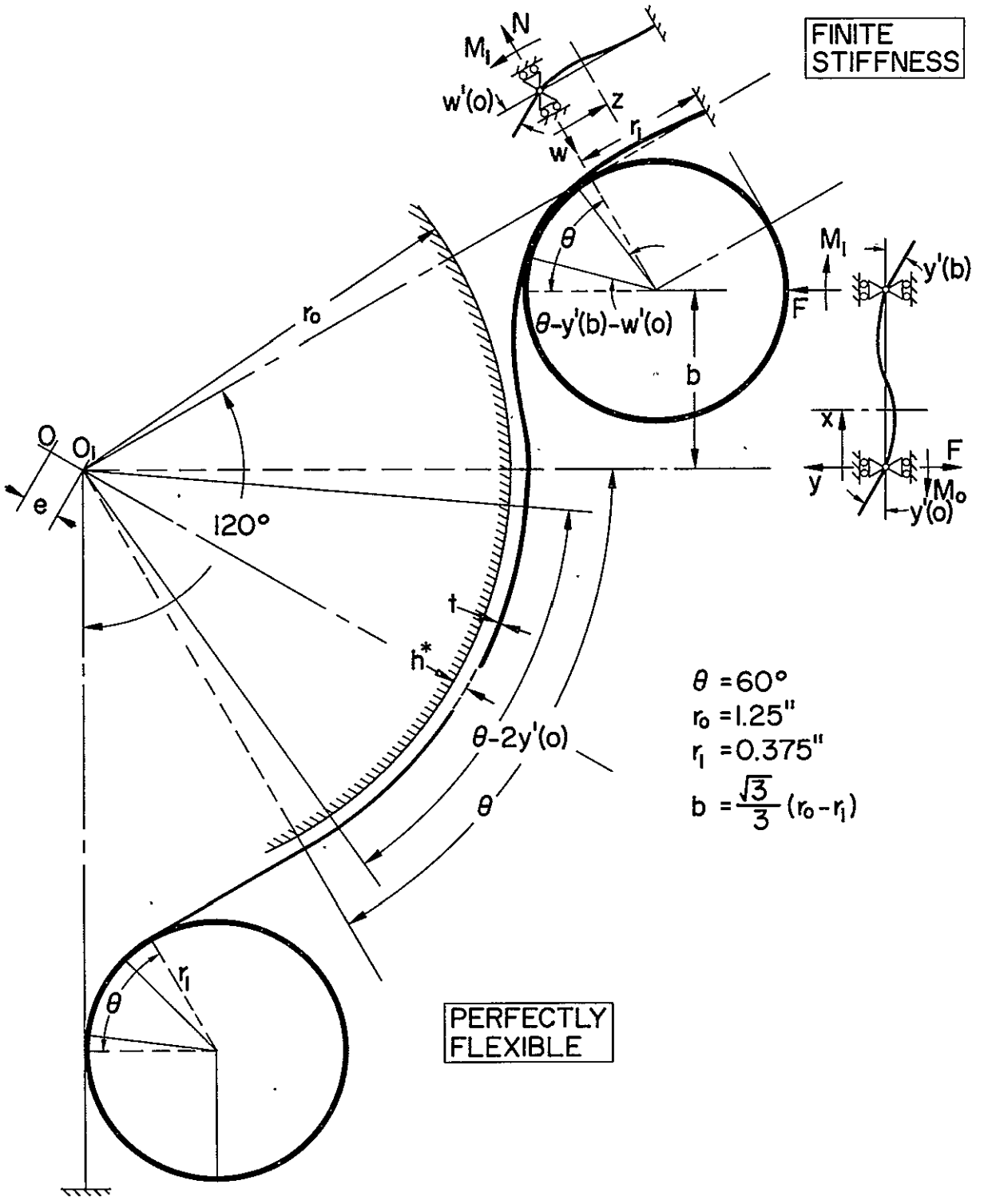

Fig. 72 Schematic Diagrams Pertinent to Estimates of Effect of Flexural Rigidity, Appendix 1.

The "slack length" $\Delta \ell_p$ is given by the integrals:

$$\Delta \ell_p = -(\Delta I + \Delta J) = \int_0^b (y'^2 - y_0'^2)\, dx + \int_0^{r_1} (w'^2 - w_0'^2)\, dz, \quad (6)$$

and the stress-strain relation can be expressed by [1]:

$$\frac{T - T_0}{Et} = \frac{L - L_0}{L_0} \approx \frac{L - L_0}{\ell_0} = \frac{-2e \sin\frac{\theta}{2} + h^* \theta - \Delta \ell_p}{\ell_0}, \quad (7)$$

so that at $\dot{e} = 0$;

$$h^* = 0.643 r_0 (6\mu r_0 \omega / T)^{2/3} = \frac{\ell_0}{Et\theta}(T - T_0) + \frac{\Delta \ell_p}{\theta}. \quad (8)$$

In order to express the "slack length" $\Delta \ell_p$ in equations (6) and (8) and its partial derivative with respect to tension $\partial \Delta \ell_p / \partial T$ in equation (2), solutions must be obtained for deflections y and w of foil sectors between the journal and the foil guide, and between the foil guide and the foil lock. Referring to the diagrams in Fig. 72, we have:

$$\frac{d^2 y}{dx^2} - \frac{T}{D} y = \frac{M_0}{D} - \frac{M_1}{D}\left(1 + \frac{M_0}{M_1}\right)\frac{x}{b} = \frac{1}{r_1}\left[\frac{r_1}{r_0} - \left(1 + \frac{r_1}{r_0}\right)\frac{x}{b}\right], \quad (9)$$

with $y = 0$ at $x = 0$ and $x = b$. (10)

Letting $X = x/b$, $Y = y/t$, $\alpha^2 = b^2 T/D$, $\beta = b^2/r_1 t$ and $\eta = r_1/r_0$, the nondimensional form of the boundary problem becomes:

$$Y'' - \alpha^2 Y = \beta\eta\left(1 - \frac{1+\eta}{\eta} X\right), \quad (11)$$

with

$$Y = 0 \text{ at } X = 0 \text{ and } X = 1 \tag{12}$$

the solution of which is:

$$Y = \frac{\beta\eta}{\alpha^2}\left[\cosh\alpha X + \frac{1-\cosh\alpha-(1+\eta)/\eta}{\sinh\alpha}\sinh\alpha X + \frac{1+\eta}{\eta}X - 1\right]. \tag{13}$$

Similarly:

$$\frac{d^2w}{dz^2} - \frac{T}{D}w = \frac{1}{r_1} - \frac{N}{D}z, \tag{14}$$

$$\text{with } w = 0 \text{ at } z = 0 \text{ and } w = w' = 0 \text{ at } z = r_1, \tag{15}$$

and letting $Z = z/r_1$, $W = w/t$, $\lambda^2 = r_1^2\,T/D$, $\bar{C} = Nr_1^3/Dt$ and $\gamma = r_1/t$, we obtain:

$$W'' - \lambda^2 W = \gamma - \bar{C}Z, \tag{16}$$

$$\text{with } W = 0 \text{ at } Z = 0 \text{ and } W = W' = 0 \text{ at } Z = 1, \tag{17}$$

the solution of which is:

$$W = \frac{\gamma}{\lambda^2}\left[\cosh\lambda Z + \frac{(\sinh\lambda-\lambda\cosh\lambda-\lambda)(1-\cosh\lambda)}{(\sinh\lambda-\lambda\cosh\lambda)\sinh\lambda}\sinh\lambda Z + \frac{\lambda(1-\cosh\lambda)}{\sinh\lambda-\lambda\cosh\lambda}Z - 1\right]. \tag{18}$$

The "slack length" $\Delta \ell_p$ and its partial derivative with respect to tension can be written as:

$$\Delta \ell_p = \frac{t^2}{b}\int_0^1 (Y'^2 - Y_o'^2)\,dX + \frac{t^2}{r_1}\int_0^1 (W'^2 - W_o'^2)\,dZ\,, \qquad (19)$$

in which the subscript $(\ )_o$ refers to the initial state at $T = T_o$, and

$$\frac{\partial \Delta \ell_p}{\partial T} = \frac{t^2 b}{D}\frac{\partial}{\partial \alpha^2}\int_0^1 Y'^2\,dX + \frac{t^2 r_1}{D}\frac{\partial}{\partial \lambda^2}\int_0^1 W'^2\,dZ\,. \qquad (20)$$

The effect of varying the flexural rigidity $D = Et^3/12(1-\nu^2)$ by changing the foil thickness is illustrated in Fig. 73 through Fig. 76 for two levels of the preload tension T_o.

It can be seen that the reduction of bearing stiffness due to flexural rigidity can be considerable, particularly in the low-speed range in which resonances occur. Although the stiffness assumes the same asymptotic value for $D = 0$ and $D \neq 0$, the difference is appreciable in the speed range of practical interest, except for very thin foils.

The reader will note that the stiffness and, therefore, the resonant frequencies are insensitive to speed, except at low RPS. This explains the experimental results presented in Fig. 4.40 of reference [1], in which the resonant frequency $f_n(N) \approx$ constant.

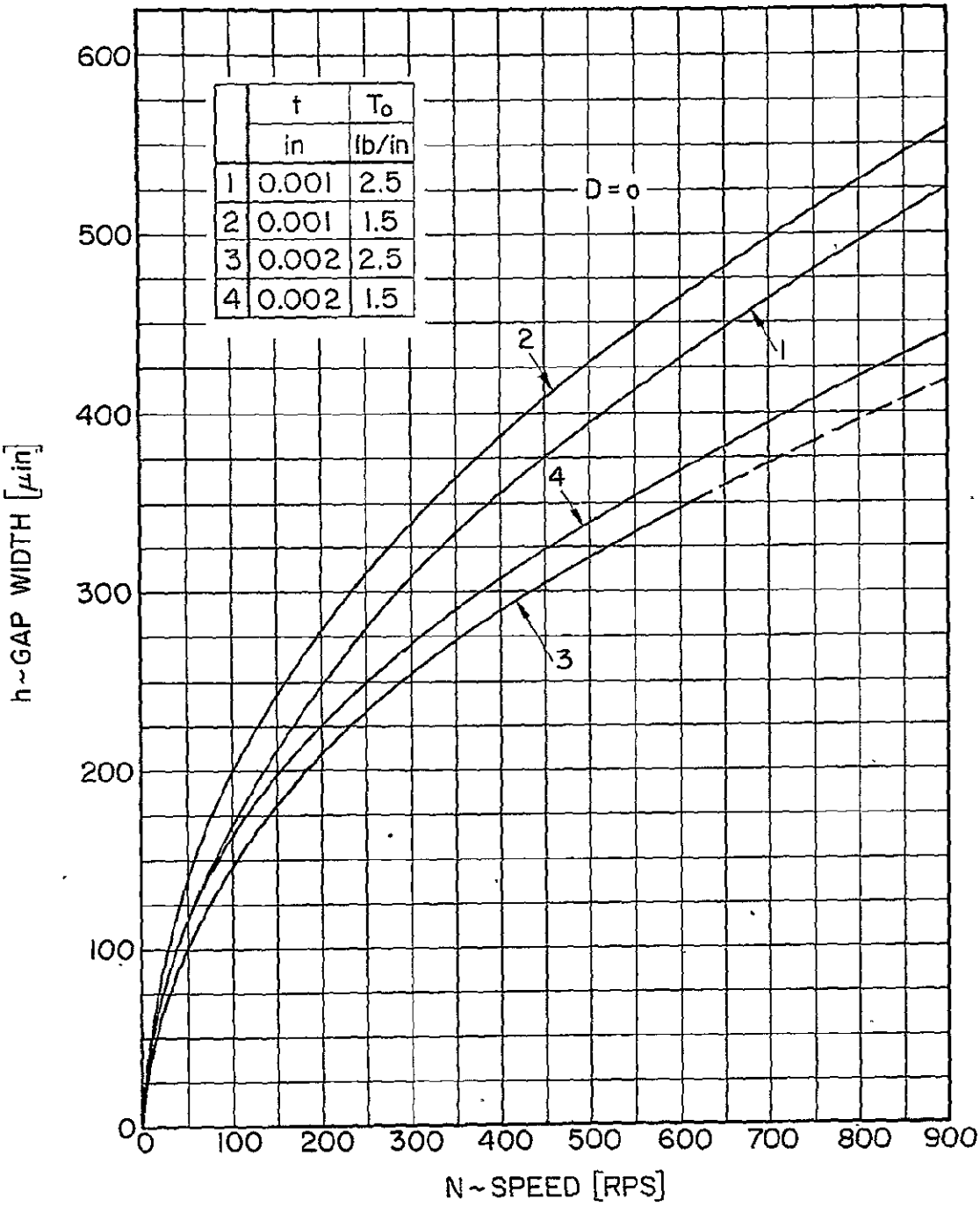

Fig. 73 Effect of Foil Thickness and Preload Tension on the Variation of Gap Width With Speed, D = 0. Appendix 1

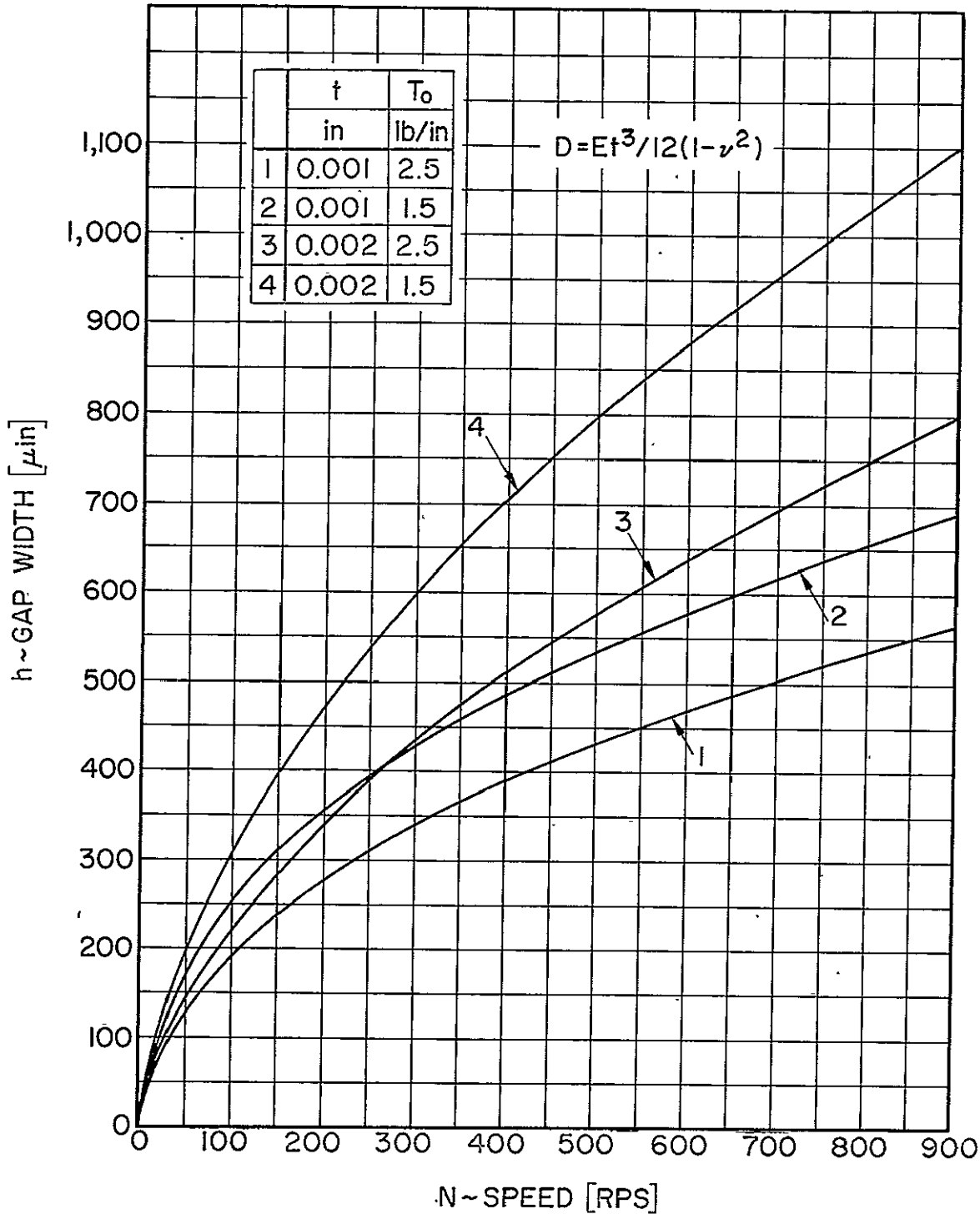

Fig. 74 Effect of Foil Thickness and Preload Tension on the Variation of Gap Width with Speed, $D \neq 0$. Appendix 1

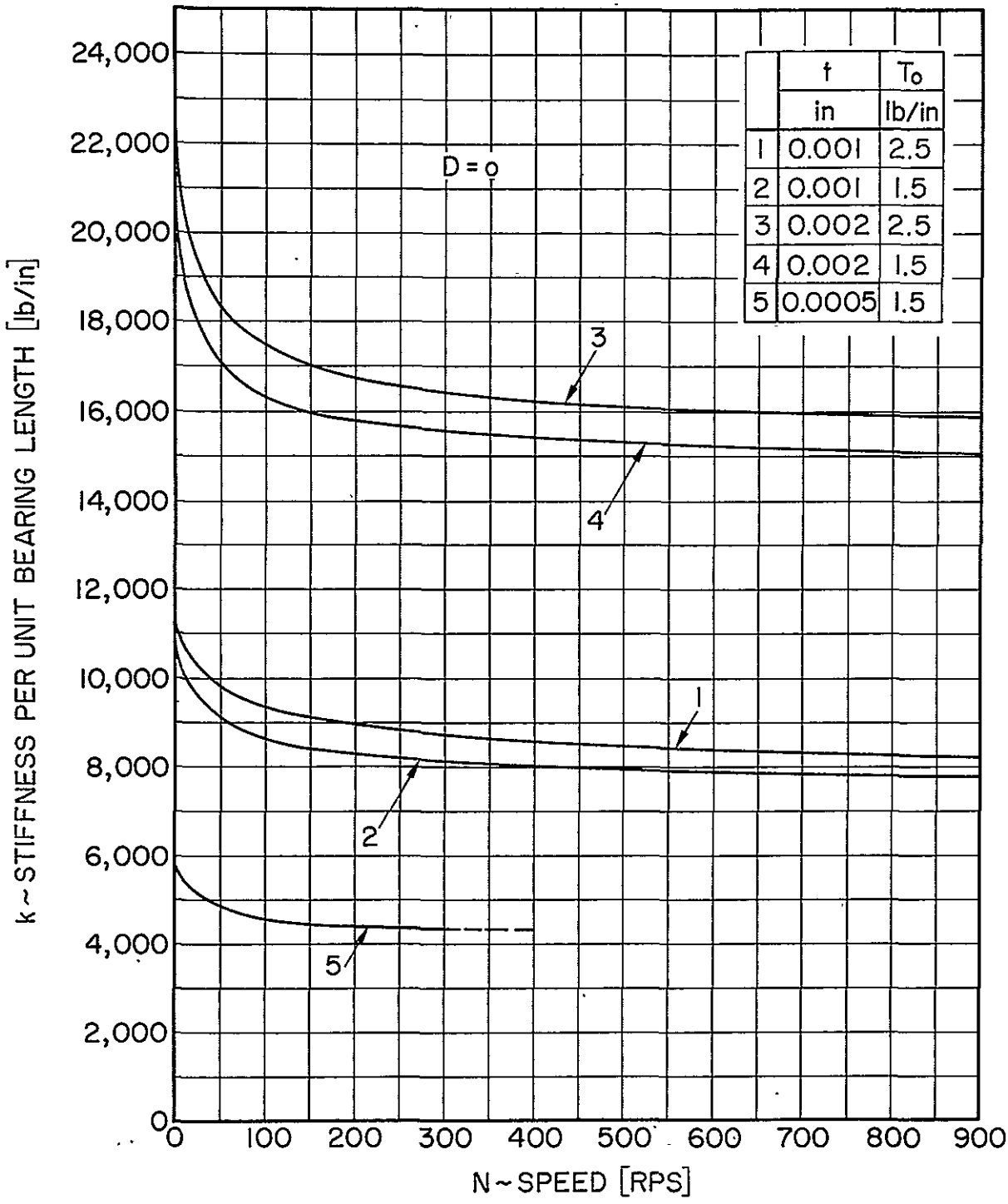

Fig. 75 Effect of Foil Thickness and Preload Tension on the Variation of Bearing Stiffness with Speed, D = O. Appendix 1

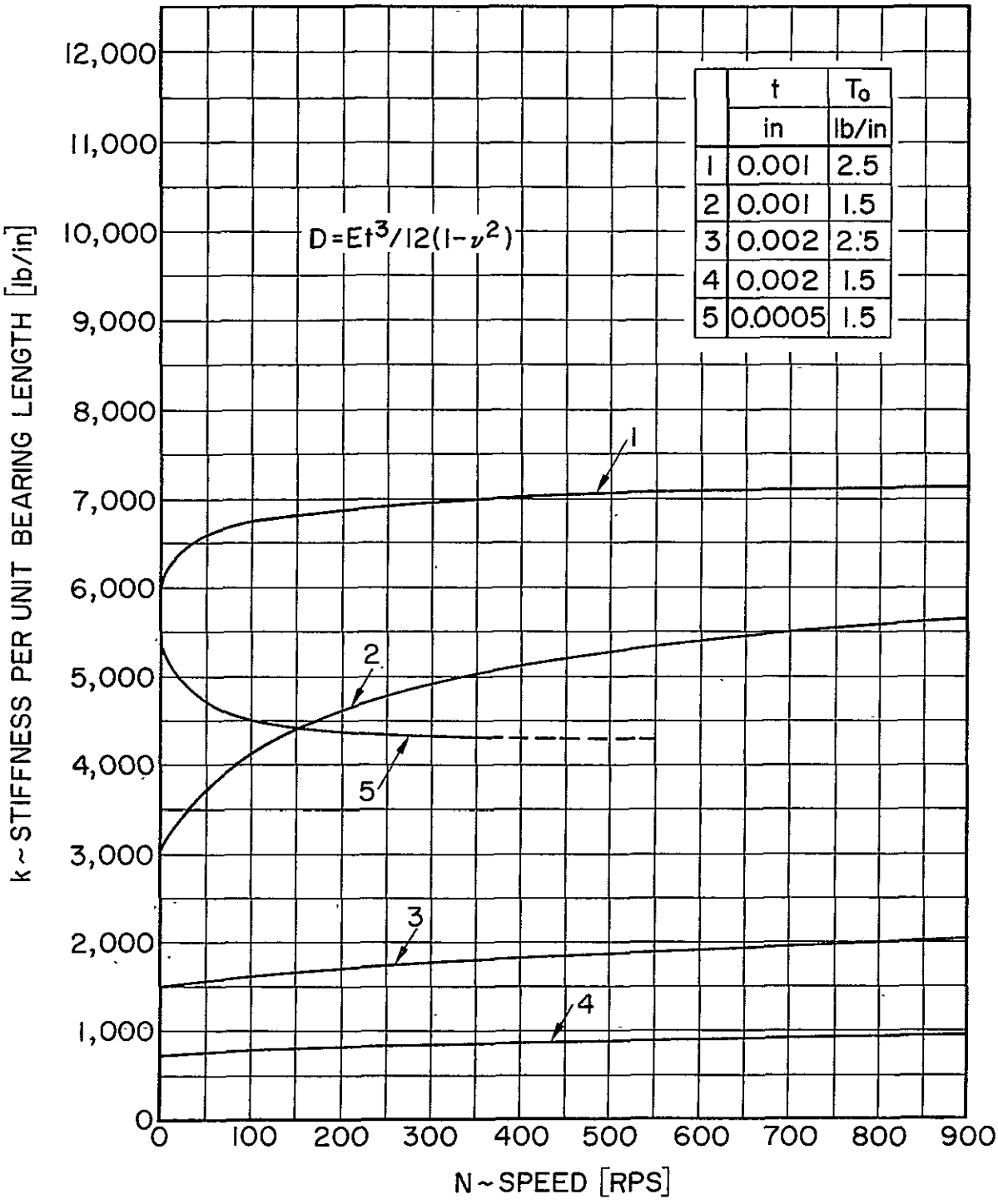

Fig. 76 Effect of Foil Thickness and Preload Tension on the Variation of Bearing Stiffness with Speed, $D \neq 0$. Appendix 1

APPENDIX 2

METHOD OF STARTING IN THE HORIZONTAL ATTITUDE

The capability of starting without a foil-lift system was demonstrated in the vertical attitude. "Dry" starting could undoubtedly be achieved also in the horizontal attitude with relatively light rotors.

The foil-lift system involving pressurization through the interior of the rotor was elaborate [3], but a much simpler system could be designed to initiate rotation when gravity loading is appreciable.

The schematic diagram in Fig. 77 shows a pressurized pad*, integral with a spring-retractable piston. The function of the pad is to lift the rotor and restore the journal to the reference (concentric) position. With the rotor weight and spring force balanced by the piston, the breakaway friction torque would be equal to that in the vertical attitude. As soon as sufficient speed is attained to generate sufficient load capacity and an adequate clearance, the pressure can be cut off and the piston automatically retracted to a safe position. The additional journal length occupied by the pad would be sensibly small, and the system would be considerably simpler than the foil lift requiring pressurization through the interior of the rotor [1,3].

*The pad is situated outside the foil bearing.

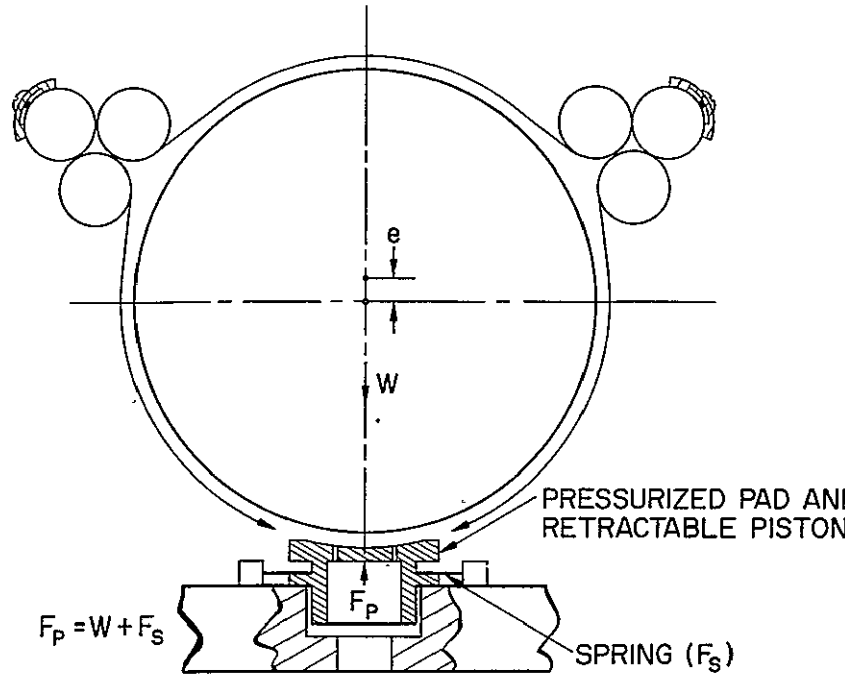

Fig. 77 Schematic Diagram of Rotor Lift, Appendix 2

APPENDIX 3

EFFECT OF PRELOAD TENSION ON THE NATURAL FREQUENCY OF THE FOIL-ROTOR SYSTEM AND ON THE FREQUENCY OF FRICTION INDUCED OSCILLATION

Friction induced oscillations are one of the most commonly encountered and easily observable types of mechanical vibrations. It is well known that external vibrations, both transverse and in the direction of sliding, can effectively reduce friction, as much as by an order of magnitude [14,15,28]. This principle was utilized in the course of the present investigation, as described in Chapter 2. On the other hand, the occurrence of self-excited vibrations during sliding is intimately connected with the variation of friction forces with the velocity of sliding [29,30,31,32].

The correlation of the natural frequencies of the foil-rotor system with the frequencies of friction induced vibrations, Fig. 78, does not depend on artificial distinctions made between "static" and "kinetic" coefficients of friction [28], or on precise differentiation between "stick-slip" and "quasi-harmonic" oscillations [30,31]. In the experiments described in Section 3.9, the first attempts to start with a preload of $T_o \approx 2.25$ lb/in produced excessively large amplitudes of vibrations during the initial stages of rotation. The problem was eliminated by reducing the preload to $T_o \approx 1.5$ lb/in.

Although the friction-induced vibrations were essentially torsional, they excited also transverse components of motion. Slow manual rotation of the rotor produced a quasi-sinusoidal, lateral vibration, the frequency of which remained nearly constant above a certain minimal speed of rotation (see also Fig. 13 in reference [31]).

The experiment consisted of varying the preload tension T_o and recording at each setting of preload (a) the frequency of the decaying vibration, f_n, following impact, and (b) the frequency of friction induced oscillation, f_{SS}. The results presented in Fig. 78 show that these frequencies coincided at $T_o \approx 2.10$ lb/in. It was inferred, therefore, that frictional vibrations induced at a preload $T_o \approx 2.25$ lb/in were in the immediate vicinity of a resonance of the foil-rotor system, resulting in large amplitudes of motion.

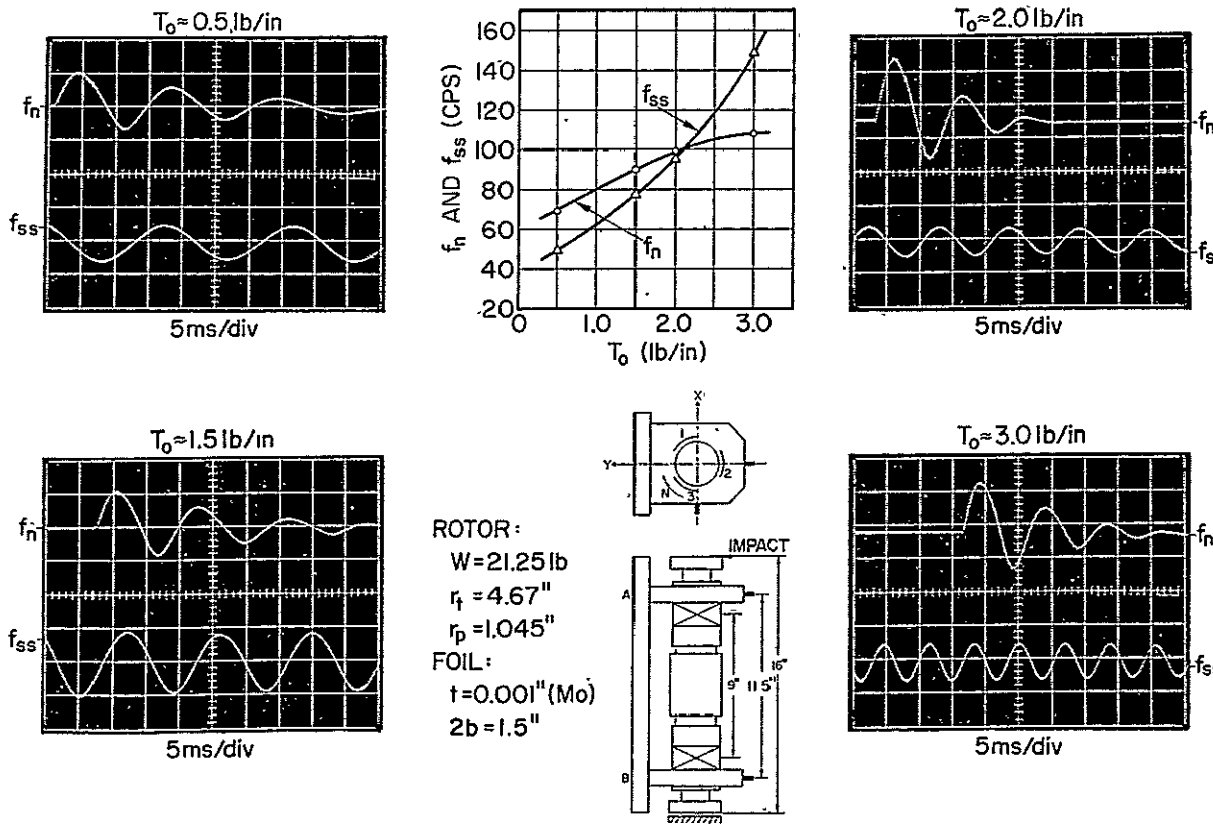

Fig. 78 Correlation of Frequencies of Friction-Induced Vibrations with the Natural Frequencies of the Foil-Rotor System, Appendix 3

40

APPENDIX 4

SUGGESTED FOIL BEARING CONFIGURATION

The basic support elements of the foil bearing tested in the course of the present investigation consisted of cylindrical guides, clamps, and a foil lock. The bearing sectors were essentially symmetrical about radial planes spaced at 120°, with the exception of a slight dissymetry introduced by the foil lock.

A suggested 4-sector configuration is illustrated schematically in Fig..79. A similar 3-sector geometry is also feasible. While the schematic diagrams in Fig. 79 are self-explanatory, the main advantages of the support shell are thought to be the following. The shell may serve as a thermal shield and a temperature equalizer, as well as a mechanical limit-stop. The narrow clearance between the shell and the outer foil-surface may furnish an appreciable amount of damping and limit the journal amplitudes at resonance.

The bearing shell may be cantilevered from one end, or mounted on spokes, with provision made for thermal expansion and additional elements of flexibility. The suggested configuration should not be interpreted beyond the limits intended by the schematic representation.

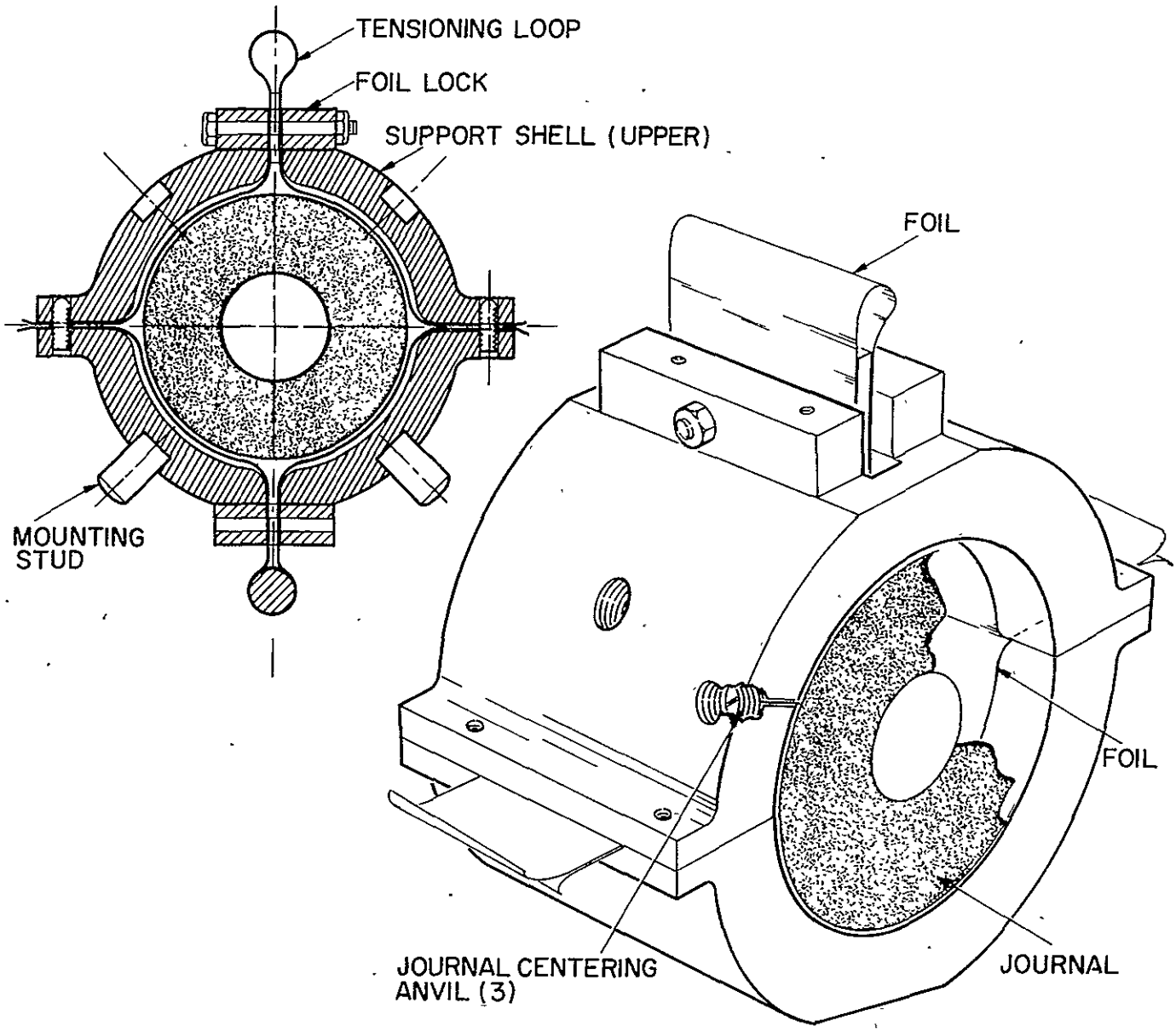

Fig. 79 Schematic Diagram of Suggested Foil-Bearing Configuration, Appendix 4

BEARINGS BRANCH SPACE POWER CONTRACTS

Final Report Distribution List

Attention:	Bearings Branch, Project Manager	(10 + reporducible)
	E.E. Bisson, MS 5-3	1
	W.J. Anderson, MS 23-2	1
	R.L. Johnson, MS 23-2	1
	B. Lubarsky, MS 3-3	1
	J.E. Dilley, MS 500-309	1
	C.H. Voit, MS 5-3	1
	H.O. Slone, MS 500-501	1
	R.E. English, MS 500-201	1
	D.G. Beremand, MS 500-201	1
	W.L. Stewart, MS 500-316	1
	Report Control Office, MS 5-5	1
	Library, MS 60-3	1
	Reliability & Quality Assurance Office, MS 500-111	1
	Technology Utilization Office, MS 3-19	1
	Office of Operations Analysis and Planning, MS 3-15	1

NASA Lewis Research Center
21000 Brookpark Road
Cleveland, Ohio 44135

Attention: Acquisitions Branch (SQT-34054) 1
NASA Scientific & Technical Information Facility
P.O. Box 5700
College Park, Maryland 20740

Attention: Library 1
NASA Ames Research Center
Moffett Field, California 94035

Attention: Library 1
NASA Flight Research Center
P.O. Box 273
Edwards, California 93523

Attention: Library 1
NASA Goddard Space Flight Center
Greenbelt, Maryland 20771

Attention: Library 1
Jet Propulsion Laboratory
4800 Oak Grove Drive
Pasadena, California 91103

Attention: Library 1
NASA Langley Research Center
Langley Station
Hampton, Virginia 23365

Attention: Library 1
NASA Manned Spacecraft Center
Houston, Texas. 77058

Attention: Library 1
NASA Marshall Space Flight Center
Marshall Space Flight Center
Marshall Space Flight Center, Alabama 35812

Attention: P.R. Miller (RNP) 1
H.D. Rochen (RNP) 1
NASA Headquarters
Washington, D.C. 20546

Attention: Library 1
Aerojet-General Corporation
1100 West Hollyvale
Azusa, California 91702

Attention: Library 1
J.B. Accinelli
Aerojet-General Corporation
Aerojet Liquid Rocket Company
Sacramento, California 98509

Attention: Library 1
Aerospace Corporation
P.O. Box 95085
Los Angeles, California 91745

Attention: M.R. Chasman 1
Air Force Aero-Propulsion Lab
Wright-Patterson Air Force Base
Dayton, Ohio 45433

Attention: Library 1
Lyle Six 1
AiResearch Manufacturing Company
402 South 36 Street
Phoenix, Arizona 85034

Attention: Library 1
AiResearch Manufacturing Company
9851 Sepulveda Boulevard
Los Angeles, California 90009

Attention: N. Grossman 1
Atomic Energy Commission
Division of Reactor Development
and Technology
Washington, D.C. 20767

Attention: N. Gerstein 1
Atomic Energy Commission
AEC-NASA Space Nuclear Systems Office
Washington, D.C. 20545

Attention: Library 1
C.M. Allen 1
Battelle Memorial Institute
Columbus Laboratories
505 King Avenue
Columbus, Ohio 43201

Attention: Library
DMIC
% Battelle Memorial Institute
Columbus Laboratories
505 King Avenue
Columbus, Ohio 43201

Attention: Library 1
Bendix Research Labs Division
Detroit, Michigan 48232

Attention: Library 1
Boeing Company
Aerospace Division
P.O. Box 3707
Seattle, Washington 98124

Attention: Library 1
A.J. Lemanski 1
Boeing Company
Vertol Division, Boeing Center
P.O. Box 16858
Philadelphia, Pennsylvania 19142

Attention: Library 1
Continental Aviation & Engineering Corporation
12700 Kercheval Avenue
Detroit, Michigan 48215

Attention: Library 1
Curtiss-Wright Corporation
Wright Aero Division
Main & Passaic Streets
Woodridge, New Jersey 07075

Attention: W. Shapiro 1
Franklin Institute Research Labs
Benjamin Franklin Parkway
Philadelphia, Pennsylvania 19103

Attention: Library 1
Space Division
General Electric Company
Evendale, Ohio 45215

Attention: Library 1
General Electric Company
Re-Entry & Environmental Systems Division
3198 Chestnut Street
Philadelphia, Pennsylvania 19104

Attention: Library 1
General Electric Company
Mechanical Technology Laboratory
R&D Center
Schenectady, New York 12301

Attention: Library
General Motors Corporation
Allison Division
Indianapolis, Indiana 46206

Attention: Library 1
Hughes Aircraft Corporation
Centinda & Teale Avenue
Culver City, California 90024

Attention: Library 1
Institute for Defense Analyses
400 Army-Navy Drive
Arlington, Virginia 22202

Attention: Library
Lear Siegler, Incorporated
3171 S. Bundy Drive
Santa Monica, California 90406

Attention: Library 1
Lockheed Missiles & Space Company
P.O. Box 504
Sunnyvale, California 94088

Attention: Library 1
McDonnell Douglas Astronautics Company
5301 Bolsa Avenue
Huntington Beach, California 92647

Attention: Library
McDonnell Douglas Astronautics Company
3000 Ocean Park Boulevard
Santa Monica, California 90406

Attention: Library 1
Massachusetts Institute of Technology
Cambridge, Massachusetts 02139

Attention: Library 1
Mechanical Technology Incorporated
968 Albany-Shaker Road
Latham, New York 12110

Attention: Library 1
National Science Foundation
Engineering Division
1800 G. Street, N.W.
Washington, D.C. 20540

Attention: Library 1
North American Rockwell Corporation
Space Division
12214 Lakewood Boulevard
Downey, California 90241

Attention: Library 1
Northern Research & Engineering Company
219 Vassar Street
Cambridge, Massachusetts 02139

Attention: S.W. Doroff ONR/463 1
Office of Naval Research
Washington, D.C. 20360

Power Information Center 1
University of Pennsylvania
3401 Market Street, Room 2107
Philadelphia, Pennsylvania 19104

Attention: Library 1
Solar
Division of International Harvester
2200 Pacific Highway
San Diego, California 92112

Attention: Library 1
Space Systems Division
Los Angeles Air Force Station
Los Angeles, California 90045

Attention: Library 1
Sunstrand Denver
2480 West 70 Avenue
Denver, Colorado 80221

Attention: Library 1
TRW Accessories Division
23555 Ecluid Avenue
Cleveland, Ohio 44117

Attention: Library 1
TRW Systems
One Space Park
Redondo Beach, California 90278

Attention: W. Crim 1
U.S. Army Engineering R&D Labs
Gas Turbine Test Facility
Fort Belvoir, Virginia 22060

Attention: Library 1
United Aircraft Corporation
Pratt & Whitney Aircraft
400 Main Street
East Hartford, Connecticut 06108

Attention: Library 1
United Aircraft Research Laboratory
East Hartford, Connecticut 06108

Attention: Library 1
Westinghouse Electric Corporation
Astronuclear Laboratory
P.O. Box 10864
Pittsburgh, Pennsylvania 15236

Attention: Library 1
Williams Research
Walled Lake, Michigan 48088

AMPEX